Letter from the Editors

Dear readers of *Acta Naturae*,

We are celebrating a kind of anniversary: we are bringing to your attention the tenth issue of our journal with the hope that you will not be disappointed. The issue opens with a review article penned by a researcher from M.V. Lomonosov Moscow State University under the guidance of M.B. Gottikh. It discusses the prospects in developing drugs with a specific inhibiting activity of HIV-integrase. Since the stage of integration of viral DNA into cellular DNA is catalyzed by viral integrase, blocking the activity of this enzyme could result in termination of viral replication and open rather favorable ways for therapeutic use. Integrase inhibitors have not been used as components of the conventional "cocktail" consisting of the inhibitors of reverse transcriptase and protease. Moreover, the problems related to the stability of mutant forms require that researchers pay close attention to new enzyme targets. Existing data are reassuring. The siRNA technology is an efficient method for "switching off" regulatory pathways, which is an alternative to the above-mentioned chemical approach. Researchers from Novosibirsk Academgorodok, under the guidance of Professor M.A. Zenkova, used this approach on cell lines in order to reduce their proliferation rate. This fundamental work has significant clinical potential. The study conducted by a group of researchers from Moscow State University under the guidance of Academician I.G. Atabekov is devoted to the *in vitro* assembly of potato virus X protein complexes. The proposed method has demonstrated the fundamental possibility of packaging foreign genetic material into virus-like particles. Two groups of authors from N.I. Pirogov Medical University (Moscow, professor O.A. Favorova) and the Fox Chase Cancer Center, Philadelphia, USA (professor J.R. Testa and professor E.P. Henske) publish pioneering studies in this issue. In one of them, the DLX5 transcriptional factor is described as a new target for anticancer therapy; the role of the rabin8 protein in the functioning of the mTORC1protein kinase complex and the protein biosynthesis associated with it are considered in the second study. Both articles have a pronounced potential clinical orientation. The article by authors from the Ufa, Novosibirsk, and Yakutsk Academic centers was written under the guidance of E.K. Khusnutdinova and aimed to perform a population analysis using mutations of the *GJB2*–35delG gene linked to hereditary hearing loss. The authors arrive at a rather interesting conclusion on the timeframe of population migrations. Several studies are usually devoted to various aspects of bioengineering. Thus, a team of authors under the guidance of Academician of the Russian Academy of Medical Sciences A.L. Gintsburg presents a study devoted to nanoantibody expression using an adenoviral vector. The article by a group of authors under the guidance of Academician M.P. Kirpichnikov focuses on the important problem of the expression of membrane proteins. The study carried out under the guidance of Academician of the Russian Academy of Medical Sciences A.M. Egorov is devoted to the technology of expression of the antibody-peroxidase detection of recombinant conjugate in the yeast system. Targeted gene delivery, another problem that is topical both in the sense of fundamentality and application, is also discussed in this issue. This direction is required for advances in gene therapy. An efficient method for interleukin-2 gene delivery into hematopoietic cells is described in the article by a group of authors from the N.F. Gamaleya Institute of Epidemiology and Microbiology. The study by a team of authors from Moscow State University and the Institute of Molecular Genetics of the Russian Academy of Sciences is devoted to the investigation of the structural features of cytoskeletal morphology by atomic force microscopy. Our intention is to continue to seek to publish studies associated with new methods of biological imaging.

The article by Doctor of Chemistry P.V. Sergiev published in the "Forum" section is devoted to the role of high performance sequencing in genome analysis. We are looking forward to your response to this publication. In future, we plan to pay the closest attention to problems related to the development of novel analytical technologies in Russia. Today, the equipment at the disposal of many institutions in the Russian Federation is worthy of admiration. Our hope is that in the nearest future Russian researchers will manage to produce breakthrough results. ●

PHARMASI

INNOVATIVE DRUG R&D RUSSIA 2011

DISCOUNT 10%*
VIP CODE — HR18ACTA

Adam Smith CONFERENCES

Adam Smith Conferences' 2nd International Forum

How to maximise the potential of a highly promising sector, and how to achieve a leading position in it?

www.drug-research-russia.com

40+ Speakers include:


Andrey Ivaschenko
Chairman of the Board of Directors
The ChemRar High-Tech Center


Dmitry Genkin
Chairman of the Board of Directors
Pharmsyntez


Evgeny Zaytsev
General Partner
Helix Ventures pharm


Igor Agamirzian
Chief Executive Officer
Russian Venture Company


Igor Goryanin
Executive Director
Biomedicine Cluster Skolkovo Innovation Center


Petr Rodionov
Director
Geropharm


Mark A. Herzog
CAE,
Executive Director
Virginia Biotechnology Association (VABIO)


Lyudmila Ogorodova
Head of Technology Platform "Medicine of the Future"


Alexey Konov
Vice-President
GC BIOPROCESS & Investment Director
Bioprocess Capital Partners


Dmitry Morozov
Chairman of the Board of Directors
BIOCAD


Alexander Gabibov
Shemyakin–Ovchinnikov Institute of Bioorganic Chemistry, Russian Academy of Sciences


Tatyana Nikolenko
Director, Infrastructure Projects, The Russian Corporation of Nanotechnologies

21—22 November 2011, Renaissance Moscow Monarch Centre Hotel

WHAT'S ON OFFER IN 2011?

- KEY FEATURE! **GOVERNMENT STRATEGIES AND POLICIES.** Plans and priorities
- THINK-TANK! **How to develop an IDEAL LIFE CYCLE for innovative drugs?**
- SPOLIGHT SESSION! **COMPANIES' ROLE** in sector development. Recent projects and initiatives
- MEETING OF MINDS! **FUNDING** and **OPPORTUNITIES FOR ATTRACTING INVESTMENT**
- SPECIAL FOCUS! **THE FUTURE OF BIOPHARMACEUTICAL CLUSTERS** in Russia. Including a review of **TECHNOLOGY PLATFORM "MEDICINE OF THE FUTURE"**
- IN-DEPTH FOCUS! **CLINICAL TRIALS** — the potential today & tomorrow
- SPECIAL DISCUSSION! **HR assets** for developing an innovative pharmaceutical sector
- THEMED DISCUSSION! **BIOSIMILARS VS. INNOVATIVE TECHNOLOGICAL DRUGS**

Sponsors: R-PHARM, GOLTSBLAT BIP, BAKER BOTTS LLP

In Cooperation with: CHEMRAR high-tech center, RUSSIAN VENTURE COMPANY

Lead Information Partner: Фармацевтический ВЕСТНИК

Official Analytical Information Partner: РЕМЕДИУМ

Information Internet Partner: Pharma.net.ua

Supporting Organisations: AIPM, Mid-Atlantic - Russia Business Council

Information Partners: Социальный навигатор, Фармацевтическая отрасль, SCRIP Intelligence, Новости GMP, Фармацевтическая промышленность, TEMPLETON THORP, ФАРМАЦЕВТ ПРАКТИК, РИАНОВОСТИ, Казахстанский фармацевтический вестник, Farmavita.Net, EUROMONITOR INTERNATIONAL, "The Pink Sheet", PharmAsia News, Pharm-Med, ActaNaturae, NewScientist, S&TRF

* Discount is not valid for persons who have already registered to participate at this conference and/or seminar(s). All discounts can only be applied at the time of registration and can not be combined. All discounts are subject to approval.

Tel: +44 20 7017 7444 | Fax: +44 20 7017 7447 | events@adamsmithconferences.com

M. V. Arkhipenko, E. K. Petrova, N. A. Nikitin, A. D. Protopopova, E. V. Dubrovin, I. V. Yaminskii, N. P. Rodionova, O. V. Karpova, J. G. Atabekov

Characteristics of Artificial Virus-like Particles Assembled *in vitro* from Potato Virus X Coat Protein and Foreign Viral RNAs

Potato virus X (PVX) and some other potexviruses can be reconstituted *in vitro* from viral coat protein (CP) and RNA. PVX CP is capable of forming viral ribonucleoprotein complexes (vRNP) not only with homologous, but also with foreign RNAs. Our data suggest that the assembly of the "mixed" vRNP *in vitro* could be started at the 5'-proximal region of the RNA, producing a helical structure of vRNPs with foreign nucleic acids. The formation of heterologous vRNP *in vitro* with PVX CP appears not to require a specific 5' end RNA nucleotide sequence, and the PVX CP seems to be able to pack foreign genetic material of various sizes and compositions into artificial virus-like particles.

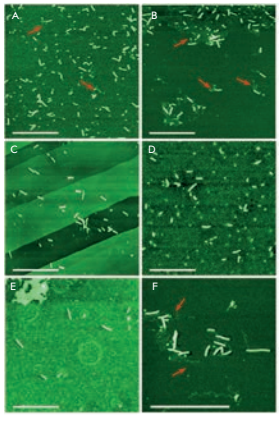

AFM images of the vRNPs assembled *in vitro* from homologous or foreign RNA and PVX CP.

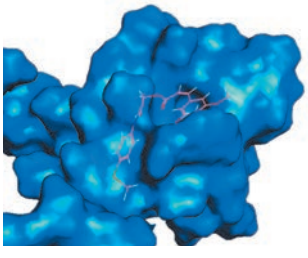

Position of compound in the active site of the transcription factor DLX5.

R. A. Timakhov, P. O. Fedichev, A. A. Vinnik, J. R. Testa, O. O. Favorova

Transcription Factor DLX5 As a New Target for Promising Antitumor Agents

The crystal structure of the human transcription factor DLX5 has been used for the screening of a library consisting of 10^6 compounds by the molecular docking technique. Compound Q12 displays the best ability to inhibit the proliferation of *Dlx5* positive mouse lymphoma cells, which correlates with the down-regulation of *c-myc* expression. Compound Q12 can be used for further chemical optimization and for the development of novel, highly efficient cancer treatments.

L. U. Dzhemileva, O. L. Posukh, N. A. Barashkov, S. A. Fedorova, F. M. Teryutin, V. L. Akhmetova, I. M. Khidiyatova, R. I. Khusainova, S. L. Lobov, E. K. Khusnutdinova

Haplotype Diversity and Reconstruction of Ancestral Haplotype Associated with the c.35delG Mutation in the *GJB2* (Cx26) Gene among the Volgo-Ural Populations of Russia

The mutations in the *GJB2* (Cx26) gene make the biggest contribution to hereditary hearing loss. The spectrum and prevalence of the *GJB2* gene mutations are specific to populations of different ethnic origins. For several *GJB2* mutations, their origin from the appropriate ancestral founder chromosome was shown, approximate estimations of "age" obtained, and presumable regions of their origin outlined. The haplotype analysis of chromosomes with the c.35delG mutation in patients with nonsyndromic sensorineural hearing loss and in population samples permitted the reconstruction of an ancestral haplotype with this mutation, established the common origin of the majority of the studied mutant chromosomes, and provided the estimated time of the c.35delG mutation carriers expansion (11,800 years) on the territory of the Volga-Ural region.

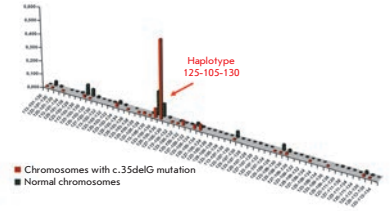

The distribution of frequencies of haplotype D13D141-D13S175-D13S143 on normal chromosomes and chromosomes with a mutation c.35delG in patients with NSHL.

ActaNaturae
JULY—SEPTEMBER 2011 VOL. 3 № 3 (10)

Founders
Ministry of Education and
Science of the Russian Federation,
Lomonosov Moscow State University,
Park Media Ltd

Address: 119991 Moscow, Russia, Leninskiye Gory, Nauchny
Park MGU, vlad.1, stroeniye 75G.
Phone/Fax: +7 (495) 930 80 06
E-mail: vera.knorre@gmail.com, enovoselova@strf.ru,
biomem@mail.ru

Номер подписан в печать 28 сентября 2011 г.
Тираж 200 экз. Цена свободная.
Отпечатано в типографии «МЕДИА-ГРАНД»

CONTENTS

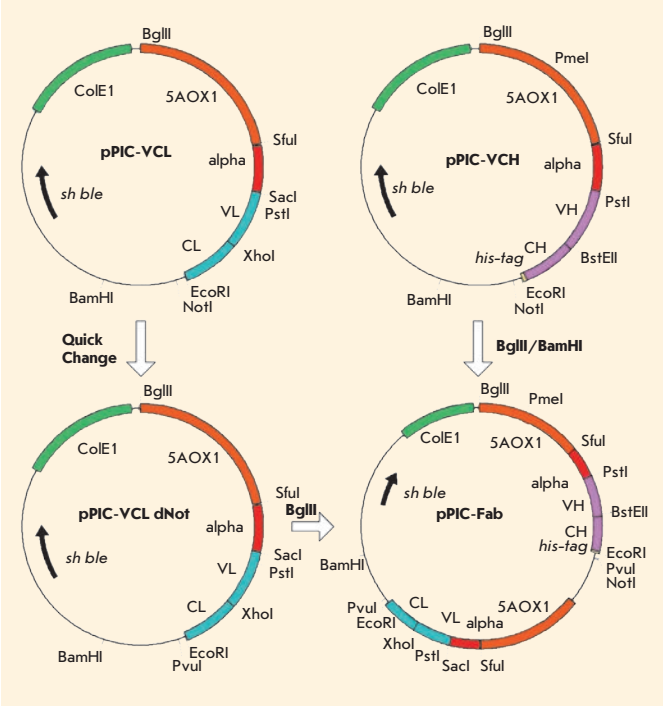

IMAGE ON THE COVER PAGE
Cloning scheme for construction of pPIC Fab plasmid. (O.V. Koliasnikov *et al.*)

High-Throughput Methods for Postgenomic Research

P.V. Sergiev
Belozersky Institute of Physico-Chemical Biology, Lomonosov Moscow State University
Department of Chemistry, Lomonosov Moscow State University
E-mail: petya@genebee.msu.ru

The rapid improvement in high-throughput genome sequencing has resulted in an avalanche-like accumulation of data on nucleotide sequences now stored in databases. Yet, our understanding of the function of genes, specifically the mechanisms underlying their expression and mutual influence, remains sketchy. High-throughput study of the expression, interactions and functional role of genes could be considred as the primary goal of postgenomic research. A methodological basis for postgenomic biology is being quickly developed in order to attain this goal.

Information on the development and functioning of living organisms, as well as data concerning the supposed response of these organisms to external stimuli, is encoded in their genome. Today, genome sequencing is an important stage in the study of any species. The genome size can vary from several hundred thousand nucleotides in some bacteria to several hundred billions in some eukaryotes. The number of genes increases along with the genome size, but only up to a certain level. Several high-throughput methods for genome sequencing have thus far been elaborated. Among these sequencing platforms are Roche/GS-FLX Titanium (500 million nucleotides per day), Illumina/HiSeq 2000 (55 billion nucleotides per day), and the ABI/SOLiD 5500xl (up to 30 billion nucleotides per day). Nowadays, the amount of nucleotide sequences continues to increase at a rapid rate. By early 2011, the major GenBank database contained as many as 126, 551, 501, 141 nucleotides. The sequencing procedure is getting cheaper, and in the foreseeable future the metagenome of the entire biosphere could well be determined.

With the advance in high-throughput methods for sequencing, new data on nucleotide sequences was obtained much faster than our undersanding of individual genes functions. In 2000, Peer Bork articulated the following problem: the function of approximately 30% of genes in each new genome as yet remains unknown. Furthermore, the validity of predicting the function of the other 70% of genes is also approximately 70%. In other words, today we are at the same point as geographers were in the epoch of great geographical discoveries. The general outline has already been made clear, but much remains to be done in order to understand the integral worldview. When studying a living organism, we are to determine the type and extent of mutual influence of all the genes whose products have an effect on each other.

To study a gene means to answer several questions (*Fig. 1*). First, it is necessary to know what happens to a cell or an organism if a gene is inactivated or temporarily "switched off." This also relates to the question of whether the mutations in the genome regions that are distant from the given gene reduce or increase the effects of the inactivation of this gene. All genes function under different conditions. Some genes are required all the time, while others are required only under certain circumstances. Studying the conditions in which a gene functions, i.e., when demand for the functioning of this gene emerges, provides a significant amount of information that helps to understand the question of the gene's role. Since gene functioning comprises several stages, our task is to study them all. Secondly, it is necessary to determine when a gene is transcribed; thirdly, we must find out when it is translated. Fourthly, one needs to know what molecules (proteins, RNA, DNA, small molecules) it interacts with. If a gene encodes an enzyme, one needs to know the reactions it catalyzes. If it is not an enzyme encoded by a gene, one needs to know the processes in which it participates. Efficient elaboration of post-genomic technologies is impossible without a procedural basis enabling the study of the functional interactions of a number of genes and their products. Moreover, it is necessary to elaborate methods that would enable the study of both

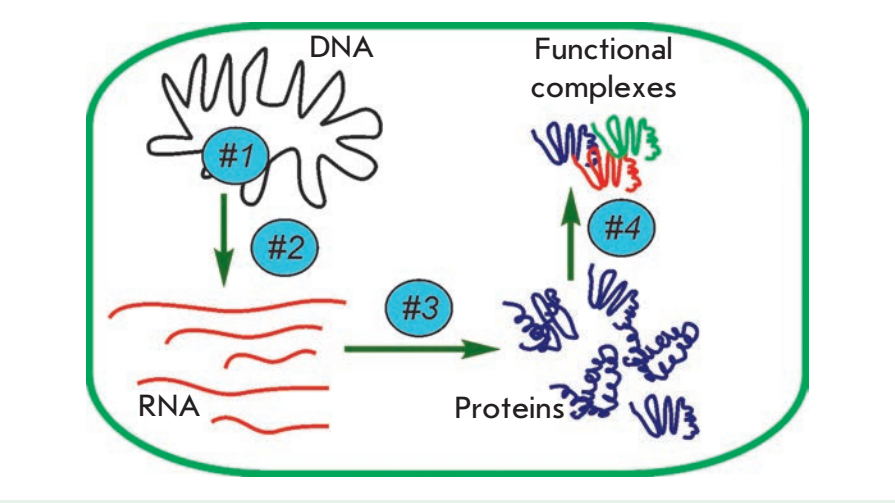

Fig. 1. Gene function scheme and questions needed to be addressed. DNA, RNA, proteins, and functional complexes are schematically shown and labelled. The gene expression pathway is shown by arrows. The questions to be answered are in blue circles: (#1) what is the phenotype of gene inactivation? (#2) How is a gene transcribed? (#3) How does mRNA correspond to a particular gene translated? (#4) What are the interaction partners of the gene expression product?

the expression of all genes under certain conditions, as well as those based on genetic manipulations with each gene from the full gene pool of an organism.

METHODS FOR STUDYING GENE EXPRESSION AT THE TRANSCRIPTION STAGE

As follows from the central dogma of molecular biology proposed by Francis Crick, gene expression involves two stages. Firstly, a gene is transcribed by RNA polymerase, yielding the proper RNA. Sometimes, it is RNA that is the functional product of a gene; in this case, gene expression is identical to RNA transcription and maturation. More frequently, the RNA copy of a gene is an mRNA and is translated by ribosomes, yielding a protein product. In order to "measure" gene expression, methods that allow to determine the amount of RNA or a protein are used. When performing post-genomic studies, it is necessary to measure the quantitative characteristics of the expression of a set of genes in the organism (ideally, all genes).

Microchip hybridization is currently the standard method for measuring the amount of all types of RNA in cells (*Fig. 2A*). The total RNA is extracted from the cells and cDNA is constructed by reverse transcription, in order to determine the gene expression level using microchips. This cDNA is modified by fluorescent dyes. Two cDNA samples stained with Cy3 and Cy5 dyes are typically compared. The mixture of cDNAs stained with different dyes is hybridized on a microchip with immobilized oligonucleotides that are complementary to the individual types of cDNA. The ratio between the fluorescence intensities of Cy3 and Cy5 in a certain spot on the microchip corresponding to a certain gene is a measure of the relative expression of this gene in the samples. Specific oligonucleotide samples, numbering between several tens of thousands to over a million, are used in modern microchips; they include the known genes of almost any model organism with a multifold excess.

Microchip technology is being gradually replaced by high-throughput sequencing technology (*Fig. 2B*). The same technologies as those used for high-throughput determination of the nucleotide sequence of individual genomes can be used to determine the whole range of RNAs present in a cell. This experiment is used to determine a large number (up to several billions) of short sequences contained in the total RNA (transcriptome). A computer analysis can be applied to align these short sequences with the genome sequence and, thereby, determine which regions of the genome are transcribed. The number of short RNA fragments referring to this gene which are detected by high-throughput sequencing can serve as a measure of gene expression.

High-throughput RNA sequencing has considerable advantages over the microchip technology, since no requirements to the preliminary annotation of this genome region as a gene are set. Thus, many earlier unknown transcripts are detected. Moreover, high-throughput RNA sequencing also permits the unbiased (i.e., not based on earlier known hypotheses) determination of the beginning and end of the transcript, as well as the variants formed by alternative processing. The results of studies of the transcriptome obtained using both microchips and high-throughput RNA sequencing are typically verified using quantitative PCR of cDNA (RT qPCR) in the case of particularly interesting genes (*Fig. 2B*). This method is based on the amplification of one cDNA fragment (amplicon) involving the quantitative determination of the resulting product, depending on the PCR cycle. With this purpose in mind, the fluorescence intensity of either a DNA-intercalating dye or a dye bound to a specially selected DNA probe is measured. In terms of its reliability, the RT qPCR method is superior to the microchip hybridization method and, to a certain ex-

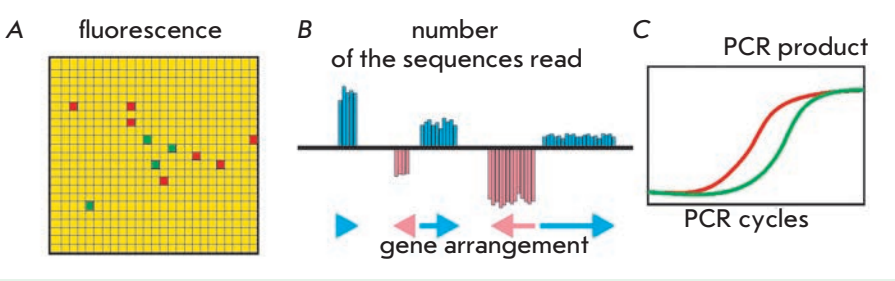

Fig. 2. High-throughput methods for studying gene transcription. *A* – Scheme of evaluation of the transcription levels by microchip hybridization. Reverse transcription is used to introduce the fluorescent label. Cy3- and Cy5-labelled cDNA derived from the samples to be compared fluoresce green and red. The rectangular grid is a microchip with immobilized oligonucleotide probes. Yellow areas correspond to the regions with equal gene expression in the compared samples, while green and red areas are those where cDNA labelled with Cy5 or Cy3, respectively, is predominant. *B* – Scheme of high-throughput transcriptome sequencing. The result of such an analysis is a plot of RNA reads of the distribution over the genome sequence. The frequency of the reads that belong to a particular transcript shown as blue and pink bars is used as a quantitative measure of the expression. *C* – Scheme of gene expression study by the quantitative polymerase chain reaction of cDNA (RT qPCR). Accumulation of two amplicons corresponding to two genes with passage of the PCR cycles is schematically shown in the plot. The earlier emergence of the PCR product attests to abundant mRNA in the transcriptome.

tent, even to high-throughput RNA sequencing. The major drawback of RT qPCR is that only one transcript can be measured in an experiment. There are several ways to overcome this disadvantage. Firstly, the use of 96- and 384-well PCR plates and proper instruments allows for the simultaneous detection of many transcripts. With modern instruments, such as the 7900HT (Applied Biosystems) or the CFX384 (Bio-Rad), the level of fluorescence intensity is measured simultaneously at four or five wavelengths. Moreover, the capability of automatic plate loading from a stack increases the maximum performance of the instrument to 20, 000 samples per run. This performance is sufficient to study the expression of all genes of bacteria and even primitive eukaryotes. Automated stations, such as the station based on Janus Extended (Perkin Elmer) mounted at the Centre for Collective Use (Moscow State University), are used to pipette this amount of PCR.

METHODS FOR STUDYING GENE EXPRESSION AT THE TRANSLATION STAGE

The expression of the genes encoding proteins involves two stages, according to the central dogma of molecular biology. mRNA formed as a result of gene transcription has to be read (translated) by a ribosome. Protein is synthesized by the ribosome according to the information encoded in mRNA. Although gene expression is regulated mostly at the transcription stage, mRNA translation can also be regulated. A number of fascinating mechanisms which regulate the translation of individual mRNAs remains to be understood. For a systemic comprehension of the mechanisms of regulation of gene expression, one should determine the relative protein amount in a cell, in addition to measuring the levels of RNA. Proteomics deals with measuring the amount of protein. This field of science is undoubtedly part of post-genomic technologies and has its own tools.

Two-dimensional protein gel electrophoresis remains the standard method for studying the combination of proteins in a cell (*Fig. 3A*). Protean (Bio-Rad) is the most commonly used system of two-dimensional gel electrophoresis. Similar to the study of the transcriptome using microchips, the comparison of two samples modified with different fluorescent dyes is most informative. Cy3 and Cy5 are typically used; they are bound to the proteins by the reaction between the hydroxysuccinimide esters of the dyes and the lysine residues in protein molecules. Protein samples modified with Cy3 and Cy5 are mixed and separated according to the isoelectric point value. The proteins which had become neutral at various pH values could be separated in this manner. The proteins are then separated according to their molecular weight using gel electrophoresis in the presence of an anionic detergent, sodium dodecyl sulfate. After protein separation, the gel is scanned on a fluorescence scanner. The relative amount of a certain protein in the initial samples can be assessed from the Cy3/Cy5 fluorescence ratio. The resolving power of each method of separation is believed to be approximately 100 protein bands. Thus, the number of protein types that can be distinguished in theory is 10, 000. Unfortunately, such a resolving power cannot be achieved in practice, because of several reasons. Firstly, the distribution of proteins in a cell over the isoelectric point and weight is not ideal. The properties of most proteins are quite similar. Secondly, the abundance of protein species in a cell varies by several orders of magnitude. Abundant proteins can be detected easily using two-dimensional gel electrophoresis, whereas it is almost impossible to detect rare proteins using this procedure. Thus, two-dimensional gel electrophoresis can be considered reliable only for the determination

of the amount of several hundreds of the most common proteins.

Protein identification from the fluorescing spots of a two-dimensional gel is performed via mass spectroscopy. Accordingly, a protein is cleaved into fragments by a specific protease, such as trypsin. Then, MALDI mass spectrometry is used to analyze fragment weights. Such instruments as Ultraflex (Brucker) and AB SCIEX 5800 (AB Sciex) are the most commonly used in modern proteomic laboratories.

Liquid chromatography, coupled with electrospray ionization mass spectrometry, is an alternative and supplementary method to two-dimensional gel electrophoresis in separating the whole cell proteome (*Fig. 3B*). The use of such systems makes the analysis of the whole proteome possible; however, the main difficulty consists in the extreme variety of the proteolytic fragments resulting from the hydrolysis of the entire pool of cell proteins. In the absence of protein modification with fluorophores, which is used in the study of proteome using two-dimensional gel electrophoresis, specific methods that would allow to compare the protein amounts in two samples using mass spectrometry only are required. Isotope labelling with iTRAQ is such a method. When using this method, protein samples are modified with chemically identical appendages consisting of two fragments. They can be split easily into special mass spectrometers that possess a fragmentation mode. Prior to fragmentation, the total weights of the appendages used to label two samples are equal. Thus, two identical peptides with chemically identical appendages that have equal weights originating from two protein samples are simultaneously analyzed in the mass spectrometer. The differences in weight appear only after the appendages are split into two fragments. Fragment weights differ, since they have a different isotopic composition. The ratio between the number of fragments with different weights will be the same as the protein ratio in the initial mixture.

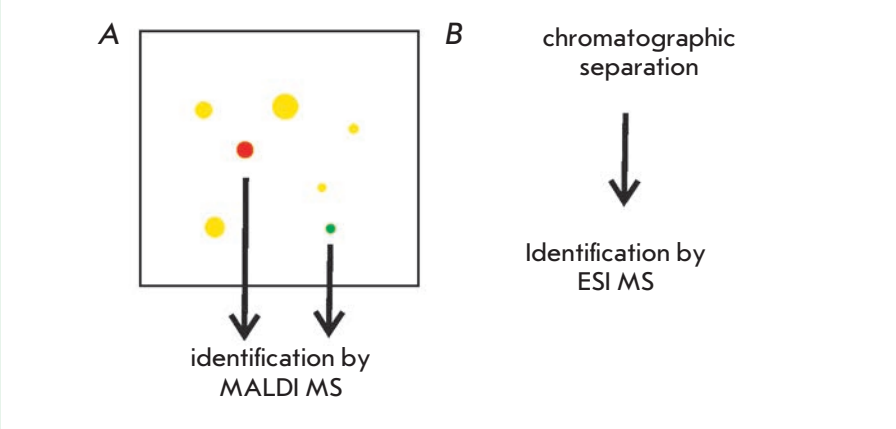

Fig. 3. Methods for studying proteome. *A* – Scheme of a quantitative comparison of proteomes in two samples by 2D gel electrophoresis. The protein samples to be compared are separately labelled with succinimide esters of the fluorescent dyes Cy3 and Cy5. After labelling, the protein samples are mixed and subjected to separation on a 2D gel. Yellow spots correspond to proteins with equal abundance in both samples, while green and red spots correspond to the proteins with different amounts. Protein identification in excised spots is accomplished via protease hydrolysis followed by peptide fingerprinting by mass spectrometry. *B* – Scheme of quantitative proteome analysis by chromatography. The total protein sample is treated with protease; the resulting peptides are separated by liquid chromatography. Peptide identification is usually performed by mass spectrometry with electrospray sample ionization.

METHODS FOR STUDYING GENE EXPRESSION USING REPORTER CONSTRUCTS

Applying the modern methods of proteomic analysis permits one to compare the amount of most cell proteins in different samples. Nevertheless, the stage at which the expression changed (transcription or translation) cannot be determined by proteomic analysis. Reporter constructs are used to study each individual expression stage, as well as the gene elements that are important for a certain mechanism of expression regulation. When using this method, the gene under study is replaced by the gene encoding the protein, whose amount in the cell can be measured easily. The genes of b-galactosidase, luciferases of different origins, and fluorescent proteins are widely used as reporter constructs. The individual elements of the gene subjected to a study that are responsible for transcription (promoter) and translation (usually, the 5'-untranslated region) can be used for the creation of a reporter construct. The amount of the reporter protein in a cell is assessed by measuring the amount of the products of the model enzyme reaction or fluorescence intensity in the case of fluorescent proteins. A similar reporter gene, whose expression is independent of the regulatory elements of the gene under study, is used as an internal control. The major problem in the use of reporter constructs is the complexity of creating them and detecting expression for the set of genes studied. The reporter construct method is very informative for one or several genes, but it is quite labour-consuming when studying a set of genes (ideally, all genes in the organism). This drawback can be overcome by using

the automated methods for cloning reporter constructs and determining their expression products. The facilities of the automated station based on Janus Extended (Perkin Elmer) mounted at the Centre for Collective Use (Moscow State University) is used in our laboratory. The automated station allows one to perform cloning, bacterial transformation, and to detect the expression of the reporter genes in automatic high-throughput mode. The genes of the red fluorescent protein from *Entacmaea quadricolor* and a cyan-modified variant of the protein from *Aequorea macrodactyla* are used as reporter genes (*Fig. 4*). As opposed to b-galactosidase and luciferases from *Photinus pyralis* and *Renilla reniformis*, the amounts of fluorescent proteins can be measured without damaging the cell or using enzymatic reactions. These advantages make the analysis of the expression of a set of reporter constructs in a single experiment considerably simpler and less expensive.

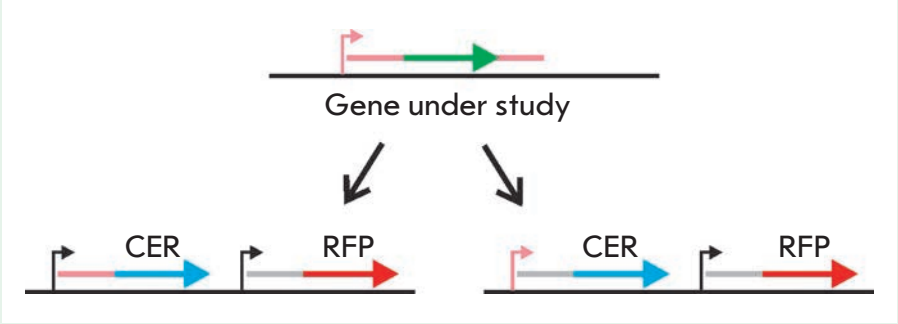

Fig. 4. Scheme for studying gene expression at the transcription and translation stages using reporter constructs. The gene under study is shown in green. The promoter and untranslated regions are shown in pink. The red fluorescent protein gene is shown in red, while the cyan fluorescent protein gene is shown in blue. The promoter (right) or 5′-untranslated region (left) under study is inserted in front of the cyan fluorescent protein gene. Expression of the red fluorescent protein is used as an internal standard.

METHODS FOR STUDYING THE GENE FUNCTION

Studying the gene function does not encompass their expression. For comprehension of the functional role of gene products, one has to ascertain what the gene product interacts with and what the consequences of the absence of a gene for a cell are. The cell components that interact with the product of a gene under study are typically detected by affinity co-purification with the gene product (protein or RNA). The cell components that are extracted, together with the protein under study or RNA, are fractionated and identified. Either the antibody to the protein under study or standard affinity tags attached to a protein by gene modification for this protein is used for affinity extraction. This procedure is easy to implement in the case of one or several proteins, but it becomes extremely labour-consuming when studying a set of proteins. At the time of writing, it is impossible to produce antibodies to each cell protein, as opposed to high-throughput-changing genes in the genome. Technologies of the same level are to be used to study the phenotype of cells lacking one of the proteins. If gene inactivation is not lethal, a strain or cell line lacking this gene is to be produced (i.e., gene knockout is to be performed). If gene inactivation results in non-viability, an artificially regulated promoter is to be incorporated in front of the gene (i.e., gene knockdown is to be performed). In order to increase the scale of these studies, methods of genome manipulations must be automated for the entire set of genes. Currently, such opportunities exist only for bacteria and yeast. Vast collections of strains of bacteria *Escherichia coli* and yeast *Saccharomyces cerevisiae* with inactivation of one of the genes have already been created. There are also partial collections of strains of these organisms in which one of the genes contains a fragment encoding the affinity tag. These collections have already made it possible to carry out a partial experimental analysis of the phenotypes of gene inactivation and study the partial cellular interactome; i.e., to perform cataloguing of the contacts between cell components.

Today, high-throughput analysis of the functional role of genes is in its early days of development. Even for the model bacterium *E. coli*, the phenotypes of the entire set of knockout strains have been analyzed only according to the rate of colony formation under various growth conditions. No overall collection of strains in which the genes important for viability are controlled by the regulated promoters has been created as of yet. Studies on the introduction of the tetracycline-activated promoter in front of *E. coli* genes that are essential for viability have been launched at the automated station based on Janus Extended (Perkin Elmer) mounted at the Centre for Collective Use (Lomonosov Moscow State University).

Combination of high-throughput methods for genome manipulations, such as creating strains containing gene “knockouts” and “knockdowns,” with methods of high-throughput analysis of gene expression could hold great promise. Such combination could allow one to uncover the effect that the activity of a gene has on another gene. Filling such a “matrix of mutual effects” will allow one to completely ascer-

tain all the regulatory pathways of a cell. The major difficulty in solving this problem is rooted in the fact that it is necessary to perform an extremely large number of experimental studies, which increases in proportion to the square number of genes. Hence, determination of the "matrix of mutual effects" for all *E. coli* genes will require 17 million experiments. It is clear that this is the maximum number, which can be reduced by restricting the screening at the expense of experiments. Systemic investigation of the influence the genes have on one another will require that the experiments be completely automated and considerably cheap to perform. Thus, the use of reporter constructs based on fluorescent proteins only, a method which was started in our laboratory, seems feasible in analyzing gene expression. This method requires significant investments to be made at the stage of creating reporter constructs; however, in future it will make possible the performance of measurements based only on fluorescence, without the use of any enzymatic reactions.

The systemic analysis of all of the stages of gene expression, the mutual effect of gene expression, functional role of gene products, and interactions between gene products is the most significant challenge in post-genomic biology. The constructed "matrix of mutual effects" will allow one to understand the functioning of the entire network of regulatory interactions inside a cell, and it has the potential of allowing control of any intracellular process. ●

The author is grateful to O.A. Dontsova for valuable comments and contribution to the manuscript.

REFERENCES

1. Watson J.D. // Genome Res. 2001. V. 11. № 11. P. 1803–1804.
2. Lewin B. Genes VIII. Upper Saddle River, N.J.: Pearson Prentice Hall. 2004. 1027 p.
3. Benson D.A., Karsch-Mizrachi I., Lipman D., Ostell J., Sayers E.W. // Nucl. Acids Res. 2011. V. 39 (Database issue). P. D32–37.
4. Kennedy J., Flemer B., Jackson S.A., Lejon D.P., Morrissey J. P., O'Gara F., Dobson A.D. // Mar. Drugs. 2010. V. 8. № 3. P. 608–628.
5. Bork P. // Genome Res. 2000. V. 10. № 4. P. 398-400.
6. Crick F.H. // Symp. Soc. Exp. Biol. 1958. V. 12. P. 138–163.
7. Ramsay G. // Nat. Biotechnol. 1998. V. 16. № 1. P. 40–44.
8. Hoen P.A., Ariyurek Y., Thygesen H.H., Vreugdenhil E., Vossen R.H., de Menezes R.X., Boer J.M., van Ommen G.J., den Dunnen J.T. // Nucl. Acids Res. 2008. V. 36. № 21. P. e141.
9. VanGuilder H.D., Vrana K.E., Freeman W.M. // Biotechniques. 2008. V. 44. № 5. P. 619–626.
10. Mathews M., Sonenberg N., Hershey J.W.B. Translational control in biology and medicine. 3rd ed. Cold Spring Harbor monograph ser. Cold Spring Harbor, N.Y.; Cold Spring Harbor Laboratory Press, 2007. 934 p.
11. Sonenberg N., Hershey J.W.B., Mathews M. Translational control of gene expression. 2nd ed. Cold Spring Harbor monograph ser. Cold Spring Harbor, N.Y.; Cold Spring Harbor Laboratory Press, 2000. 1020 p.
12. Shevchenko A., Wilm M., Vorm O., Mann M. // Anal. Chem. 1996. V. 68. № 5. P. 850–858.
13. Chakravarti B., Gallagher S.R., Chakravarti D.N. // Curr. Protoc. Mol. Biol. 2005. Chapter 10. P. Unit 10 23.
14. Link A.J. Methods in molecular biology. Totowa, N.J.: Humana Press, 1999. V. xvii, 601 p.
15. Brewis I.A., Brennan P. // Adv. Protein Chem. Struct. Biol. 2010. V. 80. P. 1–44.
16. Chalkley R. // Methods Mol. Biol. 2010. V. 658. P. 47–60.
17. Treumann A., Thiede B. // Expert Rev. Proteomics. 2010. V. 7. № 5. P. 647–653.
18. Ghim C.M., Lee S.K., Takayama S., Mitchell R.J. // BMB Rep. 2010. V. 43. № 7. P. 451–460.
19. Merzlyak E.M., Goedhart J., Shcherbo D., Bulina M.E., Shcheglov A.S., Fradkov A.F., Gaintzeva A., Lukyanov K.A., Lukyanov S., Gadella T.W., Chudakov D.M. // Nat. Methods. 2007. V. 4. № 7. P. 555–557.
20. Rizzo M.A., Springer G.H., Granada B., Piston D.W. // Nat. Biotechnol. 2004. V. 22. № 4. P. 445–449.
21. Casadaban M.J., Chou J., Cohen S.N. // J. Bacteriol. 1980. V. 143. № 2. P. 971–980.
22. Nordeen S.K. // Biotechniques. 1988. V. 6. № 5. P. 454–458.
23. Baba T., Ara T., Hasegawa M., Takai Y., Okumura Y., Baba M., Datsenko K.A., Tomita M., Wanner B.L., Mori H. // Mol. Syst. Biol. 2006. V. 2. P. 2006–2008.
24. Chu A.M., Davis R.W. // Methods Mol. Biol. 2008. V. 416. P. 205–220.
25. Butland G., Peregrin-Alvarez J. M., Li J., Yang W., Yang X., Canadien V., Starostine A., Richards D., Beattie B., Krogan N., et al. // Nature. 2005. V. 433. № 7025. P. 531–537.
26. Hu P., Janga S.C., Babu M., Diaz-Mejia J.J., Butland G., Yang W., Pogoutse O., Guo X., Phanse S., Wong P., et al. // PLoS Biol. 2009. V. 7. № 4. P. e96.
27. Howson R., Huh W.K., Ghaemmaghami S., Falvo J.V., Bower K., Belle A., Dephoure N., Wykoff D.D., Weissman J.S., O'Shea E.K. // Comp. Funct. Genomics. 2005. V. 6. № 1–2. P. 2–16.
28. Nichols R.J., Sen S., Choo Y.J., Beltrao P., Zietek M., Chaba R., Lee S., Kazmierczak K.M., Lee K.J., Wong A., et al. // Cell. 2011. V. 144. № 1. P. 143–156.

EDITORIAL NOTE

The subject matter raised is of absolute urgency. Indeed, some of the most modern equipment, including the unique kind, has recently appeared in many research institutions. This makes it possible to considerably enhance research capabilities not only at these institutions, but at other centers as well, provided that access to information is adequately ensured. The editorial board is bound on honor to spread this information, and this topic will be discussed in the next issues of the journal *Acta Naturae*.

Clinical Use of Inhibitors of HIV-1 Integration: Problems and Prospects

S. P. Korolev[1]*, Yu. Yu. Agapkina[1], M.B. Gottikh[1,2]
[1] Department of Chemistry, Lomonosov Moscow State University
[2] Belozersky Research Institute of Physico-Chemical Biology, Lomonosov Moscow State University
*E-mail: spkorolev@mail.ru
Received 04.04.2011

ABSTRACT **The HIV-1 integrase enzyme is responsible for one of the key stages of retroviral replication; it acts as a catalyst for the integration of viral cDNA into the cell's genome. Inhibitors of HIV-1 integration have been under development for over 10 years; yet, only one integration inhibitor, raltegravir, has been approved for clinical use so far. Raltegravir binds two metal ions in the enzyme's active centre and blocks one of the integration stages: the strand transfer. Unfortunately, the clinical use of raltegravir results in the development of viral resistance among some patients. Several more HIV-1 integration inhibitors are undergoing clinical trials at the moment. However, the structure and mechanism of action of those are similar to raltegravir, which results in the emergence of cross resistance with raltegravir. The present review is focused on the history of the development and clinical trials of raltegravir and its analogues, the problems connected with the emergence of viral resistance to integration inhibitors, and the prospect of their future clinical use.**

KEYWORDS **HIV-1 integrase; inhibition; mechanism of action; raltegravir.**

ABBREVIATIONS **HAART – highly active antiretroviral therapy; HIV-1 – human immunodeficiency virus type 1; IN – integrase; ST – strand transfer; AIDS – acquired immunodeficiency syndrome; AUC – area under the pharmacokinetic curve (concentration–time curve) – the change in concentration of the active component in blood plasma or serum over time; CIC_{50} – the inhibitor concentration at which the cytopathogenic effect of the virus in the infected cells decreases by 50%; CIC_{95} – the inhibitor concentration at which the cytopathogenic effect of the virus in the infected cells decreases by 95%; Cl_p – clearance, or the extraction ratio – the index showing the rate of extraction of a substance from blood plasma during the biotransformation of this substance, its redistribution in the organism, and excretion; C_{max} – the maximum or peak of concentration of an active component in blood; EC_{50} – inhibitor concentration, at which *in vivo* replication of the virus is suppressed by 50%; EC_{90} – inhibitor concentration, at which *in vivo* replication of the virus is suppressed by 90%; F – bioavailability – the fraction of a dose of unchanged drug administered orally that reaches the systemic circulation; FBS – fetal bovine serum; FDA – Federal Drug Administration (United States); IC_{50} – inhibitor concentration, at which the enzyme activity is suppressed by 50%; NHS – normal human serum; PPB – percentage plasma protein binding; $T_{1/2}$ – time by which the concentration of a drug in plasma decreases twice; WT – wild type.**

INTRODUCTION

The acquired immunodeficiency syndrome (AIDS) began as one of the most dramatic epidemics of the late 20th – early 21st centuries. AIDS is caused by the human immunodeficiency virus (HIV) afflicting the immune system of the organism. Ukraine and Russia have some of the highest rates of the spread of the HIV infection in the world. HIV prevalence among the adult population in Russia is over 1.1% [1], according to some estimates. This is precisely why the development of effective therapeutic drugs to control the spread of the virus is particularly urgent for Russia.

HIV afflicts primarily the cells of the immune system: the CD4$^+$ T-lymphocytes, macrophages, and dendritic cells. The stock of CD4$^+$ cells is gradually depleted, resulting in the subsiding of cell immunity. When a critical lymphocyte level is achieved, the organism becomes easy prey for opportunistic infections [2]. The following stages of the HIV-infection can be distinguished in the absence of antiretroviral therapy: the primary infection – acute HIV syndrome that ends with the extinction of clinical symptoms and seroconversion; the latent stage (symptom-free chronic HIV infection); symptomatic HIV infection (AIDS), which is often accompanied by the development of opportunistic infections; and the terminal stage (death) [2].

The replication cycle of HIV-1 can be tentatively divided into two phases: the early phase and the late phase (*Fig. 1*) [2, 3]. At the early stage of the life cycle, viral particles specifically bind onto the CD4 surface

protein thanks to the specific interaction between the viral coat glycoprotein gp120 and the N-terminal domain of the immunoglobulin of the CD4 protein. The binding onto the CD4 receptor allows gp120 to bind to the coreceptors (CCR5 or CXCR4) on the surface of a target cell, as well. After the binding of g120 to coreceptors, glycoprotein gp41 is incorporated into the cell membrane, resulting in the fusion of the viral coat and the cell membrane yielding a pore, through which the viral core penetrates into the cell cytoplasm [2]. After the fusion, the virus sheds its coat, and the process of reverse transcription begins. The reverse transcription of genomic RNA is carried out via the viral enzyme; reverse transcriptase, in cytoplasm. The product of reverse transcription, double-stranded cDNA, is transported into the nucleus within the pre-integration complex, which comprises a number of viral proteins, such as integrase (IN), the matrix protein (MA), reverse transcriptase, the nucleocapsid protein (NC), and the regulatory protein Vpr (Viral Protein R) [4, 5], as well as the cell proteins Ku [6], HMG I(Y) [7], BAF [8], and LEDGF/p75 [9]. The nuclear localization of IN, MA, Vpr [5], and LEDGF/p75 [9] is ensured by nuclear localization signals. After it is transported into the nucleus, a DNA copy is integrated, i.e., covalently incorporated into the genome of the host cell due to the catalytic activity of IN [3]. The late phase of the replication cycle of HIV-1 begins with the regulated expression of the proviral genome; then, processing of the synthesized viral proteins with viral protease occurs, followed by the assembly of new virions, which are released from the cell and infect new target cells, ultimately terminating the life cycle of the virus [2, 3].

Highly active antiretroviral therapy (HAART), which at the time of writing comprises 25 drugs, is used in the treatment of HIV infection [10]. These drugs mostly include nucleoside and non-nucleoside inhibitors of reverse transcriptase of HIV-1 and protease inhibitors. Moreover, entry inhibitors have recently been designed: maraviroc, which blocks the interaction between gp120 and CCR5, and enfuvirtide, which interacts with gp41 glycoprotein (*Fig. 1*). At the end of 2007, the U.S. Food and Drug Administration (FDA) approved the first integration inhibitor, Isentress™ drug, also known as raltegravir (MK-0518), an anti-AIDS agent [11].

The stage at which the viral DNA is integrated into cell DNA is one of the key stages in the replication cycle of HIV-1; therefore, IN catalyzing is considered to be one of the most attractive targets for HIV-1 inhibitors. It has been demonstrated that a virus containing a defective IN, which is incapable of catalyzing the integration of viral DNA, cannot be reproduced in cell culture [12]. Moreover, IN does not have a cell equivalent; therefore, the inhibitors that specifically suppress its catalytic activity are supposed to have no effect on the cell processes and should be less toxic for the cell and the entire organism in comparison to the inhibitors of other stages of the HIV replication cycle. Over many years, the development of integration inhibitors has been pursued, with various drugs capable of blocking IN described in minute detail in numerous reviews [13–19]. The present review is devoted to state-of-the-art studies in the field of application of raltegravir and its analogues as HAART components.

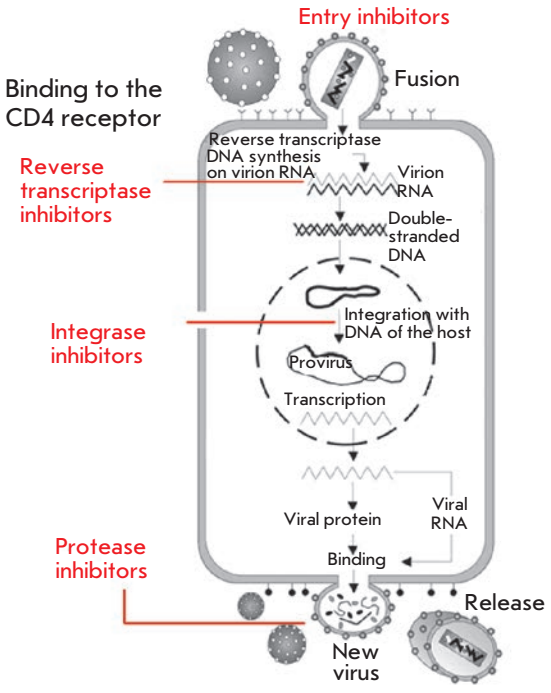

Fig. 1. HIV-1 replication cycle and HAART targets.

INTEGRASE STRUCTURE AND INTEGRATION MECHANISM

The integration process begins in cytoplasm and comprises several stages [20–22]. A DNA copy of the viral RNA contains long terminal repeats at both ends, which consist of three fragments: U3, R, and U5. At a distance of two nucleotides from the 3' terminus of each DNA strand, there is a conservative CA dinucleotide, which is found in the long terminal repeats of all retroviruses. Within the preintegration complex, IN recognizes the nucleotide sequences located at the termini of regions U3 and U5 of the viral cDNA, binds to them, and catalyzes the reaction of 3'-terminal processing. This reaction represents the endonuclease cleavage of the viral cDNA, resulting in the removal of the GT dinucleotide from the 3' terminus in each strand. Substrate cleavage is caused by the nucleophilic attack on the phosphate group between the second and third nucleotides by a water molecule [20–22].

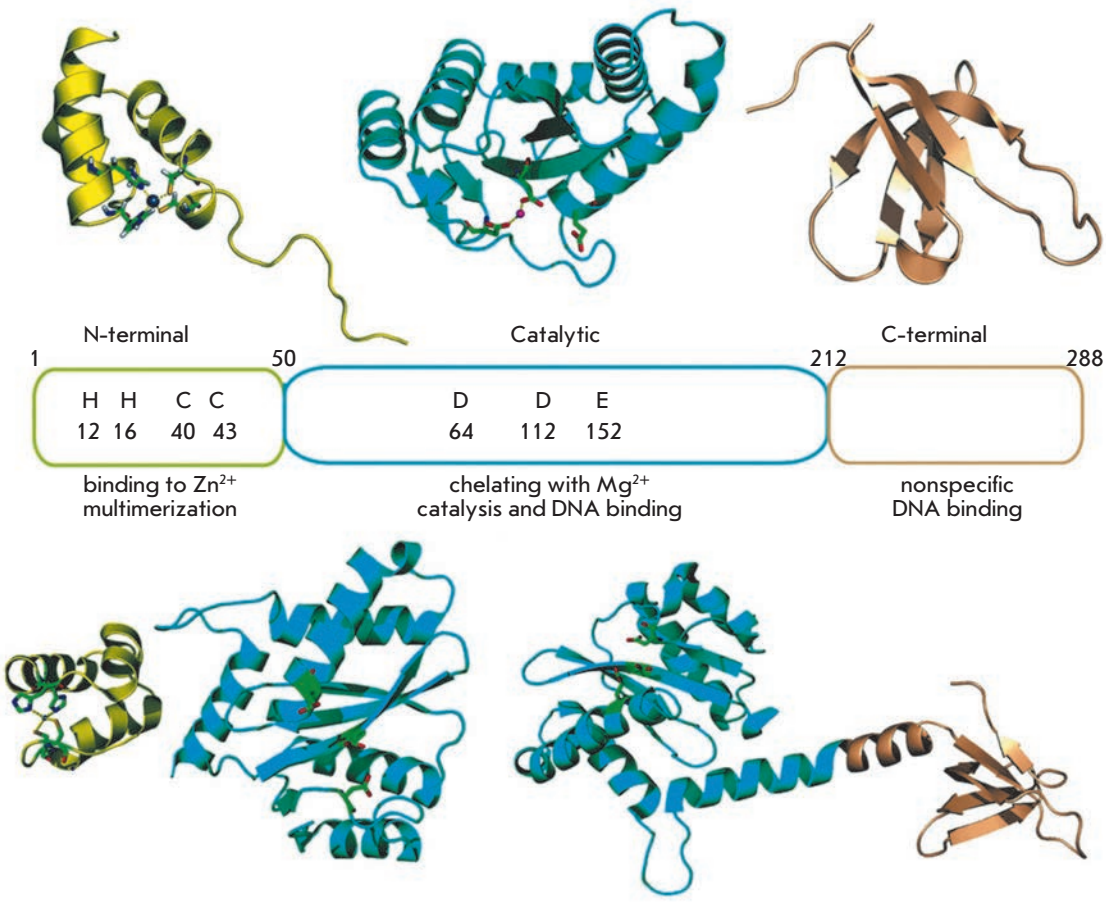

Fig. 2. Structural domains of HIV-1 integrase [14].

The pre-integration complex is then transported into the nucleus, where IN catalyzes the strand transfer (ST) stage. This stage is represented by the re-esterification reaction, which involves the nucleophilic attack on the internucleotide phosphates of both strands of cellular DNA (DNA targets) by 3'-hydroxylic groups of the processed strands of viral (substrate) DNA, yielding a covalent product. The internucleotide bonds located in different strands of the DNA target at a distance of 5 np from each other undergo re-esterification. The completion of integration requires the following processes: processing of the 5'-termini of viral DNA, polymerase addition of five lacking nucleotides, and ligation, which are performed with the participation of cell proteins [20].

In the integration process, IN is required to bind two termini of the viral DNA to the cell DNA. However, the data on the interaction between IN and DNA as yet remains quite limited. HIV-1 integrase is a protein consisting of 288 amino acid residues (32 kDa) encoded by the *pol* viral gene. IN is translated within the Gag-Pol polypeptide, which is subsequently cleaved into separate proteins by a viral protease [21]. It has been demonstrated by partial proteolysis and targeted mutagenesis that three domains can be isolated in the enzyme structure: the N-terminal domain, comprising the amino acid residues 1–50; the catalytic domain formed by residues 51–212; and the C-terminal formed by the amino acid residues 213–288 (*Fig. 2*) [20].

The N-terminal domain contains two histidine and two cysteine residues, which are conservative in retroviral integrases and retrotransportases [20]. These residues coordinate the zinc ion and participate in the formation of a catalytically active IN multimer, since it has been demonstrated that the coordination of Zn^{2+} ions stimulates IN multimerization and its activity [23]. The catalytic domain of IN contains the triad of invariant amino acid residues (D64, D116, and E152 in HIV-1) which form the active centre of retroviral integrases. The catalytic domain participates in the binding of the termini of viral DNA due to their interaction with conservative amino acid residues of the domain (primarily Q148, K156 and K159). For the integration to be possible, IN demands the presence of ions of cofactor metal ions (Mg^{2+} or Mn^{2+}), which are coordinated with two residues from the catalytic triad (D64 and D116) [21]. The least conservative C-terminal domain forms the Src homology 3-like fold; this structural motif is

involved in IN multimerization; however, it makes the greatest contribution to the formation and stabilization of DNA complexes that are either specific to the sequence or nonspecific. A non-typical double signal of nuclear localization located in the catalytic (^{186}KRK^{188}) and C-terminal (^{211}KELQKQITK^{219}) IN domains is recognized by the participants of the importine/caryopherine cellular path. This interaction is enough to involve the PIC into the cell nuclear transport system [24].

The structure of full-scale HIV-1 IN remain unknown; only the structure of separate domains and double-domain IN fragments has been determined (see [20]). These data, along with the results obtained using site-directed mutagenesis and cross-linking, have been used to design computer models of IN [25–27]. Regardless of the fact that these models often contradict each other, most researchers share the opinion that the tetrameric form of IN is the one that functions in the cell. This viewpoint was confirmed by Hare *et al.* [28], who were the first to succeed in crystallizing and decoding the structure of retroviral IN in a complex with DNA. The IN of the human foamy virus belonging to the retroviruses from the *Spumaviridae* subgroup, which was used with this purpose in mind, is active in tetrameric form. A tetramer consists of asymmetrical dimers, each of those interacts with one terminus of viral DNA and performs its integration into cellular DNA [28]. The comparative study of the catalytic characteristics of the IN of the human foamy virus and HIV-1 revealed a considerable similarity in the functioning of these two enzymes [29, 30].

Both the cellular and viral proteins that are components of the preintegration complex can affect the catalytic activity of IN. HIV-1 IN needs neither viral nor cellular cofactors for the incorporation of both ends of the viral DNA into the super-spiralized cellular DNA [31]. However, it has been demonstrated that such proteins as the NC viral protein and cellular proteins HMG I(Y) and LEDGF/p75 can enhance the integration efficiency [21, 32]. It has been known that cellular protein LEDGF/p75 immediately interacts with IN and stimulates consistent integration and IN strand transfer [33]. It is assumed that LEDGF/p75 can play the role of the chaperone with respect to IN, stabilizing its multimeric organization, and enhancing the IN affinity towards DNA [21].

DESIGNING HIV-1 INTEGRATION INHIBITORS SUPPRESSING THE STRAND TRANSFER REACTION

Since there has been no data available pertaining to the structure of HIV-1 IN, screening of libraries of chemical compounds of various classes has for a considerable period remained the primary method in the search for its inhibitors [4]. Testing of a library consisting of 250,000 compounds that ended by the year 2000 allowed specialists at Merck Pharmaceuticals (United States) to reveal a series of substances possessing the highest IN-inhibiting activity among them [34]. It appeared that all these substances are diketo compounds (DKC); notably, derivatives of 2,4-dioxobutanic acid. The inhibitors contained the so-called β-diketo acid motif, capable of coordinating cofactor metal ions in the IN active center [34]. These inhibitors manifested higher activity when inhibiting the strand transfer reaction than upon *in vitro* inhibition of the 3' processing. The most active compound, L-731.988 (*Fig. 3*), was more active by a factor of 70 with respect to the strand transfer reaction in comparison with the 3' processing reaction. Moreover, this inhibitor suppressed the development of HIV-1 in a cell culture (*Table 1*).

Table 1. Results of *in vitro* and cell studies of diketo acid L-731.988 and naphthyridine derivatives L-870.810 and L-870.812 as HIV-1 integration inhibitors

Integrase inhibitor	IC_{50}, in vitro (strand transfer), nM	CIC_{95} ex vivo
L-731.988	8–15 [34]	CIC_{50} = 1 μM [34]
L-870.810	8–15 [35]	15 nM (10% FBS) 100 nM (50% NHS) [36]
L-870.812	40 [36]	250 nM (50% NHS) [37]

The selection of virus strains stable towards the action of DKC was performed, followed by the determination of the mutation site. Replacement of the M154 (M154I) residue located in the immediate proximity of the E152 residue (a component of the catalytic triad of the enzyme) was found to exist in the IN of a strain resistant to the action of L-731.988 [34].

The interaction between L-731.988 and IN has been subsequently studied [38]. It has been demonstrated that the inhibitor, at concentrations up to micromolar ones, does not interact with the isolated enzyme. A DNA substrate, U5 or U3-terminal fragments of the viral DNA are required for its binding with the enzyme. The dissociation constant (K_d) of the integrase–L-731.988 complex determined in the presence of 100 nM of U5 substrate was equal to 75 nM, which correlated with the IC_{50} value in the strand transfer reaction. The affinity of L-731.988 upon interaction with IN bound to the processed viral DNA was higher by a factor of 100 in comparison with that upon the interaction with IN, in the absence of viral DNA (K_d = 10–20 μM). The random sequence DNA did not stimulate interaction between the inhibitor and the enzyme. Fur-

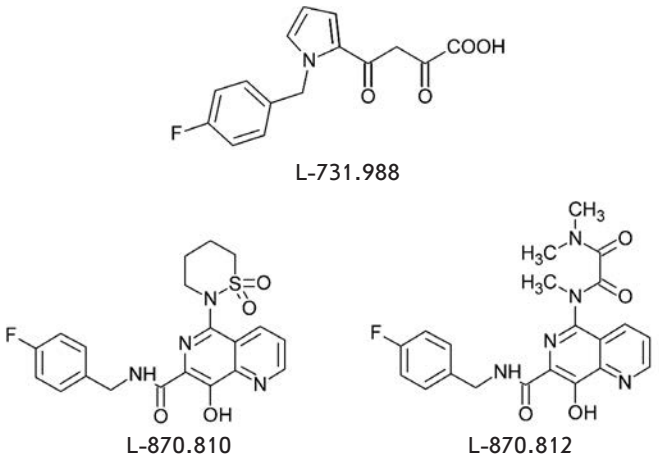

Fig. 3. Structure of HIV-1 integration inhibitors: L-731,988, L-870,810, and L-870,812.

thermore, an increase in the concentration of the DNA substrate, its excess amount being capable of acting as a DNA target, resulted in a decrease in inhibitor–IN binding. An assumption was made, based on these data, [38] that the L-731.988 inhibitor suppresses the strand transfer reaction by competing with a DNA target for its binding site; the conformation of the active enzyme–substrate complex is required for the interaction between the inhibitor and IN.

A number of other substances have a similar nature of inhibition of the IN activity; their common feature being the presence of two oxygen atoms capable of coordinating cofactor metal ions in the IN active center [39–42].

The search for DKS analogues demonstrating antiintegrase activity resulted in the design of\ naphthyridine derivatives by Merck Pharmaceuticals. The activity and selectivity of these compounds with respect to the strand transfer reaction was similar to that of DKC [43]. Among the inhibitors of this structural class, two inhibitors, L-870.810 and L-870.812, have been subjected to the most thorough study (*Fig. 2*, *Table 1*).

A naphthyridine derivative L-870.810 displaced diketo acid L-731.988 from the IN/DNA-substrate complex, which enabled one to assume the possibility of binding of these compounds to IN at a single or overlapping site [36]. The accumulation of circular viral DNA in the treated L-870.810 cells and a decrease in the amount of integrated viral DNA served as evidence of the action of this inhibitor on the integration process. The selection of virus strains that could be resistant towards the action of L-870.810 resulted in the following substitutions in the primary structure of IN: F121Y/T125K, V72I/F121Y/T125K, and V72I/F121Y/T125K/V151I [36]. The viruses carrying the corresponding mutations were less sensitive to the action of L-870.810 by a factor of 4–100 in comparison with wild-type HIV-1 [36]. Mutations in the IN gene causing viral resistance to diketo acids and naphthyridines are closely located, but not identical. All these facts attest to the possibility of the existence of both a common binding centre and a common mechanism of action in inhibitors belonging to both classes.

Inhibitor L-870.810 successfully passed the first phase of clinical trials; however, at the second phase it proved toxic to kidneys and the liver. For this reason, the trials were ended.

RALTEGRAVIR (MK-0518) – THE FIRST INHIBITOR OF HIV-1 INTEGRATION ALLOWED FOR USE

Designing raltegravir

The relative success achieved from the use of naphthyridine derivatives as IN inhibitors led to the design of inhibitors based on dihydroxypyrimidine (compound (**1**), *Fig. 4*) [45]. This compound specifically suppresses the strand transfer carried out by recombinant IN (*Table 2*); however, even micromolar concentrations of this compound are inactive in the culture of infected cells. Nevertheless, due to its pharmacokinetic indices determined in rats (good bioavailability (F = 39%) and the low clearance of blood plasma (Cl_p = 11 mg/min/kg)), this compound was selected for further structural and functional studies [45], enabling the design of this compound **(2)** *(Fig. 4)* [46]. The compound successfully inhibits the strand transfer reaction (*Table 2*) and suppresses the cytopic effect of HIV-1 in infected cells [46].

Parallel studies resulted in the design of a novel class of IN inhibitors, N-alkyl pyrimidinone derivatives, which inhibited the nanomolar concentrations of IN in *in vitro* experiments [36]. The results of the study of the inhibiting effect of compound **(3)** *(Fig. 4)*, belonging to this class, are listed in *Table 2* [47]. Moreover, compounds (**2**) and (**3**) were characterized by a strong pharmacokinetic profile and strong bioavailability in preclinical trials performed on rats, dogs, and rhesus macaques [46, 47].

An attempt was then made to combine the optimal properties of inhibitors from each of the two series in one molecule [48]. This approach resulted in the design of another N-methyl pyrimidinone derivative (compound (**4**), *Fig. 4*). However, compound (**4**) turned out to be less active (*Table 2*).

The structural and functional studies of N-methyl pyrimidinone derivatives as IN inhibitors were continued [48]. Compound MK-0518 (*Table 2*), which was given the name 'Raltegravir' (*Fig. 4*), appeared to be the

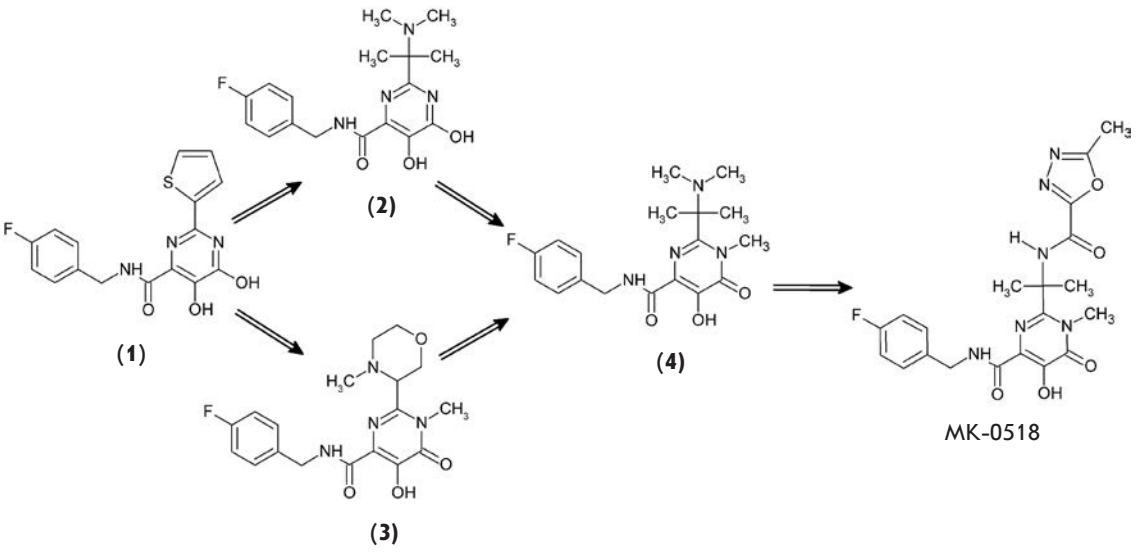

Fig. 4. Optimization of dihydroxypyrimidine (**1**, **2**) and *N*-methyl pyrimidinone carboxamides (**3**, **4**) as HIV-1 integrase strand transfer inhibitors, which led to the design of raltegravir (inhibitor MK-0518).

most active. It turned out that raltegravir has a high selectivity with respect to IN and has almost no inhibiting effect (IC_{50} > 50 μM) on such Mg^{2+}-depending enzymes as HIV-1 reverse transcriptase, HIV-1 RNAse H, hepatitis C virus RNA polymerase, and human polymerases α, β, and γ [48]. No effect of raltegravir (at concentrations of up to 10 μM) on another 150 different enzymes, receptors, and channels has been revealed. In particular, raltegravir has no effect on various cytochrome P450 isoforms (IC_{50} > 50 μM) and does not bind to the hERG ion channel [48].

Pharmacokinetics and interaction with HAART components

The pharmacokinetic profile of raltegravir has been studied on rats, dogs, and rhesus macaques [48]. The rats were given raltegravir in three different forms (OH form, as well as Na^+ and K^+ salts) at a dose of 3 mg/kg. The best results were achieved when using raltegravir salts. The amount of the compound that entered the blood upon one-time administration (AUC) was the highest for Na^+ salt; the maximum peak of compound concentration in blood (C_{max}) was attained in K^+ salt. In this case, values AUC and C_{max} were also better in the salt form of the preparation (*Table 3*). The dogs were given raltegravir in the form of the OH form or K^+ salt at a dose of 10 mg/kg. In this case, AUC and C_{max} values were also better for the salt form of the drug (*Table 3*). The crystalline OH form at a dose of 10 mg/kg was also administered to rhesus macaques, but the AUC and C_{max} indices were quite low (*Table 3*). The bioavailability of the drug administered orally (*F*) also appeared to be better for the K^+ salt in comparison with that for the OH form (*Table 3*). Hence, the pharmacokinetic profile of raltegravir in the form of Na^+ and K^+ salts was found to be preferable to that of the OH form; salt forms being characterized by improved solubility [48].

Blood plasma clearance was appreciably low in dogs and was characterized by medium values in rats and rhesus macaques (*Table 3*). Furthermore, raltegravir binding to the blood plasma proteins (PPB) of rats, dogs, and rhesus macaques has been the subject of a study (*Table 3*) [48], as well as its metabolism in the liver microsomes of these animals and humans. It appeared that the drug is metabolized by glucuronosyltransferase [48]. The same conclusion was made after studying the metabolism in hepatocytes [48] and was borne out by the results of an independent study [49]. ^1H- and ^{13}C-NMR spectroscopy was used to completely characterize the formation of a conjugate between glu-

Table 2. Results of *in vitro* and cell studies of derivatives of dihydroxypyrimidine and N-methylpyrimidinone and raltegravir (MK-0518) as HIV-1 integration inhibitors

Compound	IC_{50}, in vitro (strand transfer), nM	CIC_{95} ex vivo	Reference
(1)	10	inactive	[45]
(2)	50	60 nM (10% FBS) 78 nM (50% NHS)	[46]
(3)	60	60 nM (10% FBS) 100 nM (50% NHS)	[47]
(4)	250	1 μM (10% FBS) > 1 μM (50% NHS)	[48]
MK-0518	15	19 nM (10% FBS) 31 nM (50% NHS)	[48]

Table 3. Pharmacokinetic parameters of raltegravir determined for rats/dogs/rhesus macaques [48]

Form	AUC, μM·h	C_{max}, μM	$T_{1/2}$, h	*F*, %	Cl_p, ml/min/kg	PPB, %
OH	1.0/21/1.8	1.2/8/0.3	ND*/ND/7	37/45/8	39/6/18	74/71/85
Na^+	1.4/ND/ND	1.0/ND/ND	ND/ND/ND	ND/ND/ND	ND	ND
K^+	1.3/45/ND	1.6/24/ND	73/13/ND	45/69/ND	ND	ND

* ND – no data available.

curonide and a hydroxylic group at position 5 of the pyrimidinone ring of raltegravir [48].

The comparison of *in vivo* and *in vitro* data allowed one to suppose [48] that the pharmacokinetic profile of raltegravir for humans will be similar to the drug profile for a dog.

To achieve a therapeutic effect, it is necessary that the drug concentration 12 h after the administration (C_{12}) remain above CIC_{95} = 31 nM. With account for the data on raltegravir binding with blood plasma proteins, metabolic stability, half-excretion period, and clearance, peroral administration of raltegravir K^+ salt at a dose of at least 100 mg twice a day was proposed during the clinical trials.

The pharmacokinetic profile of raltegravir was determined both in healthy volunteers and HIV-infected patients. Two randomized placebo-controlled trials were carried out with healthy volunteers: 32 volunteers were given a single dose of raltegravir (10–1600 mg); and raltegravir was administered to 40 volunteers every 12 h for a duration of 10 days (100–800 mg) [50]. It was ascertained that raltegravir is characterized by a good assimilability; its content in blood plasma attaining the maximum level (C_{max}) as early as after 1 h. The half-excretion period of the drug ($T_{1/2}$) was equal to 7–12 h. The drug concentration in the blood becomes constant as early as 2 days after its administration; after the administration is stopped, only weak accumulation in the organism is observed [50]. Moreover, it should be noted that no considerable differences were revealed to administration of the drug in the male or female volunteers.

The pharmacokinetics of raltegravir was also studied among HIV-infected antiretroviral treatment-naïve patients [51]. It was ascertained that the AUC and C_{max} values increase in geometrical progression up to the administration of raltegravir, at a dose of 400 mg, twice a day. At a dose of 600 mg, these parameters do not increase [51]. Moreover, an approximately threefold decrease in the viral load in HIV-infected patients was observed, regardless of the dose of the administered drug [51]. Nevertheless, the latter results should be taken with great care due to the relatively small size of the sampling and short duration of the study.

The interaction of raltegravir with various components of HAART antiviral therapy in healthy volunteers has also been studied (see [52]). It appeared that the simultaneous administration of raltegravir and protease inhibitors – atazanavir and atazanavir/ritonavir mixture – increases raltegravir concentration in the blood to a certain extent, whereas ritonavir alone has almost no effect on the raltegravir concentration. The nucleotide inhibitor of reverse transcriptase, tenofir, also had a negligible effect on the raltegravir concentration. The administration of raltegravir, together with tipnavir (protease inhibitor), maraviroc (penetration inhibitor), efavirenz, and etravirine (both drugs are non-nucleoside inhibitors of reverse transcriptase), resulted in a decrease in the raltegravir concentration in healthy volunteers.

Only one study of raltegravir interaction with HAART components has been carried out on HIV-infected patients [53]. Four individuals were given raltegravir (400 mg) twice a day, together with etravirine (non-nucleoside inhibitor of reverse transcriptase); the raltegravir concentration in the blood decreased by a factor of 4. Regardless of these results, the authors provide no recommendations on changing the dose of raltegravir when administering it together with etravirine [53]. Thus, the necessity for further study of the interaction between raltegravir with HAART components in HIV-infected individuals becomes evident.

Clinical trials

Treatment upon resistance to HAART. Firstly, the study of raltegravir in HIV-infected individuals who had received HAART and acquired resistance to its components was initiated. The randomized double-blind, placebo-controlled trial (P005) was carried out during 24 weeks in research centres within the United States, Europe, Latin America, and Asia [54]. The participants included adult patients (18 years and older) with a viral load of at least 5,000 HIV RNA copies/ml and with a level of CD^+ lymphocytes of at least 50 cells/μl. The patients had also been receiving HAART on a regular basis for at least 3 months, and had laboratory-confirmed genotypic or phenotypic resistance to at least one of the

Table 4. Results of clinical trials of raltegravir

Name and duration of the trial	Therapeutic strategy	Fraction of patients with an undeterminable viral load (< 50 copies/ml)	CD4 cell count, cells/μl	Reference
Therapy upon HAART-resistance				
P005, 24 weeks	200 mg ral.*, 41 h	65	63	[54]
	400 mg ral., 44 h	56	113	
	600 mg ral., 45 h	67	94	
	Placebo, 45 hhh	13	5	
BENCHMRK-1 and -2, 96 weeks	400 mg ral., 462 h	58	123	[55]
	Placebo, 237 hhh	26	49	
Primary therapy				
P004, 4 weeks	100 mg ral., 41 h	85	221	[56]
	200 mg ral., 40 h	83	146	
	400 mg ral., 41 h	88	144	
	600 mg ral., 40 h	88	187	
	600 mg efv.*, 39 h	87	170	
STARTMRK-1 and -2, 48 weeks	400 mg ral., 281 h	86	189	[57]
	600 mg efv., 282 h	82	163	
Supporting therapy				
CHEER, 24 weeks	400 mg ral., 52 h	94	32	[58]

* ral. – raltegravir.
** efv. – efavirenz.

non-nucleoside inhibitors of reverse transcriptase, one nucleoside inhibitor of reverse transcriptase, and one protease inhibitor. Prior to the random grouping, the basic regimen of HAART was optimized for each patient; the amount of drugs administered varying from two to seven. It should be noted that the selection of antiretroviral agents for these patients was very limited due to the intolerance or HIV-1 resistance to them. Since it had been demonstrated earlier that the simultaneous administration of atazanavir (protease inhibitor) and raltegravir may result in an increase in raltegravir concentration in the blood [50], the patients were divided into two subgroups, those with atazanavir included within their basic regimen, and those without it [54].

The trial comprised 175 patients. All patients were divided into groups, which were either given varying doses of raltegravir or a placebo (*Table 4*). The clinical and demographic characteristics were similar for the groups. All patients underwent a 24-week therapy course. Raltegravir as a supplement to the optimized HAART regimen showed better efficacy in comparison with the placebo, at any given dose. A mean decrease in the viral load by 100 copies/ml was observed in all groups who were given raltegravir; it began as early as week 2 and was consistent up to week 24 (*Table 4*). The decrease in the viral load was accompanied by an increase in the $CD4^+$ cell count (*Table 4*). Joint use of raltegravir and enfuvirtid (entry inhibitor) or atazanavir within HAART particularly improved the virological and immune response. Forty-one patients left the trial because of inefficacy, 14 (11%) of the 144 who were given raltegravir and 27 (60%) of the 45 who received a placebo. It was demonstrated that raltegravir is a very safe drug: most of the side effects were of light or medium degree of severity. Only two patients left the trial as a result of the side effects of HAART (one in the raltegravir group, and one in the placebo group) [5 4].

The results of the P005 trial [54] in general are consistent with the results of the long-term trial BENCHMRK-1 and -2 [55] devoted to the study of the efficacy and safety of using raltegravir in patients who had earlier received HAART. After a 96-week study, it was found that the viral load had decreased and the CD4 cell count had increased quite considerably in patients who were given raltegravir than it had in those who received a placebo (*Table 4*). It should be mentioned that the optimum results were achieved when raltegravir was used in combination with darunavir (protease inhibitor) and enfuvirtid; the patients were naive to these drugs [55].

Primary therapy. Since raltegravir demonstrated positive results in patients who had earlier received HAART, it became attractive as a primary drug for HIV-infected patients naïve to HAART. The effect of raltegravir and efavirenz (non-nucleoside inhibitor of

reverse transcriptase) were compared in two series of clinical trials (P004 [56] and STARTMRK-1 and -2 [57]). As a supplement to these drugs, the participants were given tenofovir and lamivudin (both drugs are nucleoside inhibitors of reverse protease) (P004 [56]) or tenofovir only (STARTMRK-1 and -2 [57]). It turned out that raltegravir was no less capable of reducing the viral load to below 50 copies/ml in comparison with efavirenz; the CD4 cell count being comparable for both drugs (*Table 4*). In addition, the therapeutic effect of raltegravir was observed earlier than that of efavirenz [57]. Although the reasons for such an effect have as yet remained unclear, this property of raltegravir can be potentially used when there is a necessity for a rapid decrease in the viral load after the HIV-infection, or to reduce the risk of transplacental infection of the foetus from a HIV-infected mother. It should also be noted that in general the results demonstrated in trials P004 and STARTMRK-1 and -2 were better than those in trials P005 and BENCHMRK-1 and -2 (*Table 4*). This result posits the early commencement of raltegravir administration to HIV-infected patients.

Supporting therapy. In addition to using raltegravir as a therapeutic agent in HAART-naive patients, as well as in patients who had developed resistance to HAART components, it was proposed to substitute antiretroviral drugs with raltegravir in patients with a viral load that cannot be determined, in order to reduce the side effects. Trial CHEER [58] included 52 patients with a viral load of less than 50 copies/ml, who were earlier given enfuvertid (penetration inhibitor). Twenty-four weeks after transferring to raltegravir, the undeterminable viral load remained in 49 patients (*Table 4*). Based on these results, a conclusion can be drawn that the substitution of enfuvertid by raltegravir seems to be appreciably safe.

Safety

How safe Raltegravir is was evaluated both in HIV-infected patients naïve to HAART and in patients who developed resistance to HAART components. All studies demonstrated a strong degree of drug tolerance [51, 56, 57]. Raltegravir turned out to be safer than efavirenz upon primary therapy of HIV-infected patients [57]. How safe raltegravir is was assessed on patients who had earlier received HAART. Recurrent or progressing cancer types were detected in approximately 3.5% of patients who were administered raltegravir, whereas this index was equal to 1.7% in individuals taking a placebo. Such types of cancers as Kaposi's sarcoma, lymphoma, hepatic cancer, etc. were the most common [54]. The thorough analysis of all cases of cancer development in patients who were administered raltegravir revealed no correlation between drug administration and the emergence of malignant tumors [52].

Usage guidelines

Raltegravir successfully passed all phases of clinical trials in October 2007 and was approved by the FDA as a therapeutic agent for patients with resistance to HAART components [1]. In July 2009, the FDA also authorized the use of raltegravir for primary therapy of HIV-infected patients [59]. Raltegravir was registered under the trademark Isentress™; it is manufactured in the form of 400 mg tablets for twice-daily oral administration.

Development of resistance to raltegravir

Raltegravir has been used with appreciable success as one of the components of HAART; however, a number of patients developed resistance to this drug [60]. It was ascertained during the trial BENCHMRK-1 and -2 that 48 weeks after raltegravir administration commenced, resistance to this drug was developed in approximately 25% of patients. Virus isolates were obtained from 94 patients with resistance. No mutations in the IN genes were found in 30 isolates; whereas in the remaining 64, the development of resistance was accounted for by these mutations [60]. The resistance to strand transfer reaction is usually associated with the mutations in the IN active center [61]. It was in the active center that raltegravir-resistant virus isolates contained the primary mutations Y143R/C, Q148K/R/H, and N155H [60]. In most patients (48 out of 64), the virus had at least two mutations. Typically, it was a primary mutation and one or several secondary mutations. The primary mutation Y143R/C was associated with the secondary mutations L74A/I, E92Q, T97A, I203M and S230R; the mutation Q148K/R/H was associated with mutations G140S/A and E138K. Primary mutation N155H was associated with a number of secondary mutations: L74M, E92Q, T97A, V151I, and G163R [60]. In addition, it was ascertained that it is typical for mutations to accumulate with time. At the first instance, it refers to the Q148R substitution, which renders the virus almost unsusceptible to raltegravir. The fraction of carriers of the virus containing this mutation among raltegravir-resistant patients after undergoing therapy for 48 weeks was equal to 27%; after 96 weeks, the percentage increased to 53%. Meanwhile, the fraction of carriers of the virus with the N155H mutation shrank from 45 to 18% [60]. The probability of emergence of raltegravir-insusceptibility decreased in patients with reduced viral load (< 100,000 copies/ml) and in patients who were administered other active antiretroviral drugs.

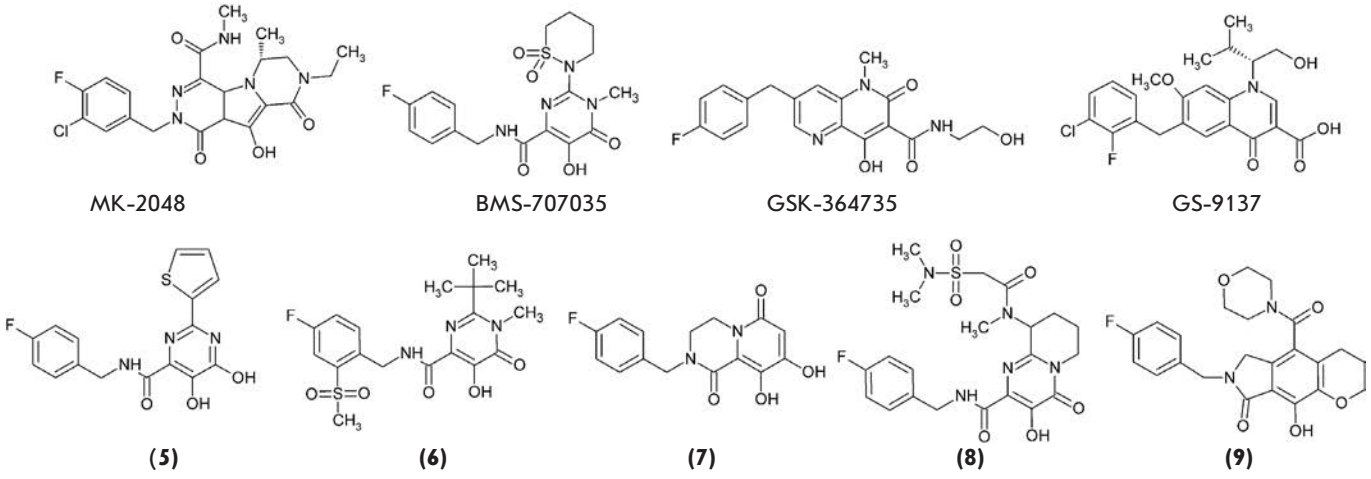

Fig. 5. Structures of HIV-1 integrase strand transfer inhibitors: MK-2048, BMS-707035, GSK-364735, GS-9137, and some new inhibitor classes: dihydroxypyrimidines **(5)**, N-methyl pyrimidinone carboxamides **(6)**, dihydroxypyrido-pyrazine-1,6-diones **(7)**, bicyclic pyrimidones **(8)**, pyrrolloquinolones **(9)**.

A similar pattern was revealed in trial P005 [54]. In 20 and 14 patients out of 35 who appeared to be unsusceptible to raltegravir, the virus contained mainly the Q148K/R/H or N144H mutation, respectively. Mutations N155H and Q148K/R/H reduced the sensitivity of HIV patients to the action of raltegravir by factors of 10 and 25, respectively. Similar to that in trial BENCHMRK-1 and -2, mutation Q148K/R/H turned out to be associated with the secondary substitutions E138K and G140S/A. The secondary mutations L74M, E92Q, and G163R were revealed, and no substitutions T97A and V151I were found in the case of N155H. The probability of resistance development decreased upon reduced viral load and when using additional HAART active components [54].

The recently obtained data in study [62] in which the effect of raltegravir on the strand carrier reaction performed by wild-type IN or IN containing a mutation G140S, Q148H, or a double mutation G140S/Q148H are also of interest. It was evident that while the G140S mutation results in the emergence of small resistance (IC_{50}(WT) = 10 nM, IC_{50}(G140S) = 30 nM), IN with the Q148H or G140S/Q148H mutations has a very high raltegravir resistance (IC_{50}(Q148H) > 70 nM, IC_{50}(G140S/Q148H) > 1000 nM). In addition, it was ascertained that the G140S mutation in the IN gene recovers the weak infectivity of the virus with the Q148H mutation to the level of the wild-type virus [62].

RALTEGRAVIR ANALOGUES — INHIBITORS OF HIV-1 INTEGRATION

The emergence of a new drug, as in the case of any other kind of innovation, results in the rapid appearance of a number of its analogues. Taking into account the approximate cost of the development, trials, and implementation of a single drug, which is equal to $ 2 million, together with the fact that only one out of three novel therapeutic agents manage to recoup this expenditure [18], it is clear that the temptation exists for pharmaceutical companies to avoid the difficulties associated with the development of a completely new drug and confine themselves to modifying the drug that is the best for the moment. Therefore, raltegravir, being the only licensed inhibitor of HIV integrase so far, is of immense interest as a starting point in the development of integration inhibitors. Raltegravir analogues are usually compounds based on diketo acids, which specifically suppress the IN strand transfer reaction due to chelating of Mg^{2+} ions in the enzyme active center [18]. In this section, we shall turn our attention to the inhibitors of strand transfer eligible for the phase of clinical trials.

MK-2048

Soon after the permission for the use of raltegravir as a therapeutic agent was obtained, Merck Pharmaceuticals attempted to design pharmacophore, typical of diketo acids and capable of interacting with the metal ion on the basis of tricyclic dihydroxypyrrole derivatives [63]. As a result, the MK-2048 inhibitor was designed (*Fig. 5*), which exhibited a high inhibition activity in all experiments (*Table 5*). The inhibitor has a good pharmacokinetic profile and, more importantly, possesses potential activity with respect to four mutant IN forms that are resistant to raltegravir. MK-2048 is currently undergoing clinical trials [18].

Table 5. Results of *in vitro* and cell studies of raltegravir analogues as HIV-1 integration inhibitors

Compound	IC_{50}, in vitro (strand transfer), nM	CIC_{95} ex vivo	Reference
MK-2048	10	35 nM (50% NHS)	[63]
BMS-707035	20	-	[16]
GSK-364735	8	EC_{50} = 1.2 nM EC_{90} = 42 nM (20% NHS)	[68]
S/GSK 1349572	2.7	EC_{50} = 0.5 nM EC_{90} = 2 nM	[13]
GS-9137 (elvitegravir)	7	EC_{50} = 0.7 nM EC_{90} = 1.7 nM (20% NHS)	[72]
(**5**) (dihydroxypyrimidine)	10	> 10 μM (10% FBS)	[48]
(**6**) (N-methylpyrimidinone)	20	10 nM (10% FBS) 20 nM (50% NHS)	[64]
(**7**) (dihydroxypyrido-pyrasine-1,6-dion)	100	310 nm (10% FBS) 310 nM (50% NHS)	[65]
(**8**) bicyclic pyrimidinone	7	16 nM (10% FBS) 31 nM (50% NHS)	[66]
(**9**) pyrrolquinolone	13	7 nM (10% FBS) 16 nM (50% NHS)	[67]

BMS-707035

The structural and functional motifs of inhibitors L-780.810 and raltegravir are combined in the structure of this inhibitor [16]. BMS-707035 differs from raltegravir only by the substitution of the oxadiazole group for the cyclic sulfonamide group (*Fig. 5*) and possesses *in vitro* inhibiting activity that is similar to that of raltegravir (*Table 5*). BMS-707035 has reached the second phase of clinical trials; however, multiple mutations emerged in the IN gene responding to the therapy, which has led to the emergence of resistant HIV strains [16]. In the beginning of 2008, the clinical trials of BMS-707035 were discontinued.

GSK-364735

The GSK-364735 inhibitor (*Fig. 5*), a naphthyridinon derivative [68], was developed by the merged Shionogi-GlaxoSmithKline Pharmaceuticals company on the basis of one of the first inhibitors of strand transfer S-1360 [42]. It was efficient in the suppression of HIV replication in MT-4 cells (*Table 5*) and possessed a low cytotoxicity (CC_{50} > 10 μM). The investigation of the action of GSK-364735 on HIV strains containing mutations in the IN gene has demonstrated that the inhibitor is more active to a certain extent with respect to the viruses with mutations T66I (by a factor of 1.2), E92Q (by a factor of 3.7), P145S (by a factor of 1.4), Q146R (by a factor of 1.7), and Q153Y (by a factor of 1.4) as compared with its activity towards the wild-type virus. However, a considerable reduction in the activity of the GSK-364735 inhibitor was observed in the case of four main mutations in the gene of HIV-1 integrase, which result in resistance development: by factors of 17 (T66K mutation), 210 (Q148K mutation), 73 (Q148R mutation), and 23 (N155H mutation) [68]. It was ascertained at the preclinical research phase that GSK-364735 has an acceptable pharmacokinetic profile; the bioavailability indices *F* (42, 12, and 32%), the half-excretion period from blood plasma $T_{1/2}$ (1.5, 1.6, and 3.9 h), and plasma clearance Cl_p (3.2, 8.6, and 2 ml/min/kg) were obtained on rats, dogs, and rhesus macaques, respectively [68]. The drug had good indices at the first phase of clinical trials: it was ascertained that GSK-364735 is capable of reducing the viral load by a factor more than 100. However, the clinical trials ceased at the second phase due to hepatotoxicity being revealed [68, 69].

S/GSK1349572

Shionogi-GlaxoSmithKline Pharmaceuticals has reported that they have designed a highly efficient inhibitor S/GSK1349572 (*Table 5*) [70]. The authors have not disclosed the structure of this compound, but they claim that the agent is capable of specific inhibition of the strand transfer reaction; the mechanism of its action being based on chelating of Mg^{2+} ions in the active centre of the IN [70]. These facts allow us to tentatively attribute S/GSK1349572 to raltegravir analogues, if not in terms of structural characteristics, then at least on the basis of its effect on IN. The use of this preparation results in the development of mutations in the IN gene; however, they are incapable of providing a high degree of virus resistance to S/GSK1349572. Interest-

ingly, the inhibitor turned out to be active with respect to the HIV strains that were resistant to raltegravir [70] and elvitegravir (see below). This drug is likely to have a different resistance profile [14]. Nevertheless, certain secondary mutations that are additional to G140S/Q148H, such as T97A, M154I or V201, induce resistance both to S/GSK1349572 and raltegravir [71]. These data point to the necessity of subjecting the emergence of HIV-1 resistance to this inhibitor to further study.

It was established by studying healthy volunteers that S/GSK1349572 has a rather positive pharmacokinetic profile; in particular, its bioavailability upon peroral administration was approximately 70%, its period of half-excretion from blood plasma $T_{1/2}$ being higher than 15 h [70]. At the time of writing, the second phase of clinical trials of S/GSK1349572 is in progress [70].

GS-9137 (elvitegravir)

The attempts to modify DKS pharmacophore made by Japan Tobacco (Japan) resulted in the design of a group of IN inhibitors based on 4-oxoquinoline, which retained the arrangement of the major functional groups that are required for the interaction with metal ions [72]. The cooperation agreement between Japan Tobacco and Gilead Sciences (United States) signed in 2005, laid the foundation for the clinical trials of the GS-9137 inhibitor (*Fig. 5*) [16] named elvitegravir, as well as the most active representative of IN inhibitors belonging to this structural class (*Table 5*). The pharmacokinetic profile of elvitegravir was studied on rats and dogs [73]. The drug had good indices of bioavailability *F* (34 and 30%), period of half-excretion from blood plasma $T_{1/2}$ (2.3 and 5.2 h) and plasma clearance Cl_p (8.3 and 17 ml/min/kg) in rats and dogs, respectively [73].

The pharmacokinetic profile of elvitegravir was studied in both healthy [74] and HIV-infected [75] volunteers. It was established that elvitegravir rapidly assimilates (3.5–4 h); an increase in C_{max} and AUC parameters was observed with an increasing elvitegravir dose. The best results were obtained when administering elvitegravir together with ritonavir (protease inhibitor) [75]. Unlike raltegravir, elvitegravir is metabolized by cytochrome P450 (CYP3A4) [74]. The stimulating action of ritonavir is probably the result of its ability to inhibit P450 cytochrome and thus maintain a higher concentration of elvitegravir. The interaction between elvitegravir and nucleoside and non-nucleoside inhibitors of reverse transcriptase and penetration inhibitor maraviroc was also studied. It turned out that these inhibitors have no considerable effect on the efficacy of elvitegravir [74].

A randomized study of the therapeutic activity of elvitegravir was performed on 278 HIV-infected patients who had earlier received HAART and developed resistance to its components [76]. The patients with a viral load of approximately 30,000 copies/ml and CD4 lymphocyte count of approximately 200 cells/μl were given the combination of elvitegravir and ritonavir once per day. After week 24 of trial, the viral load decreased by a factor of at least 10 in 90% of the patients who had been administered elvitegravir. The viral load decreased by a factor of 100 in 76% of the individuals who were given 125 mg of elvitegravir and 69% of those who were administered 50 mg of elvitegravir [76]. The study was also performed on 40 HIV-infected volunteers with a viral load of 10,000–300,000 copies/ml and an average CD4 cell count of approximately 200 cells/μl, who received elvitegravir at different doses once or twice a day or once a day in combination with ritonavir. The viral load decreased on average by a factor of 80 in the groups administered elvitegravir twice a day and those administered the combination of elvitegravir and ritonavir, after 10 days. However, no statistically significant change in the CD4 cell count has been observed [75].

A randomized double-blind study of the effect of elvitegravir on HIV-infected volunteers who were naïve to HAART was carried out for 48 weeks [77]. The patients tested were divided into two groups: one of those received a mixture of elvitegravir with cobicistat, the inhibitor of cytochrome P450; the second group was given the non-nucleoside inhibitor of reverse transcriptase efavirenz. In addition, both groups were administered two nucleoside inhibitors of reverse transcriptase, emtricitabine /tenofovir. It appeared that the fraction of patients with an undeterminable viral load in both groups reached 83% and 90% after weeks 24 and 48, respectively [77]. Thus, elvitegravir manifested a high efficacy, which was comparable with the efficacy of the commonly used antiviral agent efavirenz.

The data on the safety of elvitegravir is limited by the results of the second phase of trials, in which HIV-infected patients were given an elvitegravir/ritonavir mixture or a competitive protease inhibitor [76]. No noticeable differences between the two groups in terms of either the frequency of side-effects, or their severity, was observed. Additional studies are required to confirm how safe elvitegravir is in the treatment of HIV-infected patients. At the time of writing, elvitegravir is undergoing the third phase of clinical trials.

Analysis of resistance development in the individuals administered elvitegravir is confined to the data obtained using HIV isolates collected from the patients participating in the second phase of clinical trials [52, 78]. Primary mutations E92Q, T66I/A/K, E138K, S147G, Q148R/H/K, and N155H in HIV-1 integrase were the most frequent; they are also associated with resistance to other DKC-based inhibitors, primarily to

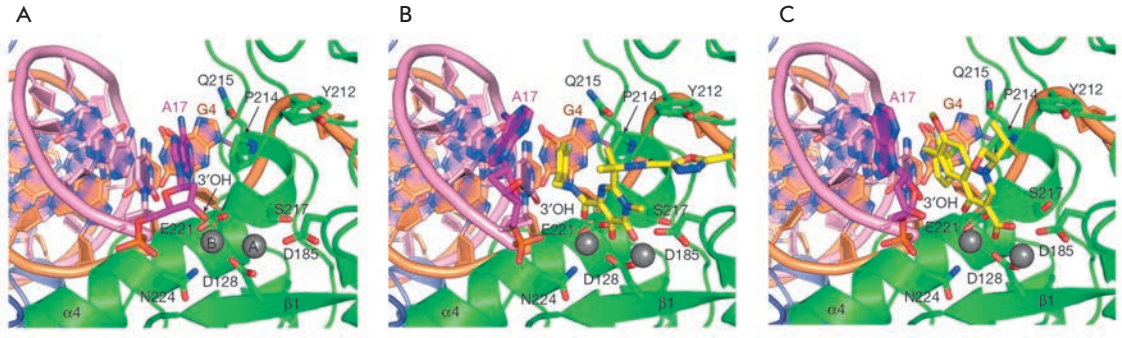

Fig. 6. Structure of the active site of human foamy virus integrase in the absence of inhibitor (A), in the presence of MK-0518 (B), and GS-9137 (C) [28].

raltegravir [79]. At least one of the primary mutations was detected in 39% of elvitegravir-resistant individuals. In addition, cross-resistance to raltegravir was detected: on average, a decrease in the susceptibility to elvitegravir by a factor of 150 also resulted in a 30-fold reduction of susceptibility to raltegravir. The cross-resistance of HIV to the action of raltegravir and elvitegravir was verified by the results of cell studies [80]. Elvitegravir-resistant HIV strains were isolated, and increased resistance to raltegravir and the derivatives of diketo acid L-731.988 and naphthyridine L-870.810 was detected [80].

New raltegravir-based inhibitors of HIV-1 integration

The conduct of a large number of studies aimed at searching for new raltegravir-based IN inhibitors resulted in the development of IN inhibitors belonging to several novel structural classes. They all specifically inhibit the strand transfer reaction and contain functional groups that are capable of chelating metal ions in the IN active centre [18]. The names of the new structural classes of IN inhibitors, the structure of individual representatives (*Fig. 5*) with the indication of their activity *in vitro* and in cell studies, and the data on studying pharmacokinetics in rats are presented in *Table 5*.

The problems of usage of raltegravir analogues as integration inhibitors

All the recorded data point to the fact that the known raltegravir analogues act upon HIV-1 integrase via the same mechanism, contain a similar structural motif, and manifest comparable activity *in vitro* and in cell studies. This type of identity casts some suspicion on the successful future application of these inhibitors as therapeutic agents. These suspicions are caused by cross-resistance of the virus to these inhibitors.

First of all, the emergence of cross-resistance can be accounted for by the similar mechanism of binding of strand transfer inhibitors to the IN complex and viral DNA [14]. As a result of the manner of binding of these compounds, they "push" the 3'-terminal hydroxyl of the processed DNA strand out of the enzyme active centre, thus blocking the integration. This binding mechanism was proposed for HIV-1 IN [81] and demonstrated for the enzyme of the human foamy virus (*Fig. 6*) [28]. Study [28] was first to show that the position of 3'-hydroxyl is occupied by the fluorobenzyl residue of the inhibitor, the fundamentally necessary structural element of all strand transfer inhibitors (*Figs. 4 and 5*).

Using data on X-ray diffraction of the catalytic domain of IN in its complex with Mg^{2+} (1BL3) [18], molecular docking of certain IN inhibitors based on DKC was performed. According to the model proposed, raltegravir interacts with the T66, E92, Y143, Q148, and N155 residues, their substitution resulting in a decrease in the susceptibility to raltegravir by a factor varying from 5 to 35 [48, 82]. Molecular docking also confirmed the fact that amino acid residues interacting with GSK-364735 and GS-9137 are identical to those interacting with raltegravir [83, 84], with an exception for G140. For the latter, a similarity is observed only in the case of elvitegravir [18]. This result correlates with the data demonstrating that the G140S mutation reduces HIV-1 susceptibility to elvitegravir by a factor of 4; and that to raltegravir, only by a factor of 1.6.

Molecular docking of certain new IN inhibitors (*Fig. 5)* demonstrated that these compounds bind to IN in a manner similar to that of raltegravir. Hence, if the results of the study [18] are valid, it is rather unlikely that new inhibitors based on raltegravir will turn out to be active with respect to HIV strains that are raltegravir-resistant and, therefore, become an adequate substitution for it.

Another problem that could complicate the successful use of integration inhibitors is the scarcity of knowledge on IN polymorphism in various subtypes of HIV-1. Until recently, only one study had been performed in which the susceptibility of 137 clinical isolates to raltegravir had been tested. Sixty of those isolates did not belong to the B-subtype [85]. No differences were revealed. However, it was demonstrated in

in vitro experiments that the IN of the C-subtype virus containing the E92Q/N155H mutation is more susceptible to raltegravir and elvitegravir by a factor of 10 as compared with the enzyme of B-subtype HIV-1 [86]. It has also been demonstrated that the mutations of the G140 residue occur less frequently in the CRF02 AG-subtype virus as compared with those in the B-subtype virus [87]. Data are available that raltegravir appears to be inefficient more frequently on individuals infected with a non-B-subtype virus [88].

ALTERNATIVE PATHS OF INHIBITION OF HIV-1 INTEGRATION

We believe that the optimal alternative way of searching for inhibitors of HIV-1 integration consists in designing inhibitors with a mechanism of action that differs from that of raltegravir and its analogues, which specifically inhibit the strand transfer. We shall provide only a brief characterization of several classes of IN inhibitors that differ from the inhibitors of strand transfer in terms of their mechanism of action, and specify certain representatives of these inhibitors.

Inhibitors of 3' processing

The inhibitors belonging to this class are likely to suppress both integration stages: both 3' processing and the strand transfer. It occurs due to the fact that they interact with the active centre of the enzyme, rather than with the enzyme–DNA substrate complex. It is an appreciably numerous class of inhibitors; styryl quinoline compounds being the best-studied inhibitors of 3' processing [89]. Styryl quinoline KHD161 (*Fig.* 7) has nearly the same effect both on 3' processing (IC_{50} = 2.4 μM) and the strand transfer (IC_{50} = 1 μM). It is capable of suppressing the cytopathic effect of HIV-1 in cells with CIC_{50} = 1.3 μM [90, 91]. IN inhibitors based on styryl quinoline are known to be incapable of destroying the pre-formed IN–DNA substrate complex and inhibiting the reaction of 3' processing with its participation. Moreover, the ability of styryl quinolines to bind onto IN depends on Mg^{2+} ions [92]. Thus, a competitive mechanism of IN inhibition with styryl quinolines, due to the interaction with a metal ion in its active centre, can be proposed.

Allosteric inhibitors

Inhibitor V-165 (*Fig.* 7), belonging to the class of 5*H*-pyrano[2,3-d:-6,5-d']dipyrimidines, prevents IN binding with the DNA substrate. It is more efficient in inhibiting the reaction of 3' processing (IC_{50} = 0.9 μM), in comparison with that of the strand transfer (IC_{50} = 16 μM) [93]. Moreover, V-165 suppresses HIV infection in a cell culture [93]. A double mutation T206S/S230N in the IN gene was successfully identified by the selection

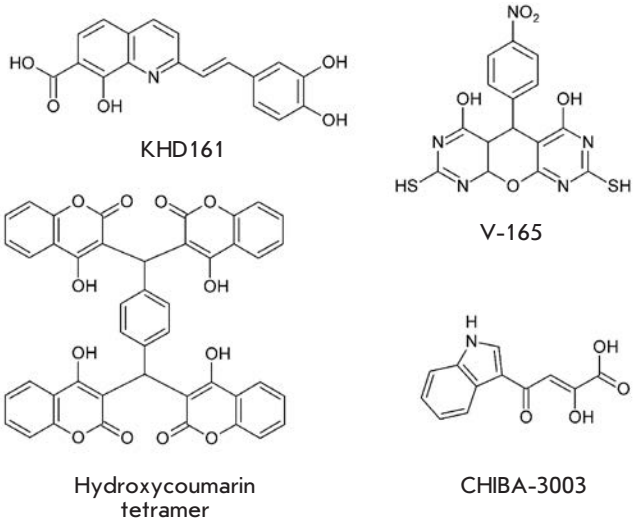

Fig. 7. Structures of KHD161, V-165, hydroxycoumarin tetramer, and CHIBA-3003.

of virus strains resistant to the inhibitor V-165, since the mutation is located in the C-terminal domain of IN, its main function consisting in DNA binding [94].

Inhibitors of integrase multimerization

The search for compounds with an effect on the interaction between the IN and components of the HIV-1 preintegration complex or on their own ability to form an active multimer is currently actively under way [95]. Hydroxycoumarin derivatives refer to the compounds that suppress IN multimerization. It has been demonstrated that hydroxycoumarin tetramer (*Fig.* 7) suppresses HIV-1 replication in a cell culture with the value CIC_{50} = 11.5 μM) [96]. It can inhibit the activity of HIV-1 integrase *in vitro*. Hydroxycoumarin tetramer inhibits 3' processing and strand transfer (IC_{50} = 1.5–2.0 μM) [96]. The benzophenone derivative of hydroxycoumarin was crosslinked to integrase in order to identify the site of inhibitor–enzyme binding [97]. Peptide ^{128}AACWWAGIK^{136}, to which the inhibitor binds, has been determined [97]. This peptide participates in the dimeric complex formation of the catalytic domain [39]. Thus, the hydroxycoumarin-based inhibitor is bound to the enzyme near the surface of contact between two monomers. The binding of hydroxycoumarin derivatives with IN near the ^{128}AACWWAGIK^{136} peptide can disturb interaction of this kind and can have an effect on the formation and stability of the catalytically active integrase multimer.

Inhibitors of the interaction between integrase and LEDGF/p75

This is the least explored direction in the search for integration inhibitors. Regardless of the fact that PIC

contains a large number of viral and cellular proteins in addition to IN, it is its interaction between IN and its cellular partner LEDGF/p75 that determines HIV-1 integration [95]. Data on the inhibitors capable of destroying the IN/LEDGF complex is rather scarce; what we know so far is that their activity is likely to be low. The CHIBA-3003 compound (*Fig.* 7) was designed using a computer simulation. It is capable of destroying the IN/LEDGF complex with IC_{50} = 35 μM [98]. The effect of the LEDGF ^{355}IHAEIKNSLKIDNLDVRNCIEAL^{377} peptide on the stability of the IN/LEDGF complex and catalytic activity of IN has been studied [99]. It appears that this peptide impedes the formation of the IN/LEDGF complex with IC_{50} = 25 μM and inhibits 3' processing and strand transfer with IC_{50} = 160 μM [99].

CONCLUSIONS

In 1996, the resources allocated to research, treatment, and prevention of the spread of HIV/AIDS amounted to 300 million USD. Since then, they have been steadily increasing, to approximately 10 million USD a year at the time of writing [18]. A considerable portion of these funds is spent on the development of new inhibitors aimed at the suppression of viral enzymes, including IN. During the 2.5 years that have elapsed since raltegravir was certified for use as a therapeutic agent against HIV-1, the major efforts of pharmaceutical companies such as Merck Pharmaceuticals, Japan Tobacco, Gilead Sciences, and Shionogi-GlaxoSmithKline Pharmaceuticals have focused on developing analogues of this drug. Yet, many raltegravir analogues are incapable of suppressing the replication of HIV-1 strains that are raltegravir-resistant [83, 84]. We consider that there is a need for a more active search for inhibitors with a different mechanism of action, which can be active with respect to the raltegravir-resistant viral strains. However, it should be mentioned that none of the inhibitors of HIV-1 integration that do not belong to the class of specific inhibitors of strand transfer has so far managed to successfully pass even the first phase of clinical trials. ●

This work was supported by the Russian Foundation for Basic Research (grants № 11-04-01004_a, 11-04-01586_a), the Grant of the President of the Russian Federation (МК-4821.2011.4), and Government Contract № 16.512.11.2193.

REFERENCES

1. http://www.unaids.org/ru
2. Simon V., Ho D.D., Abdool Karim Q. // Lancet. 2006. V. 368. № 9534. P. 489–504.
3. Turner B.G., Summers M.F. // J. Mol. Biol. 1999. V. 285. P. 1–32.
4. Miller M.D., Farnet C.M., Bushman F.D. // J. Virol. 1997. V. 71. P. 5382–5390.
5. Piller S.C., Caly L., Jans D.A. // Cur. Drug. Targets. 2003. V. 4. № 5. P. 409–429.
6. Li L., Olvera J., Yoder K., Mitchell R.S., Butler S.L., Lieber M., Martin S.L., Bushman F.D. // EMBO J. 2001. V. 20. P. 3272–3281.
7. Farnet C.M., Bushman F.D. // Cell. 1997. V. 88. P. 483–492.
8. Lin C.W., Engelman A. // J. Virol. 2003. V. 77. P. 5030–5036.
9. Vandegraaff N., Devroe E., Turlure F., Silver P.A., Engelman A. // Virology. 2006. V. 346. P. 415–426.
10. Marcelin A.G., Ceccherini-Silberstein F., Perno C.F., Calvez V. // Curr. Opin. HIV AIDS. 2009. V. 4. № 6. P. 531–537.
11. FDA approves raltegravir tablets // AIDS Patient Care STDS. 2007. V. 21. № 11. P. 889.
12. Cara A., Guarnaccia F., Reitz M.S. Jr., Gallo R.C., Lori F. // Virology. 1995. V. 208. P. 242–248.
13. Ramkumar K., Serrao E., Odde S., Neamati N. // Med. Res. Rev. 2010. V. 30. № 5. P. 750–814.
14. Mouscadet J.F., Delelis O., Marcelin A.G., Tchertanov L. // Drug Resist Updat. 2010. V. 13. № 4–5. P. 139–150.
15. De Clercq E. // Curr. Opin. Pharmacol. 2010. V. 10. № 5. P. 507–515.
16. Al-Mawsawi L.Q., Al-Safi R.I., Neamati N. // Expert Opin. Emerg. Drugs. 2008. V. 13. № 2. P. 213–225.
17. Gatell J.M. // Eur. J. Med. Res. 2009. V. 14. P. 30–35.
18. Serrao E., Odde S., Ramkumar K., Neamati N. // Retrovirology. 2009. V. 6. № 25. P.
19. Prikazchikova T.A., Sycheva A.M., Agapkina Yu.Yu., Aleksandrov D.A., Gottikh M.B. // Russ. Chem. Rev. 2008. V. 77 (5). P. 421–434.
20. Agapkina Yu. Yu., Prikazchikova T. A., Smolov M.A., Gottikh M.B. // Uspekhi Biol. Khimii. V. 45. P. 87-122.
21. Delelis O., Carayon K., Saïb A., Deprez E., Mouscadet J.-F. // Retrovirology. 2008. V. 5. P. 114.
22. Poeschla E.M. // Cell Mol. Life Sci. 2008. V. 65. № 9. P. 1403–1424.
23. Zheng R., Jenkins T.M., Craigie R. // Proc. Natl. Acad. Sci. USA. 1996. V. 93. № 24. P. 13659–13664.
24. Gallay P., Hope T., Chin D., Trono D. // Proc. Natl. Acad. Sci. USA. 2005. V. 94. P. 9825–9830.
25. Podtelezhnikov A.A., Gao K., Bushman F.D., McCammon J.A. // Biopolymers. 2003. V. 68. № 1. P. 110–120.
26. Wielens J., Crosby I.T., Chalmers D.K. // J. Comput. Aided Mol. Des. 2005. V. 19. № 5. P. 301–317.
27. Ren G., Gao K., Bushman F.D., Yeager M. // J. Mol. Biol. 2007. V. 366. № 1. P. 286–294.
28. Hare S., Gupta S.S., Valkov E., Engelman A., Cherepanov P. // Nature. 2010. V. 464. № 7286. P. 232–236.
29. Delelis O., Carayon K., Guiot E., Leh H., Tauc P., Brochon J.C., Mouscadet J.-F., Deprez E. // J. Biol. Chem. 2008. V. 283. № 41. P. 27838–27849.
30. Knyazhanskaya E.S., Smolov M.A., Kondrashina O.V., Gottikh M.B. // Acta Naturae. 2009. V. 1. № 2. P. 78-80.
31. Sinha S., Pursley M.H., Grandgenett D.P. // J. Virol. 2002. V. 76. P. 3105–3113.
32. van Maele B., Debyser Z. // AIDS Rev. 2005. V. 7. P. 26–43.
33. Yu F., Jones G.S., Hung M., Wagner A.H., MacArthur H.L., Liu X., Leavitt S., McDermott M.J., Tsiang M. // Biochemistry. 2007. V. 46. № 10. P. 2899–2908.
34. Hazuda D.J., Felock P., Witmer M., Wolfe A., Stillmock K.,

Grobler J.A., Espeseth A., Gabryelski L., Schleif W., Blau C., et al. // Science. 2000. V. 287. № 5453. P. 646–650.
35. Hazuda D.J., Anthony N.J., Gomez R.P., Jolly S.M., Wai J.S., Zhuang L., Fisher T.E., Embrey M., Guare J.P. Jr., Egbertson M.S., et al. // Proc. Natl. Acad. Sci. USA. 2004. V. 101. № 31. P. 11233–11238.
36. Summa V., Petrocchi A., Matassa V.G., Gardelli C., Muraglia E., Rowley M., Paz O.G., Laufer R., Monteagudo E., Pace P. // J. Med. Chem. 2006. V. 49. № 23. P. 6646–6649.
37. Guare J.P., Wai J.S., Gomez R.P., Anthony N.J., Jolly S.M., Cortes A.R., Vacca J.P., Felock P.J., Stillmock K.A., Schleif W.A., et al. // Bioorg. Med. Chem. Lett. 2006. V. 16. № 11. P. 2900–2904.
38. Espeseth A.S., Felock P., Wolfe A., Witmer M., Grobler J., Anthony N., Egbertson M., Melamed J.Y., Young S., Hamill T., et al. // Proc. Natl. Acad. Sci. USA. 2000. V. 97. № 21. P. 11244–11249.
39. Goldgur Y., Craigie R., Cohen G.H., Fujiwara T., Yoshinaga T., Fujishita T., Sugimoto H., Endo T., Murai H., Davies D.R. // Proc. Natl. Acad. Sci. USA. 1999. V. 96. № 23. P. 13040–13043.
40. Grobler J.A., Stillmock K., Hu B., Witmer M., Felock P., Espeseth A.S., Wolfe A., Egbertson M., Bourgeois M., Jeffrey Melamed J., et al. // Proc. Natl. Acad. Sci. USA. 2002. V. 99. № 10. P. 6661–6666.
41. Marchand C., Zhang X., Pais G.C.G., Cowansage K., Neamati N., Burke T.R., Pommier Y. // J. Biol. Chem. 2002. V. 277. P. 12596–12603.
42. Billich A. // Curr. Opin. Investig. Drugs. 2003. V. 4. № 2. P. 206–209.
43. Zhuang L., Wai J.S., Embrey M.W., Fisher T.E., Egbertson M.S., Payne L.S., Guare J.P. Jr., Vacca J.P., Hazuda D.J., Felock P.J., et al. // J. Med. Chem. 2003. V. 46. № 4. P. 453–456.
44. Cotelle P. // Recent Patents on Anti-Infective Drug Discovery. 2006. V. 1. P. 1–15.
45. Petrocchi A., Koch U., Matassa V.G., Pacini B., Stillmock K.A., Summa V. // Bioorg. Med. Chem. Lett. 2007. V. 17. № 2. P. 350–353.
46. Pace P., Di Francesco M.E., Gardelli C., Harper S., Muraglia E., Nizi E., Orvieto F., Petrocchi A., Poma M., Rowley M., et al. // J. Med. Chem. 2007. V. 50. № 9. P. 2225–2239.
47. Gardelli C., Nizi E., Muraglia E., Crescenzi B., Ferrara M., Orvieto F., Pace P., Pescatore G., Poma M., Ferreira Mdel R., et al. // J. Med. Chem. 2007. V. 50. № 20. P. 4953–4975.
48. Summa V., Petrocchi A., Bonelli F., Crescenzi B., Donghi M., Ferrara M., Fiore F., Gardelli C., Gonzalez Paz O., Hazuda D.J., et al. // J. Med. Chem. 2008. V. 51. № 18. P. 5843–5855.
49. Kassahun K., McIntosh I., Cui D., Hreniuk D., Merschman S., Lasseter K., Azrolan N., Iwamoto M., Wagner J.A., Wenning L.A. // Drug. Metab. Dispos. 2007. V. 35. № 9. P. 1657–1663.
50. Iwamoto M., Wenning L.A., Petry A.S., Laethem M., De Smet M., Kost J.T., Merschman S.A., Strohmaier K.M., Ramael S., Lasseter K.C., et al. // Clin. Pharmacol. Ther. 2008. V. 83. № 2. P. 293–299.
51. Markowitz M., Morales-Ramirez J.O., Nguyen B.Y., Kovacs C.M., Steigbigel R.T., Cooper D.A., Liporace R., Schwartz R., Isaacs R., Gilde L.R., et al. // J. Acquir. Immune. Defic. Syndr. 2006. V. 43. № 5. P. 509–515.
52. Schafer J.J., Squires K.E. // Ann. Pharmacother. 2010. V. 44. № 1. P. 145–156.
53. Ménard A., Solas C., Mokthari S., Bregigeon S., Drogoul M.P., Tamalet C., Lacarelle B., Martin I.P. // AIDS. 2009. V. 23. № 7. P. 869–871.
54. Grinsztejn B., Nguyen B.Y., Katlama C., Gatell J.M., Lazzarin A., Vittecoq D., Gonzalez C.J., Chen J., Harvey C.M., Isaacs R.D. // Lancet. 2007. V. 369. № 9569. P. 1261–1269.
55. Steigbigel R.T., Cooper D.A., Teppler H., Eron J.J., Gatell J.M., Kumar P.N., Rockstroh J.K., Schechter M., Katlama C., Markowitz M., et al. // Clin. Infect. Dis. 2010. V. 50. № 4. P. 605–612.
56. Markowitz M., Nguyen B.Y., Gotuzzo E., Mendo F., Ratanasuwan W., Kovacs C., Prada G., Morales-Ramirez J.O., Crumpacker C.S., Isaacs R.D., et al. // J. Acquir. Immune. Defic. Syndr. 2007. V. 46. № 2. P. 125–133.
57. Lennox J.L., DeJesus E., Lazzarin A., Pollard R.B., Madruga J.V., Berger D.S., Zhao J., Xu X., Williams-Diaz A., Rodgers A.J., et al. // Lancet. 2009. V. 374. № 9692. P. 796–806.
58. Towner W., Klein D., Kerrigan H.L., Follansbee S., Yu K., Horberg M. // J. Acquir. Immune. Defic. Syndr. 2009. V. 51. № 4. P. 367–373.
59. FDA notifications. Raltegravir indication extended for treatment-naive patients // AIDS Alert. 2009. V. 24. № 8. P. 93.
60. Cooper D.A., Steigbigel R.T., Gatell J.M., Rockstroh J.K., Katlama C., Yeni P., Lazzarin A., Clotet B., Kumar P.N., Eron J.E., et al. // N. Engl. J. Med. 2008. V. 359. № 4. P. 355–365.
61. Malet I., Delelis O., Valantin M.A., Montes B., Soulie C., Wirden M., Tchertanov L., Peytavin G., Reynes J., Mouscadet J.-F., et al. // Antimicrob. Agents. Chemother. 2008. V. 52. № 4. P. 1351–1358.
62. Delelis O., Malet I., Na L., Tchertanov L,. Calvez V., Marcelin A.G., Subra F., Deprez E., Mouscadet J.-F. // Nucleic. Acids Res. 2009. V. 37. № 4. P. 1193–1201.
63. Wiscount C.M., Williams P.D., Tran L.O., Embrey M.W., Fisher T.E., Sherman V., Homnick C.F., Donnette Staas D., Lyle T.A., Wai J.S., et al. // Bioorg. Med. Chem. Lett. 2008. V. 18. № 16. P. 4581–4583.
64. Di Francesco M.E., Pace P., Fiore F., Naimo F., Bonelli F., Rowley M., Summa V. // Bioorg. Med. Chem. Lett. 2008. V. 18. № 8. P. 2709–2713.
65. Wai J.S., Kim B., Fisher T.E., Zhuang L., Embrey M.W., Williams P.D., Staas D.D., Culberson C., Lyle T.A., Vacca J.P., et al. // Bioorg. Med. Chem. Lett. 2007. V. 17. № 20. P. 5595–5599.
66. Muraglia E., Kinzel O., Gardelli C., Crescenzi B., Donghi M., Ferrara M., Nizi E., Orvieto F., Pescatore G., Laufer R., et al. // J. Med. Chem. 2008. V. 51. № 4. P. 861–874.
67. Jin H., Wright M., Pastor R., Mish M., Metobo S., Jabri S., Lansdown R., Cai R., Pyun P., Tsiang M., et al. // Bioorg. Med. Chem. Lett. 2008. V. 18. № 4. P. 1388–1391.
68. Garvey E.P., Johns B.A., Gartland M.J., Foster S.A., Miller W.H., Ferris R.G., Hazen R.J., Underwood M.R., Boros E.E., Thompson J.B., et al. // Antimicrob. Agents Chemother. 2008. V. 52. № 3. P. 901–908.
69. Reddy Y.S., Min S.S., Borland J., Song I., Lin J., Palleja S., Symonds W.T. // Antimicrob. Agents Chemother. 2007. V. 51. № 12. P. 4284–4289.
70. Min S., Song I., Borland J., Chen S., Lou Y., Fujiwara T., Piscitelli S.C. // Antimicrob. Agents Chemother. 2010. V. 54. № 1. P. 254–258.
71. Vandeckerckhove L. // Curr. Opin. Invest. Drugs. 2010. V. 11. P. 203–212.
72. Sato M., Motomura T., Aramaki H., Matsuda T., Yamashita M., Ito Y., Kawakami H., Matsuzaki Y., Watanabe W., Yamataka K., et al. // J. Med. Chem. 2006. V. 49. № 5. P. 1506–1508.

73. Sato M., Kawakami H., Motomura T., Aramaki H., Matsuda T., Yamashita M., Ito Y., Matsuzaki Y., Yamataka K., Ikeda S., et al. // J. Med. Chem. 2009. V. 52. № 15. P. 4869–4882.
74. Correll T., Klibanov O.M. // Pharmacotherapy. 2008. V. 28. № 1. P. 90–101.
75. DeJesus E., Berger D., Markowitz M., Cohen C., Hawkins T., Ruane P., Elion R., Farthing C., Zhong L., Cheng A.K., et al. // J. Acquir. Immune. Defic. Syndr. 2006. V. 43. № 1. P. 1–5.
76. Zolopa A.R., Berger D.S., Lampiris H., Zhong L., Chuck S.L., Enejosa J.V., Kearney B.P., Cheng A.K. // J. Infect. Dis. 2010. V. 201. № 6. P. 814–822.
77. Cohen C., Elion R., Ruane P., Shamblaw D., DeJesus E., Rashbaum B., Chuck S.L., Yale K., Liu H.C., Warren D.R., et al. // AIDS. 2011. V. 25. № 6. P. F7–F12.
78. McColl D.J., Fransen S., Gupta S., Parkin N., Margot N., Chuck S., Cheng A.K., Miller M.D. // Antivir. Ther. 2007. V. 12. P. S11–S111.
79. Ceccherini-Silberstein F., Malet I., D'Arrigo R., Antinori A., Marcelin A.G., Perno C.F. // AIDS Rev. 2009. V. 11. № 1. P. 17–29.
80. Goethals O., Clayton R., van Ginderen M., Vereycken I., Wagemans E., Geluykens P., Dockx K., Strijbos R., Smits V., Vos A., et al. // J. Virol. 2008. V. 82. № 21. P. 10366–10374.
81. Langley D.R., Samanta H.K., Lin Z., Walker M.A., Krystal M.R., Dicker I.B. // Biochemistry. 2008. V. 47. P. 13481–13488.
82. Marinello J., Marchand C., Mott B.T., Bain A., Thomas C.J., Pommier Y. // Biochemistry. 2008. V. 47. № 36. P. 9345–9354.
83. Kobayashi M., Nakahara K., Seki T., Miki S., Kawauchi S., Suyama A., Wakasa-Morimoto C., Kodama M., Endoh T., Oosugi E., et al. // Antiviral Res. 2008. V. 80. № 2. P. 213–222.
84. Nakahara K., Wakasa-Morimoto C., Kobayashi M., Miki S., Noshi T., Seki T., Kanamori-Koyama M., Kawauchi S., Suyama A., Fujishita T., et al. // Antiviral Res. 2009. V. 81. № 2. P. 141–146.
85. an Baelen K., van Eygen V., Rondelez E., Stuyver L.J. // AIDS. 2008. V. 22. P. 1877–1880.
86. Bar-Magen T., Donahue D.A., McDonough E.I. // AIDS. 2010. V. 24. № 14. P. 2171–2179.
87. Maiga A.I., Malet I., Soulie C., Derache A., Koita V., Amellal B., Tchertanov L., Delelis O., Morand-Joubert L., Mouscadet J.-F., et al. // Antivir. Ther. 2009. V. 14. P. 123–129.
88. Sichtig N., Sierra S., Kaiser R., Daumer M., Reuter S., Schulter E., Altmann A., Fatkenheuer G., Dittmer U., Pfister H., et al. // J. Antimicrob. Chemother. 2009. V. 64. P. 25–32.
89. Mekouar K., Mouscadet J.-F., Desmaële D., Subra F., Leh H., Savoure D., Auclair C., d'Angelo J. // J. Med. Chem. 1998. V. 41. P. 2846–2857.
90. Ouali M., Laboulais C., Leh H., Gill D., Desmaele D., Mekouar K., Zouhiri F., d'Angelo J., Auclair C., Mouscadet J.-F., et al. // J. Med. Chem. 2000. V. 43. № 10. P. 1949–1957.
91. Zouhiri F., Mouscadet J.-F., Khalid Mekouar K., Desmaële D., Savouré D., Leh H., Subra F., Le Bret M., Auclair C., d'Angelo J. // J. Med. Chem. 2000. V. 43. P. 1533–1540.
92. Deprez E., Barbe S., Kolaski M., Leh H., Zouhiri F., Auclair C., Brochon J.-C., Le Bret M., Mouscadet J.-F. // Mol. Pharmacol. 2004. V. 65. № 1. P. 85–98.
93. Pannecouque C., Pluymers W., van Maele B., Tetz V., Cherepanov P., De Clercq E., Witvrouw M., Debyser Z. // Curr. Biol. 2002. V. 12. № 14. P. 1169–1177.
94. Hombrouck A., Hantson A., van Remoortel B., Michiels M., Vercammen J., Rhodes D., Tetz V., Engelborghs Y., Christ F., Debyser Z., et al. // J. Antimicrob. Chemother. 2007. V. 59. № 6. P. 1084–1095.
95. Al-Mawsawi L.Q., Neamati N. // Trends Pharmacol. Sci. 2007. V. 28. № 10. P. 526–535.
96. Mazumder A., Wang S., Neamati N., Nicklaus M., Sunder S., Chen J., Milne G.W.A., Rice W.G., Burke T.R. Jr., Pommier Y. // J. Med. Chem. 1996. V. 39. P. 2472–2481.
97. Al-Mawsawi L.Q., Fikkert V., Dayam R., Witvrouw M., Burke T.R. Jr., Borchers C.H., Neamati N. // Proc. Natl. Acad. Sci. USA. 2006. V. 103. № 26. P. 10080–10085.
98. De Luca L., Barreca M.L., Ferro S., Christ F., Iraci N., Gitto R., Monforte A.M., Debyser Z., Chimirri A. // Chem. Med. Chem. 2009. V. 4. № 8. P. 1311–1316.
99. Al-Mawsawi L.Q., Christ F., Dayam R., Debyser Z., Neamati N. // FEBS Lett. 2008. V. 582. № 10. P. 1425–1430.

Silencing of *Her2*, *CCNB1* and *PKC* Genes by siRNA Results in Prolonged Retardation of Neuroblastoma Cell Division

I. A. Akimov, E. L. Chernolovskaya*, Yu. E. Spitsyna, E. I. Ryabchikova, M. A. Zenkova
Institute of Chemical Biology and Fundamental Medicine, Siberian Branch, Russian Academy of Sciences
*E-mail: elena_ch@niboch.nsc.ru
Received 15.04.2011

ABSTRACT **Deregulation of the expression of the genes that are involved in the control of the cell cycle impairs cellular differentiation and leads to cell death. This process can result in uncontrollable cell proliferation and, subsequently, cancer development. In this study, we examined the effect of the silencing of cancer-related genes by small interfering RNAs (siRNA) targeted at mRNA of *Her2*, cyclin B1 (*CCNB1*), and protein kinase C *(PKC)* on the proliferation of human cancer cells of different origins. Maximum silencing of *CCNB1*, *Her2* (in KB-3-1, SK-N-MC, MCF-7 cells), and *PKC* (in MCF-7 cells) was achieved 72 h after transfection of the corresponding siRNAs, and 12 days after the transfection, the initial levels of the target mRNAs were fully recovered. Silencing of *Her2*, *CCNB1,* and *PKC* differently effected the proliferation of the cell lines under study. The most pronounced antiproliferative action of the investigated siRNAs was observed in neuroblastoma SK-N-MC cells (3 – 10-fold reduction in the proliferation rate) even after the recovery of the initial levels of expression of the *Her2*, *CCNB1,* and *PKC* genes. The obtained data indicate that the *CCNB1* and *PKC* genes can be used as targets in the development of drugs for neuroblastoma treatment.**

KEYWORDS **neuroblastoma; siRNA; *Her2*; *CCNB1*; *PKC*; proliferation.**

ABBREVIATIONS **C – 2'-O-methylcytosine; U – 2'-O-methyluridine; siRNA – small interfering RNA; MTT – 3-[4,5-dimethylthiazol-2-yl]-2,5-diphenyltetrazolium bromide; PBS – phosphate buffered saline; FBS – fetal bovine serum.**

INTRODUCTION

Malignant cell transformation is a complex process involving both genetic disorders and failure in the regulation of differentiation, apoptosis, and proliferation [1, 2]. The regulatory signal transduction network in a cell is cascade-like and consists of a number of duplicating paths [3]. When silencing one of the cell factors that participate in signal transduction, its function can be compensated by the activation of alternative signal paths [3]. While on one hand this further complicates the search for adequate molecular targets , on the other hand, it makes it necessary to design anti-tumor cells that would provide an irreversible antiproliferative effect by "switching off" the synthesis of the protein factors localized at the points of interception of the regulatory paths.

Hyperexpression of normal genes or expression of their mutant variants encoding transcription factors, receptors, tyrosine kinases, and other regulatory proteins can be behind the uncontrollable cell division upon cancer [2]. Suppression of the synthesis of these proteins may provide a positive effect and normalize cell proliferation [4–7].

Today, RNA interference is widely used both to study the role of genes in the regulation of the cell cycle and to reveal potential targets for designing new therapeutical agents [8–10]. Specific and efficient silencing of target genes can be achieved using chemically synthesized small interfering RNAs (siRNAs) [11]. The products of such genes as *Her2*, cyclin B1 (*CCNB1*), and protein kinase C (*PKC*) belong to different groups of proteins that participate in the regulation of the cell cycle [8, 12, 13]. Earlier, it was experimentally demonstrated and clinically verified that disorders in the expression of these genes may result in the emergence of malignant tumors in humans [12, 14–18]. The level of amplification and expression of these genes in breast or ovarian cancer cells, or cancer cells in other human organs, is considerably higher than that in the normal cells of these organs [14, 17–

32]. Moreover, high levels of expression of the *Her2*, *CCNB1*, and *PKC* genes correlate with dire prognosis: three-year survival rate, and the recurrence-free period shortens [17, 18, 22–25, 30].

The *Her2* gene (also known as *c-erb-B2* and *neu*) encodes a transmembrane glycoprotein possessing tyrosine kinase activity and belonging to the family of human epidermal growth factor receptors, which play a significant role in the regulation of the proliferation, differentiation, and mobility of human epitelial cells [33, 34]. A level of *Her2* gene expression considerably higher than the normal level was detected in the cells of humans with breast, endometrial, uterine neck, ovarian, fallopian tube, and lung cancer [25, 29, 30].

Cyclin B1 encoded by the *CCNB1* gene is a regulatory subunit of the cyclin-dependent kinase complex (CDK1) that regulates the transition from phase G_2 of the cell cycle into phase M [35]. Hyperexpression of the *CCNB1* gene usually does not immediately result in cell cycle disorder, which causes the accumulation of mutations in a cell [36]. An increased expression level of this gene, which is typical of benign and malignant human prostate tumors [37], is often the reason for aneuploidy [38]. Disturbance in the *CCNB1* gene expression could be regarded as an early warning in malignant cell transformation [17].

Protein kinase C encoded by the *PKC* gene is expressed in many human tissues and organs; it plays an important role in the transduction of the regulatory signals that activate various cell functions, including proliferation [39, 40]. A level of *PKC* gene expression higher than the normal level was detected in human cancer cells of different origins [18, 19].

It has been known that silencing of the same gene in tumor cells of different tissue origins may result in various antiproliferative effects [41]. This determines the necessity for comparing the antiproliferative action of siRNAs in different human tumor cell lines. It was earlier demonstrated that siRNAs targeted at mRNAs of the *Her2*, *CCNB1*, and *PKC* genes efficiently silence the target genes and have an antiproliferative effect on human cancer cells for 5 days following transfection [41].

In this study, we assessed the long-term consequences of short-term silencing of *Her2*, *CCNB1*, and *PKC* on the proliferation and morphology of human tumor cells. We demonstrated that siRNAs that are homologous to mRNAs of the *Her2*, *CCNB1*, and *PKC* genes silence these genes, attaining maximum effect (up to 4–22% of the control level) 72 h after transfection. These siRNAs demonstrated different efficiencies of deceleration of the division of human tumor cells of different tissue origins. We found that the antiproliferative effect of siCyc and siPKC in SK-N-MC neuroblastoma cells is retained even after the initial levels of target gene expression have been recovered. The data obtained permit the reasonable assumption that the *CCNB1* and *PKC* genes play a key role in sustaining a high proliferation rate of neuroblastoma cells, whereas their short-term silencing results in change in signal transmission paths and normalization of the rate of cell division. Thus, the *CCNB1* and *PKC* genes in SK-N-MC cells can serve as potential efficient targets for the agents targeted at neuroblastoma, including siRNAs.

EXPERIMENTAL

siRNAs

All the oligonucleotides that were used to form siRNA duplexes were synthesized at the Laboratory of RNA Chemistry, Institute of Chemical Biology and Fundamental Medicine, Russian Academy of Sciences, Siberian Branch using the solid-phase phosphiteamide method on an automatic synthesizer ASM-102U (Biosset, Russia) and extracted using high-efficiency reversed phase chromatography. The nuclease-sensitive sites in siRNA were protected by introducing 2'-O-Me-analogues of ribonucleotides into the siRNAs using the algorithm described earlier [42, 43]. According to the data of electrophoresis in polyacrylamide gel under denaturating conditions, the purity of the oligoribonucleotides was at least 95%. The following siRNAs were used in the present study: siHer homologous to the region 1297–1317 of mRNA of the human *Her2* gene (sense strand 5'-G<u>C</u>AGUUAC<u>C</u>AGUGC<u>C</u>AAUAUU-3', antisense strand 5'-<u>U</u>AU<u>U</u>GG<u>C</u>AC<u>U</u>GG<u>U</u>AAC<u>U</u>GCCC-3'); siCyc homologous to the region 189–209 of mRNA of the human *CCNB1* gene (sense strand 5'-<u>C</u>AC<u>C</u>AGGAACUCGAAAAUUUU-3', antisense strand 5'-AAUUUUCGAGUUCC<u>U</u>GG<u>U</u>GAC-3'); and siPKC homologous to region 1079–1099 of mRNA of the human *PKC* gene (sense strand GCGGC<u>C</u>AGAGAAGGAAAAAUU-3', antisense strand 5'-UUUUUCCUUCUC<u>U</u>GGCCGC<u>U</u>G-3'), 2'-O-Me-modified units are underlined. siScr (sense strand 5'-<u>C</u>AAGUCUCG<u>U</u>A<u>U</u>G<u>U</u>AG<u>U</u>GGUU-3', antisense strand 5'-C<u>C</u>AC<u>U</u>A<u>C</u>A<u>U</u>ACGAGACU<u>U</u>GUU-3') without significant homologies with the nucleotide sequences of mRNAs of mouse, rat, and human genes was used as the negative control. siRNAs were selected using the BioPredSi software [44]. siRNAs were obtained via fusion of the antisense and sense strands in a buffer of 15 mM HEPES-KOH pH 7.4, 50mM potassium acetate, and 1 mM magnesium acetate. To perform this procedure, equimolar mixtures of oligoribonucleotides (sense and antisense strands) were incubated for 2 min at 90^0C and slowly cooled to room temperature.

Cell cultures and siRNA transfection

Cell lines of human uterine neck carcinoma KB-3-1, SK-N-MC neuroblastoma, and MCF-7 breast adenocarcinoma were obtained from the collection of the Institute of Cytology of the Russian Academy of Sciences (St. Petersburg, Russia). The cells were cultivated in a DMEM medium (Dulbecco's Modified Eagle Medium) containing 10% of fetal bovine serum (FBS), 100 u/ml of penicillin, 100 μg/ml of streptomycin, and 0.25 μg/ml of amphotericin at 37°C in humid atmosphere with 5% CO_2 content. Twenty-four hours prior to the experiment, the cells in the phase of exponential growth were seeded in 6-well plates: KB-3-1 – 4×10^4, SK-N-MC – 2×10^5, MCF-7 – 8×10^4 cells/well or in 24-well plates: KB-3-1 –10^5, SK-N-MC – 1.25×10^5, and MCF-7 – 1.5×10^5 cells/well and allowed to adhere overnight. The cells were transfected with siRNA at a concentration of 200 nM; Lipofectamine 2000™ (Invitrogen, United States) or Oligofectamine™ (Invitrogen, United States) for SK-N-MC cells were used as transfection agents, in accordance with the manufacturer's protocol. The levels of specific mRNAs were determined 1–5, 7, 10, and 12 days after transfection. The cells treated only with a transfection agent or siScr/lipofectamine (oligofectamine) complex were used as the control. During the experiment, the cells were reseeded once in 3–4 days to maintain the exponential growth.

Real-time reverse transcription PCR (RT-PCR)

The total RNA was extracted from the cells using the SDS-phenol method [45]. Reverse transcription (RT) reaction was carried out in a 20 μl mixture containing 1 μg of total RNA, 5 μM of the oligo(dT_{15}) primer, 50 mM of Tris-HCl, pH 8.3, 75 mM of KCl, 3 mM of $MgCl_2$, 0.5 mM of dNTP, 5 mM of dithiothreitol, and 10 U of M-MLV reverse transcriptase from the Moloney murine leukemia virus. The reaction mixture was incubated at 42°C for 1 h. The resulting cDNA was amplified in a reaction mixture (volume 20 μl) containing 1 μl of cDNA, 10 mM of Tris-HCl, pH 8.3, 50 mM of KCl, 1.5 mM of $MgCl_2$, 0.01% Tween-20, 0.25 mM of each dNTP, 0.25 μM of each primer, 0.5 mM of EvaGreen (Biotium, United States), and 2 U of thermostable DNA polymerase *Thermus aquaticus* (produced at the Institute of Chemical Biology and Fundamental Medicine, Siberian Branch, Russian Academy of Sciences). Real-time PCR was carried out on a Bio-Rad iQ5 Multicolor Real-Time PCR Detection System instrument according to the following scheme: one cycle – 3 min, 95°C, 40 cycles – 30 s, 95°C, 30 s – 58°C, 30 c – 72°C. The amount of mRNA of each gene was standardized per the amount of mRNA of β-actin, since the level of expression of this gene is relatively constant for different types of cells. The relative level of gene expression was determined using the Bio-Rad iQ5 2.0 software (Bio-Rad Laboratories Inc., United States).

The following DNA primers were used in the present study:

Her2 forward – 5'-AGCAATGGTGTCAGTATCCAGGCT-3',
Her2 reverse – 5'-TGCAAATGGACAAAGTGGGTGTGG-3',
CCNB1 forward – 5'-AGGAAGAGCAAGCAGTCAGACCAA-3',
CCNB1 reverse – 5'-GCAGCATCTTCTTGGGCACACAAT-3',
PKC forward – 5'-GCTGTCTTTCACGATGCCCC-3',
PKC reverse – 5'-CACCCGACGACCCTGAGAGA-3',
β-actin forward– 5'-ACCAACTGGGACGACATGGAGAAA-3',
β- actin reverse – 5'-TTAATGTCACGCACGATTTCCCGC-3'.

MTT test

The number of living cells was determined using the colorimetric method based on oxidation of 3-[4,5-dimethylthiazol-2-yl]-2,5-diphenyl tetrazolium bromide (MTT) in mitochondria of living cells [46]. On day 6 after siRNA transfection, the cells were seeded from the 6-well plate to a 96-well plate, with density being 1.5×10^3 (KB-3-1), 7.5×10^3 (SK-N-MC), and 3×10^3 cells/well (MCF-7), followed by incubation over a period varying from 1 to 6 days at 37°C. Then, the MTT solution was added to the cells until the concentration reached 0.5 mg/ml. After 3 h, the culture medium was removed; the resulting formazan crystals were dissolved in dimethyl sulfoxide (100 μl/well), and the optical density of the solution was measured on a Multiscan RC multichannel photometer (Labsystems) at wavelengths of 570 and 630 nm. The results were represented as the relative proliferation rate, i.e., the rate of cell division in the sample standardized to the cell division rate in the control (taken as 100%). The proliferation rate was calculated using the following formula: $V = (D_{12} - D_7)/(\Delta t)$, where D_{12} and D_7 are the optical densities in the wells 12 and 7 days after transfection, respectively; Δt is the time interval of cell observation (i.e., 12–7 = 5 days).

Microscopic analysis

For the microscopic analysis, SK-N-MC neuroblastoma cells after transfection with siRNA preparations for 48 h were seeded (10^5 cells/well) in round coverslips with a diameter of 15 mm, which were placed into the wells of a 24-well plate. The oligofectamine-only treated cells, intact cells, and the cells transfected with siScr (controls) were incubated for 24, 48, and 72 h; whereas the cells transfected with siRNA siCyc, siPKC were incubated

for 3, 5, 7, and 12 days. After the incubation, the cells were washed with 0.5 ml of DMEM and immobilized without taking them off the coverslip with 4% paraformaldehyde in a DMEM medium. Cell preparations were then washed with PBS, treated with acetone for 5 min, and washed with PBS, again. Then, hematoxylin or Feulgen staining [47] was carried out, and the cells were incorporated into polystyrene. The stained preparations of SK-N-MC neuroblastoma cells were studied in a DM2500 light microscope with a DFC420 digital camera (Leica, Germany). Mitosis calculation was performed upon zooming ×40.

RESULTS

The *Her2*, *CCNB1*, and *PKC* genes encoding the most significant regulatory proteins of the cell cycle were selected as targets for siRNAs, since their hyperexpression is frequently associated with the emergence of various tumor diseases.

Analysis of the expression levels of the *Her2*, *CCNB1*, and *PKC* genes in KB-3-1, SK-N-MC, and MCF-7 cell lines after transfection with corresponding siRNAs

The expression of target genes was determined in the following cell lines: KB-3-1 (uterine neck carcinoma), SK-N-MC (neuroblastoma), and MCF-7 (breast adenocarcinoma). We had previously detected a high mRNA level of the *CCNB1* gene in these cell lines and a slightly lower mRNA level of the *Her2* gene; an increased mRNA level of the *PKC* gene was revealed only in MCF-7 cells [41].

The effect of siRNAs on the expression of target genes was analyzed on the basis of the following scheme: siRNA at a concentration of 200 nm was transfected to the cells; Oligofectamin™ (SK-N-MC) and Lipofectamin 2000™ (other cell lines) being used as transfection agents. 1–12 days after transfection (upon long-term experiments, the control cells were reseeded once per 3–4 days), real-time PCR was used to extract the total RNA from the cells and determine the level of specific mRNAs; the β-actin gene was used as an internal standard. The specificity of the siRNA action was inspected on the basis of the retention of the mRNA levels of β-actin and its nonhomologous target genes (*Fig. 1*).

As can be seen in *Fig. 1*, all siRNAs efficiently and specifically silence their target genes in the cell lines used; maximum silencing (up to 97–99%) being observed 72 h after transfection. siHer decreased the expression of the *Her2* gene only, having no effect on the expression of the *CCNB1* and *PKC* genes, as well as that of β-actin. Similar results were obtained when using siRNA siCyc and siPKC. Random-sequence siRNA (siScr) caused no changes in the expression level of target genes, as well.

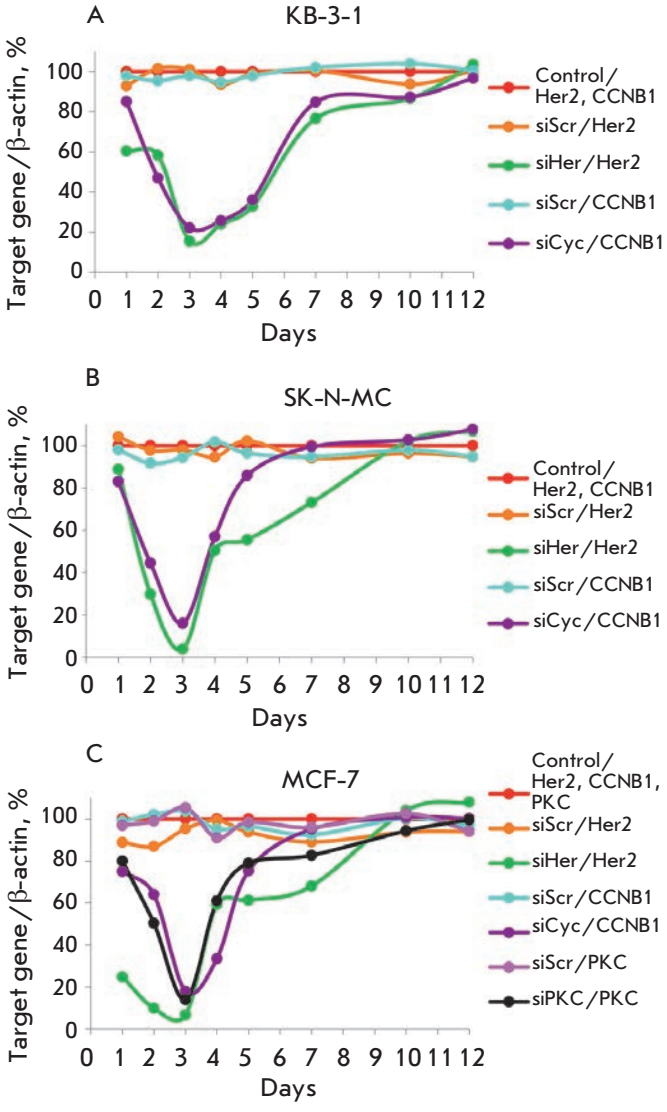

Fig. 1. Relative levels of *Her2*, *CCNB1* and *PKC* mRNAs in KB-3-1 (A), SK-N-MC (B), and MCF-7 (C) cells 1 – 12 days after siRNAs (200 nM) transfection. The level of *β-actin* mRNA was used as an internal standard. Mean values obtained from three independent experiments. The standard error of the mean < 10%. Control/*gene(s)* is the relative mRNA level of *genes* in the control cells. siRNA/*gene(s)* is the relative mRNA level of *gene(s)* in the cells after siRNA transfection.

siHer and siCyc reduced the mRNA levels of the *Her2* and *CCNB1* genes in all of the cell lines used. Seventy-two hours after transfection, the mRNA level of the *Her2* gene was equal to 15% in KB-3-1 cells, 4% in SK-N-MC cells, and 7% in the MCF-7 cell line with respect to the control. The mRNA level of the *CCNB1* gene in the KB-3-1, SK-N-MC, and MCF-7 cells 72 h after transfection with siCyc decreased to 22, 16, and

18%, respectively, as compared to the control. siPKC transfection reduced the mRNA level of the *PKC* gene in MCF-7 cells to 14% (*Fig. 1*). The data obtained attest to the fact that siHer, being an inhibitor of the *Her2* gene, has the highest efficiency in SK-N-MC and MCF-7 cell lines, whereas siCyc most considerably decreases the mRNA level of the *CCNB1* gene in SK-N-MC and MCF-7 cells (*Fig. 1*). Starting with day 4 after transfection, the mRNA level of all genes gradually increased and returned to the initial value by day 7–12 after transfection (*Fig. 1*).

As can be seen in *Fig. 1*, the kinetic curves of the relative mRNA level of the *Her2*, *CCNB1*, and *PKC* genes after transfection with specific siRNAs are U-shaped. The following regions can be visually isolated in each curve: a region corresponding to the decrease in the level of specific mRNA (days 1–3), the region where its amount increases (days 3–7), and the region in which the amount of target mRNA is stabilized at a level corresponding to its level in the control cells (days 7–12). The gradual recovery of the initial mRNA level in cells is probably associated with cell division, which results in the reduction of siRNA concentration in cytoplasm, and, therefore, in attenuation of the RNA interference effect.

Thus, the siRNAs used provide efficient silencing of the *Her2*, *CCNB1* and *PKC* genes in human tumor cells. The analysis of their expression at the mRNA level has demonstrated the specificity of the action of the siRNAs selected.

Proliferation of KB-3-1, SK-N-MC, and MCF-7 cell lines after the recovery of the initial level of *Her2*, *CCNB1*, and *PKC* gene expression

It was shown earlier that the observed anti-proliferative effect of the siRNAs under study is conditioned by the retardation of cell division rather than their death [41]. In this study, we analyzed the changes in the proliferation rate of the cells after the initial level of target gene expression was recovered. The dependence of the proliferation rate of KB-3-1, SK-N-MC, and MCF-7 cells on the expression level of *Her2*, *CCNB1*, and *PKC* was estimated using the MTT test over a period ranging from day 7 to day 12 after transfection of the corresponding siRNA (200 nm); the cell proliferation rate in the control samples was taken as 100% (*Table 1*). As expected, transfection of nonspecific siScr does not result in a reliable change in the cell proliferation rate.

The proliferation rate of the KB-3-1 cell line after the initial expression levels of target genes (*Her2*, *CCNB1*) is virtually the same as that of the control cells. On the contrary, the proliferation rate of SK-N-MC and MCF-7 cells remained low even after the expression of target genes (*Her2*, *CCNB1*) was recovered. Thus, after siHer transfection, the division rate of SK-N-MC and MCF-7 cells over the period of 7–12 days was equal to 36 and 78% of its level in the control, respectively. The proliferation rate of SK-N-MC and MCF-7 cells exposed to the action of siCyc remained at a level of 14 and 73% of its level in the control, respectively; that of siPKC was equal to 9 and 79% (*Table 1*). It should be mentioned that siPKC has the most pronounced and longest antiproliferative effect (10-fold deceleration of the division rate) on SK-N-MC neuroblastoma cells, in which the expression of the *PKC* gene cannot be detected with the methods used (see [41]). siHer and siCyc had also the most pronounced antiproliferative effect on SK-N-MC line cells. Thus, specific silencing of the genes that are responsible for cell-cycle regulation is capable of considerably decelerating and even terminating SK-N-MC cell division.

As can be seen in *Table 1*, the cell lines used can be conventionally divided into three groups: the cells in which the proliferation rate is completely recovered (KB-3-1); those in which the proliferation rate remains considerably reduced (SK-N-MC); and those in which the proliferation rate remains insignificantly reduced, after the recovery of the initial mRNA level of the target genes. The temporary silencing of the *Her2*, *CCNB1*, and *PKC* genes is unlikely to result in irreversible changes in the regulation paths of KB-3-1 cell division; therefore, the cell proliferation rate is recovered, together with the recovery of the mRNA levels of these genes. The situation is different with SK-N-MC cells: the temporary silencing of these genes apparently results in irreversible changes in the paths of proliferation regulation; therefore, the proliferation rate remains

Table 1. The effect of siRNAs on the proliferation of KB-3-1, SK-N-MC, and MCF-7 cells

siRNA, 200 nM	Proliferation rate*, %		
	KB-3-1	SK-N-MC	MCF-7
Control**	100 ± 7	100 ± 6	100 ± 3
SiScr	113 ± 10	90 ± 7	93 ± 6
SiHer	123 ± 8	36 ± 9	78 ± 2
SiCyc	112 ± 9	14 ± 4	73 ± 2
SiPKC	117 ± 14	9 ± 3	79 ± 2

* The average values over the results of three independent experiments ± the standard deviation are presented.
** Cells treated with a transfection agent only.

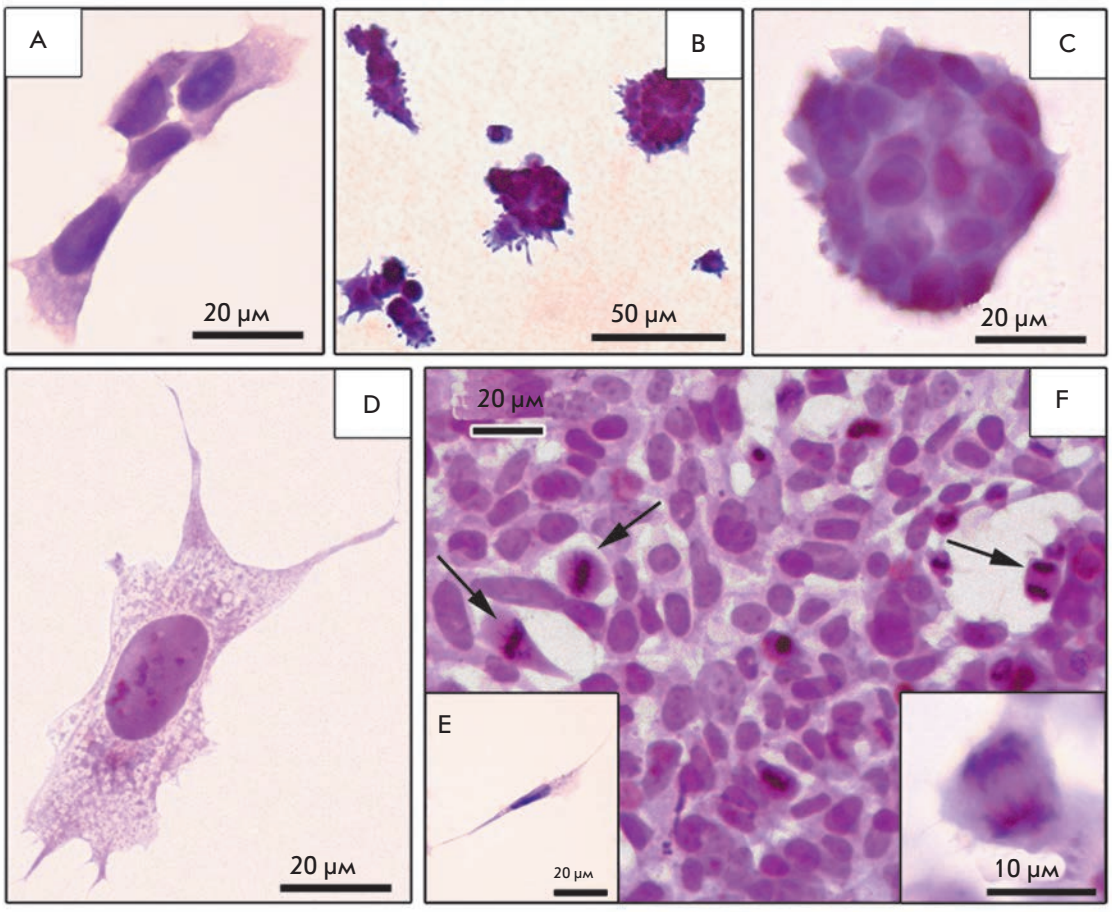

Fig. 2. Morphology of neuroblastoma SK-N-MC cells on coverslips (total preparations). A – "islet" cells; B, C – dense spherical cell aggregations; D – neuron-like cell; E – fusiform cell; F – mitoses (indicated by arrows) in the culture cells 5 days after siCyc (200 nM) transfection; the sidebar shows the divergence of the mitotic chromosomes. Staining by hematoxylin.

considerably reduced even after the mRNA levels of the target genes are recovered. In MCF-7 cells, suppression of proliferation has an intermediate character; the division rate is reduced, although not completely. This fact likely demonstrates that the role of the *Her2*, *CCNB1*, and *PKC* genes in the paths of proliferation regulation differs for these cell lines in terms of its significance.

The results obtained attest to the fact that the *PKC and CCNB1* genes are the most efficient targets for gene-targeted action on SK-N-MC neuroblastoma cells and *CCNB1* breast cancer cells, respectively. In SK-N-MC cells, the antiproliferative effect of silencing the *CCNB1* and *PKC* genes is considerably higher than that conditioned by siHer (*Table 1*).

Effect of *CCNB1* and *PKC* gene silencing on the morphological characteristics of the SK-N-MC cell culture

The study demonstrated that the most efficient silencing of the *CCNB1* and *PKC* genes is observed in a SK-N-MC human neuroblastoma cell culture (*Table 1*); therefore, we performed a microscopic study of the changes in the morphology and division of cells of this line under the action of siCyc and siPKC.

A SK-N-MC neuroblastoma cell culture treated with Oligofectamin™ (control) after 24 h of incubation is represented by different cell types (*Fig. 2*). A portion of the cells form a monolayer with "growth islets," another part of the cells forms small, dense globular aggregates. The "growth islets" of different sizes consist of flat polygonal mononuclear cells with homogeneously stained cytoplasm and non-stained vacuoles (*Fig. 2A*) connecting into networks on the coverslip surface. In most cases, the "growth islets" have appreciably distinguishable boundaries; a tendency towards merging being observed. Small spherical cells with a large nucleus, an intensely stained cytoplasm, and smooth surface can be sparsely found in the "growth islets." Spherical cell aggregates are located on the coverslip both individually and in clusters, their appearance reminding mulberries. Aggregation cells are small, intensely stained, with needle-like or rounded sprouts on the surface; cells with a smooth surface occur, as well (*Figs. 2B, C*). The cells lie tightly against each another, making it impossible to count them on total preparations. The third type of

cells that are present in the SK-N-MC neuroblastoma cell culture is large spread cells of neuron-like shape with a pale stained vacuolized cytoplasm (*Fig. 2D*). The cells contain 1–2 nuclei; multinuclear variants occur, as well. Neuron-like cells are mostly localized between the "islet" cells and stand out against the general background by their isolation. Only in extremely rare cases do they contact with the cells of other types, and even if they are localized in the center of the "growth islets," the space around them is empty.

Small, strongly elongated spindle- or needle-shaped cells with sparse vacuoles in the cytoplasm also occur in the SK-N-MC neuroblastoma cell culture (*Fig. 2E*). Thus, four morphological types of cells are revealed in preparations of SK-N-MC neuroblastoma cells at the light-optical level, no transition forms being observed upon the used method of analysis.

When incubating SK-N-MC cells treated with Oligofectamin™ for 24–72 h, the morphological characteristics of the cell types remain constant; all of the described variants being revealed on the coverslips. A considerable increase in the total amount of cells on coverslips is observed due to the "islet" cells; the "growth islets" merge, and by the end of day 3 of incubation these cells represent the main mass of the culture. Multiple mitoses are observed in the "islet" SK-N-MC culture cells during the incubation for 24–72 h (*Table 2*). The variety of sizes of spherical cell aggregates, neuron-like and spindle-like cells does not noticeably change.

The comparison of preparations of intact SK-N-MC cells and Oligofectamin™-treated cells revealed no observable changes in the morphological characteristics of the cells. Treatment with a transfection agent did not result in the emergence of new variants of cells or a noticeable change in their ratio. Transfection of SK-N-MC cells with all siRNAs did not result in the emergence of new morphological cell types, either: all preparations contained the cell varieties described above at all incubation periods. Transfection of SK-N-MC cells with siScr did not result in any noticeable changes in the ratio between different types of cells during 72 h of incubation, as compared with preparations of the oligofectamin-treated culture.

A study of the preparations of SK-N-MC neuroblastoma cells obtained after different time intervals after transfection revealed distinct morphological signs of the effect of siCyc and siPKC on the vital activity of the cells. The "seeding" dosage being equal, the cells either Oligofectamin™-treated or transfected with siScr almost completely filled the surface area of the coverslip after 3 days of incubation (*Figs. 3B,D*), whereas transfection with siCyc or siPKC abruptly decelerated cell division, their number on the coverslip on the same day being incomparably smaller (*Figs. 3E,G*). The cells transfected with siCyc and siPKC were incubated for 12 days (*Figs. 3F,H*), whereas it was necessary to reseed the cells transfected with siScr and the control cells once in 3 days. The differences in the growth rate and necessity to reseed the control and siScr transfected cells rendered it impossible to compare the morphological characteristics of the culture transfected with siCyc and siPKC with the control preparations after 5–12 days of incubation. Only the preparations incubated for 72 h after transfection could be compared.

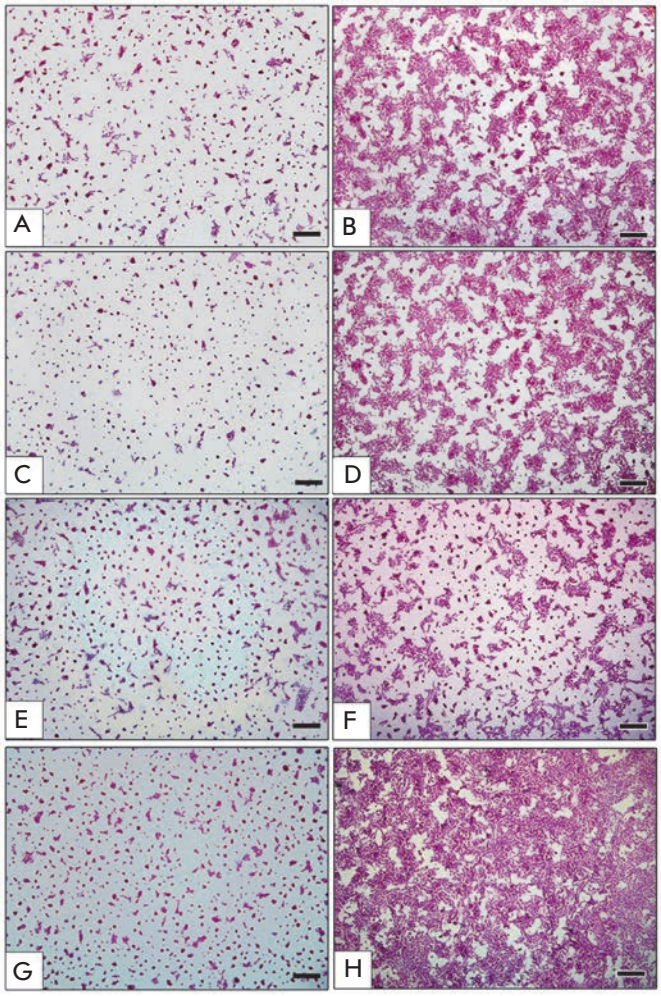

Fig. 3. Neuroblastoma SK-N-MC cells on a coverslip (total preparations). Control cells (only transfection reagent treatment): A – 1 day of incubation, B – 3 days of incubation. Transfection with 200 nM siScr: C – 1 day of incubation, D – 3 days of incubation. Transfection with siCyc: E – 3 days of incubation, F – 12 days of incubation. Transfection with siPKC: G – 3 days of incubation, H – 12 days of incubation. Staining with hematoxylin. Size bar is 200 μm.

The preparations of SK-N-MC cells transfected with siCyc and siPKC during the period contained an incomparably smaller number of "islet" cells, in comparison to the control. The major part of the population was represented by small, intensely stained cells from the globular aggregates, which included several cells at a time. Against the background of a decreasing number of "islet" cells, the relative number of neuron-like and fusiform cells was increasing. Similar to events in the control preparation, mitoses were revealed mostly in the "islet" cells; their number abruptly decreasing, especially if compared with the preparations transfected with siScr (*Table 2*).

Thus, 72 h after transfection with siCyc and siPKC, the mitotic activity of "islet" cells is considerably decreased in neuroblastoma cells and their number decreases; therefore, the ratio between the morphological types of culture cells changes and the share of neuron-like and fusiform cells increases.

Late effects (days 5–12) of the transfection of neuroblastoma cells with siCyc and siPKC differed to a certain extent. When using siCyc, the number of mitoses increased 5 days after transfection and remained at the same level over the entire observation period (*Table 2*). The cells at the mitosis stage were mostly revealed among "islet" cells (*Fig. 2E*), their number increasing, while the number of spherical cell aggregates, neuron-like and fusiform cells had not noticeably changed. It should be noted that even after 12 days of incubation, the number of neuroblastoma cells on the coverslips and the number of "islet" cells were appreciably smaller than that in the control 72 h after the transfection (*Fig. 3B,D,F*). Transfection of neuroblastoma cells with siPKC resulted in a more prolonged decrease in the mitosis number; its growth being recorded only 7 days after transfection. It continued until the end of observations (*Table 2*). Similar to the case of transfection with siCyc, mitoses were revealed mostly in the islet cells; their number increasing during the incubation. Five days after transfection with siPKC, the relative increase in the number of neuron-like and fusiform cells noted after 3 days remained constant; the number of spherical cell aggregations also did not change. The islet cells comprised the major part of SK-N-MC neuroblastoma cells 7 and 12 days after transfection; their number increased intensely due to the active mitotic division (*Table 2*). The density of cells on the coverslip 12 days after the transfection was at a maximum and exceeded that in the control and upon transfection with siCyc (*Fig. 3B,D,F,H).* Thus, transfection with siPKC results in a more prolonged blocking of mitotic division of SK-N-MC neuroblastoma cells, in comparison with siCyc transfection; however, further growth in the number of mitoses is more pronounced and results in a more intense cell culture growth. The analysis of the morphological characteristics of SK-N-MC neuroblastoma demonstrates that "islet cells" comprising the main part of the cell population, their division being suppressed, are the main target of siCyc and siPKC. The effect of siPKC appears to be more complex as compared with that of siCyc, requiring further investigation. The results of a microscopic study of SK-N-MC cell growth after silencing of the *CCNB1* and *PKC* genes (*Fig. 3*) agree well with the data on the effect of this silencing on the proliferation rate of these cells (*Table 1*).

Table 2. The number of mitoses in SK-N-MC cells 1–12 days after transfection with siCyc and siPKC (200 nm)

Day	Number of mitoses per 1,000 cells				
	Control*	SiScr	SiCyc	SiPKC	Control without transfecting agent
1	14 ± 5	16 ± 8	-	-	-
2	40 ± 16	25 ± 7	-	-	22 ± 15
3	21 ± 10	33 ± 12	15 ± 11	16 ± 7	-
5	-	-	30 ± 12	20 ± 11	-
7	-	-	28 ± 6	35 ± 5	-
12	-	-	30 ± 6	49 ± 14	-

* Cells treated with a transfection agent only.
(-) – not determined.

DISCUSSION

Today, interfering RNAs are regarded as potential therapeutic agents; a number of preparations based on them have been going through different stages of clinical trials [48]. An urgent problem is revealing the targets in which the short-term silencing results in irreversible consequences for a cancer cell, such as terminal differentiation, apoptosis, or long-term suppression of their proliferation. An appreciably large body of data on successful temporal silencing of the genes responsible for the emergence of oncologic diseases, including the *Her2*, *CCNB1,* and *PKC* genes, has been published recently [4, 6, 7, 49]. It has been demonstrated that this silencing results in a decrease in the proliferation rate of cancer cells; however, most experiments were confined to incubation of up to 96 h, whereas the fall in the mRNA level of the target gene under the action of siRNA is retained for up to 4–5 days. There had been no data concerning the duration of the effect of siRNA

on *Her2, CCNB1,* and *PKC* gene expression; therefore, we were the first to study the changes in the expression level of these genes 12 days after transfection with specific siRNAs. We were able to demonstrate that a maximum decrease in the expression level of the *Her2*, *CCNB1*, and *PKC* genes in KB-3-1, SK-N-MC, and MCF-7 cells is observed 72 h after siRNA transfection. The silencing of these genes, as it was earlier shown in [41], slows to a different extent the proliferation of tumor cells from day 3 to day 7 of their cultivation after siRNA transfection. The analysis of the kinetics of the changes in the levels of specific mRNAs has demonstrated that the initial mRNA levels are recovered as early as on day 5–day 7 after a single transfection with the corresponding siRNA, which is likely determined by the lifetime of siRNA in a cell (*Fig. 1*). The duration of the antiproliferative effect of siRNA in various cell lines considerably varies. The determination of the cell proliferation rate over a period of day 7–day 12 after siRNA transfection demonstrated that after the initial level of the target gene expression is recovered, the proliferation rate of KB-3-1 cells does not differ from the rate of cell growth in the control (that of nontreated cells, that of the cells subjected to the action of the transfection agent only, and those transfected with a random siRNA (SiScr)). The growth of MCF-7 cells transfected with specific siRNAs remained low to a certain extent as compared with the control. Thus, regardless of the pronounced antiproliferative effect of siRNA preparations revealed, in order to limit the growth of these cell lines, it is necessary to sustain the decreased level of target gene expression. This can be achieved by additional introduction of the corresponding siRNA into the cells or using short interfering hairpin RNA (shRNAs), which are expressed immediately in the target cells after their transduction with recombinant viruses (adeno-, adeno-associated , lenti- and retroviruses). However, the issue of safety in using recombinant viruses for therapeutic purposes remains far from settled [50–52].

We found that the temporary silencing of the *Her2, CCNB1,* and *PKC* genes in a SK-N-MC cell culture results in considerable slowing of cell division even after the initial mRNA level of target genes is recovered (*Table 1*). The *CCNB1* and *PKC* genes serve as the most efficient target to achieve long-term suppression of proliferation in SK-N-MC neuroblastoma cells (*Table 1*). The pronounced antiproliferative effect (5–10 times) of the short-term silencing of these genes remains for up to 12 days of incubation. It should be mentioned that the long-term antiproliferative effect of siPKC on SK-N-MC cells is quite unexpected, since no hyperexpression of the *PKC* gene is observed in these cells [41]. Nevertheless, the long-term antiproliferative effect of this specific inhibitor in SK-N-MC cells has been demonstrated; the elucidation of its reasons requires additional studies.

The proliferation rate of SK-N-MC cells remains at a considerably low level even after siCyc and siPKC have been removed from the cells and the level of their target genes returns to the initial level. This result is rather unexpected. It appears that this phenomenon can be interpreted taking into account the specific pattern of gene expression in cells of neuronal origin (to which SK-N-MC cells belong), the changes in the expression pattern under the action of the temporary silencing of target genes, and its subsequent reactivation. Thereby, even a short-term expression inhibition of the *CCNB1* or *PKC* gene is likely to result in a very slow recovery of the cell proliferation rate (or in its complete blocking) even after the initial level of the products of each target gene is recovered. It is already known that a deficiency in protein p53 is observed in this cell line; i.e., they do not contain the most important participant of the apoptosis induction chain, which appears to play a significant role in their uncontrollable proliferation [53]. It is possible that the absence of this participant in the regulatory cascade is one of the key reasons behind the difference between the consequences of a short-term inhibition of *CCNB1* and *PKC* gene expression in this cell line and the other ones that were used; their proliferation rate having recovered after the level of the target gene had returned to its initial level. It would be of interest to study the joint action of siRNAs and p53 inhibitors on the proliferation of cells of different lines. As shown by the results obtained, after the inhibition of *CCNB1* and *PKC* gene expression in a SK-N-MC cell culture, the share of neuron-like and fusiform cells characterized by a lower mitotic activity as compared with other morphological cell types in the culture was high to a certain extent. An increase in the share of these cells may attest to the induction of the initial events of cell differentiation (either reversible or irreversible), which may also be one of the reasons for the so prolonged antiproliferative effect of the selected siRNAs. To verify these hypotheses, it is necessary to study the behavior of the cells as exposed to the action of siRNAs for a longer period of time. Nevertheless, the data on long-term proliferation suppression may point to an important role played by the *CCNB1* and *PKC* genes in the aggressive proliferation of SK-N-MC.

A study of the morphology of SK-N-MC cells 3–12 days after transfection has demonstrated that temporary inhibition of the expression of the *Her2, CCNB1,* and *PKC* genes does not result in their death or terminal differentiation (which is demonstrated by the retention of different cell types in the population) and slows cell division. The gradual increase in the total amount of cells in the preparations transfected with

specific siRNAs and, in particular cells at the mitosis stage by days 10–12 of incubation, points to the fact that the duration of the antiproliferative effect of these siRNAs on neuroblastoma cells is likely limited to 12–15 days.

In this study, it was demonstrated using genetic and morphological material that the *Her2*, *CCNB1*, and *PKC* genes are efficient targets for specifically addressed siRNAs in neuroblastoma cells, since the decrease in the expression level of target genes attained with their aid results in efficient and long-term proliferation inhibition. The use of siRNAs to control the growth of tumor cells that survive chemotherapy may become one of the aspects of a complex therapy upon cancer and neuroblastoma, in particular. Until recently, low-molecular-weight compounds found empirically have been used as antitumor agents. Interfering RNAs have the potential to become the new generation of preparations that considerably outperform known ones in terms of specificity, efficacy, and nontoxicity. ●

The authors are grateful to M.I. Meshchaninova and A.G. Veniaminova for synthesis of siRNAs used in this work and A.V. Vladimirova for the assistance in dealing with cell cultures.

This work was supported by the Programs of the Russian Academy of Sciences "Molecular and Cell Biology" (grant № 22-1), "Fundamental Science for Medicine" (grant № 37), the President's Support of Leading Scientific Schools (grant № NSh-7101.2010.4), Russian Foundation for Basic Research (grant № 11-04-01017-a), and the Integration Research Program of the Russian Academy of Sciences, Siberian Branch (grant № 41).

REFERENCES

1. Sulic S., Panic L., Dikic I., Volarevic S. // Croat. Med. J. 2005. V. 46. P. 622–638.
2. Sandhu C., Slingerland J. // Cancer Detect. Prev. 2000. V. 24. P. 107–118.
3. Malumbres M., Hunt S.L., Sotillo R., Martin J., Odajima J., Martin A., Dubus P., Ortega S., Barbacid M. // Adv. Exp. Med. Biol. 2003. V. 532. P. 1–11.
4. Yuan J.P., Yan R.L., Kramer A., Eckerdt F., Roller M., Kaufmann M., Strebhardt K. // Oncogene. 2004. V. 23. P. 5843–5852.
5. Minana M.D., Felipo V., Cortes F., Grisolia S. // FEBS Lett. 1991. V. 284. P. 60–62.
6. Wu T.T., Hsieh Y.H., Hsieh Y.S., Liu J.Y. // J. Cell. Biochem. 2008. V. 103. P. 9–20.
7. Faltus T., Yuan J.P., Zimmer B., Kramer A., Loibl S., Kaufmann M., Strebhardt K. // Neoplasia. 2004. V. 6. P. 786–795.
8. Vermeulen K., van Bockstaele D.R., Berneman Z.N. // Cell Prolif. 2003. V. 36. P. 131–149.
9. Tuschl T. // Chembiochem. 2001. V. 2. P. 239–245.
10. Tabara H., Grishok A., Mello C.C. // Science. 1998. V. 282. P. 430–431.
11. Elbashir S.M., Harborth J., Lendeckel W., Yalcin A., Weber K., Tuschl T. // Nature. 2001. V. 411. P. 494–498.
12. Yarden Y. // Oncology. 2001. V. 61. P. 1–13.
13. Nishizuka Y. // Nature. 1984. V. 308. P. 693–698.
14. Ali A.S., Ali S., El-Rayes B.F., Philip P.A., Sarkar F.H. // Cancer Treat. Rev. 2009. V. 35. P. 1–8.
15. Robert N.J., Favret A.M. // Hematol. Oncol. Clin. North Am. 2007. V. 21. P. 293–302.
16. Meric F., Hung M.C., Hortobagyi G.N., Hunt K.K. // J. Am. Coll. Surg. 2002. V. 194. P. 488–501.
17. Aaltonen K., Amini R.M., Heikkila P., Aittomaki K., Tamminen A., Nevanlinna H., Blomqvist C. // Br. J. Cancer. 2009. V. 100. P. 1055–1060.
18. Koivunen J., Aaltonen V., Peltonen J. // Cancer Lett. 2006. V. 235. P. 1–10.
19. Martiny-Baron G., Fabbro D. // Pharmacological Res. 2007. V. 55. P. 477–486.
20. Revillion F., Bonneterre J., Peyrat J.P. // Eur. J. Cancer. 1998. V. 34. P. 791–808.
21. Williams T.M., Weiner D.B., Greene M.I., Maguire H.C. // Pathobiology. 1991. V. 59. P. 46–52.
22. Wright C., Angus B., Nicholson S., Sainsbury J.R., Cairns J., Gullick W.J., Kelly P., Harris A.L., Horne C.H. // Cancer Res. 1989. V. 49. P. 2087–2090.
23. Tandon A.K., Clark G.M., Chamness G.C., Ullrich A., Mcguire W.L. // J. Clin. Oncol. 1989. V. 7. P. 1120–1128.
24. Slamon D.J., Clark G.M., Wong S.G., Levin W.J., Ullrich A., Mcguire W.L. // Science. 1987. V. 235. P. 177–182.
25. Gulati S., Ytterhus B., Granli U.S., Gulati M., Lydersen S., Torp S.H. // Diagn. Pathol. 2010. V. 5. P. 18–26.
26. Soria J.C., Jang S.J., Khuri F.R., Hassan K., Lin D., Hong W.K., Mao L. // Cancer Res. 2000. V. 60. P. 4000–4004.
27. Yasuda M., Takesue F., Inutsuka S., Honda M., Nozoe T., Korenaga D. // J. Cancer Res. Clin. Oncol. 2002. V. 128. P. 412–416.
28. Song Y.M., Zhao C.L., Dong L.J., Fu M., Xue L., Huang Z., Tong T., Zhou Z., Chen A., Yang Z., et al. // Carcinogenesis. 2008. V. 29. P. 307–315.
29. Berchuck A., Rodriguez G., Kinney R.B., Soper J.T., Dodge R.K., Clarkepearson D.L., Bast R.C. // Am. J. Obstet. Gynecol. 1991. V. 164. P. 15–21.
30. Berchuck A., Kamel A., Whitaker R., Kerns B., Olt G., Kinney R., Soper J.T., Dodge R., Clarke-Pearson D.L., Marks P., et al. // Cancer Res. 1990. V. 50. P. 4087–4091.
31. Marks J.R., Humphrey P.A., Wu K., Berry D., Bandarenko N., Kerns B.J.M., Iglehart J.D. // Ann. Surg. 1994. V. 219. P. 332–341.
32. Carr J.A., Havstad S., Zarbo R.J., Divine G., Mackowiak P., Velanovich V. // Arch. Surg. 2000. V. 135. P. 1469–1474.
33. Casalini P., Iorio M.V., Galmozzi E., Menard S. // J. Cell. Physiol. 2004. V. 200. P. 343–350.
34. Yamamoto T., Ikawa S., Akiyama T., Semba K., Nomura N., Miyajima N., Saito T., Toyoshima K. // Nature. 1986. V. 319. P. 230–234.
35. Pines J., Hunter T. // Ciba Fdn. Symp. 1992. V. 170. P. 187–204.
36. Sutherland R.L., Watts C.K.W., Musgrove E.A. // J. Steroid Biochem. Mol. Biol. 1993. V. 47. P. 99–106.
37. Gomez L.A., de las Pozas A., Reiner T., Burnstein K.,

Perez-Stable C. // Mol. Cancer Ther. 2007. V. 6. P. 1534–1543.
38. Sarafan-Vasseur N., Lamy A., Bourguignon J., Le Pessot F., Hieter P., Sesboüé R., Bastard C., Frébourg T., Flaman J.M. // Oncogene. 2002. V. 21. P. 2051–2057.
39. Newton A.C. // Chem. Rev. 2001. V. 101. P. 2353–2364.
40. Clemens M.J., Trayner I., Menaya J. // J. Cell Sci. 1992. V. 103. P. 881–887.
41. Akimov I.A., Chernolovskaya E.L. // Mol. Biol. 2010. V. 44. P. 89–96.
42. Amarzguioui M., Rossi J.J., Kim D. // FEBS Lett. 2005. V. 579. P. 5974–5981.
43. Hohjoh H. // FEBS Lett. 2004. V. 557. P. 193–198.
44. Matveeva O., Nechipurenko Y., Rossi L., Moore B., Saetrom P., Ogurtsov A.Y., Atkins J.F., Shabalina S.A. // Nucl. Acids Res. 2007. V. 35. P. 1–10.
45. Chattopadhyay N., Kher R., Godbole M. // Biotechniques. 1993. V. 15. P. 24–26.
46. Carmichael J., Degraff W.G., Gazdar A.F., Minna J.D., Mitchell J.B. // Cancer Res. 1987. V. 47. P. 936–942.
47. Pearse E. Gistokhimia (Histochemistry). Moscow: Inostrannaya literatura, 1962. 962 p.
48. Castanotto D., Rossi J.J. // Nature. 2009. V. 457. P. 426–433.
49. Choudhury A., Charo J., Parapuram S.K., Hunt R.C., Hunt D.M., Seliger B., Kiessling R. // Int. J. Cancer. 2004. V. 108. P. 71–77.
50. Blankinship M.J., Gregorevic P., Chamberlain J.S. // Mol. Ther. 2006. V. 13. P. 241–249.
51. Gao G.P., Wilson J.M., Wivel N.A. // Adv. Virus Res. 2000. V. 55. P. 529–543.
52. Snyder R.O., Flotte T.R. // Curr. Opin. Biotechnol. 2002. V. 13. P. 418–423.
53. Choi M.S., Yuk D.Y., Oh J.H., Jung H.Y., Han S.B., Moon D.C., Hong J.T. // Anticancer Res. 2008. V. 28. P. 3777–3784.

Characteristics of Artificial Virus-like Particles Assembled *in vitro* from Potato Virus X Coat Protein and Foreign Viral RNAs

M. V. Arkhipenko[1], E. K. Petrova[1], N. A. Nikitin[1], A. D. Protopopova[2,3], E. V. Dubrovin[3], I. V. Yaminskii[2,3], N. P. Rodionova[1], O. V. Karpova[1]*, J. G. Atabekov[1,4]

[1] Biology Department, Lomonosov Moscow State University

[2] Advanced Technologies Center

[3] Physical Department, Lomonosov Moscow State University

[4] Belozersky Institute of Physico-Chemical Biology, Lomonosov Moscow State University

*E-mail: okar@genebee.msu.su

Received 21.04. 2011

ABSTRACT **Potato virus X (PVX) and some other potexviruses can be reconstituted *in vitro* from viral coat protein (CP) and RNA. PVX CP is capable of forming viral ribonucleoprotein complexes (vRNP) not only with homologous, but also with foreign RNAs. This paper presents the structure and properties of vRNP assembled *in vitro* upon incubation of PVX CP and RNAs of various plant and animal viruses belonging to different taxonomic groups. We have shown that the morphology and translational properties of vRNPs containing foreign (heterologous) RNA are identical to those of homological vRNP (PVX RNA – PVX CP). Our data suggest that the assembly of the "mixed" vRNP *in vitro* could be started at the 5'-proximal region of the RNA, producing a helical structure of vRNPs with foreign nucleic acids. The formation of heterologous vRNP *in vitro* with PVX CP appears not to require a specific 5' end RNA nucleotide sequence, and the PVX CP seems to be able to pack foreign genetic material of various sizes and compositions into artificial virus-like particles.**

KEYWORDS **plant viruses; RNA; viral ribonucleoproteins; translation activation.**

ABBREVIATIONS **PVX – Potato virus X; CP – coat protein; vRNP – viral ribonucleoprotein; MP – movement protein; BMV – Brome mosaic virus; PAMV – Potato aucuba mosaic virus; TMV – Tobacco mosaic virus; NMV – Narcissus mosaic virus; AltMV – Altenathera mosaic virus.**

INTRODUCTION

The protein capsid of a number of phytoviruses consists of identical coat protein subunits folded on the basis of helical symmetry. Genomic viral RNA is helically arranged between the turns of coat protein subunits and follows their folding. The possibility of reversible dissociation of virions into coat proteins and RNA followed by the *in vitro* self-assembly of viral ribonucleoproteins (vRNP) is an important feature of a number of viruses. As a result, the structure and biological activity of the virus can be reconstituted. The self-assembly (repolymerization) of a low-molecular-weight coat protein can occur in the absence of RNA, yielding particles with a structure identical to that of viruses, but possessing an unlimited length [3].

The self-assembly procedure enables one to obtain a "mixed" vRNP consisting of the viral coat protein and a heterologous RNA [4, 5]. The fact that it is possible to construct viruses containing foreign RNA creates the potential for using a "mixed" artificial vRNP to target cells and organs of plants and, possibly, animals with foreign RNA. It is convenient to use plant viruses to form "mixed" vRNPs, since they are highly stable, completely biologically safe (there are no pathogens common to both plants and animals) and the procedure of vRNP assembly is a low-cost one due to the exceptionally high level of accumulation of a number of viruses in an infected plant (4–10 g/kg of leaves).

Another advantage of vRNP is the possibility of controllable activation of the translation of the RNA encapsulated in the coat protein. Viruses and a "mixed" vRNP can change their structure under the effect of a number of factors (pH shift, phosphorylation, and the presence of certain virus-specific activating proteins).

The spiral viruses of plants, which are rather highly stable at high temperatures, non-physiological pH values of the environment and in the presence of hydro-

lytic enzymes, are preferable for the construction of vRNP. Moreover, the length of a spiral virus depends on the size of the nucleic acid; as opposed to isometric viruses, hence, vRNP formed in vitro can include RNA of unlimited length. Looking ahead, it is reasonable to assume that the spiral phytoviruses that are modified and reconstructed in a "mixed" manner can serve as containers to store and deliver "therapeutic" genes and pharmaceutical agents into cells [3].

Potato virus X (PVX) is one of the phytoviruses with a spiral structure, a typical representative of *Potexvirus* genus of the family *Flexiviridae*. PVX virions are flexible thread-like bodies 515 nm long and 13.5 nm in diameter. A viral particle contains approximately 1350 helically folded identical coat protein (CP) subunits and a viral RNA enclosed between the helix turns [6]. A turn of the primary PVX helix consists of 8.9 CP subunits. The PVX genome consists of a 6345 nt single-stranded (+)-RNA [7]. The genomic RNA contains a cap at its 5' terminus and a poly(A) sequence at its 3' terminus [8]. The RNA of PVX encodes five proteins: viral replicase (molecular weight of 165 kDa) and four proteins that are responsible for the intercellular and systemic transport of the infected material; three movement proteins (MP1, MP2, and MP3, the products of the "triple gene block") with molecular weights of 25, 12, and 8 kDa, respectively; and a coat protein with a molecular weight of 25 kDa [8].

It has been shown that the coat protein of potexviruses is capable of forming vRNP *in vitro* not only with the homologous RNA, but with certain heterologous RNAs as well [9, 10].

The present study was aimed at investigating the structure and the properties of vRNP obtained *in vitro* by the incubation of PVX CP with the RNA of a number of plant and animal viruses belonging to various taxonometric groups. The RNAs of potexviruses (NMV – narcissus mosaic virus, PAMV – potato aucuba mosaic virus, AltMV – alternanthera mosaic virus), tobamovirus (TMV – tobacco mosaic virus), bromovirus (BMV – brome mosaic virus), and Mengo picornavirus (animal virus) were used as heterologous RNAs.

EXPERIMENTAL

Purification of PVX specimens, coat protein, MP1 and PVX RNA

The PVX specimen (Russian strain) was extracted from infected plants *Datura stramonium L.* according to the procedure described by Atabekov *et al.* [11]. PVX CP was obtained by salt deproteinization [12]. RNA was extracted using the phenol technique [13] with modifications. Recombinant protein MP1 was obtained according to the procedure described earlier [14].

In vitro obtainment of vRNP

In order to obtain vRNP, the RNA and the coat protein were mixed at a RNA : CP weight ratio of 1 : 10. The incubation was carried out under the standard conditions [15]: in 20 μl of a 0.01 M tris-HCl buffer, pH 7.5 at room temperature for 20 min. The reaction was stopped by adding bromophenol blue or transferring the incubation mixture into ice (0°C).

In vitro translation

RNA translation was carried out in a cell-free protein-synthesis system consisting of a wheat germ extract according to the procedure described earlier [14], in the presence of ^{35}S-methionine for 60 min at 25°C. The amount of RNA in the sample was 40 μg/μl (for Mengovirus RNA, 25 μg/μl). Recombinant MP1 for the translational activation of RNA within vRNP was added at a PVX: MP1 molar ratio = 1 : 100; i.e., 1.4 μg of MP1 per 1 μg of RNA (20 μg of the virus).

Transmission electron microscopy

The specimens (15 μl) were sorbed onto copper grids for electron microscopy, coated with formvar film (a 0.5% formvar solution in dichloroethane was used for film coating) for 15–20 s. Then, the specimens on the grids were contrasted with a 2% uranyl acetate solution and viewed on a JEOL JEM-1011 (JEOL, Japan) electron microscope at 80 kV. The images were obtained using a Gatan Erlangshen ES500W digital camera and Gatan Digital Micrograph™ software.

Atomic force microscopy (AFM)

The scanning was performed on the Nanoscope 3a (Digital Instruments, Santa Barbara, United States) and SmartSPM (Aist-NT, Russia) microscopes in air in the resonance mode. The typical scan rate was 1 Hz. Cantilevers fpN01S with a resonance frequency of 118–190 kHz, rigidity of 5.3 N/m, and guaranteed needle bending radius of 10 nm (F.V. Lukin State Research Institute of Physical Problems, Russia) were used. FemtoScan Online software (Center for Advance Technologies, Russia) was used to process and visualize AFM images. For sample preparation, 5–10 μl of the specimen at the required concentration was applied to freshly cleaved mica or highly oriented pyrolytic graphite for 5–10 min. Then, the sample was washed twice in a drop of distilled water and air-dried.

RESULTS AND DISCUSSION

A series of vRNP were obtained by *in vitro* assembly of PVX CP and the RNAs of viruses belonging to various taxonomic groups. The RNAs of the following viruses were used as heterologous RNA: four potexviruses (PVX, NMV, PAMV, and AltMV), tobamovirus (TMV),

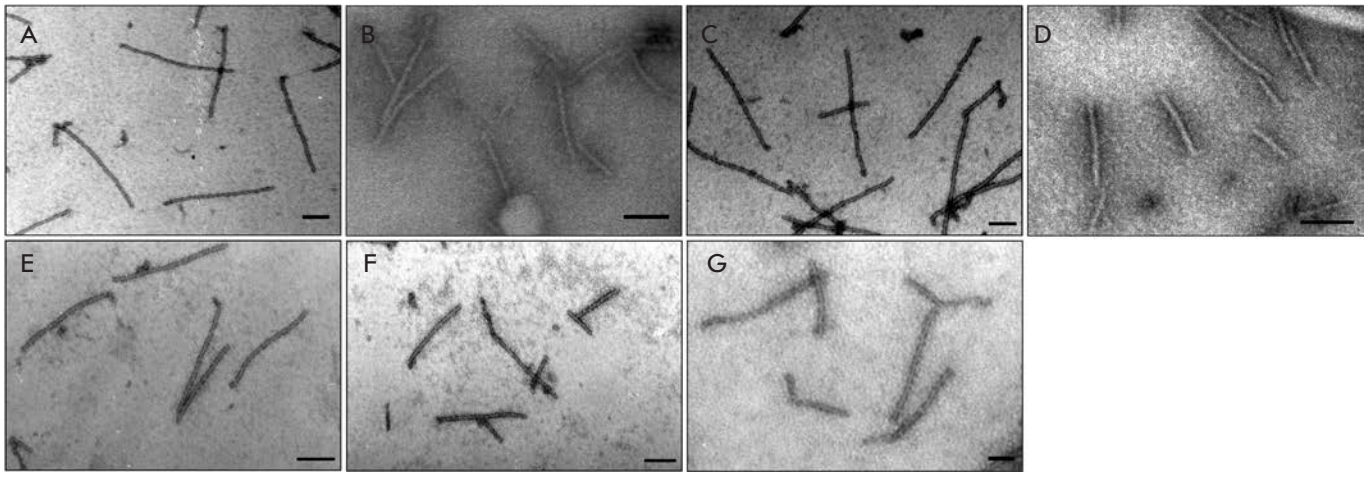

Fig. 1. TEM images of the vRNPs assembled *in vitro* from homologous or foreign RNA and PVX CP. (A) PVX RNA; (B) NMV RNA; (C) PAMV RNA; (D) total BMV RNA; (E) Mengo virus RNA; (F) TMV RNA; (G) AltMV RNA. The RNA : CP ratio (w/w) = 1 : 10. The samples were stained with 2% uranyl acetate. Scale bars represent 100 nm.

bromovirus (BMV, icosahedral virus with a functionally fragmented genome), and Mengo picornavirus (animal virus). The homologous RNA of PVX was used as a control.

The PVX CP is known not to form virus-like aggregates in the absence of RNA [16]. Particles that are morphologically indistinguishable from those obtained upon the reconstruction of PVX CP with homologous PVX RNA (*Fig. 1A*) can be observed in a transmission electron microscope (TEM) after incubation of PVX CP with heterologous RNAs of various viruses at a RNA : CP ratio = 1 : 10 (w/w) (*Figs. 1B–G*). We have already demonstrated that homologous vRNP "PVX RNA – PVX CP" are structurally identical to native PVX virions [15].

The vRNP morphology was analyzed using high-resolution AFM imaging. The vRNP particles containing homologous and heterologous RNAs were studied using this technique. The images of vRNP obtained upon the incubation of PVX CP with heterologous RNAs (*Fig. 2B–F*) are identical to those of homologous vRNP (*Fig. 2A*). The AFM data showed that the average height of a homologous and heterologous complex was 10.0 ± 0.6 and 9.9 ± 0.9 nm, respectively (*Fig. 3*). These values coincide with each other within the limits of error and correspond to the height of the native PVX (data not shown). As mentioned above, the diameter of the PVX virion is 13.5 nm [6]. The heights of the homologous complexes determined using the AFM technique agree with this value [17]. However, the height and width of a viral particle determined by AFM may vary depending on the type of probe used, the method of sample preparation, and the value of the force action. When performing measurements in air, the height of PVX virions is typically underestimated and equal to 10–11 nm. This is associated with the fact that during scanning, the microscope probe imposes pressure on the sample and flattens it to a certain extent [18].

TEM and AFM were used previously to detect single-tailed particles (STPs) with the 3' terminus of PVX RNA that was vacant of CP, and rod-like heads that resulted from the helical folding of the coat protein on the 5' terminal RNA fragment [15].

The 1 : 10 (w/w) RNA : coat protein ratio in the incubation mixture upon vRNP assembly ensures the absence of excessive unbound CP on the specimen surface. On the other hand, this amount of CP is insufficient for encapsulation of the entire RNA. As a result, AFM detects the particles in which a part of the RNA molecule within vRNP remains unbound to CP (*Figs. 2A, B, F*). It should be noted that not all short vRNPs have unbound RNA tails (*Figs. 2C–E*). This may result from the hydrolysis of the 3' RNA terminus not bound to CP due to the action of the ribonucleases in the solution or upon loading the particle suspension on the mica surface prior to the analysis.

The self-assembly of RNA with the viral CP leads to the formation of a set of vRNPs heterogeneous in length (*Fig. 3*). Particles containing a completely encapsidated RNA were not found even when analyzing the homologous vRNP (*Fig. 3A*). The most completely reconstructed PVX vRNPs reached just 300 nm, whereas the modal length of the native virions is 515 nm. The decrease in vRNP length seems to be the result of the deficiency of the coat protein in the incubation mixture (the RNA : CP ratio was 1 : 10 instead

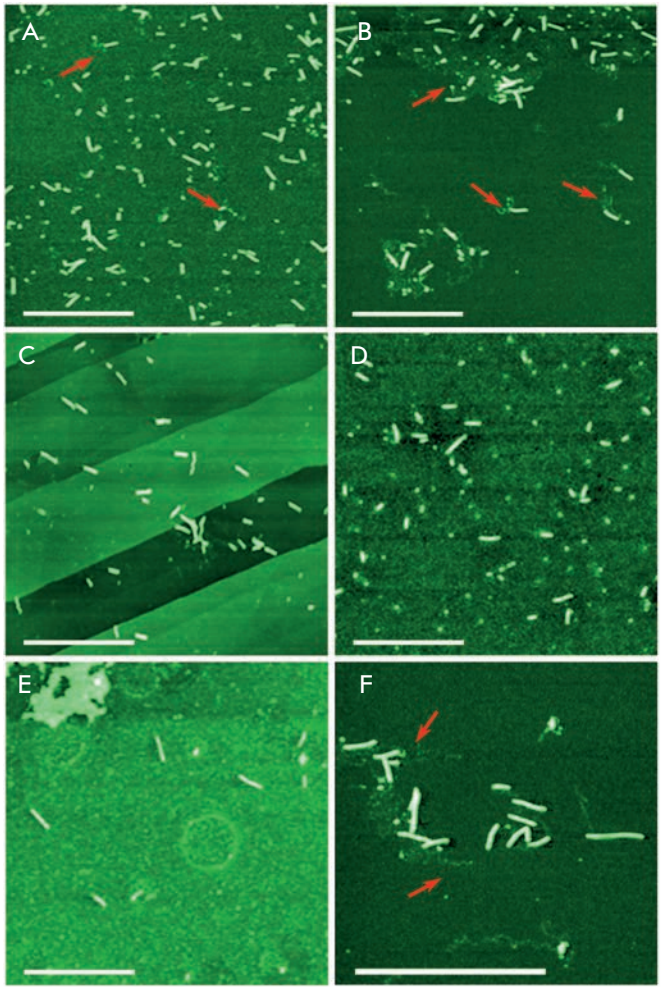

Fig. 2. AFM images of the vRNPs assembled *in vitro* from homologous or foreign RNA and PVX CP. (A) PVX RNA on mica; (B) TMV RNA on mica; (C) NMV RNA on graphite; (D) total BMV RNA on mica; (E) Mengo virus RNA on mica; (F) PAMV RNA on mica. The RNA : CP ratio (w/w) = 1 : 10. The samples were air-dried. Cantilever oscillation frequency 300–350 kHz. Arrowheads point to protein-free RNA tails. Scale bars represent 1 μm.

of the 1 : 20 ratio that is used to reconstruct the full-size PVX particles).

The increase in the amount of protein within the incubation mixture (calculated per RNA molecule) results in an increase in the length of "mixed" (heterologous) particles. Thus, at a RNA : CP ratio = 1 : 10, heterologous particles formed after protein "coating" of the RNA of potexviruses NMV, PAMV, and tobamovirus TMV were characterized by an average length of 200 nm similar to that of PVX vRNP (*Fig. 3A*). The size of the RNA of these viruses is comparable with that of PVX RNA. When using shorter viral RNAs (the total specimen of BMV RNA consists of four RNAs with lengths varying from 800 to 3234 n), the RNA : CP molar ratio decreased while the number of short particles (80–100 nm) increased (*Fig. 3B*). On the other hand, upon incubation of Mengo virus RNA (8400 n) with the PVX CP, the molar ratio increased and the average size of the particles increased to 400–450 nm (*Fig. 3B*).

Earlier, we had revealed that the RNA molecule within native particles of PVX and homologous single-tail vRNPs (PVX RNA – PVX CP) is inaccessible for translation as opposed to TMV and a number of other viruses. However, RNA translation is activated upon phosphorylation of PVX CP or upon formation of the virion or vRNP with PVX MP1 [11, 15, 19].

In the present work, we studied the translation properties and specificity of the translation activation of "mixed" vRNPs using MP1.

It was demonstrated in the control experiments that interaction between PVX RNA and PVX CP results in inhibition of RNA translation within vRNP compared to that of unbound RNA (*Fig. 4A, 1, 2*). The background translation level observed (*Fig. 4A, 2*) may result from the presence of unbound RNA because of CP deficiency upon incubation [15]. The amount of unbound RNA decreases as the RNA : CP molar ratio increases, accompanied by a drop in the background translation level [15].

On the other hand, the interaction between MP1 and vRNP consisting of homologous coat proteins and RNA results in efficient translation activation of the encapsidated PVX RNA (*Fig. 4A, 1, 3*).

It is worth mentioning that similar results were obtained by analyzing the translational activation of the heterologous RNAs within the vRNPs reconstructed from PVX CP (*Figs. 4B–F*). The addition of PVX CP to the RNA at the 10 : 1 (w/w) ratio leads to a noticeable translation suppression of BMV RNA (*Fig. 4B, 1, 2*), PAMV RNA (*Fig. 4C, 1, 2*), NMV RNA (*Fig. 4D, 1, 2*), TMV RNA (*Fig. 4E, 1, 2*), and Mengo virus RNA (*Fig. 4F, 1, 2*) within vRNP as compared with the same amount of unbound RNA. Almost complete translation suppression of encapsidated RNA can be achieved by increasing the amount of CP to the RNA : CP ratio = 1 : 30. Figure 4 shows the results for BMV RNA (*Fig. 4B, 4*), NMV RNA (*Fig. 4D, 4*), and TMV RNA (*Fig. 4E, 4*). The addition of the MP1 to the "mixed" vRNP results in translation activation (*Figs. 4B–F, 3*), the translational efficiency recovering to the level of unbound RNA (*Figs. 4B–F, 1*). The set of peptides that are formed upon RNA translation within MP1-activated vRNP is identical to the products of translation of unbound RNA as follows from Fig. 4. The results obtained lead to assume that the structures of the protein coats of the "mixed" (heterologous) and homologous vRNPs are rather similar.

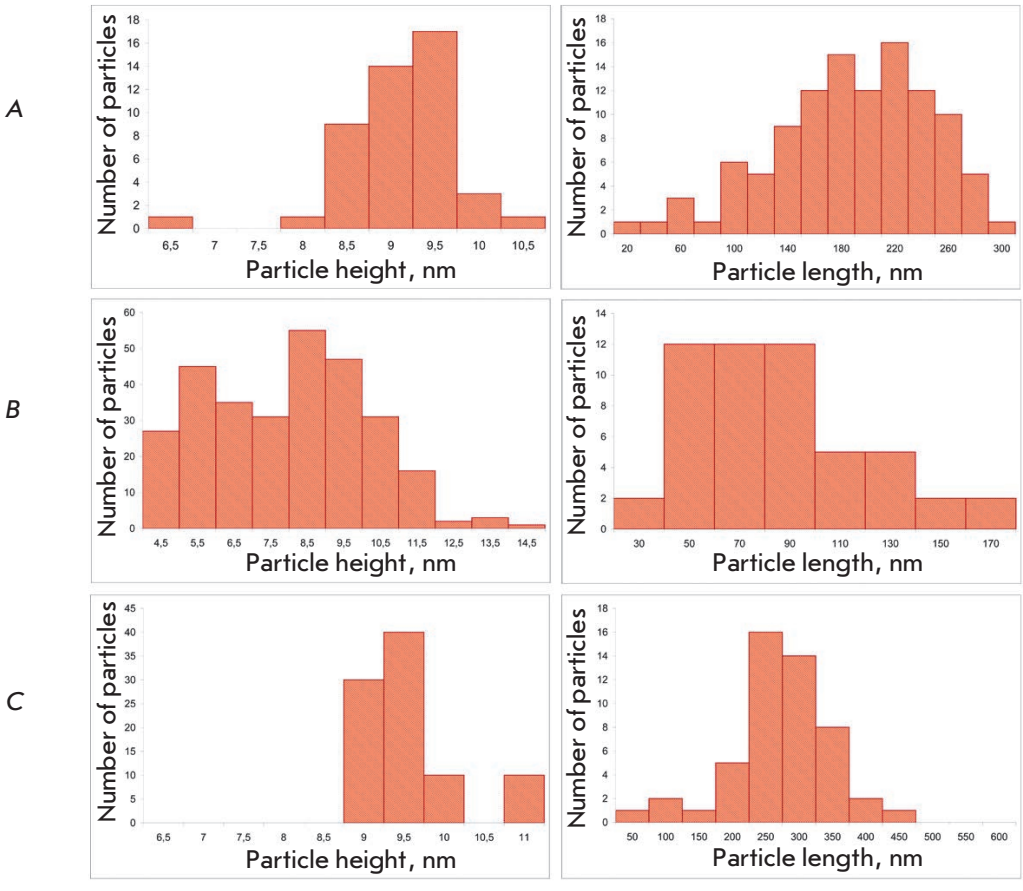

Fig. 3. Histograms showing height and length distribution of vRNP on the basis of the AFM data. PVX CP was incubated with RNA at RNA : PVX CP (w/w) ratio = 1 : 10. (A) PVX RNA; (B) total BMV RNA; (C) Mengo virus RNA.

We demonstrated previously that protein–protein interactions between CP and MP1 play a key role upon the MP1-dependent activation of the RNA translation within viral particles or homologous vRNPs [15, 20]. The fundamental role in the interaction between CP and MP1 appears to belong to the C terminus fragment of PVX CP [21]. The results of the translational activation of heterologous RNAs within "mixed" artificial vRNPs serve as new evidence of the key role of the coat protein in this phenomenon.

Specific recognition of viral RNAs by the structural protein plays a key role in the encapsidation of viral RNA genomes during the assembly of a viral particle. Assembly signals interacting with coat proteins (origin of assembly, OAS) have been identified in the RNA molecules of a number of plant viruses (TMV, BMV, turnip crinkle virus) [22–25]. In particular, the significance of the 5' terminus fragment of the genomic RNA in the processes of the assembly of the virus and replication of potexvirus RNA has been demonstrated [26].

Kwon *et al.* [27] were able to identify *in vitro* the origin of assembly of PVX within the 5' terminus fragment of PVX RNA (51–84 nt) forming a stem-loop structure (SL1). Moreover, the regulatory elements that are required for the binding of RNA to the coat protein are shown to be located in the fragment 1–107 nt of PVX RNA [28]. The data obtained by an analysis of the translational properties of heterologous vRNPs allow one to assume that the initiation of *in vitro* assembly of heterologous vRNP also starts at the 5' terminus RNA fragment and proceeds in the 5'–3' direction. This conclusion is appropriate for potexvirus RNAs (NMV, PAMV). However, the signal for specific assemby of TMV is located in the 3' terminus region; the tRNA-like 3' terminal structure and elements of the polymerase gene play a role in assembly initiation in BMV. Mengo virus RNA (genus *Cardiovirus*, family *Picornaviridae*) with a length of 8400 nt contains the virus-specific protein VPg [29] at its 5' terminus; the protein is bound to the RNA via the phosphodiester bond; its 3' terminus is polyadenylated [30]. It is not quite clear which sites are recognized by the PVX CP upon initiation of the "coating" of heterologous RNAs; although based on the results of translational activation, this process is likely to start at the 5' terminus. It is most surprising that the translation of Mengo virus RNA, which has an internal translation origin site, is also inhibited upon binding to PVX CP and activated

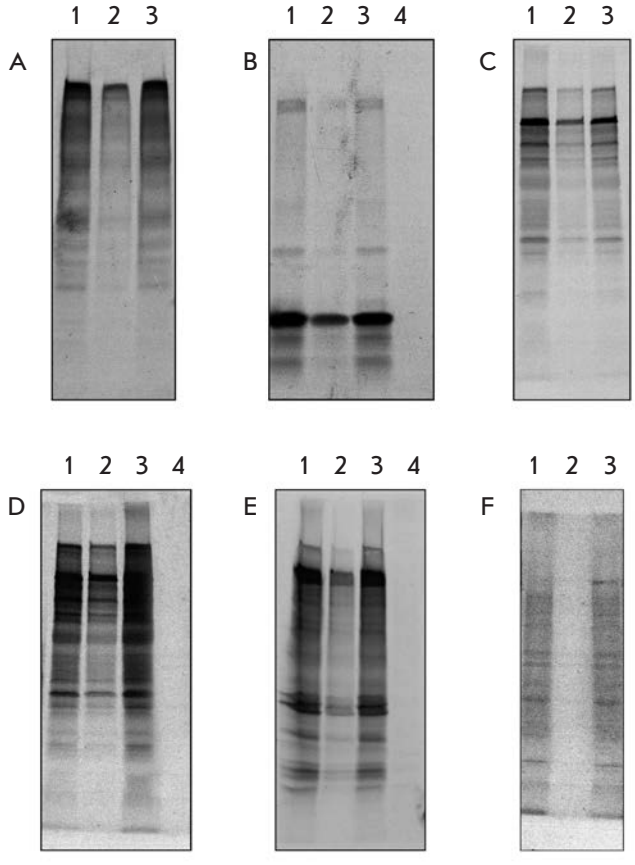

Fig. 4. *In vitro* translational activation of RNA within vRNP. vRNP are formed upon incubation of PVX CP with homologous and foreign RNAs at weight ratio = 10 : 1, except for lane 4 at sections B, D, E, where the CP : RNA ratio = 30 : 1. Electrophoretic analysis (in 8–20% denaturating polyacrylamide gel) of ^{35}S labeled translation products produced in wheat germ extract. (A) PVX RNA; (B) total BMV RNA; (C) PAMV RNA; (D) NMV RNA; (E) TMV RNA; (F) Mengo virus RNA. Lane 1 is RNA; Lane 2 – RNA + PVX CP; Lane 3 – (RNA + PVX CP) + MP1.

upon addition of MP1. Thus, it is plausible that the initiation of vRNP is determined by the protein at least in the case of PVX CP, and probably in the case of the papaya mosaic virus, too (according to Abouhaidar and Bancroft [31]). The assembly of the coat protein of PVX and heterologous RNAs is initiated at regions that differ considerably in terms of localization and structure from the ones in the case of RNA interaction with its "own" protein.

It can be assumed under the conditions of our experiment that PVX CP recognizes not a specific nucleotide sequence, but a certain structure of the 5' terminus fragment of the RNA, which initiates the formation of vRNP.

CONCLUSIONS

The incubation of various foreign heterologous RNAs with PVX CP *in vitro* has been shown to result in the formation of the vRNPs having morphology and translational properties similar to those of homologous vRNPs. It can be assumed that a protein coat will be formed upon interaction of a heterologous RNA and PVX CP similar to the coat of homologous particles in terms of its structure. The *in vitro* formation of heterologous vRNPs with the participation of PVX CP seems to be initiated at the 5' terminus of an RNA molecule and to be independent of the specific nucleotide sequence of the 5' terminus RNA fragment. As a result, PVX CP is capable of packaging foreign genetic material of different sizes into an artificial virus-like particle. Neither the heterologous nor homologous RNA within vRNP is accessible for ribosomes. However, it becomes translationally active upon incubation of the resulting vRNPs with PVX MP1. Binding of MP1 to one of the termini of the PVX virion induces conformation changes in the terminal subunits of the coat protein, which results in the destabilization (remodelling) and transition of the protein helix into a metastable state. The following MP1-dependent translational disassembly of PVX particles occurs rapidly and, most likely, in cooperation with the release of unbound RNA and protein subunits at early stages of the translation [20]. It is quite likely that the same mechanism is responsible for the translational activation of "mixed" vRNPs, with the participation of MP1, described above.

Coat proteins of plant viruses with a helical structure could be used to design and deliver into target organs artificial "hybrid" nanoparticles (vRNP) capable of *in vivo* disassembly under the control of various factors. ●

This study was supported in part by the Russian Foundation for Basic Research (grant № 10-04-000-89a) and the Ministry of Education and Science of the Russian Federation (Government Contract № 02.740.11.0789). The authors are grateful to AIST-NT Company, and personally to M. Savvateev for the AFM analysis of the specimens.

REFERENCES

1. Butler P.J.G. // Philos. Trans. R. Soc. London. B. 1999. V. 354. P. 537.
2. Klug A. // Philos. Trans. R. Soc. London B. 1999. V. 354. P. 531.
3. Atabekov J.G. // Nanotechnology in Russia. 2008. V. 3 (1-2). P. 128-137.
4. Atabekov J.G., Novikov K., Vishnichenko K., Kaftanova A.S. // Virology. 1970. V. 41. P. 519.
5. Fraenkel-Conrat H., Singer B. // Philos. Trans. R. Soc. London. B. 1999. V. 354. P. 583.
6. Tollin P., Wilson H.R. // The Filamentous Plant Viruses in the Plant Viruses 4 / Ed. Milne R.C. New York: Plenum Press, 1988. P. 51–83.
7. Skryabin K.G., Morozov S.Yu., Kraev A.S., Rozanov M.N., Chernov B.K., Lukasheva L.I., Atabekov J.G. // FEBS Lett. 1988. V. 240. P. 33–40.
8. Morozov S.Yu., Miroshnichenko N.A., Zelenina D.A., Fedorkin O.N., Solovyev A.G., Lukasheva L.I., Karasev A.V., Dolja V.V., Atabekov J.G. // J. Gen. Virol. 1991. V. 72. P. 2039–2043.
9. Novikov V.K., Kimazev V.Z., Atabekov J.G. // Dokl. Acad. Nauk. SSSR. 1972. V. 204. P. 1259-1262.
10. Erickson J.W., Bancroft J.B. // Virology. 1978. V. 90. P. 60–66.
11. Atabekov J.G., Rodionova N.P., Karpova O.V., Kozlovsky S.V., Poljakov V.Y. // Virology. 2000. V. 271. № 2. P. 259–263.
12. Goodman R.M., Horne R.W., Hobart J.M. // Virology 1975. V. 68. P. 299–308.
13. Fraenkel-Conrat H., Singer B., Tsugita A. // Virology. 1961. V. 14. P. 54–58.
14. Karpova O.V., Ivanov K.I., Rodionova N.P., Dorokhov Yu.L., Atabekov J.G. // Virology. 1997. V. 230. P. 11–21.
15. Karpova O.V., Zayakina O.V., Arkhipenko M.V., Sheval E.V., Kiselyova O.I., Poljakov V.Yu., Yaminsky I.V., Rodionova N.P., Atabekov J.G. // J. Gen. Virol. 2006. V. 87. № 9. P. 2731–2740.
16. Kaftanova A.S., Kiselev N.A., Novikov V.K., Atabekov J.G. // Virology. 1975. V. 65. P. 283–287.
17. Kiseleva O.I., Yaminsky I.V., Karpova O.V., Rodionova N.P., Kozlovsky S.V., Arkhipenko M.V., Atabekov J.G. // J. Mol. Biol. 2003. V. 332. № 2. P. 321–325.
18. Nikitin N.A., Sushko A.D., Arkhipenko M.V., Rodionova N.P., Karpova O.V., Yaminsky I.V. // Colloid Journal. 2011. V. 73 (4). P. 523–530.
19. Karpova O.V., Arkhipenko M.V., Zayakina O.V., Nikitin N.A., Kiselyova O.I., Kozlovsky S.V., Rodionova N.P., Atabekov J.G. // Mol. Biol. (Mosk.). 2006. V. 40 (4). P. 628–634.
20. Rodionova N.P., Karpova O.V., Kozlovsky S.V., Zayakina O.V., Arkhipenko M.V., Atabekov J.G. // J. Mol. Biol. 2003. V. 333. № 3. P. 565–572.
21. Zayakina O., Arkhipenko M., Kozlovsky S., Nikitin N., Smirnov A., Susi P., Rodionova N., Karpova O., Atabekov J. // Mol. Plant. Pathol. 2008. V. 9. № 1. P. 37–44.
22. Butler P.J. // J. Gen. Virol. 1984. V. 65. № 2. P. 253–279.
23. Choi Y.G., Rao A.L. // J. Virol. 2003. V. 77. № 18. P. 9750–9757.
24. Miller E.D., Plante C.A., Kim K.H., Brown J.W., Hemenway C. // J. Mol. Biol. 1998. V. 284. № 3. P. 591–608.
25. Qu F., Morris T.J. // J. Virol. 1997. V. 71. № 2. P. 1428–1435.
26. Sit T.L., Leclerc D., AbouHaidar M.G. // Virology. 1994. V. 199. № 1. P. 238–242.
27. Kwon S.J., Park M.R., Kim K.W., Plante C.A., Hemenway C.L., Kim K.H. // Virology. 2005. V. 334. № 1. P. 83–97.
28. Lough T.J., Lee R.H., Emerson S.J., Forster R.L., Lucas W.J. // Virology. 2006. V. 351. № 2. P. 455–465.
29. Lee Y.F., Nomoto A., Detjen B.M., Wimmer E. // Proc. Natl. Acad. Sci. USA. 1977. V. 74. № 1. P. 59–63.
30. Yogo Y., Wimmer E. // Proc. Natl. Acad. Sci. USA. 1972. V. 69. № 7. P. 1877–1882.
31. Abouhaidar M.G., Bancroft J.B. // Virology. 1980. V. 107. № 1. P. 202–207.

Transcription Factor DLX5 As a New Target for Promising Antitumor Agents

R. A. Timakhov[1,2,3*], P. O. Fedichev[1], A. A. Vinnik[1], J. R. Testa[3], O. O. Favorova[2]
[1] Quantum Pharmaceuticals, Russia
[2] Pirogov Russian National Research Medical University
[3] Fox Chase Cancer Centre, Philadelphia, USA
E-mail: timakhov@gmail.com
Received 11.05.2011

ABSTRACT **The crystal structure of the human transcription factor DLX5 has been used for the screening of a library consisting of 10^6 compounds by the molecular docking technique. *In vitro* tests of the 14 top-rated ligands showed that compound Q12 displays the best ability to inhibit the proliferation of *Dlx5* positive mouse lymphoma cells, which correlates with the down-regulation of *c-myc* expression. Compound Q12 has low toxicity on normal human ovarian epithelial cells and mouse lymphoma cells with absent expression of *Dlx5*, and can be used for further chemical optimization and for the development of novel, highly efficient cancer treatments.**
KEYWORDS **DLX5; transcription factor; small molecules; cancer; molecular docking.**
ABBREVIATIONS **DLX5 – human transcription factor, encoded by gene *DLX5* (Distall-less homeobox gene 5); Dlx5 – mouse transcription factor encoded by gene *Dlx5*; K_d – binding (affinity) constant; NSCLC - non-small cell lung cancer; siRNA – small interfering RNA, RT-PCR – reverse transcription polymerase chain reaction.**

INTRODUCTION

A wide range of drugs have been used in modern clinical practice in order to control cancer [1–3]. However, even if all the available drugs were to be used, the proportion of patients who respond to the therapy would remain rather small. For this reason is critically necessary to design new efficient targeted methods for cancer treatment based on a deep comprehension of the mechanisms of tumor growth.

Recent discoveries reveal that the transcription factor DLX5 displays oncogenic activity. The overexpression of the *DLX5* gene in mammalian cells stimulates cell proliferation [4] and can be observed in endometrial carcinoma, non-small cell lung cancer (NSCLC), and small cell lung cancer [5, 6]. The knockdown of the *DLX5* expression using siRNA in mouse and human cancer cells results in the arrest of cell proliferation [4, 7]. New data point to the fact that DLX5 has a direct effect on the expression of protooncogene *c-myc* [8]. All these facts allow us to regard DLX5 as a promising target for which specific ligands that have the properties of oncogenesis inhibitors can be found.

Attempts have frequently been made to use the so-called "high throughput screening" to solve the problem of the search for the ligands of a certain protein [9–13]. This screening is carried out on a cell culture or on an *in vitro* model, using an earlier prepared compound library. The logistics and cost of the studies required for the experimental validation of a significant number of molecules is prohibitively high in many cases. On account of these reasons, in the present study we used the algorithm earlier elaborated to search for inhibitors of new protein targets, based on the analysis of the crystal structure of a target protein [14]. The algorithm is based on the molecular docking of chemical compounds to the known 3D model of a target protein, which predicts the possible position of a compound in the protein–ligand binding site, the calculation of the molecular dynamics being used to refine the binding energies for the best suiting compounds. As shown in our study, as well as in previous studies [14–19], this multi-level approach is not only efficient, but it also considerably reduces the amount of experiments to be carried out. In this case, it enabled the discovery of several ligands of the transcription factor DLX5 that have potential for cancer therapy.

EXPERIMENTAL

Ligand preparation and molecular docking

In order to optimize the time of computational screening, the ENAMINE library consisting of 10^6 compounds was clustered using the Jarvis–Patrick algorithm [20, 21] with acceleration [22], which is contained in the QUANTUM software package. The so-called Tanimoto metric was calculated using the Daylight molecular

fingerprints, which were selected as the measure of molecular similarity [23]. The parameters of clusterization were selected in such a manner that each cluster consisted, on average, of approximately 10 related structures; the total number of non-clustered molecules being no higher than 20% of the initial amount of the library compounds. The compounds representing the centroids of clusters were then selected for further screening. In order to enhance the speed of molecular docking, from the entire centroid library were selected the molecules with the low molecular weight. All the selected compounds were extracted from the sdf files provided by ENAMINE and processed in the batch-mode. The library had not been additionally enriched with molecules active towards oncotargets or by any other methods. The typization of protein and ligands, as well as *in silico* screening, was carried out using the corresponding tools from the QUANTUM software package.

The software predicts the binding (affinity) constants (K_d) between small molecules and a target protein with an accuracy of approximately one order of magnitude, through the estimation of their intermolecular interactions, by using accurate models of atomic forces in an aqueous environment [14, 24–26]. The hierarchy of physical models of intermolecular interactions was used for calculations. In order to initially find the position of a ligand in the active site of a protein and estimate the binding energy of the protein–ligand complex, docking of the ligand to the rigid protein structure was carried out; the results were then refined using the flexible protein model. The modified model of inter and intramolecular interactions AMBER/GAFF were used [27] in order to estimate the potential energy of interaction. The free energy was estimated using the linear interaction model [28]. An aqueous environment was simulated using the modified generalized Born model [25]. The algorithm was described earlier [14], where it was used to search for the inhibitors of protein–protein interactions.

Molecular docking of the molecules from the initial compound library was performed to the rigid structure of the DLX5 2DJN protein obtained from the Protein Data Bank (PDB) [29]. The region of the 3D structure that was selected for molecular docking was 2 x 2 x 2 nm in size. The ligands with the best predicted binding energies were recalculated to the models with a flexible protein [14, 15]. In order to verify that the selected molecules had not been described earlier, the following facts were checked: whether or not these compounds and/or their analogues had been contained in the database or had been mentioned in the reviews devoted to the known inhibitors.

Cell cultures

In the present study we used the earlier characterized [30] line 42 of T-cell lymphoma from Akt2-transgenic mice (42-936, 42-577, and 42-588) and line 72 (wtl36). The cells were incubated in the Iscove's MDM medium containing 10% of fetal bovine serum (FBS).The other cell lines were incubated in the RPMI medium with 10% of FBS. All cell cultures were kept at 37^0C at an atmosphere of 5% CO_2. Potential inhibitors of DLX5 (Dlx5) were added to the medium containing 10^5 tumor cells at a concentration of 10 μM followed by incubation for 96 h at 37^0C. The cell proliferation was assessed using the CellTiter 96 Aqueous One Solution Assay (Promega) in accordance with the manufacturer's protocol. Each experiment was repeated at least three times.

RNA extraction and real-time RT-PCR

The RNA was extracted from the line 42 mouse T-cell lymphoma cells after incubation with compound Q12 and DMSO for 96 h using the RNAqueous® Kit, in accordance with the manufacturer's protocol. Real-time RT-PCR (repeated at least in triplicates) was carried out in a specialized service of the Fox Chase Cancer Center. The samples for estimation of the expression of the *c-myc*, *Dlx5*, and *Tbp* genes were synthesized at Applied Biosystems.

RESULTS AND DISCUSSION

Screening for the new ligand molecules specific to DLX5 has been carried out with The QUANTUM software suite, based on the analysis of the protein crystal structure [14, 24–26]. This approach not only enables the identification of the molecules with potential to bind with a certain protein, but also allows us to minimize the quantity of false positive results, when the molecules with a high binding energy predicted *in silico* manifested no functional activity in the experiment. The search was made more complicated by the absence of preliminary data on the binding of the known compounds with DLX5 protein; therefore, blind studies were performed. The best molecules and all their structural analogues from the original ENAMINE library were sorted on the basis of their predicted binding energy. According to the results of molecular docking, 100 ligands were selected; 14 of those with the best predicted binding energy of DLX5 protein were ordered and synthesized at ENAMINE company; then, they were tested on cell cultures. *Figure 1* shows an example of molecular docking with an active DLX5 site of one of these ligands.

The cells of the earlier characterized line 42 of T-cell lymphoma from Akt2-transgenic mice [4, 30] were used as a model to verify the specific activity of the selected ligands. These cells bear a clonal chromosome rearrangement –chromosome 6 inversion, which results in

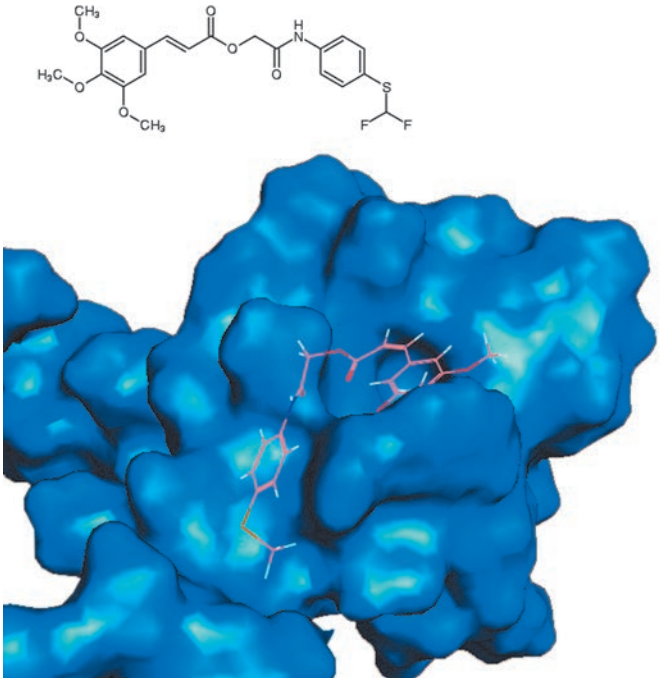

Fig. 1. Molecular docking of one compound selected for further experiments: chemical structure and position of compound in the active site the transcription factor DLX5.

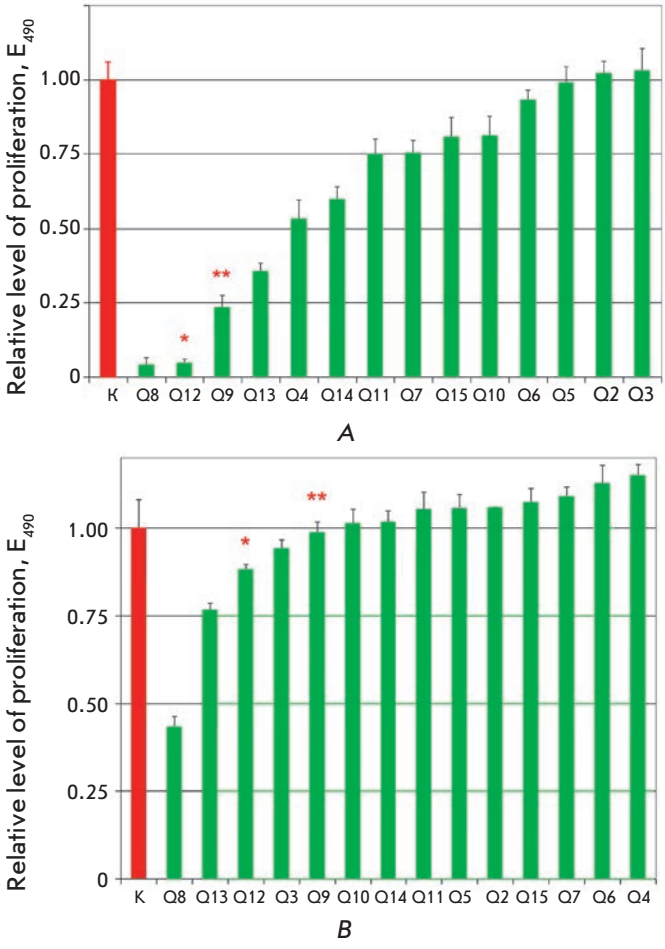

Fig. 2. Experimental estimation of the properties of 14 compounds, for which high binding energy for the 3D structure of DLX5 was predicted: their efficacy was estimated by the impact on proliferation of Dlx5 positive mouse lymphoma cells 42-936 (A) and cytotoxicity measured by the impact on proliferation of normal human ovarian epithelial cells (B). K - is the level of proliferation in the control. The columns depicting the effect of the most promising compounds are labeled with asterisks (Q12(*) and Q9(**)).

the translocation of the *Dlx5* gene into the region under control of the T-cell enhancer and in the overexpression of Dlx5 protein. Lymphoma cells 42-936 were incubated with each of the 14 selected DLX5 ligands; the impact of the ligands on proliferation was assessed. As can be seen in *Fig. 2A*, the ligands demonstrate different efficacies of impact on the proliferation of lymphoma cells; compounds Q8, Q12, Q9, and Q13 manifested the best inhibitory activity. The possible nonspecific cyto-toxic action of the selected compounds was tested on normal human ovarian epithelial cells without DLX5 expression (*Fig. 2B*). When comparing with the control, it can be seen that most ligand molecules, with the exception of the compounds Q8 and Q13, manifest no significant cyto-toxicity. Since Q8 and Q13 manifested a cytotoxic effect, they were eliminated from further consideration. Compounds Q12 and Q9 were selected for further studies as the most promising ones.

In order to eliminate the possibility of a nonspecific impact of compounds Q12 and Q9 on cells of the lymphoid series, their action was tested on T-cell lymphoma cells of line 72 with absent expression of *Dlx5* from Akt2-transgenic mice (*Fig. 3*). Cells of line 72 contain another type of chromosome rearrangement, a translocation between chromosomes 14 and 15 (t(14:15)), which results in an increased expression of protooncogene *c-myc* [*30*]. *Figure 4* shows the results of the effect of compound Q12 on the proliferation of an additional two subtypes of lymphoma cells expressing *Dlx5* (42-577 and 42-588), as well as the proliferation of the human lymphoma cells Jurkat and Molt16 not expressing *DLX5*. A general conclusion can be made from the data presented in *Figs. 3 and 4* that compounds Q9 and Q12 have no effect on the proliferation of cells not expressing *Dlx5*; however, they are highly efficient in the suppression of the proliferation of cells in which this factor is expressed.

It is known that the DLX5 transcription factor can directly control the expression of protooncogene *c-myc*

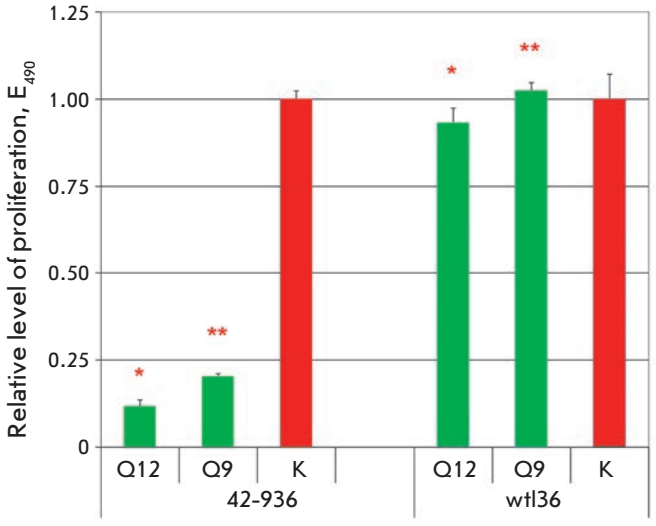

Fig. 3. The selectivity of compounds Q12 and Q9 on mouse lymphoma cells. Left panel: the impact of compounds on proliferation of Dlx5-positive mouse lymphoma cells 42-936. Right panel: the impact of compounds on proliferation of Dlx5-negative mouse lymphoma cells wtl36. Additional labeling is identical to that in *Fig. 2.*

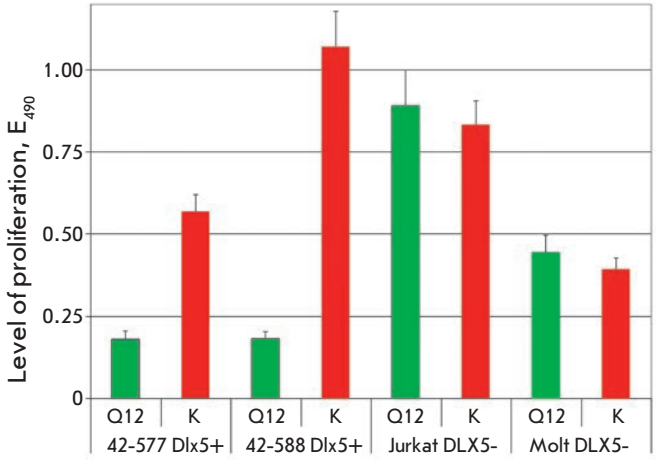

Fig. 4. Selectivity of compound Q12 on human lymphoma cells. On the left: proliferation of Dlx5-positive mouse lymphoma cells 42-577 and 42-588. On the right: proliferation of DLX5-negative human lymphoma cells Jurkat and Molt16. Additional labeling is identical to that in *Fig. 2.*

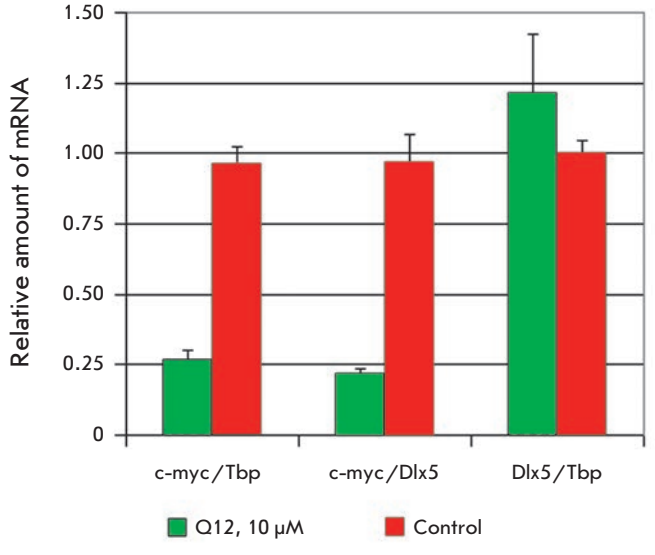

Fig. 5. Real-time RT-PCR. The measurement of the expression of *c-myc* and *Dlx5* in mouse lymphoma cells 42-936, after cultivation with 10 μM compound Q12 by the mRNA level. Tbp is the TATA-binding protein.

[8, 30]. The impact of Q12 on the expression of *c-myc* in the lymphoma cells 42-936 expressing *Dlx5* was studied by real-time RT-PCR. *Figure 5* shows the levels of mRNA of c-myc with respect to the endogenous control, mRNA of TATA-binding protein (Tbp) or mRNA of Dlx5, as well as mRNA of Dlx5 with respect to mRNA of Tbp in the presence of 10 μM Q12 and without any addition of it. It can be seen that the expression of *c-myc* decreases considerably under the action of Q12, while the expression of *Dlx5* remains intact. These results agree with the conception of the inhibitory effect of ligand Q12 on the transcription activity of the Dlx5 factor. Although these data need to be tested on a larger number of cell lines, it is tempting to make a preliminary conclusion on the specificity of binding between the transcription factor DLX5 and ligand Q12 based on the results of this study.

The approaches used in this study made it possible to experimentally identify the most active inhibitors of Dlx5 (DLX5) out of those that were tested. Further plans include optimizing the structure of the resulting compounds in terms of parameters such as the enhancement of efficacy, reduction of possible nonspecific toxicity, and the enhancement of the metabolic stability. The next stage of this study assumes that the activity and toxicity of the optimized compounds will be assessed *in vivo,* and their K_d will be measured directly.

CONCLUSIONS

With the aim of verifying the fundamental possibility of using the DLX5 transcription factor as a target for anti-tumor agents and designing drugs that can suppress the development of certain types of human tumors (T-lymphomas, lung and ovarian cancer), a search for specific ligands of the DLX5 factor was performed

based on the analysis of its crystal structure. It was shown that more than 50% of compounds which were selected by docking technique are capable at micro-molar concentrations to inhibit the proliferation of mouse lymphoma cells expressing *Dlx5*. Moreover, most of the compounds active on Dlx5 positive lymphoma cells had no effect on other types of cells that do not express this transcription factor, which serves as evidence of the specificity of the selected molecules. Compounds Q12 and Q9 were found to be the best in terms of the ratio between the parameter characterizing the efficacy and the absence of nonspecific cytotoxicity. The observed decrease in the expression of *c-myc* under the action of Q12 attests to the inhibitory effect of this ligand on the transcriptional activity of the Dlx5. The compounds discovered are the first described low-molecular-weight ligands of DLX5 which can be used for subsequent chemical optimization and the development of highly efficient anti-tumor agents. ●

This study was carried out within the framework of inter-institute collaboration between the Pirogov Russian National Research Medical University (Division of Molecular Biology and Medical Biotechnology) and the Fox Chase Cancer Center (Philadelphia, United States), in cooperation with Quantum Pharmaceuticals. The authors are grateful to E.G. Getmantsev and L.I. Men'shikov for their assistance in performing the calculations and for the many productive discussions.

REFERENCES

1. Albain K.S., Nag S.M., Calderillo-Ruiz G., Jordaan J.P., Llombart A.C., Pluzanska A., Rolski J., Melemed A.S., Reyes-Vidal J.M., Sekhon J.S., et al. // J. Clin. Oncol. 2008. V. 26. P. 3950–3957.
2. Shepherd F.A., Pereira J.R. // N. Engl. J. Med. 2005. V. 353. P. 123–132.
3. Kris M.G., Natale R.B., Herbst R.S., Lynch Jr. T.J., Prager D., Belani C.P., Schiller J.H., Kelly K., Spiridonidis H., Sandler A., et al. // JAMA. 2003. V. 290. № 16. P. 2149–2158.
4. Tan Y., Timakhov R.A., Rao M., Altomare D.A., Xu J., Liu Z., Gao Q., Jhanwar,S.C., Di Cristofano A., Wiest D.L., et al. // Cancer Res. 2008. V. 68(5). P. 1296–1302.
5. Pedersen N., Mortensen S., Sorensen S.B., Pedersen M.W., Rieneck K., Bovin L.F., Poulsen H.S. // Cancer Res. 2003. V. 63. № 8. P. 1943–1953.
6. Maxwell G.L., Chandramouli G.V.R., Dainty L., Litzi T.J., Berchuck A., Barrett J.C., Risinger J.I. // Clin. Cancer Res. 2005. V. 11. P. 4056–4066.
7. Kato T., Sato N., Takano A., Miyamoto M., Nishimura H., Tsuchiya E., Kondo S., Nakamura Y., Daigo Y. // Clin. Cancer Res. 2008. V. 14. P. 2363–2370.
8. Xu J., Testa J.R. // J. Biol. Chem. 2009. V. 284. P. 20593–20601.
9. Broach J.R., Thorner J. // Nature. 1996. V. 384. P. 14–16.
10. Young K., Lin S., Sun L., Lee E., Modi M., Hellings S., Husbands M., Ozenberger B., Franco R. // Nat. Biotechnol. 1998. V. 16. P. 946–950.
11. Hamasaki K., Rando R.R. // Anal. Biochem. 1998. V. 261. P. 183–190.
12. Moore K.J., Turconi S., Miles-Williams A., Djaballah H., Hurskainen P. // J. Biomol. Screen. 1999. V. 4. P. 205–214.
13. Dunn D., Orlowski M., McCoy P., Gastgeb F., Appell K. // J. Biomol. Screen. 2000. V. 5. P. 177–188.
14. Joce C., Stahl J.A., Shridhar M., Hutchinson M.R., Watkins L.R., Fedichev P.O., Yin H. // Bioorg. Med. Chem. Lett. 2010. V. 20. № 18. P. 5411–5413.
15. Okimoto N., Futatsugi N., Fuji H., Suenaga A., Morimoto G., Yanai R., Ohno Y., Narumi T., Taiji M. // PLoS Comput. Biol. 2009. V. 5. № 10. P. 1–13.
16. Doman T., Huo S., Wang J., Cieplak P., Kollman P.A., Kuntz I.D. // J. Med. Chem. 2002. V. 45. P. 1412–1419.
17. Masukawa K.M., Kollman P.A., Kuntz I.D. // J. Med. Chem. 2003. V. 46. P. 5628–5637.
18. Kuhn B., Gerber P., Schulz-Gasch T., Stahl M.J. // J. Med. Chem. 2005. V. 48. P. 4040–4048.
19. Ferrara P., Curioni A., Vangrevelinghe E., Meyer T., Mordasini T. // J. Chem. Inf. Model. 2006. V. 46. P. 254–263.
20. Jarvis R.A., Patrick E.A. // IEEE Trans. Comput. 1973. V. 22. № 11. P. 1025–1034.
21. Willett P. Similarity and Clustering in Chemical Information Systems. N.Y. USA: John Wiley & Sons, Inc., 1987. 266 p.
22. Li W. // J. Chem. Inf. Model. 2006. V. 46. № 5. P. 1919–1923.
23. Flower D.R. //J. Chem. Inf. Comput. Sci. 1998. V. 38. P. 379–386.
24. Fedichev P.O., Men'shikov L.I. // Arxiv preprint. 2006. arXiv:cond-mat/0601129v3
25. Fedichev P.O., Getmantsev E.G., Menshikov L.I. // J. Comput. Chem. 2011. V. 32. № 7. P. 1368–1376.
26. Men'shikov L.I., Fedichev P.O. // Rus. J. Phys. Chem. 2011. V. 85. № 5. P. 906–908.
27. Case D.A., Darden T.A., Cheatham III. T.E., Simmerling C.L., Wang J., Duke R.E., Luo R., Walker R.C., Zhang W., Merz K. M., et al. // AMBER 11. 2010. University of California, San Francisco.
28. Hansson T., Marelius J., Åqvist J. // J. COMP-AID MOL DES. 1996. V. 12. P. 27–35.
29. Berman H.M., Westbrook J., Feng Z., Gilliland G., Bhat T.N., Weissig H., Shindyalov I.N., Bourne P.E. // Nucl. Acids Res. 2000. V. 28. P. 235–242.
30. Timakhov R.A., Tan Y., Rao M., Liu Z., Altomare D.A., Pei J., Wiest D.L., Favorova O.O., Knepper J.E., Testa J.R. // Genes Chromosomes Cancer. 2009. V. 48. № 9 P. 786–794.

Haplotype Diversity and Reconstruction of Ancestral Haplotype Associated with the c.35delG Mutation in the *GJB2* (Cx26) Gene among the Volgo-Ural Populations of Russia

L. U. Dzhemileva[1*], O. L. Posukh[2], N. A. Barashkov[3], S. A. Fedorova[3], F. M. Teryutin[3], V. L. Akhmetova[1], I. M. Khidiyatova[1], R. I. Khusainova[1], S. L. Lobov[1], E. K. Khusnutdinova[1]
[1]Institute of Biochemistry and Genetics, Ufa Research Center, Russian Academy of Sciences
[2]Institute of Cytology and Genetics, Siberian Branch, Russian Academy of Sciences
[3]Yakut Research Center of Complex Medical Problems, Siberian Branch, Russian Academy of Medical Sciences
*E-mail: dzhemilev@anrb.ru
Received 23.03.2011

ABSTRACT **The mutations in the *GJB2* (Cx26) gene make the biggest contribution to hereditary hearing loss. The spectrum and prevalence of the *GJB2* gene mutations are specific to populations of different ethnic origins. For several *GJB2* mutations, their origin from appropriate ancestral founder chromosome was shown, approximate estimations of "age" obtained, and presumable regions of their origin outlined. This work presents the results of the carrier frequencies' analysis of the major (for European countries) mutation c.35delG (*GJB2* gene) among 2,308 healthy individuals from 18 Eurasian populations of different ethnic origins: Bashkirs, Tatars, Chuvashs, Udmurts, Komi-Permyaks, Mordvins, and Russians (the Volga-Ural region of Russia); Byelorussians, Ukrainians (Eastern Europe); Abkhazians, Avars, Cherkessians, and Ingushes (Caucasus); Kazakhs, Uzbeks, Uighurs (Central Asia); and Yakuts, and Altaians (Siberia). The prevalence of the c.35delG mutation in the studied ethnic groups may act as additional evidence for a prospective role of the founder effect in the origin and distribution of this mutation in various populations worldwide. The haplotype analysis of chromosomes with the c.35delG mutation in patients with nonsyndromic sensorineural hearing loss (N=112) and in population samples (N =358) permitted the reconstruction of an ancestral haplotype with this mutation, established the common origin of the majority of the studied mutant chromosomes, and provided the estimated time of the c.35delG mutation carriers expansion (11,800 years) on the territory of the Volga-Ural region.**
KEYWORDS **hereditary nonsyndromic sensorineural hearing loss; *GJB2* (Cx26) gene; c.35delG mutation; ancestral haplotype; populations of the Volga-Ural region.**

INTRODUCTION

Hereditary deafness is a frequent disorder in humans: it is recorded in 1/1,000 newborns. The etiology and pathogenesis of this disease are still to be clarified; however, approximately half of the cases of hereditary deafness are a result of genetic disorders [1].

The hereditary forms of innate hearing loss are characterized by clinical polymorphism and genetic heterogeneity. In the nuclear genome, about 114 loci were mapped and 55 genes were identified, whose mutations to a certain extent cause hearing loss. About 80% of all cases of hereditary nonsyndromic hearing loss fall within the category of autosomal-recessive forms; 15–20% – autosomal-dominant, and about 1% - the form linked with the X-chromosome and mitochondrial forms of deafness [2].

The most frequent cause of nonsyndromic autosomal recessive hearing loss in humans is the mutations in the *GJB2* gene (gap junction β2, subunit β2 of the gap junction protein), localized in the chromosomal region 13q11–q13 and coding connexin 26 (Cx26), which is the transmembrane protein involved in the formation of connexons. Connexons are structures consisting of six protein subunits, which form cellular channels, ensuring a fullblown ion exchange among adjacent cells. This facilitates the maintenance of the homeostasis of endolymph in cochlea tissues. Recently, the fine structure of intercellular channels formed by connexin 26

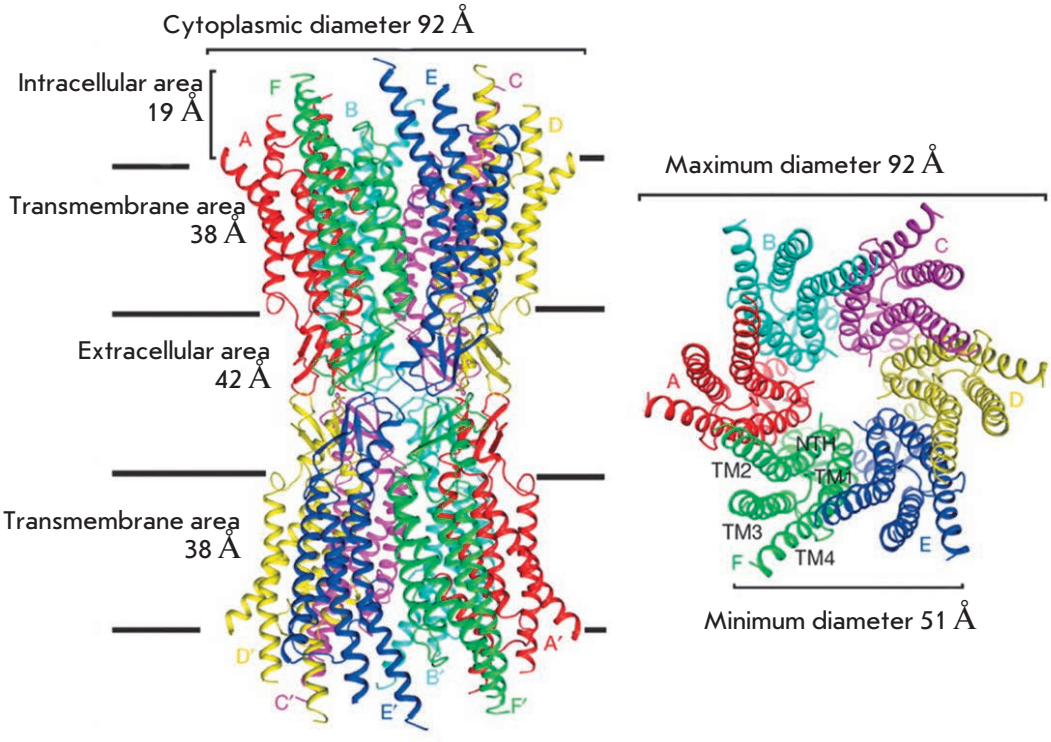

Fig. 1. Structure of intercellular channels formed by molecules of connexin 26. A, B, C, D, F, E and A′, B′, C′, D′, F ′, E′ - connexin 26 molecules in connexones of neighboring cells; TM 1-4 – transmembrane protein segments of Cx26; NTH - N-terminal helix of protein Cx26. Figure was adapted from [3] by permission from Macmillan Publishers Ltd.

was reported (*Fig. 1*) [3]. When there are defects in connexin 26, the functioning of the intercellular channels is irreversibly disrupted in the tissues of the internal ear and endolymph homeostasis is not restored: a factor that is necessary for normal sound perception [4].

So far, in the *GJB2* gene, over 150 pathogenic mutations (mainly recessive), several polymorphisms and sequencing variants whose role in the pathogenesis of hearing loss is still unclear, have been described [2]. The spectrum and frequencies of the *GJB2* gene mutations are characterized by significant interpopulation differences. The racial and/or ethnic specificity of the spread of several *GJB2* gene mutations is preconditioned in some cases by the founder effect, as well as by, in all likelihood, the geographic and social isolation of some populations. Researchers have managed to show the origin of some *GJB2* gene mutations from an ancestor founder chromosome, to obtain approximate estimations of the "age" of the mutations, and to outline suggested regions where they appeared [5–10]. The mutation c.35delG (p.Gly12Valfsx1) is the most frequent in Europe. It first emerged, according to various estimates, 10,000 to 14,000 years ago on the territory of the Middle East or Mediterranean region (probably on the territory of modern Greece) [10–12] and spread in Europe with the migrations of the neolithic population of *Homo sapiens* [6]. Haplotype analysis of the chromosomes with mutation c.235delC (p.Leu79Cysfsx3) in populations of Japan, Korea, China, and Mongolia has allowed to put forward a hypothesis about the founder effect regarding the origin and distribution of this mutation in East Asia and to estimate its "age" (~11,500 years) and presumed appearance in the Lake Baikal region, from where it spread, by way of sequential migrations, over Asia [7]. The "age" of the mutation c.71G>A (p.Trp24X), most widespread in India, has also been assessed (~7,880 years) [8]. The ethnic specificity of the mutation c.167delT (p.Leu56Argfsx26) and mutation c.427C > T (p.Arg143Trp) was shown for populations of the Ashkenazi Jews [5] and for some populations of Western Africa (Ghana) [13, 14], respectively.

In Russia, several research groups have studied the hereditary forms of deafness [15–32]. In most cases, they have considered the genetic-epidemiological and clinical-genetic peculiarities of the inherited forms of hearing loss, and a series of papers are devoted to the molecular-genetic analysis of the *GJB2* gene or its single mutations [17–21, 25–30]. Some authors have obtained data on the specificity of the range and frequency of separate mutations in the *GJB2* gene function in the studied region. For instance, the most frequent mutations in the Siberian populations (Yakuts and Altaians) are IVS1 + 1G>A [27] and c.235delC [25], respectively. The populations of the Volga-Ural region, as generally in the European part of the continent, predominantly exhibit the mutation c.35delG [18–22, 28]. Local differences in the carrier frequency of the

mutation c.35delG are probably related to the genetic history of some populations, and factors of population dynamics, and migration routes of the c.35delG carriers in the world. The available data on the contribution of the *GJB2* mutations to the development of a pathology in patients with nonsyndromic sensorineural hearing loss (NSHL), living in the Volga-Ural regions, and the population-based data on the carrier frequency of the most significant recessive mutation c.35delG permitted an adequate assessment of the haplotypic diversity of the chromosomes bearing the mutation c.35delG, the reconstruction of the possible ancestor haplotype linked to that mutations, and the estimated time of its appearance on the territory of the Volga-Ural regions, which represents the eastern border of the habitat of the mutation c.35delG.

EXPERIMENT

The material taken for the haplotypic analysis and estimates of the "age" of c.35delG of the gene *GJB2* was 56 DNA samples (112 chromosomes) obtained from patients with NSHL, residing in the Volga-Ural regions, in which the mutation.35delG was identified in the homozygote state (32 Russians, 10 Tatars, 1 Bashkirs, 4 Ukrainians, 2 Armenians, and 7 individuals of mixed ethnicity). The control group included 179 (358 chromosomes) healthy individuals from three ethno-geographical groups of the Russians ($N = 86$); Tatars ($N = 62$); and Bashkirs ($N = 31$) without this mutation.

To analyze the carrier frequency of c.35delG 2,308 DNA samples were used, which were obtained from healthy individuals-representatives of different populations of the Volga-Ural region, Central Asia, Northern Caucasus, Eastern Europe, and Siberia, belonging to four language families (*Table 1*).

The blood samples were obtained during expeditions between the years of 2000 and 2010, after receiving the informed written consent of the participants in the study. The genomic DNA was extracted from peripheral blood using the phenol-chloroform extraction method.

The present scientific-research work was approved by the local committee for biomedical ethics at the IBG UNT of the Russian Academy of Sciences (Ufa).

Screening of the c.35delG mutation in the *GJB2* gene

The screening of the mutation c.35delG in the *GJB2* gene was carried out with the allele-specific amplification of fragments of the coding region of the *GJB2* gene using the primers listed in *Table 2*. The results were visualized by vertical electrophoresis in a 10% polyacrylamide gel (PAAG) with further staining of the ethidium bromide solution in the standard concentration and viewing in ultraviolet rays.

Analysis of haplotypes and estimate of the "age" of the mutation c.35delG

For the analysis of the haplotypes and the estimated age of the mutation c.35delG in the *GJB2* gene, three high-polymorphic microsatellite CA-markers were used: D13S175, D13S141, and D13S143 [6, 9, 10, 12, 36], flanking the DFNB1 locus, which contains the *GJB2* gene. The physical and genetic localization of the markers at chromosome 13 and genetic distances between them, as well as the *GJB2* gene, were identified on the basis of the Marshfield genetic linkage map (http://www.ncbi.nlm.nih.gov/mapview/). The total physical distance of the flanked region was ~ 2 Mb. (*Fig. 2*). The choice of the markers was preconditioned to fall with the strive to get the possibility of comparable data, as earlier these markers were used for the assessment of the age of mutations in the gene *GJB2* in different populations [6, 9, 10, 12, 36].

The STR-markers were genotyped using PCR at the thermocycler (Eppendorf), and appropriate oligonucleotide primers were used (*Table 2*). Products of the

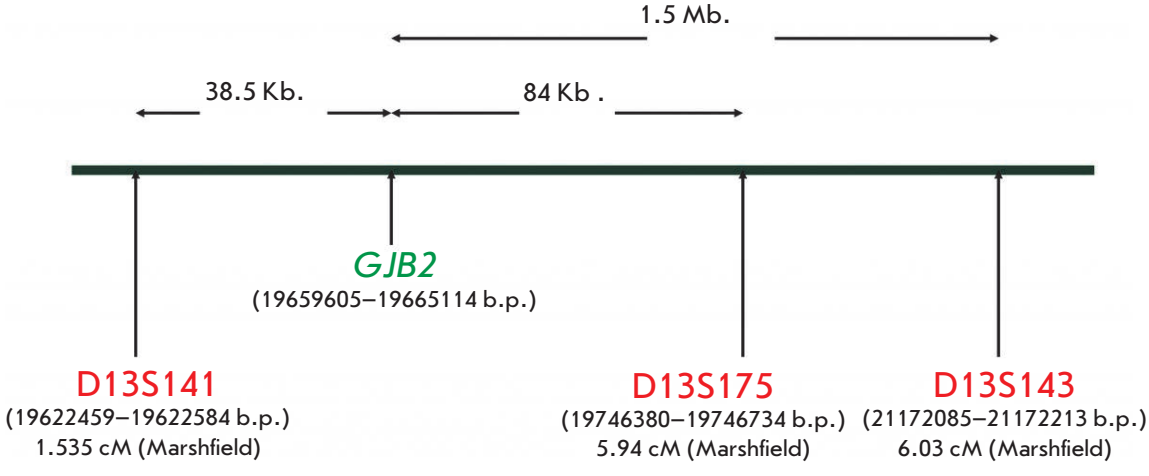

Fig. 2. Localization of the microsatellite markers D13S141, D13S175, and D13S143, flanking the *GJB2* gene, on chromosome 13. The distance between the *GJB2* gene and the markers is indicated by arrows.

Table 1. Carrier frequencies of the c.35delG mutation in 18 ethnic groups dwelling on the territory of Eurasia

Population	Linguistic affiliation (group)	Region	N	Number of heterozygote carriers of the mutation c.35delG / total numbers of individuals tested (carrier frequency)
Eastern Europe				
Byelorussians	Indo-European / Slavic	The Republic of Belarus (disperse sample)	97	6/97 (0.062)
Ukrainians	Indo-European / Slavic	Kharkov region and Poltava region, Ukraine	90	3/90 (0.033)
Volga-Ural region				
Russians	Indo-European / Slavic	Yekaterinburg, the Russian Federation (RF)	92	2/92 (0.022)
Bashkirs	Altaic / Turkic	Baimakskii, Burzyanskii, Abzelilovskii, Kugarchinskii, Salavatskii, and Arkghangelskii districts, the Republic of Bashkortostan, RF	400	1/400 (0.003)
Tatars	Altaic / Turkic	Al'met'evskii and Yelabuzhskii districts, the Republic of Tatarstan, RF	96	1/96 (0.010)
Chuvashs	Altaic / Turkic	Morgaushskii district, the Chuvash Republic, RF	100	0/100
Mordvins	Uralic / Finno-Ugric	Staroshaiginskii district, the Republic of Mordovia, RF	80	5/80 (0.062)
Udmurts	Uralic / Finno-Ugric	Malopurginskii district of the Udmurt Republic and Tatyshlinskii district of the Republic of Bashkortostan, RF	80	3/80 (0.037)
Komi-Permyaks	Uralic / Finno-Ugric	Kachaevskii district, the Komy-Permyak Autonomous District, RF	80	0/80
Central Asia				
Kazakhs	Altaic / Turkic	Alma-Atinskaya region, Kyzylordinskaya region, and Abaiskii district, Kazakhstan	240	2/240 (0.008)
Uighurs	Altaic / Turkic	Alma-Atinskaya region, Kazakhstan	116	1/116 (0.009)
Uzbeks	Altaic / Turkic	The Republic of Uzbekistan (disperse sample)	60	0/60
Caucasus				
Abkhazians	North-Caucasian / Adygo-Abkhaz	Abkhazia and Georgia (disperse sample)	80	3/80 (0.038)
Avars	North-Caucasian / Dagestan	Gumbetovskii district, the Republic of Dagestan, RF	60	0/60
Cherkessians	North-Caucasian / Adygo-Abkhaz	The Karachaevo-Cherkess Republic, RF	80	1/80 (0.013)
Ingushes	North-Caucasian / Nakh	Nazran' district, the Republic of Ingushetia, RF	80	0/80
Siberia				
Altaians	Altaic / Turkic	The Republic of Altai, RF	230	0/230
Yakuts	Altaic / Turkic	Megino-Kangalasskii, Amginskii, Churapchinskii, Tattinskii, Verkhnevilyuiskii, Vilyuiskii, Nyurbinskii, and Suntarskii uluses (districts), the Republic of Sakha (Yakutia), RF	247	1/247 (0.004)

Table 2. Sequences of primers used for amplification

Locus	Name and nucleotide sequence of primers	Detection method	Reference
GJB2 (13q11-q12)	35delG F 5'-CTTTTCCAGAGCAAACCGCCC-3' 35delG R 5'-TGCTGGTGGAGTGTTTGTTCAC-3'	Visualization of PCR fragments in 10% PAAG	[15]
D13S141	F- 5'-GTCCTCCCGGCCTAGTCTTA-3' R-5'-ACCACGGAGCAAAGAACAGA-3'		[33]
D13S143	F-5'-CTC ATG GGC AGT AAC AAC AAAA-3' R-5'-CTT ATT TCT CTA GGG GCC AGC T-3'		[34]
D13S175	F-5'-TAT TGG ATA CTT GAA TCT GCT G-3' R-5'-TGC ATC ACC TCA CAT AGG TTA-3'		[35]

PCR-reaction were separated by vertical electrophoresis (glass size 20 × 20 cm, Helicon, Russia) in 10% PAAG and 5% glycerin. The gels were stained with silver ions.

The linkage disequilibrium between alleles of the 13th-chromosome loci was calculated using the following formula:

$$\delta = (Pd - Pn)/(1 - Pn),$$

where δ is the measure of linkage disequilibrium, *Pd* is the frequency of the associated allele among mutant chromosomes, and *Pn* is the frequency of the same allele among intact chromosomes [37].

The statistical significance of differences in the frequencies of the alleles of the studied markers on 112 chromosomes containing c.35delG and 358 chromosomes without this mutation was assessed using the standard χ^2 test 2x2 (the MedStat software).

The age of expansion of the founder haplotype bearing the mutation c.35delG in the *GJB2* gene was estimated via the genetic clock approach [38], which is based on the definition of the number of generations (*q*) from the moment of the mutation appearance in the population to the present, proceeding from the ratio of linkage disequilibrium in terms of polymorphous markers linkage with the locus of the disorder. This age was calculated using the following formula:

$$q = \log[1 - Q/(1 - Pn)]/\log(1 - \Theta),$$

where *q* is the number of generations since the moment the mutation appeared in the population, *Q* is the share of mutant chromosomes without the founder haplotype, *Pn* is the frequency of the allele of the founder haplotype in the population, and Θ is the recombinant fraction. The value of Θ was computed given the physical distance of the markers from the location of the mutation, stemming from the ratio 1 cM = 1,000,000 b.p.

The value for the allele association was estimated by the coefficient of standard linkage disequilibrium according to [39]:

$$\Delta St = \frac{p - q}{\sqrt{(p + q)(2 - p - q)}},$$

where *p* and *q* are the frequencies of the alleles or haplotypes of the normal (*p*) and mutant (*q*) chromosomes.

The haplotypic diversity indicator equivalent to the expected heterozygosity was calculated using the formula:

$$h = (1 - \sum x_i^2) N / (N - 1),$$

where *x* is the frequency of each haplotype in the population, and *N* is the sample size [40].

RESULTS AND DISCUSSION

In many populations worldwide, the main contributor to the development of nonsyndromic sensorineural hearing loss (NSHL) is the mutations of the *GJB2* gene. In most European populations, up to 40–50% of cases of NSHL are preconditionally caused by one of the major recessive mutations of this gene, c.35delG, which is revealed in the homozygous or compound-heterozygous state [41]. In connection with this, many researchers have analyzed the carrier frequency of c.35delG in a variety of populations in the world. A large-scale study which embraced 17 European countries showed that the mean carrier frequency of the c.35delG mutation amounts to 1.96% (1/51), ranging from 2.86% (1/35) in South-European countries to 1.26% (1/79) in Northern Europe [42]. In the Mediterranean region, the highest carrier frequency of c.35delG were observed in Greece (3.5%), in the southern regions of Italy (4.0%), and in France (3.4%) [43]. As a result of the meta-analysis of the c.35delG carrier frequency in over 23,000 individuals from different populations, carried out on the basis of the data published between the years of 1998 and 2008, the average regional frequencies of c.35delG were determined in the European (1.89%), American (1.52%), Asian (0.64%), and African (0.64%) populations, as well as in Oceania (1%). Also, the decreasing gradient of the carrier frequency of c.35delG (from 2.48 to 1.53%) from

south to north in European populations and from west to east (from 1.48 to 0.1%) in Asian populations [44] was confirmed.

Carrier frequency of the mutation c.35delG

An analysis of the carrier frequency of the mutation c.35delG in 18 populations of Russia and the former Soviet states was carried out (*Table 1*).

High carrier frequencies of the c.35delG were revealed in two Eastern European populations: Ukrainians (3.3%) and Byelorussians (6.2%). In the Turkic-speaking populations of the Volga-Ural region, the carrier frequencies of the mutation c.35delG were 1.0, 0.3, and 0% in Tatars, Bashkirs and Chuvashs, respectively. In the Finno-Ugric populations of the Volga-Ural region, the c.35delG mutation was present with a high carrier frequency of 6.2% in Mordvins, 3.7% in Udmurts, and it was absent in Komi-Permyaks. These frequency fluctuations among the studied populations of the Volga-Ural region are likely due to the specific features of the historic development of these populations in the region, or could be the consequence of the relatively small size of the samples. Earlier, a high carrier frequency of c.35delG (4.4%) was found in Estonians, an apparent exception for Northern European populations, who typically have low frequencies of c.35delG [42]. These data, as well as the data obtained during other studies [15, 20–22, 28, 29], indicate the significant variation in the carrier frequency of c.35delG among indigenous populations of the Volga-Ural region. The carrier frequency of the c.35delG, singled out in Russians (2.2%), was comparable to the results for the Russian population in the Central region of Russia [15, 18, 28]. In the Turkic-speaking populations of Central Asia (Kazakhs, Uighurs, and Uzbeks) the mutation c.35delG with a low carrier frequency was observed in Kazakhs (0.8%), Uighurs (0.9%), and it was absent in Uzbeks. In the Turkic-speaking populations of Siberia (Yakuts and Altaians) a relatively low carrier frequency of the mutation c.35delG (0.4%) was revealed in the Yakut population but was not detected in Altaians. The North Caucasus region was in the past one of the crucial migration corridors in Eurasia. It is characterized by a high diversity of the population and a complex historical development of its resident ethnoses. In the North Caucasus populations (Abkhazians, Avars, Cherkessians, and Ingushes), the mutation c.35delG was discovered only in Abkhazians (3.8%) and Cherkessians (1.3%).

The spatial distribution of the carrier frequency of the mutation in the Eurasian populations obtained on the basis of our own data and that of relevant published information on the c.35delG available as of 2010 [24] is presented in *Fig. 3*.

The data obtained significantly added to the picture of the mutation c.35delG distribution in Eurasia: European regions of Russia, just as the European part of the continent on the whole, are characterized by a high frequency of c.35delG, and this mutation is widespread in the polyethnic population of the Volga-Ural region. However, the mechanisms of its spreading and time of appearance in the Volga-Ural region are yet to be studied. To answer these questions, we carried out a haplotypic analysis of the chromosomes carrying c.35delG and those without it, using three high-polymorphous microsatellite CA-markers: D13S175, D13S141, and D13S143 [6, 9, 10, 12, 36], which flank the locus DFNB1 containing the *GJB2* gene (*Fig. 2*).

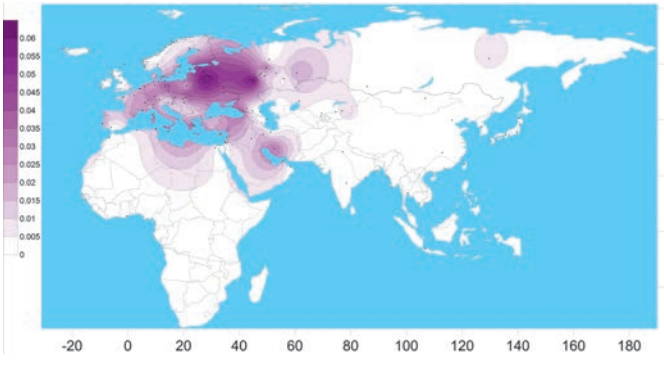

Fig. 3. The spatial distribution of the carrier frequency of the c.35delG mutation in the *GJB2* gene in the populations of Eurasia (performed using the program SURFER 9.0 Golden Software Ink).

Frequencies of alleles of loci D13S141, D13S175, and D13S143

Table 3 lists the distribution of frequencies for the alleles of microsatellite markers D13S141, D13S175, and D13S143 in the NSHL patients (c.35delG-mutant chromosomes) and in the control sample (normal chromosomes), including three ethnic groups (Russians, Tatars, and Bashkirs).

In other studies, the area sized 2 Mb and covered by these three markers allowed for the calculation of the approximate number of past generations since the start of the expansion of the proposed founder haplotype, including mutations of the *GJB2* gene, in the populations of India (mutation p.Trp24X) [8] and Morocco (c.35delG) [9]. A panel consisting of 8 STR-markers (D4S189, D13S1316, D13S141, D13S175, D13S1853, D13S143, D13S1275, and D13S292) and 2 SNP-markers was applied in dating the splicing site IVS1 + 1G>A mutation of the *GJB2* gene in the Yakut population [27]. The age of the mutations c.35delG and c.235delC was computed using the 6 SNP-markers [6, 7]. In later stud-

Table 3. Distribution of allele frequencies of microsatellite markers D13S141, D13S175, and D13S143 in patients with NSHL (chromosomes with the c.35delG mutation) and in the control sample (normal chromosomes)

Allele (b.p.)	Chromosomes with c.35delG mutation (N=112)		Normal chromosomes (N=358)		χ^2	P (95% significance level)
	Number of chromosomes	Allele frequency	Number of chromosomes	Allele frequency		
D13S141						
113	0	0	10	0.027±0.008	0.3131	0.6
123	26	0.232±0.031	211	0.589±0.026	43.458	0.000
125	84	0.750±0.042	112	0.312±0.024	67.058	0.000
127	2	0.017±0.002	25	0.069±0.013	4.2629	0.045
D13S175						
101	3	0.026±0.012	21	0.058±0.01	1.793	0.300
103	8	0.071±0.021	88	0.245±0.02	15.875	0.000
105	91	0.812±0.036	157	0.438±0.02	47.866	0.000
107	1	0.008±0.007	30	0.083±0.01	7.763	0.005
109	6	0.053±0.024	38	0.106±0.01	2.783	0.100
111	0	0	7	0.019±0.007	2.222	0.150
113	3	0.026±0.01	17	0.047±0.01	0.897	0.064
D13S143						
126	1	0.008±0.007	0	0	3.192	0.04
128	1	0.008±0.007	5	0.013±0.006	0.169	0.65
130	90	0.80±0.048	283	0.79±0.021	0.088	0.81
132	6	0.05±0.026	26	0.07±0.013	0.490	0.54
134	12	0.11±0.016	37	0.10±0.013	0.012	0.89
136	2	0.017±0.021	3	0.008±0.004	0.727	0.55
138	0	0	4	0.011±0.005	3.278	0.05

ies aimed at clarifying the age of the mutation c.35delG in Greece, two STR-markers, D13S175 and D13S141, and six SNP-markers were used [12].

D13S141. The marker D13S141 has seven allelic variants [9, 12]; however, only four of them were revealed in the ethnic groups from the Volga-Ural region. The allele 123 (D13S141) frequency is significantly higher ($\chi^2 = 43.458$; $p = 0.000$) on chromosomes of individuals from the control group (59%), whereas in NSHL patients, it is only 23%. The allele 125 (D13S141) is observed in the mutant chromosomes with a frequency of 75%, which is significantly higher than in normal chromosomes (31%) ($\chi^2 = 67.058$; $p = 0.000$), and it matches the data on the allele 125 (D13S141) dominance on chromosomes with the mutation c.35delG in NSHL patients from Morocco, Greece, Palestine, and Israel [9, 10, 12, 45].

D13S175. The marker D13S175 has eight allelic variants [9, 10, 12], of which seven are present in the ethnic groups of the Volga-Ural region. The allele 105 (D13S175) on c.35delG chromosomes is observed at a frequency of 81.2%, which is significantly higher in comparison with the normal chromosomes (43.8%) ($\chi^2 = 47.866$; $p = 0.000$), and allele 103 (D13S175) was significantly more frequent in the controls ($\chi^2 = 47.866$; $p = 0.000$ and $\chi^2 = 15.87$; $p = 0.000$, respectively) (*Table. 3*). Earlier, it was shown that, on the chromosomes with the mutation c.35delG in NSHL individuals from Tunisia, Algeria, Morocco, and Greece, allele 105

(D13S175) was also very frequent (from 67 to 100%) [9, 12, 46]. Allele 111 (D13S175) was not observed on the chromosomes of individuals with NSHL but it was present in 2% of the chromosomes of people with no hearing problems.

D13S143. The marker D13S143 has eight allelic variants [9, 12], of which seven are present in the ethnic groups residing in the Volga-Ural region. Allele 130 (D13S143) is the most frequent both on normal chromosomes (79%) and c.35delG chromosomes (80%), and allele 134 (D13S143) is more often detected on chromosomes of c.35delG-mutant individuals ($\chi^2 = 9.909$; $p = 0.005$).

An analysis of the distribution of the allele frequencies of three microsatellite loci D13S141, D13S175, and D13S143 on normal and c.35delG chromosomes revealed a pronounced misbalance in linkage between the specific alleles of these markers and mutation c.35delG in the *GJB2* gene (*Table. 3*). The degree of association of the out-gene microsatellite loci under study vividly reflects the standard coefficient of the allele association (ΔSt) [39]. The greatest degree of linkage with the mutation c.35delG is typical of allele 125 of the marker D13S141 (ΔSt = -0.438) and allele 105 of the marker D13S175 (ΔSt = -0.386).

Haplotype analysis and age of c.35delG mutation

Given the data we obtained during the study of the polymorphism of the markers D13S141, D13S175, and D13S143, and the linkage disequilibrium of some of their alleles with the mutation c.35delG in the *GJB2* coding region, we suggested that they may be evidence of the presence of a single ancestor haplotype, which carries this mutation. As a result, for three polymorphic loci, haplotypes of members of each of the 56 families with hereditary deafness and healthy donors were constructed. A precise identification of the haplotype by the alleles D13S175–D13S143–D13S141 is possible for 112 mutant chromosomes with c.35delG and 358 normal chromosomes.

In all of the chromosomes analyzed, 59 different variants of haplotypes were revealed, of which 52 were found on normal chromosomes and 25 on c.35delG-mutant chromosomes (*Table 4*).

The distribution of the haplotypes on 358 normal chromosomes is characterized by a high value of haplotypic diversity ($h = 0.943$), the frequency of the most wide-spread haplotype 123-105-130 amounts to 17.8%, and 11 other haplotypes are found at frequencies exceeding 2%. For the distribution of haplotype frequencies on 112 chromosomes with the mutation c.35delG, a lower value of the haplotypic diversity ($h = 0.645$) is typical, the haplotype 125-105-130 is the most frequently found (59%), and the frequency of six haplotypes exceeds 2%. Seven haplotypes rarely occurring on the mutant chromosomes (below 2%) were not detected on normal chromosomes. The graphic mapping of the occurrences of the haplotypes D13S141–D13S175–D13S143 on the normal chromosomes of healthy donors and c.35delG-mutant chromosomes in NSHL patients is illustrated in *Fig. 4*.

An analysis of the distribution of the haplotypes D13S141–D13S175–D13S143 on normal chromosomes in people of different ethnic origins (Russians, Tatars, and Bashkirs) showed differences in the spectrum of haplotypes in the surveyed ethnic groups and statistically significant differences in the frequencies of the haplotypes ($\chi^2 = 57.335$; $p = 0.000$; d.f. = 56). In Russians

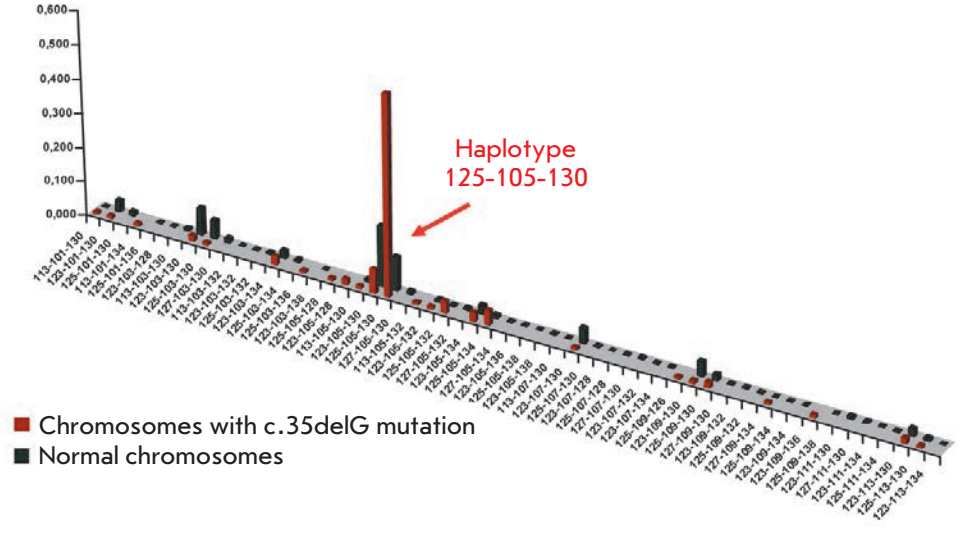

Fig. 4. The distribution of frequencies of haplotype D13D141-D13S175-D13S143 on normal chromosomes and chromosomes with a mutation c.35delG in patients with NSHL (nonsyndromic sensorineural hearing loss). Along the vertical and horizontal axes the frequency of the haplotype and the names of the haplotype are indicated, respectively. The arrow shows the haplotype 125-105-130.

Table 4. Frequencies of haplotypes D13S141-D13S175-D13S143, identified in chromosomes of patients with the c.35delG / c.35delG genotype and in normal chromosomes of healthy donors living in the Volga-Ural region

Haplotypes	Patients with c.35delG\c.35delG		Overall control		Russians		Tatars		Bashkirs	
	Absolute value	Frequency	Absolute value	Frequency	Absolute value	Frequency	Absolute value	Frequency	Absolute value	Frequency
113-101-130	1	0.009	1	0.002	0	0	1	0.008	0	0
123-101-130	1	0.009	12	0.033	4	0.023	7	0.056	1	0.016
125-101-130	0	0	4	0.011	4	0.023	0	0	0	0
113-101-134	1	0.009	0	0	0	0	0	0	0	0
125-101-136	0	0	1	0.002	1	0.006	0	0	0	0
123-103-128	0	0	1	0.002	0	0	1	0.008	0	0
113-103-130	0	0	3	0.008	2	0.012	1	0.008	0	0
123-103-130	2	0.018	28	0.078	13	0.076	12	0.097	3	0.048
125-103-130	1	0.009	20	0.055	12	0.070	4	0.032	4	0.064
127-103-130	0	0	5	0.013	4	0.023	0	0	1	0.016
113-103-132	0	0	1	0.002	0	0	1	0.008	0	0
123-103-132	0	0	1	0.002	0	0	1	0.008	0	0
125-103-132	0	0	2	0.005	1	0.006	1	0.008	0	0
123-103-134	3	0.027	8	0.022	2	0.012	4	0.032	2	0.032
125-103-134	0	0	3	0.008	3	0.017	0	0	0	0
125-103-136	1	0.009	0	0	0	0	0	0	0	0
123-103-138	0	0	1	0.002	0	0	1	0.008	0	0
125-105-128	1	0.009	0	0	0	0	0	0	0	0
123-105-128	2	0.018	0	0	0	0	0	0	0	0
113-105-130	1	0.009	3	0.008	3	0.017	0	0	0	0
123-105-130	8	0.071	64	0.178	25	0.145	24	0.194	15	0.242
125-105-130	66	0.590	35	0.097	24	0.140	5	0.040	6	0.097
127-105-130	0	0	3	0.008	3	0.017	0	0	0	0
113-105-132	1	0.009	0	0	0	0	0	0	0	0
123-105-132	1	0.009	3	0.008	0	0	2	0.016	1	0.016
125-105-132	4	0.036	1	0.002	1	0.006	0	0	0	0
127-105-132	0	0	2	0.005	2	0.012	0		0	0
123-105-134	3	0.027	9	0.025	3	0.017	4	0.032	2	0.032
125-105-134	5	0.045	4	0.011	3	0.017	1	0.008	0	0
127-105-134	0	0	1	0.002	0	0	1	0.008	0	0
123-105-136	0	0	2	0.005	0	0	2	0.016	0	0
125-105-138	0	0	1	0.002	0	0	1	0.008	0	0
123-105-138	0	0	1	0.002	1	0.006	0	0	0	0
113-107-130	0	0	1	0.002	0	0	1	0.008	0	0
123-107-130	1	0.009	16	0.044	4	0.023	4	0.032	8	0.129
125-107-130	0	0	1	0.002	1	0.006	0	0	0	0
123-107-128	0	0	1	0.002	0	0	0	0	1	0.016
125-107-128	0	0	1	0.002	0	0	1	0.008	0	0
127-107-130	0	0	2	0.005	0	0	2	0.016	0	0
123-107-132	0	0	1	0.002	0	0	1	0.008	0	0
123-107-134	0	0	1	0.002	0	0	1	0.008	0	0
125-109-126	1	0.009	0	0	0	0	0	0	0	0
123-109-130	1	0.009	16	0.044	9	0.052	4	0.032	3	0.048
125-109-130	2	0.018	7	0.019	6	0.035	1	0.008	0	0
127-109-130	0	0	1	0.002	1	0.006	0	0	0	0
123-109-132	0	0	2	0.005	1	0.006	1	0.008	0	0
125-109-132	0	0	1	0.002	1	0.006	0	0	0	0
127-109-134	1	0.009	1	0.002	0	0	0	0	1	0.016
125-109-134	0	0	1	0.002	1	0.006	0	0	0	0
123-109-134	0	0	1	0.002	1	0.006	0	0	0	0
123-109-136	1	0.009	0	0	0	0	0	0	0	0
125-109-138	0	0	1	0.002	1	0.006	0	0	0	0
123-111-130	0	0	3	0.008	0	0	3	0.024	0	0
127-111-130	0	0	2	0.005	1	0.006	0	0	1	0.016
123-111-134	0	0	1	0.002	0	0	1	0.008	0	0
125-111-134	0	0	1	0.002	0	0	0	0	1	0.016
123-113-130	2	0.018	8	0.022	6	0.035	1	0.008	1	0.016
125-113-130	1	0.009	3	0.008	2	0.012	1	0.008	0	0
123-113-134	0	0	1	0.002	0	0	0	0	1	0.016
Haplotypic diversity	0.645		0.943		0.944		0.917		0.946	
Total, chromosomes	112		358		172		124		62	
Number of haplotype variants	25		52		32		32		16	

Table 5. Association and linkage disequilibrium of markers D13S141, D13S175, and D13S143 with the mutation c.35delG

Marker	Allele	P (95% significance level)	χ^2	Δ
D13S141	125	<0.001	67.05872	0.636179
D13S175	105	<0.001	47.8665	0.666045
D13S143	130	0.81	0.08801	0.062381

Table 6. The number of generations which passed since the time of the c.35delG mutation spread in the Volga-Ural region

Marker	Number of generation since the time of the mutation's appearance in the population (q)	Number of years which passed from the start of expansion	Start of expansion
D13S175 (allele 105)	470	11800	9800 B.C.
D13S141 (allele 125)	133	3300	1300 B.C.
Mean value	301	7500	5500 B.C.

(172 analyzed chromosomes), 32 of the 59 haplotypes were revealed in the total sample; in Tatars (124 chromosomes analyzed), 32 of the 59; and in Bashkirs (62 chromosomes), 17 of the 59 haplotypes.

In Russians, the most widespread haplotypes were 123-105-130 (14.5%), 125-105-130 (14.0%), and 123-103-130 (7.6%), while the remaining 29 occurred at different frequencies: from 0.6% (12 haplotypes) to 7.0% (haplotype 125-103-130). On normal chromosomes in Tatars, the haplotypes 123-105-130 and 123-103-130 occurred most often at frequencies of 19.4 and 9.7%, respectively, and the frequencies of the remaining 30 varied from 0.8% (19 haplotypes) to 5.6% (haplotype 123-101-130). In Bashkirs, the haplotypes 123-105-130 (24.2%), 123-107-130 (12.9%) and 125-105-130 (9.7%) were most often recorded, and their total frequency reached 46.8%. The frequencies of the remaining 14 haplotypes varied from 1.6% (9 haplotypes) to 6.4% (haplotype 125-103-130). Besides, in each ethnic group, specific haplotypes (D13S141–D13S175–D13S143), non-occurring in other groups, were observed at low frequencies: in Russians, 14 haplotypes; in Tatars, 15; and in Bashkirs, 4.

An analysis of the haplotypes D13S141-D13S175-D13S143 revealed that there is a higher frequency of haplotype 125-105-130 on chromosomes with the c.35delG mutation compared to the chromosomes of healthy donors ($\chi^2 = 64.866$, $p < 0.001$), as well as an ethnic specificity of the spectra and frequencies of occurrence of the haplotypes D13S141–D13S175–D13S143 in three ethnic groups of healthy donors.

Table 5 shows data on the association and linkage disequilibrium of marker D13S175, D13S143, and D13S141 alleles carrying the mutation c.35delG.

The values of the linkage disequilibrium parameter were greatest in alleles 105 and 125 of D13S175 and D13S141 markers, respectively, located proximally relative to the gene *GJB2*, and the lowest in alleles of the distal D13S143 marker. Stemming from the values of χ^2 and the linkage disequilibrium parameter δ, the most probable founder haplotype (the ancestor haplotype) seems to consist of the alleles 125-105-130 (*Fig. 4*). The haplotype 125-105-130 was revealed on 59% of all chromosomes carrying c.35delG, which is reliably higher ($p < 0.001$) than the frequency of this haplotype (9.7%) on normal chromosomes.

To calculate the number of generations since the start of the spread of the c.35delG mutation in the populations of the Volgo-Ural region, we selected two markers: D13S175 and D13S141. The selection criterion for these markers was relatively high values of χ^2 and measure of linkage disequilibrium δ; statistically significant differences in the frequency distribution of these marker alleles in chromosomes with and without c.35delG were also considered.

No statistically significant differences in the frequency distribution of alleles of the marker D13S143 between c.35delG and intact chromosomes (*Table. 3*), and concurrently a minimum value of the linkage disequilibrium parameter, were observed (*Table 5*). The prevalence of the allele 130 of this STR-marker in two groups of chromosomes (with and without the c.35delG mutation) formally explains the absence of statistically significant differences. Nevertheless, given the statistically significant differences obtained for two other STR-markers, which are closer to the c.35delG mutation, the existence of the ancestor haplotype for c.35delG, embracing the area covered by the D13S141-D13S175-D13S143 markers, and its subsequent "tailing" at the expense of recombination and mutation events during the numerous generations seem likely. However, the absence of a statistically significant association of the most frequent allele 130 (D13S143) and the ancestor haplotype provided grounds for excluding D13S143 from markers using which the number of generations was computed (*Table 6*).

After the beginning of divergence of the c.35delG-mutant ancestor haplotype in the populations of the

Volga-Ural region, from 133 to 470 generations (on average 301 generations) passed. At the estimate of the age (in years) of the ancestor haplotype reconstructed on the territory of the Volga-Ural region, the duration of one generation, as in other studies, was considered equal to 25 years (*Table 6*).

The time over which the expansion of the c.35delG-mutant chromosomes has been present within the population of the Volga-Ural region ranges from 3,300-11,800 years (mean is ~ 7,500). However, such estimates of the number of generations (based on the physical distance) often lead to the overestimation of the "age" of the mutation, because it is the probable (not the observed) value for the mutation events that is considered; therefore, with this approach, researchers do not orientate mean values. Instead, they choose the most distant marker, which is linked however to the locus of the disease, i.e. the so-called boundary of the stable haplotype [47]. In the given case, it is the D13S175 marker. If one presumes that the number of generations calculated with the use of this marker is more accurate, then the most likely time of expansion of the founder haplotype with the mutation c.35delG in the populations of the Volga-Ural region is ~ 11,800 years. Such dating of the beginning of c.35delG expansion in the Volga-Ural region matches the results obtained in studies with the use of different DNA markers (SNP- and STR-markers) in other populations of Eurasia (10,000–14,000 years ago) [9–12].

The results of the haplotype analysis, estimates of the age of the c.35delG mutation, and data on the descending gradient to fit carrier frequency from south to north in the European populations allow to suggest that the Middle East and Mediterranean regions (probably, modern Greece) are the most probable centers of c.35delG origin, from where, together with Neolithic migrations of man, it widely propagated throughout Europe [9–12]. An analysis of the haplotypic diversity (using STR-markers) and approximate assessment of the age of c.35delG in the Volga-Ural region favor to a great extent the "traditional" Neolithic hypothesis about the origin and spread of this mutation.

Considering the unified time continuum of the start of c.35delG spread in Eurasia, obtained with the use of various systems of DNA markers (SNP- and STR-markers), an assessment of the world haplotypic diversity of the mutant chromosomes accounting for the integral set of DNA markers is required to get an unambiguous answer to the question of the center of origin of the c.35delG mutation.

CONCLUSIONS

The analysis of the carrier frequency of the mutation c.35delG in the *GJB2* gene in Eurasian populations has revealed a tendency towards gradient decrease in the c.35delG frequency from West to East, starting from the populations of Eastern Europe and the Volga-Ural region, with average frequencies of 3.3 and 1.4%, respectively; a low frequency (0.8–0.9%) in Central Asian populations, a minimum frequency (0.4%) in Yakuts residing in Eastern Siberia; and the absence of c.35delG in Altaians (Southern Siberia).

A haplotype analysis of the c.35delG-mutant chromosomes has allowed us to reconstruct the ancestor haplotype carrying this mutation and to confirm the unified origin of most of the studied mutant chromosomes of NSHL patients living in the Volga-Ural region. The estimated time of expansion of the c.35delG mutation carriers we obtained (11,800 years ago) fits the world values of the "age" of this mutation (10,000–14,000 years).

The body of data collected should help clarify or review existing ideas about the center and time of origination of the c.35delG mutation (*GJB2*), as well as the factors that define its occurrence worldwide. ●

This work was supported by a Grant of the Russian Foundation for Basic Research (№ 09-04-01123-a), Federal Target-Oriented Programs "Scientific and Scientific-Pedagogical Personnel of Innovative Russia in 2009–2013" (№ 16.740.11.0190, 16.740.11.0346) and for 2010–2012 (№ 02.740.11.0701), as well as by the Russian Ministry of Education and Science (Government Contracts P325 and P601) and Government Contract № 16.512.11.2047.

REFERENCES

1. Marazita M.L., Ploughman L.M., Rawlings B., Remington E., Arnos K.S., Nance W.E. // Am. J. Med. Genet. 1993. V. 46. № 5. P. 486–491.
2. van Camp G., Smith R. // 2009. http://webhost.ua.ac.be/hhh/
3. Maeda S., Nakagawa S., Suga M., Yamashita E., Oshima A., Fujiyoshi Y., Tsukihara T. // Nature. 2009. V. 458. №7238. P. 597–602.
4. Kikuchi T., Kimura R.S., Paul D.L., Adams J.C. // Anat. Embryol. (Berl.). 1995. V. 191(2). P. 101–118.
5. Morell R.J., Friderici K.H., Wei S., Elfenbein J.L., Friedman T.B., Fisher R.A. // N. Engl. J. Med. 1998. V. 339. P. 1500–1505.
6. van Laer L., Huizing E.H., Verstreken M., van Zuijlen D., Wauters J.G., Bossuyt P.J., van de Heyning P., McGuirt W.T., Smith R.J. // J. Med. Genet. 2001. V. 38. P. 515–518.
7. Yan D., Ke X., Blanton S.H., Ouyang X.M., Pandya A., Du L.L., Nance W.E., Liu X.Z. // Hum. Genet. 2003. V. 114. P. 44–50.
8. RamShankar M., Girirajan S., Dagan O., Ravi Shankar H.M., Jalvi R., Rangasayee R., Avraham K.B., Anand A. // J. Med. Genet. 2003. V. 40. P. 68.

9. Abidi O., Boulouiz R., Nahili H., Ridal M., Noureddine A.M., Tlili A., Rouba H., Masmoudi S., Chafik A., Hassar M., et al. // Genet. Test. Mol. Biomark. 2007. V. 12. №4. P. 569–574.
10. Kokotas H., Grigoriadou M., Villamar M., Giannoulia-Karantana A., del Castillo I., Petersen B.M. // Genet. Test. Mol. Biomark. 2010. V. 14. №2. P. 183–187.
11. Najmabadi H., Cucci R., Sahebjam S., Kouchakian N., Farhadi M., Kahrizi K., Arzhangi S., Daneshmandan N., Javan K., Smith R.J.H. // Hum. Mutat. 2002. V. 504. P. 135–138.
12. Kokotas H., van Laer L., Grigoriadou M., Ferekidou E., Papadopoulou E., Neou P., Giannoulia-Karantana A., Kandiloros D., Korres S., Petersen M.B. // Am. J. Med. Genet. 2008. V. 146A. P. 2879–2884.
13. Brobby G., Müller-Myhsok B., Horstmann R. // N. Engl. J. Med. 1998. V. 338 (8). P. 548–550.
14. Hamelmann C., Amedofu G.K., Albrecht K., Muntau B., Gelhaus A., Brobby G.W., Horstmann R.D. // Hum. Mutat. 2001. V. 18. № 1. P. 84–85.
15. Anichkina A., Kulenich T., Zinchenko S., Shagina I., Polyakov A., Ginter E., Evgrafov O., Viktorova T., Khusnitdonova E. // Eur. J. Hum. Genet. 2001. V. 9. P. 151.
16. Nekrasova N.U., Shagina I.A., Petrin A.N., Polyakov A.V. // Med. genet. 2002. V. 1. № 6. P. 290-294.
17. Zinchenko R.A., Elchinova G.I., Barishnikova N.V., Polyakov A.V., Ginter E.K. // Russian Journal of Genetics. 2007. V. 43. № 9. P. 1246-1254.
18. Zinchenko R.A., Zinchenko S.P., Galkina V.A. // Russian Journal of Genetics. 2003. V. 39. № 9. P. 1275-1284.
19. Osetrova A.A., Sharonova E.I., Rossinskaya T.G., Zinchenko R.A. // Med. genet. 2010. № 9. P. 30-40.
20. Khidyatova I.M, Dzhemileva L.U., Khabibulin R.M., Khusnutdinova E.K. // Mol. biol. 2002. V. 36. № 3. P. 438-441.
21. Khusnutdinova E.K., Dzhemileva L.U. // Vestn. Bioteh. and Physico-Chemical Biolog. 2005. № 1. P. 24-31.
22. Dzhemileva L.U., Barashkov N.A., Posukh O.L., Khusainova R.I., Akhmetov V.L., Kutuev I.A., Tadinova V.N., Fedorova S.A., Khidyatova I. M., Khusnutdinova E.K. // Med. Genet. 2009. № 8. P. 20-28.
23. Dzhemileva L. U., Posukh O. L., Tazetdinov A. M., Barashkov N. A., Zhuravskii S. A., Ponidelko S. N., Markova T. G., Tadinova V. N., Fedorova S. A., Maksimova N. R., Khusnutdinova E. K. // Russian Journal of Genetics. 2009. № 7. P. 982-991..
24. Dzhemileva L.U., Barashkov N.A., Posukh O.L., Khusainova R.I., Akhmetova V.L., Kutuev I.A., Gilyazova I.R., Tadinova V.N., Fedorova S.A., Khidiyatova I.M., et al. // J. Hum. Genet. 2010. V.55. № 11. P. 749–754.
25. Posukh O.L., Pallares-Ruiz N., Tadinova V., Osipova L., Claustres M., Roux A.F. // BMC Med. Genet. 2005. V. 6. № 12. P. 1–7.
26. Barashkov N.A., Dzhemileva L.U., Fedorova S. A., Maksimova N.R., Khusnutdinova E. K. // Vest. otorin. 2008. № 5. P. 23-28.
27. Barashkov N.A., Dzhemileva L.U., Fedorova S. A., Terutin F.M., Fedorova E.E., Gurinova E.E., Alekseeva S.P., Kononova S.K., Nogovicina A.N., Khusnutdinova E.K. // Med. genet. 2010. V. 9. № 7 (97). P. 22-33.
28. Shokarev R.A., Amelina S.S., Kriventsova N.V. // Med. genet. 2005. V. 4. № 12. P. 556- 567.
29. Shokarev R.A., Amelina S.S., Zinchenko S.N., Elchinova G.I., Khlebnikova O.O., Blisnez E.A., Tverskaya S.M., Polyakov A.V., Zinchenko R.A. // Med. genet. 2006. V. 5. P. 38-43.
30. Boghkova V.P., Hashaev Z.H., Umankaya T.A. // Biophis. 2010. V. 55. № 3. P.514-525.
31. Tavartkiladze G.A., Polyakov A.V., Markova T.G., Lalayanz M.R., Blisnez E.A. // Vestn. otorin. 2010. № 3. P.1-18.
32. Tazetdinov A.M., Dzhemileva L.U., Khusnutdinova E.K. // Russian Journal of Genetics. 2008. V. 44. № 6. P. 725-733.
33. Denoyelle F., Weil D., Maw M. // Hum. Mol. Genet. 1997. V. 12. № 6. P. 2173–2177.
34. Petrukhin K.E., Speer M.C., Cayanis E., Bonaldo M.F., Tantravahi U., Soares M.B., Fischer S.G., Warburton D., Gilliam T.C., Ott J. // Genomics. 1993. V. 15. № 1. P. 76–85.
35. Brown K.A., Janura A., Karbani G., Parrys G., Noble A., Crockford G., Bishop D.T., Newton V.E., Markham A.F., Mueller R.F. // Hum. Mol. Genet. 1996. V. 5. P. 169–173.
36. Rothrock C.R., Murgia A., Sartorato E.L., Leonardi E., Wei S., Lebeis S.L., Yu L.E., Elfenbein J.L., Fisher R.A., Friderici K.H. // Hum. Genet. 2003. V. 113. P. 18–23.
37. Bengtsson B.O., Thompson G. // Tissue Antigens. 1981. V. 18. P. 356–363.
38. Risch N., de Leon D., Ozelius L. // Nat. Genet. 1995. V. 9. № 2. P. 152–159.
39. Krawczak M., Konecki D.S., Schmidtke I. // Hum. Genet. 1988. V. 80. P. 78–80.
40. Nei M. Molecular Evolutionary Genetics. New York: Columbia University Press, 1987. 275 p.
41. Petersen M., Willems P. // Clin. Genet. 2006. V. 69. P. 371–392.
42. Gasparini P., Rabionet R., Barbujani G., Melchionda S., Petersen M., Brondum-Nielsen K., Metspalu A., Oitmaa E., Pisano M., Fortina P., et al. // Eur. J. Hum. Genet. 2000. V. 8. №1. P. 19–23.
43. Lucotte G. // Int. J. Pediatr. Otorhinolaryngol. 2007. V. 71. P. 741–746.
44. Mahdieh N., Rabbani B. // Int. J. Audiol. 2009. V. 48. P. 363–370.
45. Shahin H., Walsh T., Sobe T., Lynch E., ·King M.-C., Avraham K.B., Kanaan M. // Hum. Genet. 2002. V. 110. P. 284-289.
46. Belguith H., Hajji S., Salem N., Charfeddine I., Lahmar I., Amor M.B., Ouldim K., Chouery E., Driss N., Drira M., et al. // Clin. Genet. 2005. V. 68. P. 188–189.
47. Slatkin M., Rannala B. // Annu. Rev. Genomics Hum. Genet. 2000. V. 1. P. 225–249.

Effective Genetic Expression of Nanoantibodies by Recombinant Adenoviral Vector *in vitro*

I.Yu. Gribova[1], S.V. Tillib[2], I.L. Tutykhina[1], M.M. Shmarov[1], D.Yu. Logunov[1], L.V. Verkhovskaya[1], B.S. Naroditskii[1*], A.L. Gintsburg[1]

[1] Gamaleya Research Institute for Epidemiology and Microbiology

[2] Institute of Gene Biology, Russian Academy of Sciences

*E-mail: bsnar1941@yahoo.com

Received 12.05.2011

ABSTRACT **The present study is devoted to the feasibility of expressing the single-domain mini-antibody (nanoantibody) selected from the library of sequences of the variable domains of special single-stranded antibodies derived from an immunized camel, a gene of which was introduced into eukaryotic cells within a recombinant adenoviral vector. A vector bearing the gene of a single-domain nanoantibody was obtained using the AdEasy Adenoviral Vector System (Stratagene). This method of delivering the nanoantibody gene facilitates efficient expression of this gene and functional activity of the nanoantibody. The results obtained can be used to produce passive immunizing tools against pathogens or new-generation immunobiological antitoxic medication.**

KEYWORDS **recombinant adenoviral vector; nanoantibodies; genetic immunization.**

ABBREVIATIONS **HEK-293 – human embryonic kidney cell culture; His_6-tag - amino acid motif in proteins consisting of six histidines; HA-tag – epitope tag (YPYDVPDYA) derived from the haemagglutinin molecule; PFU – plaque-forming unit; PCR – polymerase chain reaction; PT-PCR – reverse transcription polymerase chain reaction; GAPDH - glyceraldehyde 3-phosphate dehydrogenase.**

INTRODUCTION

Antibodies are the primary tools of the immune system, which participate in the protection of the organism against pathogenic microorganisms. The significance of antibodies is growing as researchers become aware of their potential not only as tools to be used in diagnostics, but in therapy as well [1]. Antibodies have been successfully used to treat certain forms of oncological conditions. Over the past decades, monoclonal antibodies have been widely used in diagnostics and for research purposes. Yet, the conventional methods used to obtain monoclonal antibodies, based on dealing with animal-origin cells, make difficult their use as therapeutic agents. Introduction of these monoclonal bodies into the human organism may result in the onset of an undesirable immune reaction, particularly, if used repeatedly [2]. In order to prevent the emergence of such an immune response, the following approaches have been developed: production of recombinant immunoglobulins in which the regions that are not responsible for antigen recognition are replaced by corresponding fragments of human origin (humanized antibodies), or removal of the domains that are not involved in antigen binding (mini-antibodies). The so-called recombinant technologies, based on the use of libraries comprising sequences from human antibodies, have found increasing application over the past decade. When constructing these libraries, variable domains of the heavy and light strands are linked in the expression vector via random screening within one reading frame via the linker sequence [3]. It is rather laborious to deal with cumbersome libraries of these single-stranded antibodies (scFv), and only in rare cases is a highly affine antibody finally obtained. Certain difficulties are associated with the instability of genetic constructions, the low level of product expression, and its solubility [4].

A significant breakthrough in this field has been the detection of non-canonical antibodies in members of the Camelidae biological family. These antibodies do not contain light strands and represent a dimer of shortened heavy strands [5, 6]. An immune response with the participation of these antibodies can be induced by conventional immunization. There are a number of advantages in using the repertoire of these non-canonical antibodies to create libraries of sequences of variable domains (for the heavy strand only). The single-domain structure of the recognizing

variable domain stipulates a small size of the antigen-binding fragment (mini-antibodies), high stability, and solubility [7].

Thanks to their structure, mini-antibodies can be used to reveal epitopes that are hidden for the conventional immunoglobulins. The expression from a single gene simplifies genetic engineering procedures and, therefore, the work with the libraries containing the sequences of variable domains. Low immunogenicity (conditioned by the high homology of the sequences of mini-antibodies with a variable domain of heavy strands of human IgG3) and the relative simplicity of the humanization procedure open broad opportunities for the application of mini-antibodies in the design of novel pharmaceutical agents [8].

These features of the structure of mini-antibodies and the simplicity with which their genes can be manipulated enable efficient and economical production of large amounts of a mini-antibody, using various expression systems [9].

The use of the prokaryotic expression system to produce mammalian proteins has to do with the possibly low functional activity of the proteins obtained, due to the absence of a system for post-translational modification in prokaryotic cells. Moreover, no matter how thorough the purification, the final product can still be contaminated with pyrogenes.

One of the promising methods for delivering genetic material to target cells is the use of viral vectors. Expression constructions bearing one or several recombinant genes are incorporated into the viral genome using methods of genetic engineering. Vectors based on the genome of the adeno-associated virus have been proposed in a number of studies [10, 11] for delivery of mini-antibody genes to target cells.

Adenoviral vectors are among the most universal tools used for delivery and expression of recombinant genes in mammalian cells. It is known that recombinant adenoviruses efficiently transfer the genes of bacterial and viral antigens, cytokines, growth factors, and other proteins to the target cells, ensuring a high level and duration of target gene expression [12]. Adenoviral vectors are capable of transducing both dividing and postmitotic cells. Adenoviral DNA remains in its extrachromosomal form, whereas the recombinant virus is excreted from the organism within 4–5 weeks [13, 14].

The production of recombinant adenoviruses is characterized by the following feature: the virus is capable of reproducing only *in vitro* in special cell lines, which ensures the vector's safety [15].

The fact that recombinant adenoviral vectors can be used efficiently for the expression of antigen-binding fragments of antibodies is borne out by the example of mini-antibodies to the cell epitope (the epidermal growth factor receptor (erbB-2) and anthrax toxin component) [16, 17].

The aim of the present work is to examine how recombinant adenoviral vectors can be used for delivery and efficient expression of single-domain mini-antibodies (nanoantibodies) obtained using the novel technology of generation of special single-stranded antibodies extracted from camel. The nanoantibody earlier obtained and characterized to the cell cytokeratine-8 [18] was selected as the model antibody. It was subsequently used to demonstrate the fundamental possibility of expressing the single-domain antibodies obtained by immunization of members of the Camelidae family via recombinant adenoviruses.

EXPERIMENTAL

Enzymes

In this study, restriction endodeoxyribonucleases, T4 DNA ligase, alkaline phosphatase (CIAP) purchased from Fermentas MBI (Lithuania), and Taq-polymerase purchased from Promega (United States) were used.

Cell lines

The HEK-293 cell line (human embryonic kidney cell culture transformed by the E1-region of human adenovirus serotype 5) and H1299 cell line (human lung cancer cells) were used. The cells were cultured in a DMEM medium containing 10% of fetal bovine serum (FBS) purchased from HyClone (United States).

Production of the cDNA clone encoding the single-domain mini-antibody (nanoantibody) which specifically recognizes the endogenous mouse cytokeratin-8

Antibody aCyK-V_HH, which specifically recognizes mouse cytokeratin-8, was obtained earlier by S.V. Tillib's research group (Institute of Gene Biology, Moscow) in collaboration with the laboratory headed by S. Muyldermans (Vrije Universiteit Brussel) and used (via binding to the fluorescent protein sequence) to obtain fluorescent nanoantibodies (or chromobodies) aimed at demonstrating the new method for tracing antigens in a living cell. It should be noted that the aCyK-V_HH nanoantibody was one of the first antibodies to endogenous structural eukaryotic proteins. The first stage of its production comprised immunization of the Bactrian camel (*Camelus bactrianus*) with a protein extract from mouse soft tissue cells (predominantly from the liver). The subsequent selection procedure, based on the phage display method, was performed as described in the online supplement to

the article [18]. The fundamental stage after selection of the most enriched antibody clones was the identification of the unknown antigen recognized by these nanoantibodies. The proteins from the nanoantibody-binding region upon Western blotting were additionally separated by electrophoresis to obtain individual products. Western blotting was then used to analyze the recognition of each product by a nanoantibody. The product recognized by a nanoantibody was identified using mass spectrometrical analysis of its trypsin hydrolysate. The resulting nanoantibody aCyK-V_HH recognized cytokeratin-8, a fact attested to via the immunofluorescent staining of C2C12 (mouse myoblast cell line) with these antibodies, revealing the characteristic distribution of cytokeratin intermediate filaments in the cytoplasm.

The nanoantibody aCyK-V_HH produced in the bacterial periplasm was modified by binding an antigen-recognizing sequence of two additional small fragments, epitope of influenza virus haemogglutinine (HA-tag) and six histidine residues (His_6-tag), in order to purify it and simplify its detection.

Obtaining recombinant adenovirus

Plasmids and the recombinant adenoviral vector were obtained using the gene of antibody to cytokeratin *aCyK-V_HH*. The nucleotide sequence encoding the nanoantibody was obtained by chemical synthesis in "Evrogen" JSC. The AdEasy Adenoviral Vector System (Stratagene, United States) was used in order to construct the pAd-aCyK-V_HH plasmid vector containing the genome of the recombinant adenovirus with E1 region deletion, and a transgene expression cassette incorporated instead of it via homologous recombination in *E. coli* cells. The recombinant adenovirus was obtained via transfection of HEK-293 cell lines with the pAd-aCyK-V_HH plasmid construct linearized on the PacI site. Lipofectamine 2000 (Invitrogen, United States) was used for the transfection, according to the manufacturer's recommendations. The recombinant human adenovirus of serotype 5 with E1 region deletion and an incorporated transgene-free cassette expression (Ad-null) inserted instead of it was used as the control.

To accumulate adenoviral preparations, an infected cell suspension (10^7 PFU of the virus per Petri dish with a diameter of 15 cm) was coated to the HEK-293 cell monolayer with 50–70% confluence. The infected cell suspension was destroyed by three freeze-thaw cycles and clarified by centrifuging (2000 rpm, 10 min, +4°C).

The titres of the specimens Ad5-aCyK-V_HH and Ad-null (10^8 PFU/ml) were determined by the plaque formation technique in the HEK-293 cell culture.

Infection of cells with a recombinant adenovirus

Approximately 10^6 cells of the H1299 line were infected with recombinant adenoviruses. The cells were seeded to ~ 70% of the monolayer, cultivated for 24 h, and infected with the recombinant adenovirus (the multiplicity of infection being 100 PFU/cell) in a DMEM medium containing 2% of FBS. Two hours after the viral preparation was introduced, the medium was collected, the cell culture was washed, and a fresh DMEM medium was added. The medium from the infected cells was collected 72 h after infection and concentrated by centrifuge ultrafiltration through a membrane with a nominally intercepted molecular weight of 10 kDa. After thickening by a factor of 10, the supernatant was fractioned in a 10% polyamide gel and used for immune blotting analysis.

Antigen preparation

Homogenized mouse liver lysate (BALB/c line) was obtained via extraction with the use of a RIPA buffer (50 mM Tris-HCl, pH 8.0, 150 mM NaCl, 1% NP-40, 0.5% sodium deoxycholate, protease inhibitor kit (Roche, Switzerland)). The concentration of the total protein in the specimens was determined by the Bradford method (Sigma-Aldrich, United States). The specimens with an equal protein concentration were applied to the gel to be separated by electrophoresis.

Polyacrylamide gel electrophoresis and immunoblotting

Cellular proteins were separated by polyacrylamide gel electrophoresis by the Laemmli procedure under denaturing conditions in the presence of sodium dodecyl sulphate. Protein Test Mixture 4 (Serva, Germany) was used as the molecular weight standard. After the gel electrophoresis, the proteins were placed onto a Hybond-P PVDF membrane (GE Healthcare, United States) using a TE70 Semi-Dry Transfer Unit (Hoefer Scientific, United States) in accordance with the manufacturer's recommendations. The nanoantibodies were detected using the Monoclonal Anti-HA–Peroxidase antibody (Sigma-Aldrich, United States). The immobilized proteins were detected using ECL Plus Western Blotting Detection Reagents (GE Healthcare, United States) in accordance with the manufacturer's recommendations. The chemilumenscent radiation was recorded with the aid of an Amersham Hyperfilm ECL X-ray film (GE Healthcare, United States).

RESULTS

As a result of the earlier performed selection of the phage library of the antigen-binding domains of single-stranded antibodies, DNA from the pHEN4 phagemid

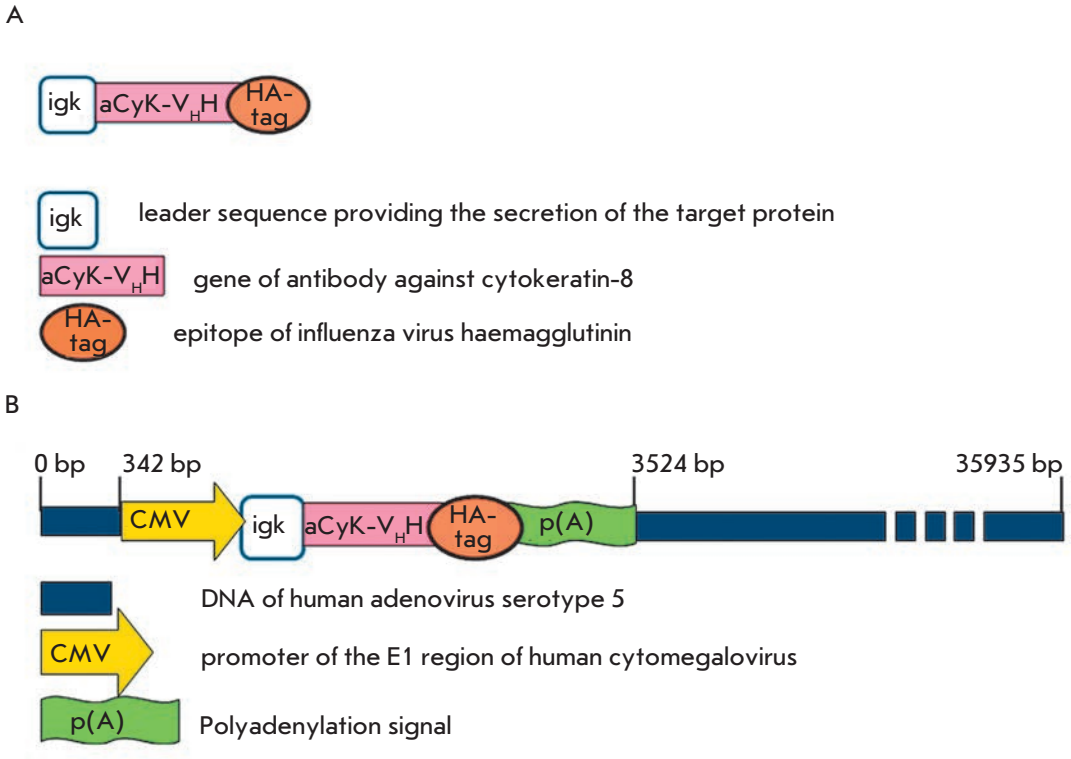

Fig. 1. Schematic description of the genetic constructions used. A – Genetic construction containing the gene of nanoantibody against cytokeratin. B – The recombinant adenovirus genome bearing the gene of nanoantibody against cytokeratin.

with an insertion encoding the nanoantibody, which has a high affinity towards the structural cytoplasmatic mouse protein, cytokeratin-8, was collected. The data on the structure of the target protein were obtained via mass spectrometric identification. The nucleotide sequence encoding the nanoantibody was cloned in the recombinant adenoviral vector.

A leading peptide of the mouse immunoglobulin κ-chain was bound to its N-terminus, in order to ensure efficient extracellular expression of a nanoantibody. The HA-tag, which is effectively recognized by commercial antibodies, a requirement for confirming nanoantigen expression at the protein level, was bound to the C-terminus of the nanoantibody. *Figure 1* shows the scheme of the resulting construct.

In order to construct the adenoviral vector, the sequence encoding the HA-tag-labelled aCyK-V_HH antibody was cloned in the shuttle plasmid vector pShuttle-CMV (Stratagene, United States). This vector contains terminal fragments of the human adenovirus serotype 5 genome, the expression cassette containing the human cytomegalovirus promoter (CMV) and polyadenylation signal. The presence of the insertion and its orientation were confirmed by restriction mapping.

The recombinant plasmid adenoviral vector bearing the target gene was obtained via homologous recombination in *E. coli* cells. The plasmid construct obtained contained the replication initiation site ori, the gene of antibody resistance, and a cassette with the target gene within the adenoviral genome. The main advantage of this method is the potential utilization of *E. coli* cells as the main tools for cloning, recombination, and production of adenoviral DNA in preparative amounts. The opportunity to perform the homologous recombination in *E. coli* cells makes it possible to deal with the individual clones containing plasmid constructs only with recombinant adenoviruses, which eliminates the possibility of contamination with a wild-type adenovirus.

The shuttle plasmid construct bearing the expression cassettes with the nanoantibody gene was linearized on the PmeI site and introduced along with pAd-EASY (Stratagene) to *E. coli* BJ5183 cells by electroporation. Recombinant clones obtained by homologous recombination were collected on the selective kanamycin-containing medium (50 μg/ml). The presence of recombinant clones of nucleotide sequences encoding the aCyK-V_HH antibody and human adenovirus serotype 5 fibre in plasmid DNA was analyzed by PCR with specific primers and via restriction mapping, using HindIII restrictase, which enables one to obtain a restriction pattern that is typical for the human adenovirus genome.

HEK-293 cells were transfected with a plasmid cleaved at the PacI site and containing the recombinant adenovirus genome with E1 region deletion and the expression cassette with a transgene inserted instead of it. The resulting recombinant adenovirus Ad5-aCyK-

V_HH was analyzed by PCR using the primer pair that was complementary to the target gene, the hexon gene of human adenovirus serotype 5, and the E1 region of the adenovirus in order to control the possible presence of replication-competent viral particles.

Detection of the expression of the nanoantibody gene within the recombinant adenovirus Ad5-aCyK-V_HH

The expression of the target gene within the recombinant human adenovirus serotype 5 Ad5-aCyK-V_HH was analyzed at the level of the mRNA. With this purpose in mind, the cells of the HEK-293 line that are permissive for human adenovirus serotype 5 were infected with the recombinant virus Ad5-aCyK-V_HH. The total RNA of infected cells was used to produce DNA, which was analyzed by PCR with primers specific to the sequence of the nanoantibody gene to mouse cytokeratin 8, to viral DNA, and the constitutively expressed gene of glyceraldehyde-3-phosphate dehydrogenase (GAPDH). HEK-293 cell lines infected with Ad-null virus (*Fig. 2A*) were used as the negative control. RT PCR was used to demonstrate that the recombinant adenoviral vector expresses mRNA of the nanoantibody gene to cytokeratin and can be used to analyze protein production.

Nanoantibody expression at the translational level was analyzed in H1299 cells infected with the recombinant adenovirus carrying the gene of nanoantibody to aCyK-V_HH tagged with HA-epitope of the influenza virus (Ad5-aCyK-V_HH), and the recombinant adenovirus containing the transgene-free expression cassette (Ad-null). The presence of a nanoantibody in the culture medium containing the infected cells was measured by immunoblotting with antibodies to HA-epitope of the influenza virus conjugated with horseradish peroxidase (*Fig. 2B*).

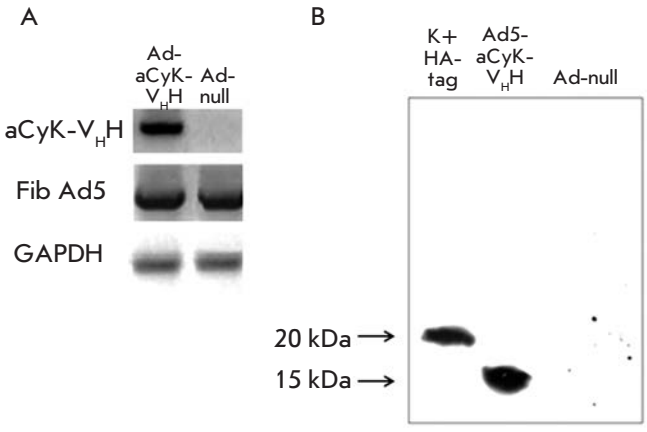

Fig. 2. The analysis of anti-cytokeratin nanoantibody expression in cells infected with recombinant adenovirus. A – Expression of anti-cytokeratin nanoantibody gene in cells infected with recombinant adenovirus Ad5-aCyK-VHH was analyzed using reverse transcription (RT)-PCR, cDNA encoding this gene was amplified by PCR with primers specific to the gene of the anti-cytokeratin nanoantibody (aCyK-VHH), Ad5 fiber gene (Fib Ad5), and house-keeping gene GAPDH. A recombinant adenovirus with no transgenic insertions in the E1 deletion region of the adenoviral genome (Ad-null) was used as the specificity control. B – The expression of the anti-cytokeratin nanoantibody was detected by hybridization with anti-HA antibodies in a Western blot analysis. A protein with a molecular weight of 15 kDa was detected in the cultural fluid of cells infected with the recombinant adenovirus. The (His_6)-tagged nanoantibody produced in E. coli was used as the control of the specificity of the interaction between anti-HA antibodies and the target protein.

Biological activity

The specificity of a nanoantibody expressed by the adenoviral vector to cytokeratin was confirmed by means of comparison of the interaction between the antigene and the proteins of the cultural fluid from the cells infected with recombinant adenovirus, and the interaction between the antigene and the antibody purified from *E. coli* periplasm.

The lysates of mouse liver and cerebrum cells were fractioned in a polyacrylamide gel, transferred to the PVDF membrane, which was incubated with the cultural medium of the cells infected with Ad5-aCyK-V_HH. The expressed nanoantibody served as the primary antibody to the target protein (mouse cytokeratin-8, 55 kDa) detected in the total lysate. The membrane was simultaneously incubated with antibodies aCyK-V_HH produced in *E. coli* periplasm.

Figure 3 shows the results of an electrophoresis of protein lysates in polyacrylamide gel and the data obtained by immunoblotting with nanoantibodies aCyK-V_HH after development by secondary antibodies to the HA-epitope of the influenza virus conjugated with horseradish peroxidase.

Immunoblotting results attest to the fact that the antibody expressed by the adenovirus has the same specificity as the antibody synthesized in *E. coli* periplasm, its gene being cloned in the recombinant adenovirus.

DISCUSSION

At the time of writing, there were a number of technologies capable of producing mini-antibodies with a predetermined specificity. Only quite recently was it revealed that, in addition to the canonical antibodies, functionally active noncanonical single-stranded antibodies were produced in relatively large amounts in members of the Camelidae family. Therefore, it is now possible to obtain mini-antibodies on the basis of

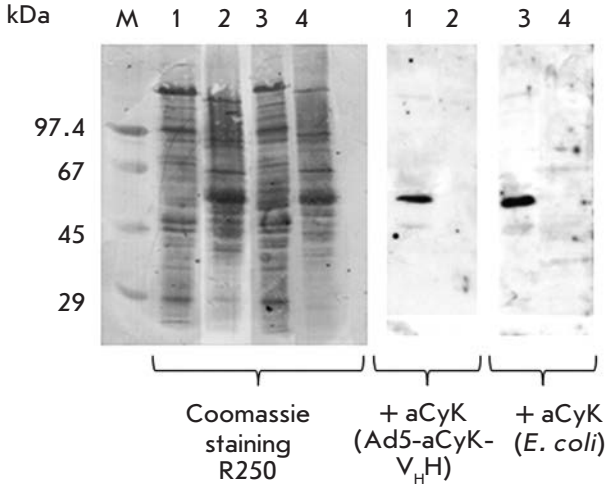

Fig. 3. Western blot detection of the functional activity of nanoantibodies. Total cell extracts of liver (lanes 1, 3) and brain (lanes 2, 4) cells were separated on a SDS–PAGE and electrophoretically transferred to a PVDF-membrane. The specific interaction of the target protein (~ 55 kDa) with the anti-cytokeratin nanoantibodies obtained in the cultural fluid of cells infected with the recombinant adenovirus and periplasm of *E. coli* was detected by immunoblotting.

libraries containing the antigen-recognizing domains of single-stranded antibodies of immunized animals. Noncanonical antibodies consist of a dimer with a single shortened heavy immunoglobulin chain (containing no light chains). Single-domain mini-antibodies (nanoantibodies) are genetically engineered derivatives of the antigen-recognizing domains of these noncanonical antibodies. The selection of clones of a mini-antibody with the predetermined specificity from the library of sequences of the entire repertoire of antigene-recognizing domains of noncanonical antibodies obtained from immunized camel is based on the highly efficient procedure of functional selection of filamentous phage particles containing both an exposed mini-antibody on the surface, and the DNA encoding it within the phage particle (phage display).

Mini-antibodies produced by this technology are characterized by high stability, solubility, and low immunogenicity. Mini-antibodies can be produced (selected) to any antigens and any antigen epitopes, including conservative ones, which often cannot be produced using the conventional procedure. Since the encoding nucleotide sequence is known for each mini-antibody, it is possible to produce the corresponding protein in any of the known expression systems (prokaryotic and eukaryotic).

It is economically viable to produce protein preparations of mini-antibodies in *E. coli* cells, yeast, or CHO cells. When injecting these preparations to experimental animals (or patients), their very short lifetime in the organism (less than 24 h) should be taken into account. The period of therapeutic action of preparations based on mini-antibodies can be increased using the vector systems, providing that the synthesis of the active agent takes place immediately in the infected cells of the organism. Recombinant adenoviruses are the optimal expression system for solving such problems. Their safety and efficiency has been proved in a number of clinical trials performed globally; the time needed to produce a target protein is approximately 20 days.

The potential application of recombinant adenoviral vectors for the expression of the genes of the antigen-recognizing fragments of single-stranded antibodies obtained from Bactrian camel was studied in this work. It was demonstrated that expression of the nanoantibody gene using the adenoviral vector is possible. Transgene expression was confirmed at the level of the RNA transcript and protein product. The specific interaction of the nanoantibody secreted by eukaryotic cells with a target protein attests to the fact that its functional activity is retained. Further studies are necessary for a qualitative estimation of the efficiency of nanoantibody expression using a recombinant adenovirus.

CONCLUSIONS

The delivery of the gene of a single-domain mini-antibody (nanoantibody) selected from the library containing sequences of the variable domains of specific single-stranded antibodies of immunized camel to eukaryotic cells using the recombinant adenoviral vector provides efficient expression and functioning of the nanoantibody. The results of this study can be used for the production of passive immunization agents for protection against pathogens, or for the design of new-generation immunobiological antitoxic preparations. ●

REFERENCES
1. Deyev S. M., Lebedenko E. N. // Acta Naturae. 2009. V. 1. №1. P. 32-50.
2. Stern M., Herrmann R. // Critical Rev. Oncol./Hematol. 2005. V. 54. P. 11–29.
3. Robinson C.R., Sauer R.T. // Proc. Natl. Acad. Sci. USA. 1998. V. 95. P. 5929–5934.
4. Worn A., Pluckthun A. // J. Mol. Biol. 2001. V. 305. P. 989–1010.
5. Hamers-Casterman C., Atarhouch T., Muyldermans S., Robinson G., Hamers C., Songa E.B., Bendahman N., Hamers R. // Nature. 1993. V. 363. P. 446–448.
6. Tillb S.V. // Molecular Biology. 2011. V. 45. №1. P. 77-85.
7. van der Linden R.H., Frenken L.G., de Geus B., Harmsen M.M., Ruuls R.C., Stok W., de Ron L., Wilson S., Davis

P., Verrips C.T. // Biochim. Biophys. Acta. 1999. V. 1431. P. 37–46.
8. Vincke C., Loris R., Saerens D., Martinez-Rodriguez S., Muyldermans S., Conrath K. // J. Biol. Chem. 2009. V. 284. P. 3273–3284.
9. Ghassabeh G., Muyldermans S., Saerens D. // Curr. Trends Monoclonal Antibody Development and Manufacturing. / Ed. Shire S.J. N.Y.: Springer, 2010. P. 29–48.
10. Campana V., Zentilin L., Mirabile I., Kranjc A., Casanova P., Giacca M., Prusiner S.B., Legname G., Zurzolo C. // Biochem. J. 2009. V. 418. P. 507–515.
11. Zuber C., Mitteregger G., Schuhmann N., Rey C., Knackmuss S., Rupprecht W., Reusch U., Pace C., Little M., Kretzschmar H.A., et al. // J. Gen. Virol. 2008 V. 89. P. 2055–2061.
12. Shmarov M.M., Sedova E.S., Verkhovskaya L.V., Rudneva I.A., Bogacheva E.A., Barykova Yu.A., Shcherbinin D.N., Lysenko A.A., Tutykhina 14. I.L., Logunov D.Y., et al. // Acta Naturae. 2010. V. 2. №1. P. 111-118.
13. Tutykhina I.L., Bezborodova O.A., Shmarov M.M., Logunov D.Y., Neugodova G.L., Nemtsova E.R., Naroditsky B.S., Yakubovskaya R.I., Gintsburg A.L. // Protein Expr. Purif. 2009. V. 65. P. 100–107.
14. Tutykhina I.L., Bezborodova O.A., Verkhovskaia L.V. Shmarov M.M., Logunov D.Iu., Nemtsova E.R., Narodnotskiĭ B.S., Iakubovskaia R.I., Gintsburg A.L. // Molecular Genetics, Microbiology, and Virology. 2009. № 1. P. 27-31.
15. Tutykhina I.L., Logunov D.Y., Shcherbinin D.N., Shmarov M.M., Tukhvatulin A.I., Naroditsky B.S., Gintsburg A.L. // J. Mol. Med. 2011. V. 89. P. 331–341.
16. Arafat W.O., Gómez-Navarro J., Buchsbaum D.J., Xiang J., Wang M., Casado E., Barker S.D., Mahasreshti P.J., Haisma H.J., Barnes M.N., et al. // Gene Therapy. 2002. V. 9. P. 256–262.
17. Kasuya K., Boyer J.L., Tan Y., Alipui D.O., Hackett N.R., Crystal R.G. // Mol. Therapy. 2005. V. 11. P. 237–244.
18. Rothbauer U., Zolghadr K., Tillib S., Nowak D., Schermelleh L., Gahl A., Backmann N., Conrath K., Muyldermans S., Cardoso M.C., et al. // Nature Meth. 2006. V. 3. P. 887–889.

Rabin8 Protein Interacts with GTPase Rheb and Inhibits Phosphorylation of Ser235/Ser236 in Small Ribosomal Subunit Protein S6

A. A. Parkhitko[1,2,3*], O. O. Favorova[1], E. P. Henske[2,3]
[1]Pirogov Russian National Research Medical University
[2]Fox Chase Cancer Center, Philadelphia, USA
[3]Brigham and Women's Hospital, Harvard Medical School, USA
*E-mail: parhitko@mail.ru
Received 18.05.2011

ABSTRACT **The mammalian target of rapamycin (mTOR) is a serine/threonine kinase that in association with Raptor, mLST8, PRAS40 and Deptor forms a complex (mTORC1) playing the key role in the regulation of protein biosynthesis, transcription, cellular metabolism, apoptosis and autophagy; mainly via direct phosphorylation of S6 kinases. mTORC1 is activated by growth factors and amino acids via the activation of Rheb GTPase. In the current study, we demonstrate for the first time that the over-expression of Rabin8, which functions as a guanine nucleotide exchange factor for Rab8 GTPase, suppresses phosphorylation of Ser235/Ser236 in ribosomal protein S6. Downregulation of Rabin8 using small interfering RNA (siRNA) increases the phosphorylation of Ser235/Ser236 in ribosomal protein S6. Furthermore, Rabin8 can be immunoprecipitated with Rheb GTPase. These results suggest the existence of a novel mechanism of mTORC1 regulation and its downstream processes. Since Rabin8 is a known regulator of ciliogenesis, a potential link can exist between regulation of Rheb/mTORC1 and ciliogenesis.**
KEYWORDS **complex mTORC1; Rheb; Rabin8; small ribosomal unit protein S6.**
ABBREVIATIONS **DMEM – Dulbecco's Modified Eagle's Medium; FBS – fetal bovine serum; GAP protein – GTPase-activating protein; mTOR – mammalian target of Rapamycin; Rheb – Ras homologue enriched in brain; siRNA – small interfering RNA; TBST – Tris-Buffered Saline and Tween 20.**

INTRODUCTION

Highly conserved serine/threonine protein kinase mTOR (mammalian target of rapamycin) belongs to the family of phosphatidyl inositol 3' kinase-related kinases (PIKK) and is the key enzyme of the mTOR-signaling pathway controlling the accumulation of the cell mass in many eukaryotes. mTOR as a catalytic subunit is a component of two hetero-olygomeric complexes, mTORC1 and mTORC2, that have different functions. mTORC1 is a functional dimer containing two subunits of each one of the following proteins: mTOR, Raptor (regulatory associated protein of mTOR), mLST8 (mammalian lethal with sec-13), PRAS40 (proline-rich AKT substrate 40 kDa), and Deptor (DEP-domain-containing mTOR-interacting protein) [1, 2]. mTORC1 phosphorylates a wide range of effectors regulating the processes of protein synthesis, cell proliferation, apoptosis, and autophagy in response to external signals [3, 4]. mTORC1 regulates translation through the direct phosphorylation of 4E-BP (translation initiation factor 4E binding protein), which binds and inhibits the initiation factor 4E and phosphorylation of S6K1 and S6K2 [5]. These kinases activate translation by phosphorylating protein S6, as well as a number of other proteins (SKAR, PDCD4, eEF-2K, eIF4B). The level of protein S6 phosphorylation using phospho-specific antibodies against Ser235/Ser236 is used to assess the kinase activity of mTORC1 [6].

The activity of mTORC1 is regulated by a number of various stimuli, such as growth factors, amino acids, glucose, and oxygen. Two key mechanisms are used in this regulation: a targeted modification of the components of this complex or regulation of Rheb GTPase, which directly interacts with mTORC1 and activates it when it is bound to GTP. The major Rheb GTPase regulator is a heterodimeric complex consisting of two tumor growth suppressor proteins: tuberin, containing conservative GAP domain, and hamartin, which stimulates the transition of Rheb GTPase from an active GTP-bound form into an inactive GDP-bound form. In-

activation of these proteins leads to the constitutive activation of Rheb GTPase, which activates mTORC1. As a result, the protein synthesizing activity is increased, and uncontrolled cell proliferation is observed [7].

It has also been demonstrated that tuberin and hamartin have an effect on the formation of primary cilia [8]. Interaction of Rab8 GTPase and guanine nucleotide exchange factor Rabin8 [9] activates Rab8 and promotes GDP release and GTP binding [10], which is involved in regulation of primary cilia formation.

Based on that, it was hypothesized that Rabin8 regulates Rheb GTPase, the major regulator of mTORC1. In the present study we showed that Rabin8 overexpression resulted in a decrease of mTORC1 activity, whereas downregulation of both Rabin8 and tuberin using siRNAs resulted in the activation of mTORC1. We also showed that Rabin8 protein could be co-immunoprecipitated with Rheb GTPase. Based on these data, we concluded that Rabin8 protein acts as a negative regulator of mTORC1 through binding to Rheb GTPase.

EXPERIMENTAL

Reagents and specimens

HEK293 (human embryonic kidney) cells (ATCC, United States) were grown in DMEM with or without 10% fetal bovine serum (FBS) (Gibco, United States) added. Antibodies against Rabin8 protein (Proteintech, United States), tuberin (Abcam, United States), Myc, β-actin and mTOR, phosphospecific antibodies against Ser235/Ser236 in ribosomal protein S6 (Cell Signalling, United States), and rabbit IgG (Santa Cruz Biotechnology, United States) were used.

Transfection

Fugene 6 (Roche, United States) was used for the transfection of HEK293 cells with plasmid constructs; for the transfection with various siRNA, Trans-IT TKO reagent (Mirus, United States) was used according to the manufacturer's protocol. HEK293 cells were transfected with pcDNA3.1 control vector, vector expressing Rabin8, pCMVTag3A control vector, or vector expressing Myc-Rheb fusion protein separately or together. Twenty-four hours after the transfection, the cells were washed twice and the medium, either with or without growth factors, was added. Twenty-four hours after the medium was replaced, the activity of mTORC1 was analyzed based on the phosphorylation of ribosomal protein S6 using phosphospecific antibodies against Ser235/Ser236 in protein S6. HEK293 cells were also transfected with the control, Rabin8 or tuberin siRNAs (Dharmacon, United States). Twenty-four hours after the transfection, the cells were washed twice and the medium, either with or without growth factors, was added.

Co-immunoprecipitation

Cells were collected in lysis buffer (Cell Signaling, United States) and cell extracts were incubated with antibodies against Rabin8 or Myc for 12 h at 4°C. The resulting complexes were precipitated by incubation with protein-A-agarose for 1 hr at 4°C, followed by centrifugation. The proteins were eluted by adding a Laemmli buffer, loaded onto denaturing gradient 4–20% polyacrylamide gel, and transferred onto polyvinyl membranes (Immobilon-P, Millipore, United States) after the electrophoresis. The membranes were blocked in a TBST buffer (137 mM NaCl, 0.1% Tween 20, 20 mM Tris, pH 7.6) (Cell Signaling, United States) containing 5% of milk for 1 h, followed by incubation with the selected primary antibodies at 4°C for a night. After the membranes were washed twice in a TBST buffer for 5 min, the corresponding secondary antibodies (Amersham, United States) were added. The membranes were washed three times in a TBST buffer for 10 min; the chemiluminescent signal was recorded by exposing with X-ray film (Kodak, United States) using a chemiluminescence kit (Perkin Elmer, United States).

RESULTS

Rabin8 decreases activity of mTORC1

The role of Rabin8 protein in the regulation of mTORC1 was studied using HEK293 cell line, the most widely used model in such experiments [11]. The cells were transfected with pcDNA3.1 control vector (*Fig. 1, lanes 1, 3, and 5*) or Rabin8 (*Fig. 1, lanes 2, 4, and 6*). In the case of the control vector, if the medium contained growth factors (*Fig. 1, lane 1*) mTORC1 was activated, which was measured by the phosphorylation level of ribosomal protein S6 (the bottom panel). In the absence of growth factors (*Fig. 1, lane 3*), mTORC1 activity was partially inhibited; the subsequent short-term stimulation of the cells after starvation with the medium containing growth factors (*Fig. 1, lane 5*) resulted in the complete reactivation of mTORC1. A high level of Rabin8 expression (top panel) had no effect on the activity of mTORC1 (*Fig. 1, lane 2*) in the medium containing growth factors; however, it resulted in a decrease of mTORC1 activity in the absence of growth factors (*Fig. 1, lane 4*), and after reactivation of mTORC1 with the medium containing growth factors (*Fig. 1, lane 6*).

Inhibition of expression of Rabin8 or tuberin results in activation of mTORC1

The data obtained using over-expression of Rabin8 was confirmed using siRNAs, synthetic short RNA duplex-

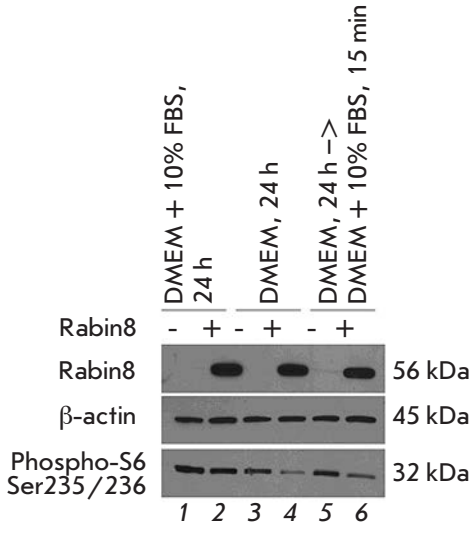

Fig. 1. Rabin8 overexpression suppresses mTORC1 activity in HEK293 cells (*lanes 4, 6*). The cells were transfected with control vector pcDNA3.1 (*lanes 1, 3, 5*) or with Rabin8 (*lanes 2, 4, 6*). Activity of mTORC1 was analyzed by levels of ribosomal protein S6 phosphorylation with phospho-specific antibody against S6 (Ser235/Ser236) in the presence of growth factors (*lanes 3,4*), absence of growth factors (*lanes 3, 4*), and after 15-min stimulation of cells grown in the growth-factor-free medium with the medium containing growth factors (*lanes 5,6*). The levels of Rabin8 and β-actin were measured using immunoblot analysis with specific antibodies.

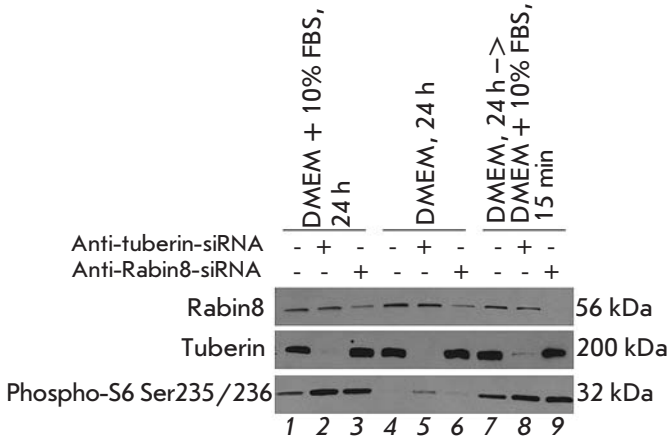

Fig. 2. Downregulation of Rabin8 using siRNA activates mTORC1 activity in HEK293 cells (*lanes 3,9*), as well as downregulation of tuberin used here as a positive control (*lanes 2,8*). Activity of mTORC1 was analyzed in the same manner as in Fig. 1 in the presence of growth factors (*lanes 1–3*), in the absence of growth factors (*lanes 4–7*), and after 15-min stimulation of cells grown in the growth-factor-free medium with the medium containing growth factors (*lanes 7–9*). The levels of Rabin8 and tuberin were measured using immunoblot analysis with specific antibodies. Control siRNA – *lanes 1,4,7*.

es which initiate the targeted degradation of mRNA that is complementary to them. The following siRNAs were used as the negative and positive controls: siRNA without the complementary sequence in the human genomic mRNA (the control siRNA), and siRNA against mRNA of tuberin, the protein forming a heterodimeric complex with hamartin, as mentioned above. This complex inhibits the activity of Rheb GTPase and, therefore, the activity of mTORC1. After transfection with control siRNA (*Fig. 2, lanes 1, 4, and 7*), similar to the transfection with control vector (see *Fig. 1*), the presence of growth factors in the medium (*Fig. 2, lane 1*) resulted in the activation of mTORC1. In the absence of growth factors (*Fig. 2, lane 4*), mTORC1 activity was inhibited. A short-term (15 min) stimulation of the cells grown in the medium without growth factors reactivated mTORC1 (*Fig. 2, lane 7*). The decrease in the expression of both tuberin and Rabin8 proteins that was observed after transfection of siRNAs against mRNA of these proteins stimulated mTORC1 activity in the presence of growth factors (*Fig. 2, lanes 2 and 3*). In the absence of growth factors, the activity of mTORC1 in the cells transfected with siRNA against tuberin mRNA marginally increased (*Fig. 2, lane 5*). The activity of mTORC1 remained unchanged after the transfection of siRNA against Rabin8 mRNA (*Fig. 2, lane 6*), in comparison with the transfection of the control siRNA; mTORC1 activity was higher than in the control after reactivation with the medium containing growth factors (*Fig. 2, lanes 8 and 9*).

Co-immunoprecipitation of Rabin8, Rheb, and mTOR proteins

As follows from the obtained results, Rabin8 is a negative regulator of mTORC1. We studied the possibility of interaction between Rabin8, Rheb, and mTOR using transfection in HEK293 by simultaneous transfection of pcDNA3.1 and pCMVTag3A control vectors (*Fig. 3A, lane 1*) or two vectors expressing Rabin8 and Myc-Rheb fusion protein (*Fig. 3A, lanes 2–4*) in a medium with (*Fig. 3A, lanes 1 and 2*) or without growth factors (*Fig. 3A, lane 3*), as well as after short-term stimulation of the cells grown for 24 hr without growth factors (*Fig. 3A, lane 4*). In order to study the interaction between Rabin8 and Rheb, the co-immunoprecipitation of cell lysates with antibodies against Rabin8 was carried

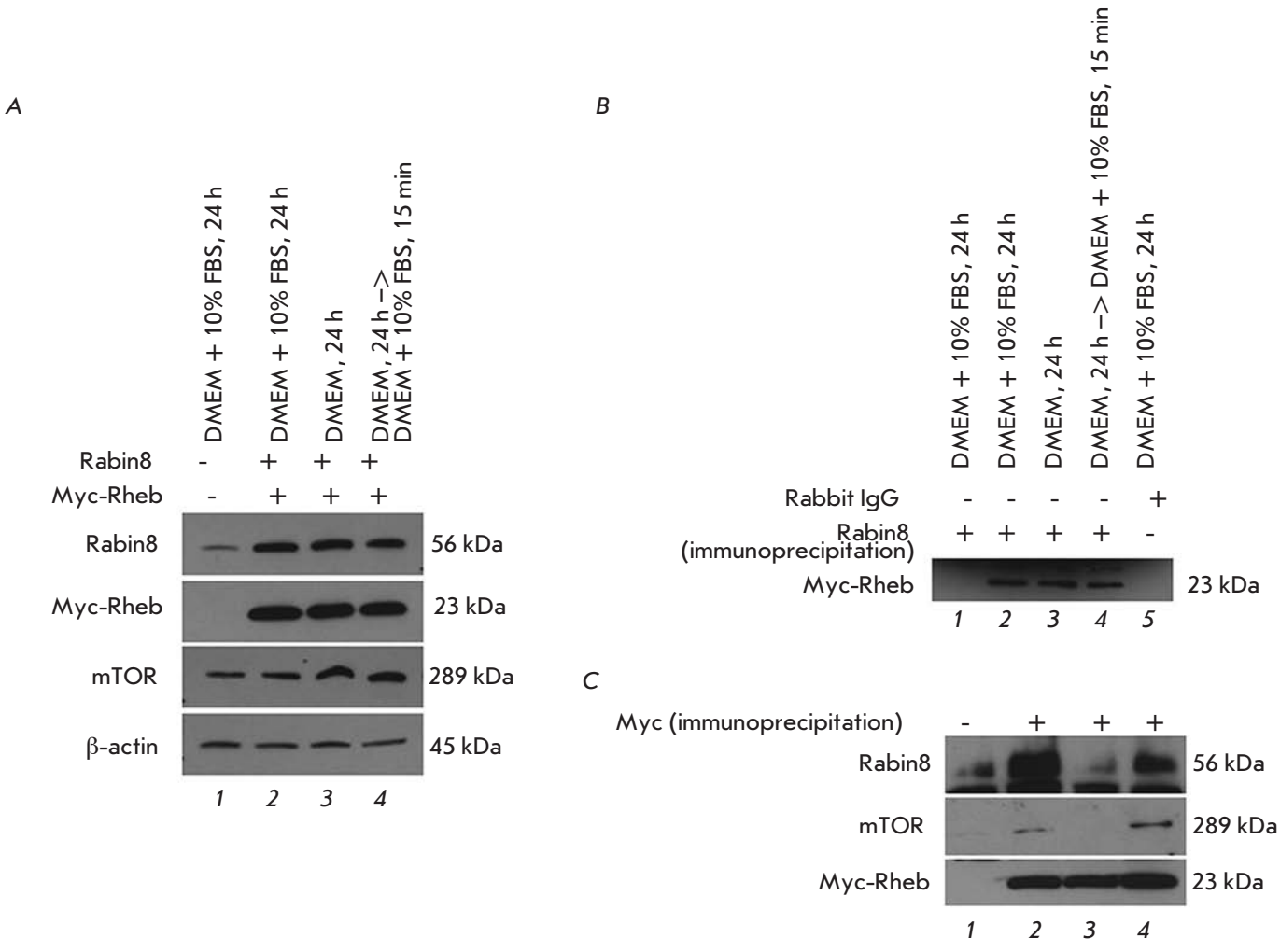

Fig. 3. Co-immunoprecipitaion of Rabin8 and Rheb overexpressed in HEK293 cells after transfection with proper vectors. The levels of Rabin8, tuberin, mTOR and β-actin were measured using immunoblot analysis with specific antibodies. (a) The expression levels of Rabin8, Myc-Rheb, and mTOR after co-transfection with control vectors pcDNA3.1 and pCMVTag3A (*lane 1*) or Rabin8 and Myc-Rheb (*lanes 2–4*) in the presence of growth factors (*lanes 1,2*), absence of growth factors (*lane 3*), and after 15-min stimulation of cells grown in media without growth factors with media containing growth factors (*lane 4*). (b) Co-immunoprecipitation using the lysates from Fig. 3a with antibodies against Rabin 8 (*lanes 1–4*) or control rabbit IgG (*lane 5*) and immunoblot analysis with antibody against Myc. The lysate from Fig. 3a (*lane 2*) was used for the co-immunoprecipitation with control rabbit IgG antibody. (c) Co-immunoprecipitation using the lysates from Fig. 3a with antibodies against Myc and immunoblot analysis with antibody against Rabin8, mTOR, and Myc.

out, followed by immunoblotting with antibodies against Myc epitope of the Myc-Rheb fusion protein (*Fig. 3B*). It was found that the interaction of Rheb with Rabin8 was independent of the presence of growth factors in the medium (*Fig. 3B, lanes 2–4*). Rheb was not detected after immunoprecipitation with antibodies against Rabin8 in the control lysate without expression of Myc-Rheb (*Fig. 3B, lane 1*) or in the lysate in which non-specific control rabbit IgG was used for co-immunoprecipitation (*Fig. 3B, lane 5*). In order to confirm the interaction between Rabin8 and Rheb proteins, reciprocal co-immunoprecipitation was carried out. Cell lysates were incubated with antibodies against Myc epitope of Myc-Rheb fusion protein; antibodies against mTOR and Rabin8 were used for the subsequent immunoblotting. As expected, Rheb and mTOR interacted in the presence of growth factors in the medium (*Fig. 3B, lanes 2 and 4*). Rheb and Rabin8 interacted in the medium containing growth factors as well (*Fig. 3B, lanes 2 and 4*); however, neither interaction between Rheb and Rabin8 nor between Rheb and mTOR was detected in the absence of growth factors (*Fig. 3B, lane 3*).

DISCUSSION

In the present study we first demonstrated that Rabin8 regulates phosphorylation of Ser235/Ser236 in ribosomal protein S6. It has been previously shown that Ser235/Ser236 is phosphorylated by protein kinase S6K1 as a result of the activation of mTORC1, whereas the inhibitor of mTORC1, rapamycin, completely blocks phosphorylation of these residues under any conditions [2]. In accordance with this, the phosphorylation level of Ser235/Ser236 in protein S6 can be used as a convenient indicator of mTORC1 kinase activity. The obtained data suggest that Rabin8 regulates the activity of this complex. However, the role of the phosphorylation of protein S6 in the regulation of protein synthesis has not been completely determined. Transgenic mice were generated in which all amino acid residues in protein S6 were replaced with nonphosphorylatable alanine residues; however, the level of protein synthesis in different cell types in these mice remained the same as in wild-type mice [12].

We determined the phosphorylation of Ser235/Ser236 in protein S6 under various conditions, such as after cell growth in the medium containing growth factors (DMEM + 10% FBS), after growing the cells in the medium without growth factors (DMEM), and after short-term stimulation with growth factors (DMEM –> DMEM + 10% FBS) of the cells grown in the medium containing no growth factors. Since the regulation of mTORC1 is performed at several levels, the use of different growth conditions makes it easier to better understand the possible regulation mechanisms [13]. In all cases, we used DMEM medium containing amino acids, since the absence of amino acids results in the complete inhibition of mTORC1 regardless of its negative regulator tuberin [14]. The absence of growth factors activates GAP protein tuberin, which stimulates the transition of Rheb GTPase from the active GTP-bound form into inactive GDP-bound form, resulting in the inhibition of mTORC1 [15, 16]. Under these conditions, any changes inhibiting the GAP activity of tuberin or stimulating the transition of Rheb GTPase into an active form will activate mTORC1, which was indeed observed.

We also used the short-term stimulation of the cells grown in a growth-factor-free medium by growth factors to differentiate the changes in the activity of mTORC1, which occur at different rates. We found that if cells grow in a complete medium containing growth factors, the decrease in Rabin8 expression stimulated mTORC1 activity; however, Rabin8 overexpression was not sufficient to inhibit this complex. In a medium without growth factors, the decrease in Rabin8 expression was insufficient for the reactivation of the mTORC1; however, Rabin8 overexpression enhanced the inhibition of mTORC1. Rabin8 overexpression decreased the reactivation of mTORC1 resulted from the short-term stimulation by the medium with growth factors, while the decrease in Rabin8 expression stimulated reactivation. These results suggest that Rabin8 suppresses the activation of mTORC1 by growth factors.

We demonstrate for the first time that Rabin8 is bound to the major regulator of mTORC1, Rheb GTPase, which is important for the understanding of the regulation mechanism of mTORC1 by Rabin8 protein. However, it is possible that Rabin8 may interact with other components of mTORC1 as well, since we detected the catalytic subunit mTOR in complex with Rabin8 and Rheb after immunoprecipitation.There is also a possibility of mediated interaction between Rabin8 and Rheb via an unknown protein or tuberin/hamartin. However, considering that both Rab8 and Rheb belong to the family of GTPases and participate in the regulation of primary cilia formation [9], we suppose that Rabin8 has an effect on the activity of mTORC1 via Rheb GTPase. Co-immunoprecipitation experiments support this assumption, since no attenuation of the interaction between Rabin8 and Rheb proteins was detected in the growth-factor-free medium when using antibodies against Myc epitope in Myc-Rheb protein. Meanwhile, the interaction between Rheb and mTOR was abrogated, which agrees with previously published data [1]. No interaction between Rabin8 and Rheb proteins was detected in the reciprocal co-immunoprecipitation experiments for Rabin8, which can account for the different affinities of antibodies towards these proteins.

The possibility of interaction between the Rabin8 and Rheb proteins suggests a novel Rheb-dependent mechanism of regulating the primary cilia formation, which is independent of the activity of mTORC1 [8]. According to this assumption, after interaction between Rheb and Rabin8, redistribution of the Rheb function from the regulation of mTORC1 to the regulation of primary cilia formation occurs. The link between the disruption of the ciliogenesis function and various diseases isolated into a separate group of ciliopathies has recently been established. In particular, this group includes such diseases as polycystic kidney disease, the Bardet-Biedl syndrom, etc. [17]. The link between the disruption of ciliogenesis and obesity has recently been revealed [18]. In addition, primary cilia regulate the activity of the Hedgehog and Wnt signaling pathways, and disruption of their activity is involved in tumor development in various organs [19]. It should also be mentioned that activation of mTORC1 is observed in many types of tumors [20] and is required for their progression. Therefore, understanding of the regulation mechanisms and the relationship between the mTORC1 complex and the processes of primary cilia formation should result in

the emergence of new approaches to the treatment of ciliopathies, obesity, and oncological diseases. ●

This study was carried out within the framework of inter-institute collaboration between the Pirogov Russian State Medical University (Division of Molecular Biology and Medical Biotechnology) and the Fox Chase Cancer Center (Philadelphia, United States). The authors are grateful to O.G. Kulakova and D.I. Khabibullin for helpful discussions.

REFERENCES

1. Sengupta S., Peterson T.R., Sabatini D.M. // Mol. Cell. 2010. V. 40. P. 310–322.
2. Zoncu R., Efeyan A., Sabatini D.M. // Nat. Rev. Mol. Cell. Biol. 2011. V. 12. P. 21–35.
3. Chan E.Y. // Sci. Signaling. 2009. V. 2. P. pe51.
4. Mizushima N. // Curr. Opin. Cell Biol. 2010. V. 22. P. 132–139.
5. Wullschleger S., Loewith R., Hall M.N. // Cell. 2006. V. 124. P. 471–484.
6. Ma X.M., Blenis J. // Nat. Rev. Mol. Cell. Biol. 2009. V. 10. P. 307–318.
7. Astrinidis A., Henske E.P. // Oncogene. 2005. V. 24. P. 7475–7481.
8. Hartman T.R., Liu D., Zilfou J.T., Robb V., Morrison T., Watnick T., Henske E.P. // Hum. Mol. Genet. 2009. V. 18. P. 151–163.
9. Nachury M.V., Loktev A.V., Zhang Q., Westlake C.J., Peranen J., Merdes A., Slusarski D.C., Scheller R.H., Bazan J.F., Sheffield V.C., et al. // Cell. 2007. V. 129. P. 1201–1213.
10. Hattula K., Furuhjelm J., Arffman A., Peranen J. // Mol. Biol. Cell. 2002. V. 13. P. 3268–3280.
11. Sancak Y., Bar-Peled L., Zoncu R., Markhard A.L., Nada S., Sabatini D.M. // Cell. 2010. V. 141. P. 290–303.
12. Ruvinsky I., Sharon N., Lerer T., Cohen H., Stolovich-Rain M., Nir T., Dor Y., Zisman P., Meyuhas O. // Genes Dev. 2005. V. 19. P. 2199–2211.
13. Peterson T.R., Laplante M., Thoreen C.C., Sancak Y., Kang S.A., Kuehl W.M., Gray N.S., Sabatini D.M. // Cell. 2009. V. 137. P. 873–886.
14. Smith E.M., Finn S.G., Tee A.R., Browne G.J., Proud C.G. // J. Biol. Chem. 2005. V. 280. P. 18717–18727.
15. Ballif B.A., Roux P.P., Gerber S.A., MacKeigan J.P., Blenis J., Gygi S.P. // Proc. Natl. Acad. Sci. USA. 2005. V. 102. P. 667–672.
16. Manning B.D., Tee A.R., Logsdon M.N., Blenis J., Cantley L.C. // Mol. Cell. 2002. V. 10. P. 151–162.
17. Hildebrandt F., Benzing T., Katsanis N. // N. Engl. J. Med. 2011. V. 364. P. 1533–1543.
18. Mok C.A., Heon E., Zhen M. // Clin. Genet. 2010. V. 77. P. 18–27.
19. Duldulao N.A., Li J., Sun Z. // Protein Cell. 2010. V. 1. P. 726–736.
20. Courtney K.D., Corcoran R.B., Engelman J.A. // J. Clin. Oncol. 2010. V. 28. P. 1075–1083.

Bacterial Synthesis and Purification of Normal and Mutant Forms of Human FGFR3 Transmembrane Segment

S. A. Goncharuk[1,2,*], M. V. Goncharuk[1,2], M. L. Mayzel[1], D. M. Lesovoy[1], V. V. Chupin[1], E. V. Bocharov[1], A. S. Arseniev[1], M. P. Kirpichnikov[1,2]

[1] Shemyakin and Ovchinnikov Institute of Bioorganic Chemistry, Russian Academy of Science

[2] Biology Department, Lomonosov Moscow State University

*E-mail: ms.goncharuk@gmail.com

Received 17.05.2011

ABSTRACT **The fibroblast growth factor receptor 3 (FGFR3) is a protein belonging to the family of receptor tyrosine kinases. FGFR3 plays an important role in human skeletal development. Mutations in this protein, including Gly380Arg or Ala391Glu substitutions in the transmembrane (TM) region, can cause different disorders in bone development. The determination of the spatial structure of the FGFR3 TM domain in a normal protein and in a protein with single Gly380Arg and Ala391Glu mutations is essential in order to understand the mechanisms that control dimerization and signal transduction by receptor tyrosine kinases. The effective system of expression of eukaryotic genes in bacteria and the purification protocol for the production of milligram amounts of both normal TM fragments of FGFR3 and those with single pathogenic mutations Gly380Arg and Ala391Glu, as well as their ^{15}N- and [^{15}N, ^{13}C]-isotope-labelled derivatives, were described. Each peptide was produced in *Escherichia coli* BL21(DE3)pLysS cells as a C-terminal extension of thioredoxin A. The purification protocol involved immobilized metal affinity chromatography and cation- and anion-exchange chromatography, as well as the fusion protein cleavage with the light subunit of human enterokinase. The efficiency of the incorporation of target peptides into DPC/SDS and DPC/DPG micelles was confirmed using NMR spectroscopy. The described methodology of production of the native FGFR3 TM domain in norma and with single Gly380Arg and Ala391Glu mutations enables one to study their spatial structure using high-resolution heteronuclear NMR spectroscopy.**

KEYWORDS **membrane protein; FGFR; bacterial expression; purification; detergent solubilization; NMR.**

ABBREVIATIONS **FGFR - Fibroblast growth factor receptor family; FGFR3 - Fibroblast growth factor receptor 3; RTK - receptor tyrosine kinase; TM - transmembrane (domain of membrane protein); DPC — dodecylphosphocholine; DPG — dodecylphosphoglycerol; SDS - sodium dodecyl sulfate; TFE — 2,2,2-trifluoroethanol.**

INTRODUCTION

The fibroblast growth factor receptor 3 (FGFR3) belongs to the family of receptor tyrosine kinases (RTKs). This protein consists of an extracellular component with three immunoglobulin-like domains, a hydrophobic transmembrane (TM) domain, and an intracellular component with two tyrosine kinase domains. Specific ligands (fibroblast growth factors) and heparin are bound to the immunoglobulin-like domain of FGFR3, thus stabilizing the dimer complex consisting of two receptor molecules and providing signal transduction inside the cell [1, 2]. FGFR3 plays an important role in the processes of human growth and development (both embryonic/neonatal and that in an adult organism). Mutations in this protein may result in various disorders in the development of connective tissues and skeleton [3–5]. FGFR3 has also been known to participate in tumor formation [5, 6]. In particular, Gly380Arg and Ala391Glu mutations in the TM region of FGFR3 cause lethal dysplasia [7] and the Crouzon syndrome with acanthosis nigricans [8], respectively. The Ala391Glu mutation occurs both upon disorders in skeletal development and upon oncogenesis [6]. The Ala391Glu mutation is considered to stabilize FGFR3 dimerization in the cell membrane, resulting in uncontrollable signal transduction and the emergence of a pathology [9, 10]. However, the detailed mechanism of FGFR3 functioning has not been fully revealed. The approach that has been most frequently used in modern structural biology assumes the division of the membrane protein under study into components and studying the individual water-soluble components of the molecule and its TM regions [11–15]. It is extremely important to obtain a high-resolution structure of the native TM domain of human FGFR3

and that of the domain with Gly380Arg or Ala391Glu mutation to understand the mechanisms that control their dimerization and functioning, because these fragments act as the linking units between the extracellular and intracellular RTK domains and directly participate in signal transduction inside the cell.

In this paper, an efficient system of gene expression and purification protocol are described which enable one to produce preparative amounts of the FGFR3 TM fragment both in norma and with single Gly380Arg and Ala391Glu mutations, as well as their ^{15}N- and [^{15}N, ^{13}C]-labelled derivatives. The designed approach of producing TM peptides facilitates the study of their structure by high-resolution heteronuclear NMR spectroscopy.

EXPERIMENTAL

In this study, we used *Escherichia coli* strains XL-10-Gold (Stratagene, United States) and BL21(DE3)pLysS (Stratagene, United States), plasmids pGEMEX-1 (Promega, United States) and pGEMEX-1/TRX-TMS [16]. Oligonucleotides were synthesized by Evrogen (Russia). DNA was sequenced at the Inter-institute Center of Shared Use GENOME (Russia). The reagents purchased from CIL (United States) were used to introduce the isotope labels ^{15}N and ^{13}C. The completely deuterized dodecylphosphoglycerol (DPG) was produced by enzymatic transphosphatidylation from completely deuterized dodecylphosphocholine (DPC) and glycerol in the presence of phospholipase D [17].

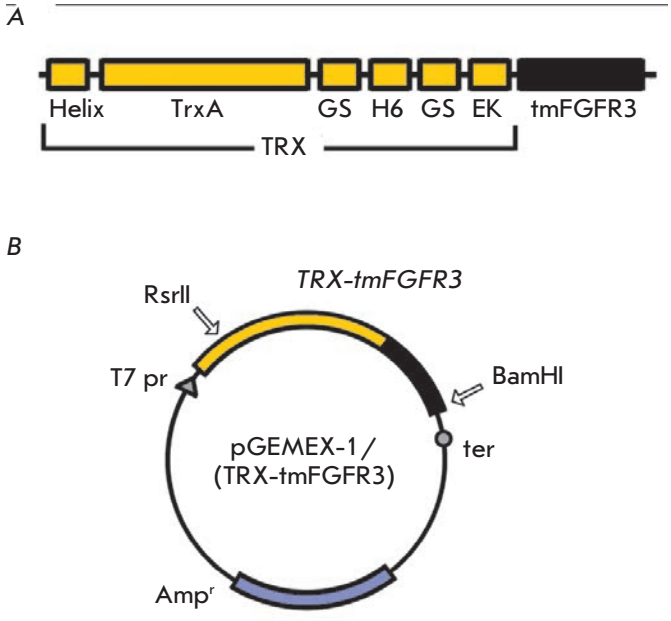

Fig. 1. Schematic representation of (A) TRX-tmFGFR3 fusion proteins and (B) expression vectors. Helix – N-terminal fragment of a membrane-active protein from *Helicobacter pylori*; TrxA – thioredoxin A of *E.coli*; GS – GlySerGlySerGly aminoacid sequence; H6 – hexahistidine sequence; EK – enterokinase light chain cleavage site; tmFGFR3 – target transmembrane peptide from FGFR3 in norma or with Gly380Arg and Ala391Glu single point mutations; *Amp^r* – ampicillin resistance gene.

Gene cloning

Plasmid vectors for the expression of peptide genes as fusion proteins with thioredoxin A were constructed as described previously [12, 16–19]. The genes encoding TM fragments of human FGFR3 (*tmFGFR3*) (amino acid residues 357–399 of the normal FGFR3 (*tmFGFR3-nat*) and 357–399 of FGFR3 with point mutations G380R (*tmFGFR3-R*), and A391E (*tmFGFR3-E*)) were assembled using six chemically synthesized oligonucleotides with partially overlapping nucleotide sequences. The codons used were optimized for the gene expression in *E. coli* cells. The restriction site BamHI and the sequence encoding the enterokinase recognition site were introduced into the 3' and 5' terminal primers, respectively. The same sequence was added to the 3' terminus of the carrier protein gene (*TRX*) amplified using PCR from the pGEMEX-1/(TRX-TMS) vector [16]. The recombination of the *TRX* and *tmFGFR3* genes was performed using PCR yielding *TRX-tmFGFR3*. The expression plasmids pGEMEX-1/(TRX-tmFGFR3) (*Fig. 1B*) were obtained by cloning *TRX-tmFGFR3* fragments treated with RsrII and BamHI restriction endonucleases into pGEMEX-1/(TRX-TMS) vectors linearized with the same proteases [16]. The validity of the nucleotide sequence within expression cassettes was confirmed by DNA sequencing on both strands.

Selection of cultivation conditions for the recombinant *E. coli* strain

Fusion protein genes were expressed in the *E. coli* cells BL21(DE3)pLysS. The cells were cultured in rich and minimal media; both chemical induction of protein synthesis (TB and M9 media) and autoinduction [20] (media BYM5052, M5052, C750501', or M50501, *Table 1*) being used. When selecting the optimal conditions for protein synthesis, an inducing agent, isopropyl-β-D-thiogalactoside (IPTG), was added into the cell culture that was cultivated at 28°C and attained the optical density of OD_{550} ~1.5 AU (TB medium) or ~0.6 AU (M9 medium) up to the final concentrations of 1, 0.25, 0.05, 0.01, and 0 mM. Cultivation was continued for 15 h at 250 rpm and a temperature of 37°C; for 40 h (TB) or 60 h (M9) at 25°C; and 60 h (TB) or 72 h (M9) at 13°C. In the case of autoinduction media, the cells were cultivated at 300 rpm and a temperature of 18°C for 4 (BYM5052)

Table 1. Composition of the auto-induction media used

Medium	Studier[a]	Na_2HPO_4 (mM)	KH_2PO_4 (mM)	Bacto trypton	Yeast extract, %	Glycerol	Na_2SO_4, $MgSO_4$, NH_4Cl, Glucose, Lactose, Metals
BYM5052	ZYM-5052	+	+	2%	1%	+	+
M5052	N-5052	25	25		0.0002%	+	+
C750501'	C-750501	+	+		0.0002%	+	+
M50501	C-750501	25	25		0.0002%	0.5%	+

[a]Auto-induction medium that is taken as a basis.
Note: Components with a concentration equal to the one used by Studier [20] are marked with a + sign.

or 7 days (M5052, C750501', or M50501). The optimal temperature, IPTG concentration, and cultivation time were determined using Tris-glycine SDS-PAGE electrophoresis.

Gene expression

A M9 medium containing 0.0002% of yeast extract, $^{15}NH_4Cl$, and [U-^{13}C]-glucose (^{15}N,^{13}C-labelling) or $^{15}NH_4Cl$ and nonenriched glucose (^{15}N-labeling) was used for the preparative obtaining of labelled proteins. In order to produce target fusion proteins, IPTG was added into the cell culture with OD_{600} ~ 0.6 AU (M9 medium, isotope labelling) or 1.5 AU (TB medium, no labelling) up to a final concentration of 0.05 mM and the temperature was reduced from 28 to 13°C. The cells were cultivated at 250 rpm for 72 h. The cells were then harvested and stored at −20°C.

Target protein purification

The biomass obtained from 1 L of the culture was suspended in 50 ml of lysing buffer (50 mM Tris, pH 8.0, 150 mM NaCl, 10 mM imidazole, 1% Triton X-100, 0.2 mM phenylmethylsulfonyl fluoride), destroyed by ultrasound, centrifuged, and filtered through a membrane (pore size 0.22 μm). The clarified lysate was applied to a column with Chelating Sepharose FF (Amersham Bioscience, United States) preliminarily charged with Ni^{2+} and balanced with buffer A (50 mM Tris, pH 8.0, 250 mM NaCl, 1% Triton X-100) containing 10 mM imidazole. The resin was successively washed with buffer A containing 10 mM imidazole and the same buffer containing 40 mM imidazole. The protein was eluted with buffer A containing 175 mM imidazole. The eluate was diluted by a factor of 11 with buffer containing 17 mM Tris, pH 8.0, 20 mM NaCl, and 1% Triton X-100; then, the light chain of recombinant human enterokinase was added [21] at a ratio of 25 units of enzyme per 1 mg of TRX-tmFGFR3. The mixture was incubated for a night at room temperature and applied to a column with Chelating Sepharose FF balanced with buffer B, pH 8.0 (20 mM Tris, 40 mM NaCl, 1% Triton X-100, 16 mM imidazole). The unbound to the resin fraction was collected, pH was decreased to 4.55 using concentrated acetic acid, filtered through a membrane (pore size 0.22 μm), and applied to a column with SP Sepharose FF (Amersham Bioscience, United States) balanced with buffer B, pH 4.55. After the fraction was applied, the resin was washed with the same buffer. The unbound to the resin fraction was collected, the pH was brought to 9.0 using NaOH, filtered through the membrane (pore size 0.22 μm), and applied to a column with Q Sepharose FF (Amersham Bioscience, United States) balanced with buffer C (20 mM Tris, pH 8.8, 1% Triton X-100). The peptides were eluted with a linear NaCl gradient (0−1 M). After incubation with a 10% trichloroacetic acid (TCA) solution, the purified peptides were washed thrice with acetone and vacuum-dried. The purity and identity of the purified peptides to the target ones were confirmed by gel electrophoresis, MALDI mass spectroscopy (Daltonics Ultraflex II TOF/TOF, Bruker Daltonik, Germany), and NMR spectroscopy.

Solubilization of tmFGFR3 in a membrane-like environment

For preliminary folding into a helical conformation the specimens of isotope labelled tmFGFR3 were dissolved in a TFE/H_2O (60/40) mixture with 2 mM tris(2-carboxyethyl)phosphine (TCEP) added in order to prevent the formation of nonspecific intermolecular disulfide bonds. Complete solubilization was achieved using 10 freeze (in liquid nitrogen)/thaw cycles. Homogenized specimens were obtained under ultrasonication (ultrasonic bath D-78224 Singen/Htw (Elma, Germany)) at the thaw stage in each cycle. The solubility and formation of the secondary structure of tmFGFR3 in the TFE/H_2O mixture was controlled using ^{1}H/^{15}N-bestHSQC NMR spectra [22−24] by analyzing the signal width and signal dispersion. A solution of tmFGFR3 in TFE/H_2O was

Table 2. Efficiency of the method of fusion proteins (TRX-tmFGFR3) and target peptides (tmFGFR3) production

TM-peptide	Molecular weight, kDa	Aminoacid sequence of a TM fragment[a]	EK[b], u/mg	Yield[c], mg/ml	
				TRX-tmFGFR3	tmFGFR3
tmFGFR3-nat	4.6	L^{357}PAEEELVEADEAGSVYAGILSYGVGFFLFILVVAAVTLCRLR^{399}	25	40	6
tmFGFR3-R	4.7	L^{357}PAEEELVEADEAGSVYAGILSY**R**^{380}VGFFLFILVVAAVTLCRLR^{399}	30	20	4
tmFGFR3-E	4.7	L^{357}PAEEELVEADEAGSVYAGILSYGVGFFLFILVV**E**^{391}AVTLCRLR^{399}	30	50	7

[a] The putative TM domains are indicated as gray boxes. The point mutations Gly380Arg (tmFGFR3-R) and Ala391Glu (tmFGFR3-E) appear in bold.
[b] Activity of the enterokinase light chain required to hydrolyze 1 mg of TRX-tmFGFR3 fusion proteins.
[c] The average yield (per 1 L of bacterial culture in M9 minimal media) of the fusion proteins (TRX-tmFGFR3) and purified peptides (tmFGFR3), including their ^{15}N- and [^{15}N-, ^{13}C]-labelled derivatives. The yields were estimated by the intensity of the Coomassie blue-stained bands in SDS-PAGE and by weighing pure, dried tmFGFR3 peptides.

mixed with the necessary amount of detergents and/or lipids dissolved in TFE/H_2O to obtain a detergent (lipid)/peptide ratio ranging from 120 to 40. The resulting mixture was lyophilized (ModulyoD-230 Freeze Dryer, Thermo, Canada) and dissolved in H_2O/D_2O (10/1) with 10 freeze/thaw cycles (under ultrasonic action) to attain protein homogeneity and complete incorporation into detergent micelles or lipid bicelles. Heteronuclear NMR spectra of tmFGFR3 peptides incorporated into supramolecular complexes were obtained at 40°C, the pH varied from 3.5 to 6.5 on an AVANCE spectrometer (Bruker, Germany) equipped with a cryogenically cooled high-sensitivity sensor, with a proton operating frequency of 700 MHz.

RESULTS AND DISCUSSION

System of *tmFGFR3* gene expression

Peptides with a primary structure corresponding to the full-length TM fragment of FGFR3 (tmFGFR3) with regions adjacent to the hydrophobic fragment (normal, tmFGFR3-nat and that with pathogenic point mutations G380R (tmFGFR3-R) or A391E (tmFGFR3-E)) were studied in this work (*Table 2*).

Due to the rapid proteolytic degradation of small peptides during their expression in bacterial cells, tmFGFR3 was obtained as thioredoxin A (TrxA) fusion protein, as described earlier [12] (*Fig. 1A*). Six histidine residues (H6), the recognition site of the human enterokinase light chain (EK), and mobile glycine-rich fragments Gly-Ser-Gly-Ser-Gly (GS) on both sides from H6 were incorporated between the TrxA and tmFGFR3 fragments of the fusion protein. The highly specific enzyme EK selectively hydrolyzes the peptide bond located immediately after the recognition site (with the exception of the Lys-Pro bond). The amino acid sequence Helix is located at the N terminus of the fusion protein [12], facilitating the elimination of the toxicity of some TM peptides with respect to the host cell (no data are provided). The genes encoding the fusion proteins Helix-TrxA-GS-H6-GS-EK-tmFGFR3 (hereinafter referred to as TRX-tmFGFR3) were incorporated into pGEMEX-1 plasmid vectors under the transcriptional control of the T7 promoter yielding pGEMEX-1/(TRX-tmFGFR3) expression vectors (*Fig. 1B*).

To produce proteins, *E. coli* BL21(DE3)pLysS cells were used, since an acceptable level of expression of target genes can be provided by these cells. When selecting between autoinduction [20] and chemical induction, the choice in favor of the former is justified by the absence of the necessity to add an inducing agent when the cell culture attains a certain optical density. The yields of the target proteins being comparable, the induction by IPTG wins out economically, since [U-^{13}C]-glucose can be used as the only carbon source, instead of the more expensive [U-^{13}C]-glycerol for ^{13}C isotope labelling.

The cultivation conditions at which maximum accumulation of the target proteins was observed were determined by testing the media used for protein synthesis induction using IPTG (TB and M9), as well as the auto-induction media proposed by FW Studier [20], taken with certain modifications (*Table 1*). The yeast extract was added to the media intended for the production of isotope-labelled peptide derivatives (M5052 – to introduce ^{15}N, and M9, C750501', and M50501 – to introduce [^{15}N, ^{13}C]) to obtain a concentration of 0.0002%. It was shown experimentally that this concentration of the yeast extract promotes the maximum increase in the yield of the target protein without having an effect on the ^{15}N and ^{13}C incorporation in the target protein. Considering the high cost of [U-^{13}C]-glycerol, we carried out a number of experiments to determine the

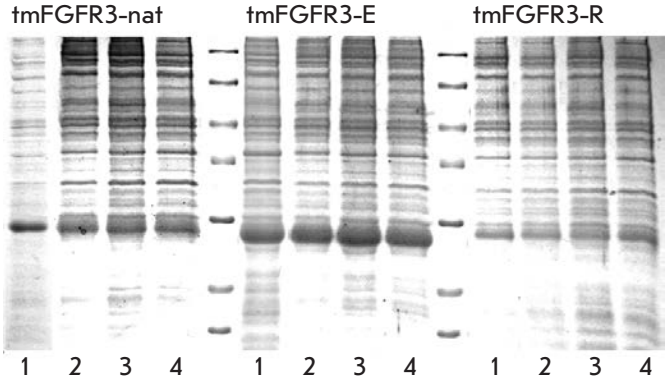

Fig. 2. Efficiency of production of TRX-tmFGFR3 fusion proteins in M9 minimal salt and M5052, C750501′ and M50501 auto-induction media. Coomassie blue-stained 14% Tris-glycine SDS-PAGE shows the fractionation of the lysate of whole cells producing TRX-tmFGFR3-nat, TRX-tmFGFR3-E and TRX-tmFGFR3-R. Recombinant strains were grown in: *1* – M9 medium, 13°C after induction with 0.05 mM IPTG; *2* — M5052 auto-induction medium, 18°C; *3* — M50501 auto-induction medium, 18°C; and *4* – C750501′ auto-induction medium, 18°C. Equivalents of 20 µL of cell culture were loaded into each lane. Protein molecular weight markers: 116.0, 66.2, 45.0, 35.0, 25.0, 18.4, and 14.4 kDa (top-down).

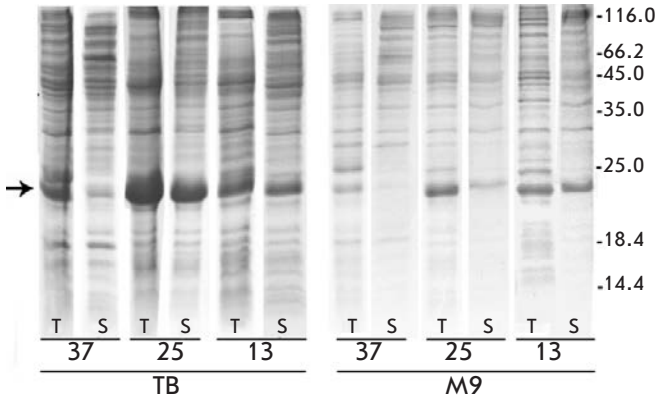

Fig. 3. Efficiency of production of TRX-tmFGFR3-E target fusion proteins in rich (TB) and minimal (M9) media depending on growth temperature (37°C, 25°C, 13°C) after IPTG induction. Coomassie blue-stained 14% Tris-glycine SDS-PAGE analysis of TRX-tmFGFR3-E cell lysate (0.05 mM IPTG). Protein molecular weight markers (kDa) are shown on the right. The arrow on the left indicates TRX-tmFGFR3-E target fusion protein. 5 (TB) or 10 µL (M9) of cell culture were loaded into each lane. T — total cellular protein; S — soluble protein fraction.

optimal glycerol concentration in the auto-induction medium at which maximum accumulation of the target product was observed. It appeared that a decrease in glycerol concentration by a factor of 1.5, along with a twofold fall in phosphate concentration in the culture medium (M50501 medium), either has no effect on the yield of the target products (tmFGFR3-nat and tmFGFR3-R) or enhances its accumulation (tmFGFR3-E) (*Fig. 2*). This fact makes it possible to considerably reduce the cost of the production of [^{15}N, ^{13}C]-labelled preparations by using the auto-induction principle.

Bacterial cells transformed with the appropriate vector were cultivated at 18°C in the case of auto-induction; or at 37, 25, and 13°C (after IPTG was added) when using chemical induction. The decrease in the cultivation temperature promotes maintenance of the protein in soluble form [12]. Thus, in the case of chemical induction, when cultivating cells both in rich (TB) and minimal (M9) media at high temperature (37°C), after adding IPTG, the fusion proteins mostly accumulated within inclusion bodies. With the temperature decreasing to 25°C, protein solubility increased; the inclusion bodies contained half of the protein. At 13°C, all fusion proteins were observed mostly in soluble form (*Figs. 2 and 3*).

The dependence of the gene expression level on the cultivation temperature or concentration of the inducing agent in case of chemical induction (1.0, 0.25, 0.05, and 0.01 mM IPTG) was assessed using SDS-PAGE electrophoresis. Based on the analysis results, a rich TB medium was used to produce target proteins (13°C after the induction) without incorporation of isotope labels. When using the M9 and M50501 media, the yield of fusion proteins appeared to be comparable (*Fig. 2*); therefore, the M9 medium (13°C after the induction) was selected for the production of preparative amounts of isotope-labelled target proteins. A maximum yield of all TRX-tmFGFR3 or their ^{15}N- or [^{15}N, ^{13}C]-labelled derivatives was attained at 0.05 mM IPTG.

Fusion protein purification

After cell lysis, fusion proteins were purified using immobilized metal affinity chromatography (IMAC). In order to prevent the precipitation of target proteins, the non-ionic detergent Triton X-100 was used at this or subsequent purification stages. The purity of the protein preparations obtained by IMAC was at least 80%. The molecular weights of the fusion proteins determined on the basis of their electrophoretic mobility (SDS–PAGE, tricine buffer) (*Fig. 4*) were similar to the calculated values.

The fusion proteins TRX-tmFGFR3 purified by IMAC were cleaved using the human enterokinase

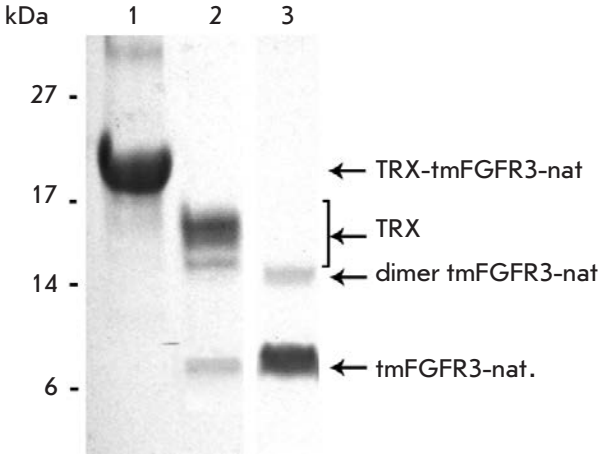

Fig. 4. Efficiency of purification of tmFGFR3-nat: *1* – purified fusion protein, *2* – products of enterokinase cleavage, *3* – purified tmFGFR3-nat. Arrows on the right indicate: TRX-tmFGFR3-nat fusion protein, TRX fusion partner, tmFGFR3-nat dimer and monomer compounds. Coomassie blue-stained 14% Tricine SDS-PAGE. Calculated molecular weights: TRX-tmFGFR3-nat – 19.6 kDa, tmFGFR3-nat – 4.6 kDa.

light chain (EK) [21] (*Fig. 1A*). When optimizing the reaction conditions for each peptide, the efficiency of the subsequent purification studies was accounted for. An optimal composition of the reaction mixture was obtained by diluting the fractions containing the fusion protein by a factor of 11 (see the EXPERIMENTAL section). EK (30 units per 1 mg of fusion protein TRX-tmFGFR3) was used for complete isolation of tmFGFR3 peptides from the partner protein (*Fig. 4*).

After the fusion protein had been cleaved for a night, IMAC was performed to remove the TRX fragment and the residual amounts of fusion proteins from the reaction mixture. The concentration and additional purification of tmFGFR3-target peptides using two successive stages of cation-exchange and anion-exchange chromatography at pH values ensuring the maximum charge and affinity of the target polypeptides towards ion-exchange resins were used to obtain protein preparations with a purity of at least 97%. The results of SDS–PAGE electrophoresis attest to the efficiency of TRX-tmFGFR3-E hydrolysis and tmFGFR3-E purification (*Fig. 4*). The data on the purification and efficiency of the proposed protocol for tmFGFR3-nat and tmFGFR3-R are identical. The electrophoretical mobility of tmFGFR3 corresponds to that of peptides mostly in monomeric conformations. The purity and correspondence of the purified peptides to the target tmFGFR3 were confirmed by mass spectroscopy analysis (*Fig. 5*) and NMR spectroscopy.

As mentioned above, tmFGFR3 peptides were obtained in the presence of Triton X-100. The high optical density of the aqueous solution of Triton X-100 impedes the use of the optical methods of analysis and determination of the secondary peptide's structure in this detergent using CD spectroscopy. In the case of NMR spectroscopy (see below), even trace amounts of Triton X-100 in the sample had a negative effect on the properties of the membrane-like environment that was used for structural studies, as well as the spatial structure of the protein. Peptides with Triton X-100 were precipitated with TCA, followed by washing of the precipitate with cooled acetone, in order to efficiently remove the detergent from the solution [12]. High efficiency of Triton X-100 removal from protein samples was confirmed by NMR spectroscopy. Using the procedure described, the yield of target proteins was brought up to 4–8 mg/l of the culture. The purity of the recombinant proteins and the degree of [^{15}N, ^{13}C]-label incorporation were at least 97%.

Solubilization of tmFGFR3 in the membrane-like environment

The selection of a medium imitating the surroundings of an object in the cell membrane is of exceptional significance for a successful study of structure and functions [23]. The composition of a membrane-like environment that would be optimal for NMR studies is determined by the following main parameters: size of supramolecular particles with tmFGFR3 incorporated into them; sample monodispersity; the absence of aggregation and sample stability; implementation of the native helical conformation; and tmFGFR3 dimerization. How closely the tmFGFR3 supramolecular complexes in the selected membrane-like environment met these criteria was estimated using NMR spectroscopy. Both detergent micelles and lipid bicelles of different compositions were used as membrane-like media. The total quality of the samples in terms of the possibility of carrying out further structural studies by NMR spectroscopy was assessed using two-dimensional spectra ^{1}H/^{15}N-bestHSQC and ^{1}H/^{15}N-TROSY. The total number of allowed cross-peaks within the region of the NH-signals of glycerol residues, dispersion, broadening, and signal doubling were analyzed.

It should be noted that both zwitterionic and charged deuterized detergents, which provide a possibility of imitating partially charged cell membranes, are often required to perform structural studies of membrane proteins and peptides by NMR methods. Today, SDS is the only commercially available detergent that is completely deuterized and negatively charged. This

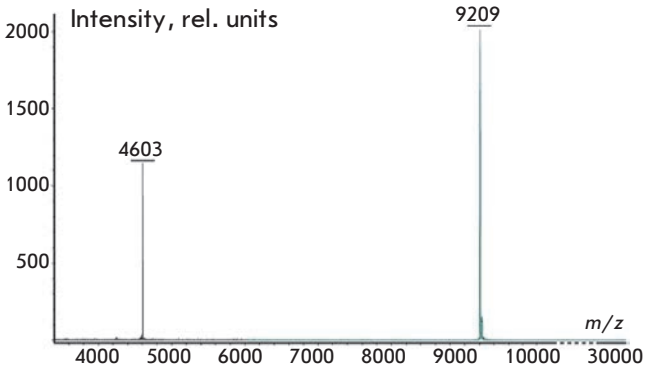

Fig. 5. Results of mass-spectroscopy analysis of the purified tmFGFR3-nat. The peaks in the spectrum correspond to tmFGFR3-nat monomer (m/z 4603) and dimer (m/z 9209) compounds.

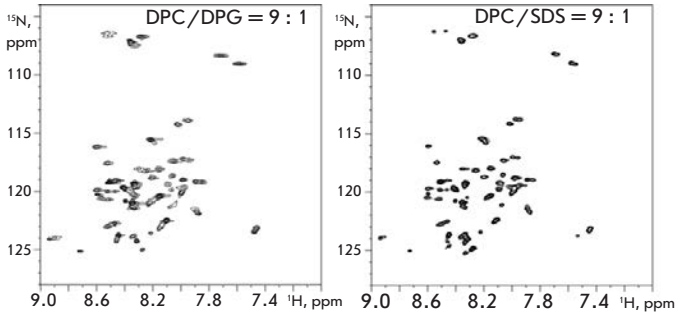

Fig. 6. $^{1}H/^{15}N$-bestHSQC NMR spectra of tmFGFR3-nat in DPC/DPG (left) and DPC/SDS (right) micelles. Temperature is 40°C, pH 5.7, and detergent/peptide molar ratio is 40.

detergent has no structural analogues among the phospholipids that are components of biological membranes; therefore, the use of SDS to simulate membrane properties is not always reasonable. In this study, we made an attempt to use completely deuterized DPG synthesized by us, in order to generate a partially negative charge on the micellar surface. The structure of the polar head of DPG is identical to that of phosphatidylglycerol, the main negatively charged phospholipid within bacterial membranes. The use of DPG allows to better simulate the properties of biological membranes as compared with SDS.

We selected tmFGFR3-nat solubilization conditions, which made it possible to study its spatial structure and dimerization. The best results upon solubilization of the tmFGFR3-nat peptide were obtained when using the mixed micelles of completely deuterized DPC/DPG (9/1 mol/mol) and DPC/SDS (9/1 mol/mol). The total number of peaks, good signal dispersion (being considerably higher than the corresponding values for the peptide in random conformation, which attests to the formation of the secondary structure), and small line width in the $^{1}H/^{15}N$-bestHSQC spectrum totally correspond to its secondary structure and the hydrodynamic size expected based on the amino acid sequence of the peptide (*Fig. 6*). The presence of cross-peak doubling in $^{1}H/^{15}N$-bestHSQC spectra, as well as the dependence of the relative intensities in these doublets on the number of tmFGFR3-nat molecules incorporated in one micelle (*Fig. 6*), points to the successful determination of the tmFGFR3-nat dimerization conditions that are suitable for structural studies using heteronuclear NMR spectroscopy.

CONCLUSIONS

The elaborated system of gene expression and purification protocol enables to produce recombinant transmembrane peptides tmFGFR3, including the isotope labelled derivatives to milligram amount, which are required for structural and functional studies. The relatively small size of the peptide complexes in the membrane-like environment attests to the possibility of obtaining the spatial structure of tmFGFR3-nat in dimeric state using high-resolution heteronuclear NMR spectroscopy [12, 24]. The conformation of the tmFGFR3-nat dimer was determined recently, and the study of the processes accompanying the specific association of tmFGFR3-E and tmFGFR3-R is now under way. The proposed technology of recombinant peptides production will help better understand the mechanism underlying the functioning, as well as signal transduction, with the participation of the FGFR3 receptor, as well as shed light on the molecular mechanisms of different disorders in human skeletal development, wich are directly associated with mutations in the FGFR3 TM domain. ●

This study was supported by the Russian Foundation for Basic Research, the Program of the Russian Academy of Sciences "Molecular and Cell Biology," and Federal Target-Oriented Programs "Scientific and Scientific-Pedagogical Personnel of Innovative Russia in 2009–2013" (P1276 and 16.740.11.0195), as well as the Federal Target-Oriented Program "Research and Development on Priority Directions of Scientific-Technological Complex of Russia in 2007–2012" (16.512.11.2172).

REFERENCES

1. Pantoliano M.W., Horlick R.A., Springer B.A., van Dyk D.E., Tobery T., Wetmore D.R., Lear J.D., Nahapetian A.T., Bradley J.D., Sisk W.P. // Biochemistry. 1994. V. 33. P. 10229–10248.
2. Shi E., Kan M., Xu J., Wang F., Hou J., McKeehan W.L. // Mol. Cell Biol. 1993. V. 13. P. 3907–3918.
3. Vajo Z., Francomano C.A., Wilkin D.J. // Endocr. Rev. 2000. V. 21. P. 23–39.
4. Passos-Bueno M.R., Wilcox W.R., Jabs E.W., Sertie A.L., Alonso L.G., Kitoh H. // Human Mutat. 1999. V. 14. P. 115–125.
5. Cappellen D., de Oliveira C., Ricol D., Diez de Medina S.G., Bourdin J., Sastre-Garau X., Chopin D., Thiery J.P., Radvanyi F. // Nat. Genet. 1999. V. 23. P. 18–20.
6. van Rhijin B., van Tilborg A., Lurkin I., Bonaventure J., de Vries A., Thiery J.P., van der Kwast T.H., Zwarthoff E.C., Radvanyi F. // Eur. J. Hum. Genet. 2002. V. 10. P. 819–824.
7. Webster M.K., Donoghue D.J. // EMBO J. 1996. V. 15. P. 520–527.
8. Meyers G.A., Orlow S.J., Munro I.R., Przylepa K.A., Jabs E.W. // Nat. Genet. 1995. V. 11. P. 462–464.
9. Merzlyakov M., Chen L., Hristova K. // J. Membr. Biol. 2007. V.215. P.93-103.
10. Li E., You M., Hristova K. // J. Mol. Biol. 2006. V. 356. P. 600–612.
11. MacKenzie K.R., Prestegard J.H., Engelman D.M. // Science. 1997. V. 276. P. 131–133.
12. Goncharuk M.V., Schulga A.A., Ermolyuk Ya.S., Tkach E.N., Goncharuk S.A., Pustovalova Yu.E., Mineev K.S., Bocharov E.V., Maslennikov I.V., Arseniev A.S., et al. // Mol. Biology (Moscow). 2011. V. 45. in press.
13. Bocharov E.V., Mineev K.S., Volynsky P.E., Ermolyuk Y.S., Tkach E.N., Sobol A.G., Chupin V.V., Kirpichnikov M.P., Efremov R.G., Arseniev A.S. // J. Biol. Chem. 2008. V. 283. P. 6950–6956.
14. Mineev K.S., Bocharov E.V., Pustovalova Y.E., Bocharova O.V., Chupin V.V., Arseniev A.S. // J. Mol. Biol. 2010. V. 400. P. 231–243.
15. Bocharov E.V., Mayzel M.L., Volynsky P.E., Mineev K.S., Tkach E.N., Ermolyuk Y.S., Schulga A.A., Efremov R.G., Arseniev A.S. // Biophys. J. 2010. V. 98. P. 881–889.
16. Kirpichnikov M.P., Goncharuk M.V., Ermolyuk Y.S., Goncharuk S.A., Schulga A.A., Maslennikov I.V., Arseniev A.S. // Tekhnologii Zhivikh Sistem. 2005. V. 2. P. 20-27.
17. Schmitt J.D., Amidon B., Wykle R.L., Waite M. // Chem. Phys. Lipids. 1995. V. 77. P. 131–137.
18. Bocharov E.V., Mayzel M.L., Volynsky P.E., Goncharuk M.V., Ermolyuk Y.S., Schulga A.A., Artemenko E.O., Efremov R.G., Arseniev A.S. // J. Biol. Chem. 2008. V. 283. P. 29385–29395.
19. Bocharov E.V., Pustovalova Y.E., Pavlov K.V., Volynsky P.E., Goncharuk M.V., Ermolyuk Y.S., Karpunin D.V., Schulga A.A., Kirpichnikov M.P., Efremov R.G., et al. // J. Biol. Chem. 2007. V. 282. P. 16256–16266.
20. Studier F.W. // Protein Expr. Purif. 2005. V. 41. P. 207–234.
21. Gasparian M.E., Ostapchenko V.G., Schulga A.A., Dolgikh D.A., Kirpichnikov M.P. // Protein Expr. Purif. 2003. V. 31. P. 133–139.
22. Schanda P., Lescop E., Falge M., Sounier R., Boisbouvier J., Brutscher B. // J. Biomol. NMR. 2007. V. 38. P. 47–55.
23. Kim H.J., Howell S.C., van Horn W.D., Jeon Y.H., Sanders C.R. // Prog. Nucl. Magn. Reson. Spectrosc. 2009. V. 55. P. 335–360.
24. Jura N., Endres N.F., Engel K., Deindl S., Das R., Lamers M.H., Wemmer D.E., Zhang X., Kuriyan J. // Cell. 2009. V. 137. P. 1293–1307.

Recombinant Production of Horseradish Peroxidase Conjugates with Fab Antibodies in *Pichia pastoris* for Analytical Applications

O.V. Koliasnikov[1,2#], V.G. Grigorenko[2*#], A.M. Egorov[2], S. Lange[3], R.D. Schmid[3]
[1]Kolmogorov Advanced Education and Science Center, Lomonosov Moscow State University
[2]Department of Chemistry, Lomonosov Moscow State University
[3]Institute of Technical Biochemistry, University of Stuttgart
*E-mail: vitaly@immunotek.ru
The authors provided equivalent contributions to the study.
Received 05.05.2011

ABSTRACT **Recombinant immunoconjugates of marker enzymes with antigens or antibodies present considerably more advantages than those obtained by conventional methods of chemical synthesis; i.e. they are homogeneous, have a strictly determined stoichiometry, and retain the functional activity of both a marker protein and an antigen/antibody. Based on the pPICZαB shuttle vector, we first managed to obtain a recombinant conjugate of key marker enzyme horseradish peroxidase (HRP) with *Fab* fragments of antibodies against atrazine. The resulting genetic construction allows us to switch to any other antibody sequence, via the simple re-cloning of variable parts and an additional reporter enzyme. Conjugates were successfully produced in the *Pichia pastoris* methylotrophic yeast expression system. The target activity of the conjugates (both enzymatic and antigen-binding) has been demonstrated by ELISA method.**
KEYWORDS **horseradish peroxidase; antibodies; recombinant conjugates; *Pichia pastoris* expression.**
ABBREVIATIONS **HRP – horseradish peroxidase; ELISA – enzyme-linked immunosorbent assay; BSA – bovine serum albumin; PCR – polymerase chain reaction; TMB – 3,3',5,5'-tetramethylbenzidine; ABTS – 2,2'-azinobis(3-ethylbenzothiazoline-6-sulphonic acid).**

INTRODUCTION

Enzyme immunoassays for the detection and quantitative analysis of various substances are based on coupling of marker enzymes such as horseradish peroxidase (HRP, EC 1.11.1.7]) with antigens or antibodies. However, all major approaches used for the chemical conjugation of proteins and haptens result in the partial inactivation of the enzyme and conjugate heterogeneity, which affects the specificity and sensitivity of the ELISA. Genetic engineering can be used to obtain recombinant conjugates of proteins with antigens or antibodies. Such conjugates present a number of advantages; firstly, they have a homogenous composition, secondly, they possess 1 : 1 stoichiometry, thirdly they retain the functional activities of both the marker protein and that of the antigen/antibody, in addition to the reproducibility and the fact that they are relatively simple to produce. Recombinant conjugates of antibodies with alkaline phosphatase [1–3], luciferase [4], and peroxidase *Arthromyces ramosus* [5] were obtained earlier.

The recombinant conjugate of HRP with the earlier obtained fatty-acid-binding protein (FABP) [6] was expressed in *Escherichia coli* cells and used as an immunotracer when performing immunoenzyme assay aimed at the early diagnosis of myocardial infarction.

The functional expression of the recombinant conjugate of HRP and antibody fragments in *E. coli* is associated with a number of difficulties, since there is no post-translational glycosylation of proteins in *E. coli* cells, resulting in low solubility and aggregation of the expressed/obtained protein. This problem can be solved by replacing the expression system. For instance, it has been shown that methylotrophic yeast *Pichia pastoris* is a more suitable organism/system for antibody expression than *E. coli* cells [7, 8].

HRP [9] and antibody fragments [10] were successfully expressed individually in *P. pastoris* cells, both in the single-stranded form scFv [11, 12] and in a Fab form [13]. Moreover, certain immunoconjugates have

also been created using this expression system [14–16]. It has been demonstrated that gene expression in the *P. pastoris* system in the secreted form considerably simplifies the scaling of the process for biochemical applications [17].

The recent advance in the functional expression of HRP and antibodies in secreted form paves the way for the construction of recombinant HRP–antibody conjugates to be used in immunoassays. Firstly, we obtained recombinant conjugates of HRP and Fab-fragments of antibodies against atrazine, in order to study the opportunities provided by this approach. In these chimeric proteins, the peroxidase part is combined with the N- and C-terminal parts of the heavy chain of an antibody via a short linker sequence. The universal vectors for the expression of conjugates of HRP and variable chains of Fab fragments of antibodies were obtained (a simple replacement of the variable part of a heavy and light chain of any other antibody by re-cloning at the PstI/BstEII and BamHI/XhoI sites, respectively) in the secreted form in *P. pastoris* cells. A functionally active HRP–Fab (atrazine) conjugate was obtained, possessing antigen-binding properties that are similar to those of monoclonal antibodies, which has been attested by single-stage competitive immunoassay of atrazine (IC_{50} ~ 3 ng/ml).

EXPERIMENTAL

Reagents

The reagents were purchased from the companies Sigma, Fluka, and Difco and used without further purification. Protein electrophoresis (SDS-PAGE) was performed according to the standard procedure, using a low molecular weight protein kit (LMW, Bio-Rad) as the molecular weight standards. The preparative work with DNA was performed using a QIA prep Spin Miniprep Kit and a QIAquick Gel extraction Kit (Qiagen, Germany). Enzymes for DNA restriction and modification were purchased from New England Biolabs, Boehringer-Mannheim, GIBCO-BRL-Life technologies, and MBI. Oligonucleotides for sequencing and PCR were purchased from ARK Scientific, MWG Biotech, or Interactiva (Germany).

Data processing and presentation

The gene engineering part of the study was planned using CloneManager software (Scientific & Educational Software, Cary, United States). The spatial structures of immunoconjugates were simulated and visualized on the InsightII (BioSym Inc., United States) software package (BioSym Inc., United States) on an SGI R4400 operating station. The experimental data were prepared for publication using software from the OpenOffice.org (www.openoffice.org) and GIMP (GNU Image Manipulation Program) packages.

Microorganisms, media, plasmids, and oligonucleotides

E. coli strain DH5α was used for genetic manipulations, and *E. coli* strain BL21(DE3) pLysS (Novagen) was used for intermediate production of the protein. The cells were cultured in an LB medium (1% yeast extract, 1% Peptone, 0.5% NaCl) supplemented with 25 mg/l of Zeocin (Invitrogen).

Preparing competent cells. *E. coli* cells were grown overnight in 50 ml of the LB medium until OD_{600} was 0.4–0.6 and were isolated from the culture medium by centrifugation (3500 rpm, 4°C) for 10 min. The cell precipitate/pellet was re-suspended in a TSS buffer (buffer based on a LBS medium containing 10 g of PEG-6000, 5 ml of DMSO, and 0.6 g of $MgCl_2$ in 100 ml; pH 6.5) and then kept on ice for 1 h, aliquoted (200 μl), and quickly frozen at –80°C.

Recombinant antibodies and their conjugates with HRP were expressed using *P. pastoris* X33 (Invitrogen) and shuttle vector pPICZαB (Invitrogen) for cloning.

The NotI site was removed using forward and reverse primers (*Table*). A three-stage PCR was used (primers listed in the *Table*), in order to incorporate the *HRP* gene behind the gene of the heavy antibody chain and to remove the restriction sites BspCI, ApaI, PstI, BstEII, BglII, XhoI, BamHI, SacI, and PvuI.

DNA modification and cell transformation

Manipulations with DNA included the standard procedures [18]. *E. coli* cells were transformed via the addition of plasmids or a ligation mixture to the unfrozen competent cells. *P. pastoris* cells were also transformed by plasmids preliminarily linearized at the PmeI site via electroporation.

P. pastoris cultivation and secretion of the recombinant conjugate

P. pastoris cells were cultivated in a YPD medium (1% yeast extract, 2% Peptone, 2% *D*-glucose). The target protein was synthesized in the glucose-free YP medium, using 0.5 vol % methanol as an inducing agent. The YPDS medium (YPD containing 1 M sorbitol) was used for transformation of *P. pastoris* cells. The solid medium contained 1.5% of Bacto Agar. The transformants were grown in the YPDS medium at 30°C under stirring (200 rpm) until OD_{600} = 15 units was obtained. The cells were centrifuged at 3,000 *g* and 4°C, washed with YP medium, and OD_{600} was brought to 1. The induction was performed for 96 h by adding 0.5 vol % metha-

nol every 24 h. The supernatant was concentrated via membrane ultrafiltration (Amicon, 10 kDa).

Synthesis of bovine serum albumin (BSA) conjugated with atrazine

The mixture of 1 mg of atrazine derivative (4-chloro-6-(isopropylamino)-1,3,5-triazine-2-(6-amino-caproic acid)) (~ 3.2 μmol), 1.7 mg of N-hydroxysuccinimide (~ 15 μmol), 6.6 mg of N,N'-dicyclohexylcarbodiimide (~ 30 μmol) in 130 μl of 1,4-dioxane was stirred for 8 h at room temperature. The precipitate was isolated by centrifuging on a desktop centrifuge (12,000 rpm, 30 s). The supernatant was added dropwise to the BSA solution (2 mg) in 3 ml of 0.13 M $NaHCO_3$. The reaction mixture was left in a dark place for 3 h. The reaction product was applied to a PD-10 column that was preliminarily balanced with a phosphate-buffered saline (PBS), pH 7.5. A total of 16 fractions (0.5 ml each) were collected and analyzed spectrophotometrically (at 220 and 260 nm). The fractions with the highest $OD_{220/260}$ ratio were combined to be used in further experiments.

Determination of activity of the recombinant conjugate by ELISA

ELISA was performed overnight using plates ("NUNC" MAXI-SORP) with the preliminarily sorbed BSA-atrazine (1 : 100 dilution) conjugate or BSA (10 μg/ml) in a 10 mM carbonate buffer, pH 9.0, at 4°C. The samples of supernatant of a *P. pastoris* culture medium were successively diluted in PBS, added into the plate wells, and incubated at 37°C for 1 h. Then, the plate was washed thrice with PBS containing 0.1% of Tween-20 (PBS-T), and 50 μl of a TMB substrate mixture was added (0.6 mg/ml TMB and 8 mM H_2O_2 in 0.1 M acetate buffer, pH 5). The reaction was stopped by adding 50 μl of 2 M H_2SO_4; the optical density was measured at 450 nm.

Competitive ELISA for determining atrazine

150 μl of the calibration sample (0.1, 1.0, 10, 20, 50, 100, 500 ng/ml of atrazine in PBS-T) and 40 μl of a recombinant conjugate solution were placed into plate wells with the preliminarily sorbed BSA-atrazine conjugate and incubated at 37°C for 1 h. The plate was washed three times with PBS-T, and 50 μl of the TMB substrate mixture was added into each well. The reaction was stopped by adding 50 μl of 2 M H_2SO_4; the optical density was measured at 450 nm.

RESULTS AND DISCUSSION

Recombinant conjugates are chimeric proteins combining the structural components of both marker enzymes and an antigen/antibody. The use of modern approaches has almost solved the problem of obtaining such recombinant enzymes as alkaline phosphatase, β-galactosidase, luciferase, and horseradish peroxidase that are used as markers in the ELISA methods. However, the production of recombinant conjugates is an appreciably complicated task, since it remains thus far impossible to reliably predict the structure of the desired conjugate; hence, loss of the functional activity of both the marker enzyme and antigen is possible, due to the incorrect folding of two components.

Recombinant conjugates comprising bacterial enzymes (β-galactosidase and alkaline phosphatase) that can be easily expressed in soluble form in *E. coli* cells, as well as some other enzymes, were earlier obtained. The major problem associated with the use of β-galactosidase and alkaline phosphatase within conjugates is their tetrameric and dimeric structures, respectively, which results in a considerable increase in conjugate affinity in comparison with a free antibody. This phenomenon is particularly undesirable when designing ELISA competitive schemes. Meanwhile, horseradish peroxidase, one of the marker enzymes that have been most widely used in ELISA, is expressed in *E. coli* cells only in the form of inclusion bodies, which until recently has impeded the obtaining of an active enzyme.

The recent advance in the heterologous expression of antibody genes in the cells of methylotrophic yeast *P. pastoris* offers great opportunities for using this system for the synthesis of the conjugates of horseradish conjugates with antibodies in the secreted soluble and functionally active forms.

Designing the expression vector to obtain a recombinant conjugate of HRP with a Fab fragment of antibodies in *P. pastoris*

The expression system for obtaining recombinant conjugates of HRP and Fab fragments of antibodies was elaborated on the basis of the pPICZαB vector. The genetic construction was placed under the control of the AOX promoter containing the PmeI site for the subsequent linearization and recombination into the yeast genome. The vector also contains the signal sequence of α-factor, which is necessary for the directed secretion of recombinant protein into the culture medium. Gene s*h ble* provides zeocin resistance of both *E. coli* and *P. pastoris* cell types. The possibility of introducing a hexahistidine sequence at the C-terminus of the recombinant protein is provided to simplify the procedures of extraction and purification of the product.

We used the plasmids earlier obtained (pPIC-VCL and pPIC-VCH [19] containing the corresponding fragments of variable regions of the light and heavy chains of K4E7 monoclonal antibody against atrazine [20], respectively) as the starting material (*Fig. 1*). Both these

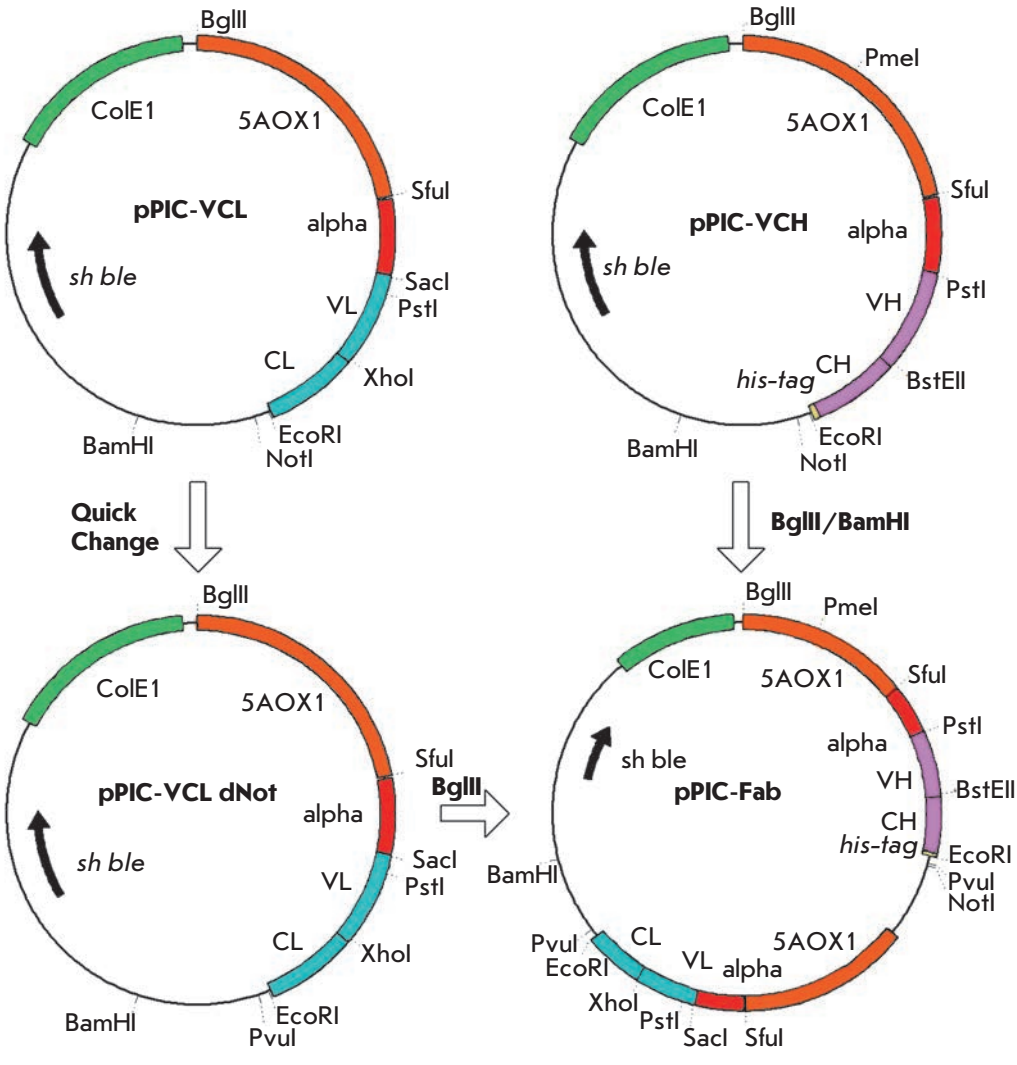

Fig. 1. Cloning scheme for construction of pPIC Fab plasmid.

vectors contained the NotI site behind the cloned gene.

To design the universal construction, we planned to leave only one NotI site in the vector behind the gene of the antibody heavy chain. PCR (the QuickChange mode [21]) using a special primer pair (*Table*) was employed to remove the NotI site from the pPIC-VCL plasmid. The vector obtained by this procedure is known as pPIC-VCL dNot. Then, the BglII/BamHI fragment of the pPIC-VCH plasmid containing the heavy-chain gene was cloned at the BglII site of plasmid pPIC-VCL dNot prior to the light chain gene. The expression vector pPIC-Fab was used. The cloning scheme is given in *Fig. 1*.

The universal pPIC-Fab gene obtained contains SacI/XhoI and PstI/BstEII site pairs for simple cloning of the genes of the heavy and light chains, encodes the C-terminal hexahistidine fragment for simplifying the purification of the target protein using metal chelate chromatography, and the NotI site for cloning the marker protein (such as HRP, green fluorescent protein (EGFP), luciferase, etc.) at the C-terminus of the heavy chain of the antibody.

A vector for the expression of the recombinant conjugate of peroxidase with Fab fragments of antibodies was designed simultaneously. For the simplicity of cloning, restriction sites PstI, BstEII, BglII, XhoI, SacI, PvuI, ApaI, BamHI and BspCI were removed using the primers listed earlier (*Table*) from the initial *HRP* gene [22] that was preliminarily cloned in the corresponding pPIC vector. Either before the *HRP* gene or behind it the fragments of antibody genes were simultaneously cloned. Thus, three-stage PCR was used to obtain two genetic constructions in which the *HRP* gene was linked with the sequence encoding the N-terminal region of the variable part of the heavy Fab chain or the C-terminal region of the constant part of the heavy chain via a short linker sequence $(Gly_4Ser)_3$ (*Fig. 2*). It should be mentioned that in order to avoid the formation of

Forward (F) and reversed (R) primers used for generation of genetic constructs with PCR. The introduced mutations are indicated in bold and underlined in primer sequences

Target gene	Restriction site destroyed		Primer sequence*
HRP	NotI	R	5′-CGATCGAGCC GCG**AT**GGCCG CCAGC-3′
HRP	NotI	F	5′-GCTGGCGGCC **AT**CGCGGCTC GATCG-3′
Fab VCH		R	5′-AGGCACAGCT ATAGGTACG-3′
Fab VCH		F	5′-TGAGAACCTC CACCGCCGCA GTCGCGCGGT ACG-3′
HRP		R	5′-GCGGCGGTGG AGGTTCTCAG TTAACGCCGA CTTTCTACG-3′
HRP	PstI, BspCI	R	5′-GA**C**CGCATGA AGGCTGC**T**GT CG-3′
HRP	PstI, BspCI	F	5′-AC**A**GCAGCCT TCATGCG**G**TC G-3′
HRP	BstEII, ApaI	R	5′-AC**T**CTAGCCG GCGG**T**CCCTC-3′
HRP	BstEII, ApaI	F	5′-GG**A**CCGCCGG CTAG**A**GTGAC-3′
HRP	XhoI	R	5′-GAACCG**T**TCG AGTGATCTAG-3′
HRP	XhoI	F	5′-AGATCACTCG A**A**CGGTTCAG-3′
HRP	SacI	R	5′-GATCAGGAGC T**G**TTCTCATC-3′
HRP	SacI	F	5′-AA**C**AGCTCCT GATCAGATTG-3′
Fab VCL	NotI	R	5′-ATCGGTACCT CGATCGAGCC GCG**AT**GG-3′
Fab VCL	NotI	F	5′-TGAAGTGGTA CGGCGATGC-3′

* The nucleotide sequence regions that were changed are highlighted.

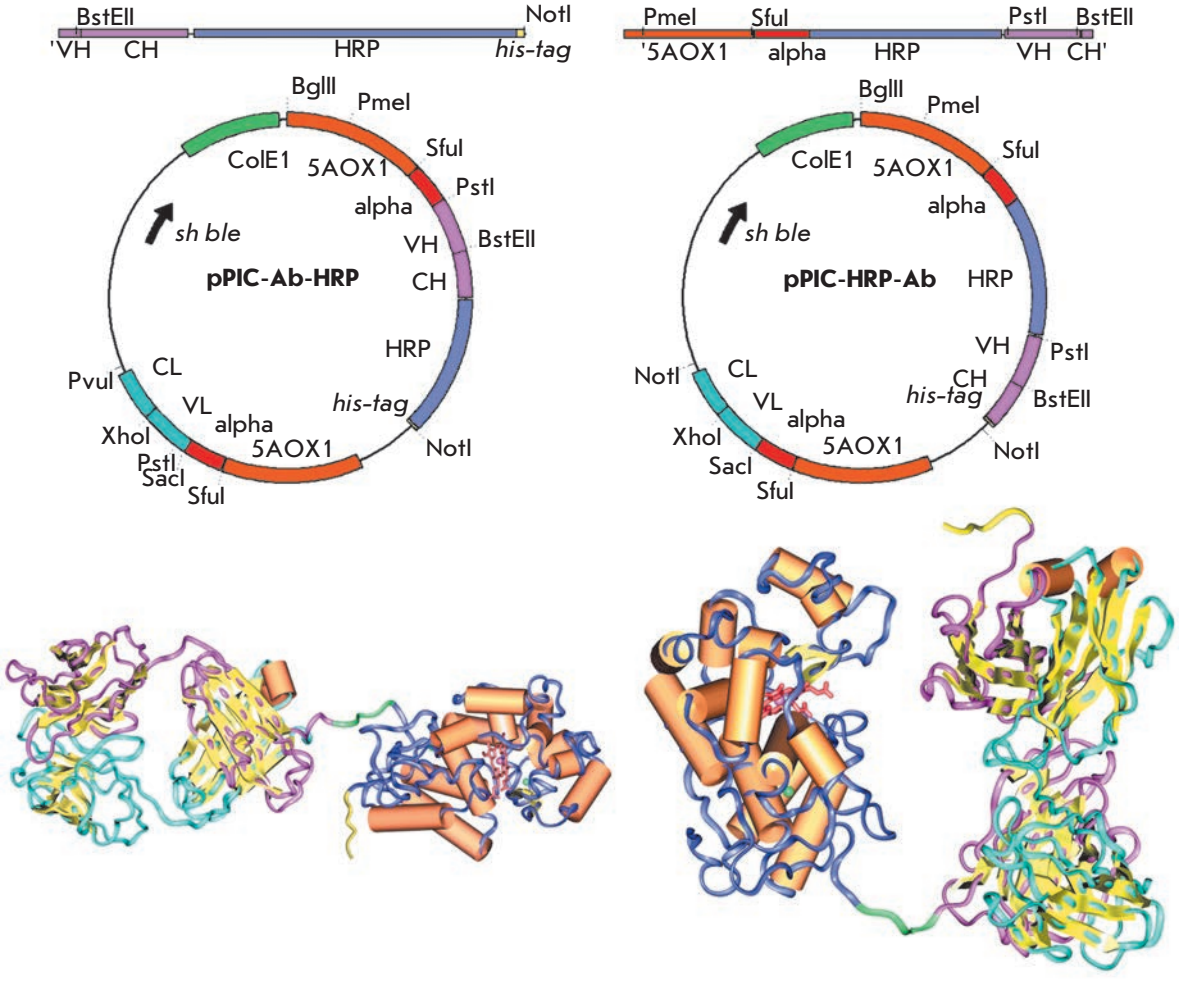

Fig. 2. General versatile expression vectors for recombinant conjugates of *HRP* with Fab antibody fragments production. The spatial models of recombinant conjugates of Fab-HRP and HRP-Fab are shown in the left and right panels, respectively.

nonfunctional dimers of the light chain, genetic constructions were cloned in the pPIC-Fab vector at the sites PmeI/BstEII and BstEII/NotI, respectively; the heavy chain was selected for the cloning of the marker protein gene. The mutual arrangement of genes in plasmids pPIC-Ab-HRP and pPIC-HRP-Ab was confirmed by restriction analysis and sequencing.

Expression and purification of recombinant conjugates Fab-HRP and HRP-Fab

P. pastoris X33 cells (Invitrogen) were transformed via the plasmid vectors pPIC-Ab-HRP and pPIC-HRP-Ab using electroporation with an efficiency of approximately 100 clones per 10 μg of plasmid DNA. The expression of the target protein was tracked by increasing the peroxidase activity in the supernatant of the culture medium, reaching a plateau on day 5 of cultivation. Ten clones were analyzed with each construction. The HRP activity with respect to the TMB substrate was detected only in three clones out of 20: two clones (1.1, 1.2) corresponding to pPIC-Ab-HRP and one clone (8) corresponding to pPIC-HRP-Ab. These clones were selected for further consideration.

As shown by SDS-PAGE electrophoresis (the data are not provided), the blurred bands located below the band at 100 kDa correspond to the recombinant conjugates HRP-VCH and VCH-HRP. This blurriness of the bands is accounted for by the microheterogeneity of conjugates, conditioned by excessive glycosylation that is typical for *P. pastoris*; correlating with our data and the data published on the expression of the *HRP* gene [9]. A considerably greater excess (by a factor of 3–4) of light-chain molecules was observed (the band at 25 kDa) in comparison with that found during the expression of the Fab fragment [19]. Unexpectedly, it occurred that the recombinant conjugated manifested no enzymatic activity toward another peroxidase substrate, ABTS, as opposed to TMB. It is well known that the site of binding with ABTS is located in the hydrophobic region on the HRP surface, in the so-called "Phe patch" zone [25]. This zone is noticeably distant from the active site of HRP, and it can be assumed that the substrate binding to it is complicated due to steric reasons – as a result of excessive glycosylation or the presence of a Fab fragment of antibody. The first hypothesis is more probable, since the same effect is observed under both positions of the heavy chain of the antibody with respect to HRP. Moreover, a similar effect was earlier observed upon expression of the *HRP* gene in *P. pastoris* (the data have not been published).

The total yield of recombinant conjugates was approximately 3–10 mg per 1 l of the *P. pastoris* culture supernatant. A relatively low yield of secreted conjugates correlates with the yield upon expression of

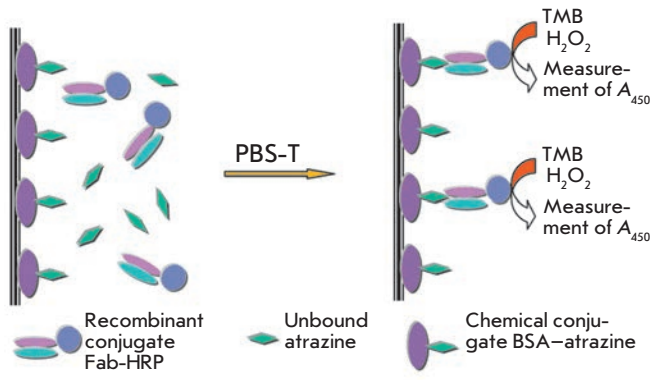

Fig. 3. ELISA scheme for atrazine determination.

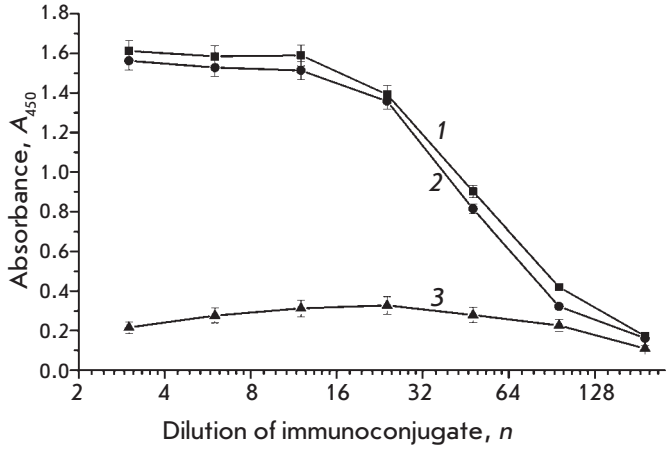

Fig. 4. Titration of recombinant conjugates: 1 – Fab-HRP (clone 1.1); 2 – Fab-HRP (clone 1.2); 3 – HRP-Fab (clone 8).

the *HRP* gene only. We believe that one of the factors that have a negative effect on the yield of the secreted product is the excessive glycosylation of the peroxidase component of the conjugate, which is typical of *P. pastoris* cells. In order to verify this hypothesis, it may be reasonable to remove all N-glycosylation sites in HRP or replace HRP with another reporter protein, such as EGFP.

Characterization of recombinant conjugates by ELISA

In order to confirm the antigen-binding activity of recombinant conjugates, we selected the scheme of indirect competitive single-stage ELISA (*Fig. 3*) carried out on the wells with an immobilized atrazine–BSA conjugate. The binding of recombinant conjugates to atrazine was preliminarily studied (*Fig. 4*). The data obtained attest to the presence of both catalytic and antibody

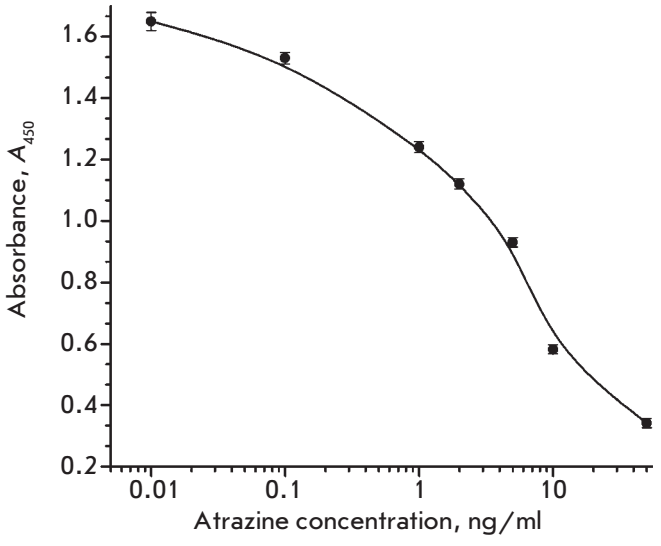

Fig. 5. Calibration curve for atrazine determination in competitive ELISA with recombinant conjugate of Fab-HRP (clone 1.1).

activity in all three clones. However, the low activity of the HRP-Fab sample (clone 8) in comparison with the C-terminal conjugate Fab-HRP (clones 1.1 and 1.2) may attest to the fact that the mutual spatial arrangement of two components of the chimeric protein in this case results in a decrease in the catalytic activity of peroxidase. The samples of recombinant conjugates Fab–HRP (clones 1.1 and 1.2) have similar characteristics, and specimen 1.1 was used for further ELISA determination of atrazine. The typical calibration diagram (*Fig. 5*) allows one to determine the atrazine concentration over a wide range, from 0.1 to 50 ng/ml; the variation coefficient being no higher than 8%. IC_{50} is equal to 3 ng/ml, which agrees well with the results of atrazine determination by a two-stage ELISA procedure using recombinant Fab fragments of the same antibody K411B [19] and with the data on the single-chain mini-antibody (scFv) obtained earlier in *E. coli* [24]. Meanwhile, in the initial monoclonal antibody, the IC_{50} value was equal to 0.2 ng/ml [19]. As is evident in the majority of similar cases, the fact that the IC_{50} value differs from that of recombinant antibodies is in all likelihood connected with the bivalence of the initial monoclonal antibody.

Thus, the recombinant conjugates of peroxidase with Fab fragments of antibody against atrazine obtained in the present study possess functional activity and can be used to determine atrazine via ELISA.

CONCLUSIONS

The possibility of using a recombinant, functionally active HRP (as a marker enzyme) conjugated with Fab fragments of the antibody against atrazine was shown for the first time. In the present study, recombinant conjugates were obtained in which the Fab fragment of an antibody is bound both to the N- and the C- terminuses of the marker enzyme. Both these variants manifest immunological and catalytic activity.

The functional secretion of recombinant conjugates of HRP with Fab fragments of antibodies offers opportunities for broad application in ELISA. The results obtained will be used to design highly sensitive immunobiosensors of a new generation, based on the recombinant DNA technology. ●

The study was partially supported by the German Federal Ministry of Science and Technology (BMBF, grant № 0311574).

REFERENCES

1. Rau D., Kramer K., Hock B. // J. Immunoassay Immunochem. 2002. V. 23. № 2. P. 129–143.
2. Tachibana H., Takekoshi M., Cheng X.J., Nakata Y., Takeuchi T., Ihara S. // Clin. Diagn. Lab. Immunol. 2004. V. 11. №1. P. 216–218.
3. Mousli M., Turki I., Kharmachi H., Saadi M., Dellagi K. // J. Virol. Meth. 2007. V. 146. №1–2. P. 246–256.
4. Patel K.G., Ng P.P., Kuo C.C., Levy S., Levy R., Swartz J.R. // Biochem. Biophys. Res. Commun. 2009. V. 390. № 3. P. 971–976.
5. Joosten V., Roelofs M.S., van den Dries N., Goosen T., Verrips C.T., van den Hondel C.A., Lokman B.C. // J. Biotechnol. 2005. V. 120. № 4. P. 347–359.
6. Grigorenko V., Andreeva I., Borchers T., Spener F., Egorov A. // Anal. Chem. 2001. V. 73. № 6. P. 1134–1139.
7. Robin S., Petrov K., Dintinger T., Kujumdzieva A., Tellier C., Dion M. // Mol. Immunol. 2003. V. 39. № 12. P. 729–738.
8. Cupit P.M., Whyte J.A., Porter A.J., Browne M.J., Holmes S.D., Harris W.J., Cunningham C. // Lett. Appl. Microbiol. 1999. V. 29. № 5. P. 273–277.
9. Morawski B., Lin Z., Cirino P., Joo H., Bandara G., Arnold F.H. // Protein Eng. 2000. V. 13. № 5. P. 377–384.
10. Pennell C.A., Eldin P. // Res. Immunol. 1998. V. 149. № 6. P. 599–603.
11. Fischer R., Drossard J., Emans N., Commandeur U., Hellwig S. // Biotechnol. Appl. Biochem. 1999. V. 30. Pt 2. P. 117–112.
12. Freyre F.M., Vazquez J.E., Ayala M., Canaan-Haden L., Bell H., Rodriguez I., Gonzalez A., Cintado A., Gavilondo J.V. // J. Biotechnol. 2000. V. 76. № 2–3. P. 157–163.
13. Takahashi K., Yuuki T., Takai T., Ra C., Okumura K., Yokota T., Okumura Y. // Biosci. Biotechnol. Biochem. 2000. V. 64. № 10. P. 2138–2144.
14. Andrade E.V., Albuquerque F.C., Moraes L.M., Brigido M.M., Santos-Silva M.A. // J. Biochem. (Tokyo.) 2000. V. 128.

№ 6. P. 891–895.
15. Luo D., Geng M., Schultes B., Ma J., Xu D.Z., Hamza N., Qi W., Noujaim A.A., Madiyalakan R. // J. Biotechnol. 1998. V. 65. № 2–3. P. 225–228.
16. Powers D.B., Amersdorfer P., Poul M., Nielsen U.B., Shalaby M.R., Adams G.P., Weiner L.M., Marks J.D. // J. Immunol. Meth. 2001. V. 251. № 1–2. P. 123–135.
17. Hellwig S., Emde F., Raven N.P., Henke M., van der Logt P., Fischer R. // Biotechnol. Bioeng. 2001. V. 74. № 4. P. 344–352.
18. Sambrook J., Fritsch E.F., Maniatis T. Molecular Cloning: A Laboratory Manual. Cold Spring Harbor, N.Y.; Cold Spring Harbor Lab. Press, 1989.
19. Lange S., Schmitt J., Schmid R.D. // J. Immunol. Meth. 2001. V. 255. P. 103–114.
20. Giersch T. // J. Agric. Food Chem. 1993. V. 41. № 6. P. 1006–1011.
21. Braman J., Papworth C., Greener A. // Methods Mol. Biol. 1996. V. 57. P. 31–44.
22. Grigorenko V., Chubar T., Kapeliuch Yu., Borchers T., Spener F., Egorov A. // Biocatal. Biotransform. 1999. V. 17. P. 359–397.
23. Ferrari R.P., Traversa S., de Gioia L., Fantucci P., Suriano G., Ghibaudi E.M. // J. Biol. Inorg. Chem. 1999. V. 4. № 1. P. 12–20.
24. Kramer K., Hock B. // Food Agric. Immunol. 1996. V. 8. P. 97–109.

Atomic Force Microscopy Study of the Arrangement and Mechanical Properties of Astrocytic Cytoskeleton in Growth Medium

Yu.M. Efremov[1*], E.V. Dzyubenko[1,2], D.V. Bagrov[1], G.V. Maksimov[1], S.I. Shram[2], K.V. Shaitan[1]
[1] Biological Department, Lomonosov Moscow State University
[2] Institute of Molecular Genetics, Russian Academy of Sciences
*E-mail: yu.efremov@gmail.com
Received 23.05.2011

ABSTRACT **Astrocytes are quite interesting to study because of their role in the development of various neurodegenerative disorders. The present work describes an examination of the arrangement and mechanical properties of cytoskeleton of living astrocytes using atomic force microscopy (AFM). The experiments were performed with an organotypic culture of dorsal root ganglia (DRG) obtained from a chicken embryo. The cells were cultivated on a gelatinous substrate and showed strong adhesion. AFM allows one to observe cytoskeleton fibers, which are interpreted as actin filaments and microtubules. This assumption is supported by confocal microscopy fluorescence imaging of α-tubulin and fibrillar actin. Mapping of the local Young's modulus of a living astrocyte showed that the stiff areas correspond to the sites where the cytoskeleton fibers are located. Thus, the data obtained indicate that AFM is a promising method to study neural cells cytoskeleton integrity and arrangement in *in vitro* models of neurodegeneration.**
KEYWORDS **atomic force microscopy; dorsal root ganglia; force spectroscopy; confocal microscopy; cytoskeleton.**
ABBREVIATIONS **AFM –atomic force microscopy; DRG – dorsal root ganglia; GFAP – glial fibrillary acidic protein.**

INTRODUCTION

Astrocytes are one of the main cell types in the central nervous system, where they have several functions: they direct and stimulate neuron migration during development; they sustain the neuronal microenvironment and modulate the immune response via antigen presentation [1]. The study of astrocyte morphology is of great interest due to their significant role in the pathogenesis of many common diseases of the central and peripheral nervous systems, such as ischemic stroke, Alzheimer's disease, AIDS-related dementia [2], diabetic retinopathy [3], etc. These pathologies are accompanied by substantial morphological and physiological rearrangements in neural cells and by changes in gene expression [2, 4]. They are also typically accompanied by changes in the cytoskeleton structure [5].

Atomic force microscopy (AFM) has been used in biological studies for a significant period of time for the visualization of biomolecules [6, 7] and cells [8–10] and for the assessment of their mechanical characteristics [11, 12]. AFM allows one to obtain a 3D image of a living cell in the growth medium and also perform manipulations on it at micro- and nano-scale. Cytoskeleton can usually be observed on cell images obtained in contact mode [9, 13]. Measuring the Young's modulus makes it possible to get important information on the physiological and functional state of cells [14, 15]. In the current work, AFM has been used to study an organotypic culture of dorsal root ganglia (DRG) obtained from a chicken embryo. The astrocyte cytoskeleton structure has been examined, and the contribution of the cytoskeleton into the local Young's modulus of a cell has been revealed. The data on the cytoskeleton arrangement obtained by AFM were compared with confocal microscopy data.

EXPERIMENTAL

Cell culture

An organotypic culture of dorsal root ganglia (DRG) was obtained from a chicken embryo according to the standard procedure described elsewhere [16]. Briefly, to prepare gelatin-coated 35 mm Petri dishes, 2 ml of a 0.5% gelatin solution was placed into sterile dishes, incubated for 1 h at 37°C, and removed. Dorsal root gan-

glia were isolated from an 11- or 12-day-old chicken embryo under a binocular microscope and placed into the gelatin-coated Petri dishes. 2 ml of the F12 medium (Biolot, Russia) containing pyruvate, glutamine, penicillin, streptomycin and 10% of horse blood serum was added into each dish.

In order to enhance cell adhesion and prolong the lifetime of the primary culture, nerve growth factor (NGF 7S) was added at a final concentration of 5 ng/ml. The obtained samples appear as a mixed primary culture of neurons and astrocytes. These two cell types have clear morphological differences and therefore can easily be distinguished [1]. In order to detect astrocytes, immunocytochemical staining for glial fibrillary acidic protein (GFAP) (an astrocytic marker protein) was performed in accordance with a procedure described in [17].

Atomic force microscopy

The atomic force microscopy experiments were carried out on a Solver BIO atomic-force microscope ("NT-MDT", Russia) equipped with a 100x100x7 μm^3 scanner and a closed-loop feedback system. The morphology intrinsic to living cells is likely to be retained for several hours, and the AFM experiments were performed only on the cells that had this type of morphology. The optical microscope, combined with the AFM, was used to choose the scanning region.

The measurements were performed in the culture medium using contact and semi-contact modes (the semi-contact mode did not help to improve the image quality; the information on the cytoskeleton was not available; therefore, we present only the images obtained in contact mode) using silicon nitride cantilevers MSCT-AUHW (former Veeco Instruments, now Bruker, USA). Trace and retrace topography and feedback error signal were recorded during each scan. The mechanical force acting on the cell, measured using the force-distance curves, was adjusted to be as small as possible (the typical value was equal to 1–4 nN) [18]. Comparison of the trace and retrace profiles was the criterion of correct feedback adjustment and validity of the obtained data. After the optimal scanning parameters were selected, the trace and retrace profiles showed good agreement, which indicated that there were no considerable distortions of the structure under the impact of the cantilever. The feedback error signal made it easier to reveal small surface relief heterogeneities [19]. The images were processed using ImageAnalysis ("NT-MDT", Russia) and FemtoScan Online (Advanced Technologies Center, Russia) software.

In the force spectroscopy experiments, AFM was used to capture the force curves. A force curve is a plot showing the elastic force acting on the cantilever as a function of the vertical scanner displacement [20, 21]. To record a force curve, the cantilever is first pushed against the selected sample point. When the cantilever moves down, the approach curve is recorded, the maximum interaction force can be adjusted and is typically 2-3 nN. Then, the cantilever is lifted, providing the retract curve. Rectangular PNP-DB cantilevers (NanoWorld, Switzerland) and triangular MSCT-AUHW (former Veeco Instruments, now Bruker, USA) cantilevers made of silicon nitride were used for the force spectroscopy. Before the measurements, the rigidity of the rectangular cantilevers was determined using the Sader method [22, 23]; the rigidity values specified by the manufacturer were used for triangular cantilevers. The deflection was calibrated using the force curve obtained above the Petri dish surface. The Young's modulus was calculated based on the approach curves using EF3 and the ImageAnalysis software ("NT-MDT", Russia). In this software, the Sneddon's modification of the Hertz model is used [9, 24].

Confocal microscopy and fluorescent staining

The specimens were fixed, stained with α-tubulin antibodies (DM1α, Santa Cruz Biotechnology, United States), and treated by the secondary antibodies conjugated with Alexa 594 (Alexa594 anti-mouse polyclone, Invitrogen, United States). Staining for astrocyte marker GFAP was performed in a similar way: after incubation with primary antibodies (GFAP, Abcam, England), secondary antibodies conjugated with Alexa 546 (Alexa546 anti-rabbit polyclone, Invitrogen, United States) were added. Rhodamine–phalloidin conjugate was used for actin staining. Fixation and staining were performed according to [17].

The confocal microscopy experiments were carried out using a LSM 510 META microscope (Carl Zeiss, Germany). Actin was visualised using an oil immersion objective lens Plan-Apochromat 100x "Carl Zeiss" (aperture 1.4), excitation wavelength 543 nm, spectral detection range 530–600 nm, and confocal diaphragm with 164 μm diameter. The image size was 1024 × 1024 pixels (85 nm/pixel).

Tubulin was visualised using an oil immersion objective lens Plan-Apochromat 100x "Carl Zeiss" (aperture 1.4), excitation wavelength 543 nm, spectral detection range 615–700 nm, and confocal diaphragm with 184 μm diameter. The image size was 1024 × 1024 pixels (85 nm/pixel).

GFAP was visualised using an oil immersion objective lens 63x "Carl Zeiss" (aperture 1.4), excitation wavelength 514 nm, spectral detection range 530–600 nm, and confocal diaphragm with 124 μm diameter. The image size was 1024 × 1024 pixels (127 nm/pixel).

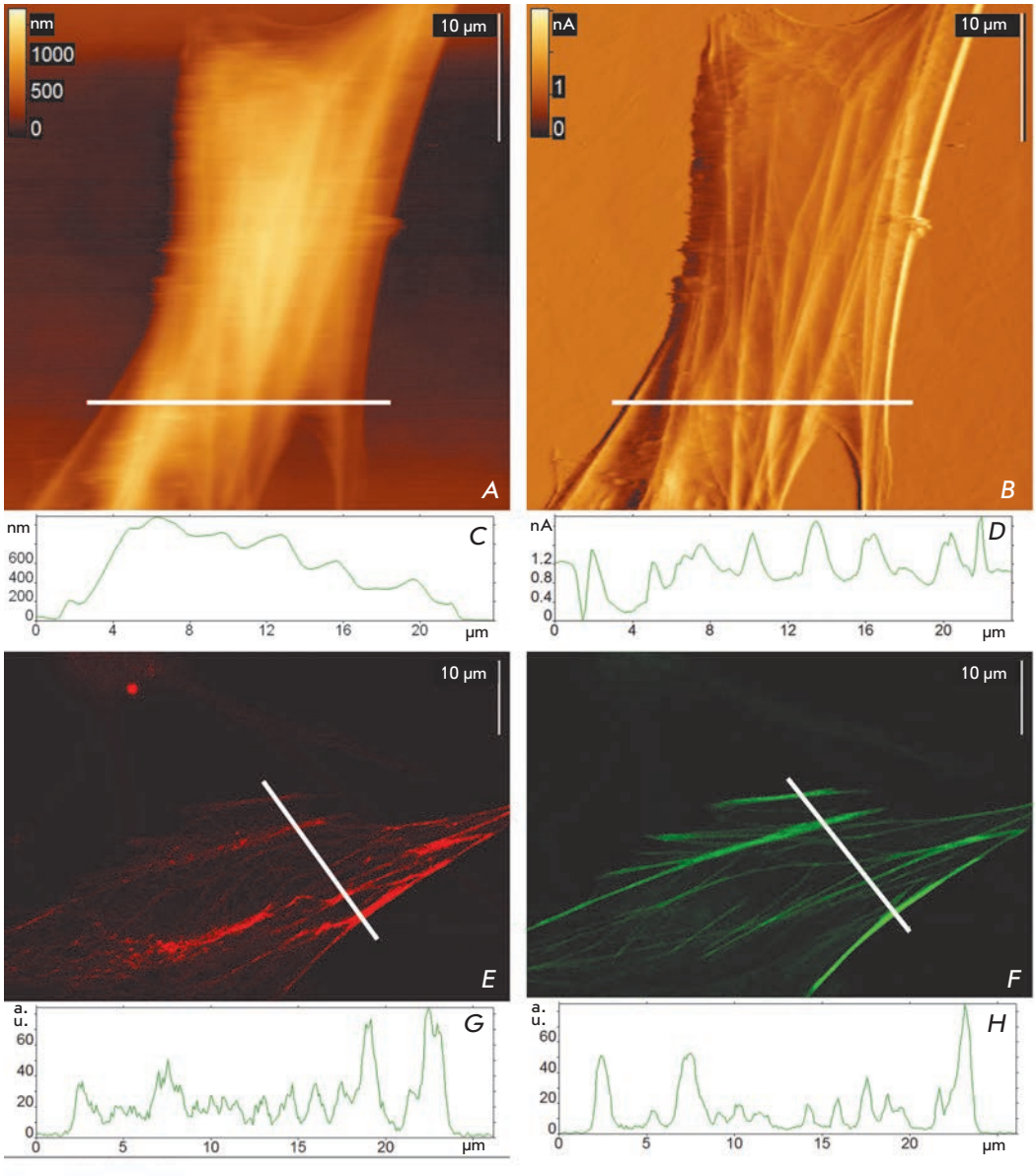

Fig. 1. Visualization of the astrocyte cytoskeleton with AFM and confocal microscopy. Typical images are presented. *A* – the topographical image of the living astrocyte in growth medium. *B* – the corresponding contact error image. *C* – the height profile of the astrocyte measured with AFM along the white line on the topographical image. *D* – the contact error profile measured along the same line. *E* – immunocytochemical staining of α-tubulin microtubules (DM1A + Alexa594). *F* – staining of actin filaments with fluorescent phalloidin. *G,H* – profiles of the fluorescence intensity measured along the white lines on corresponding fluorescent images.

RESULTS AND DISCUSSION

Visualization of astrocyte cytoskeleton using confocal and atomic force microscopy

Studying living cells with AFM is a technically and methodically complex task, since living cells are very soft and thus are easily deformed by the cantilever; they require special conditions to keep viability and must be strongly bound to the substrate [10]. Accurate selection of the sample preparation method and elaborate adjustment of the scanning parameters are necessary to obtain reproducible results.

Well-adhered cells cultured for 10 days were selected for scanning. The topographic images of living astrocytes obtained in contact mode show that the cells have an uneven surface with extended (fibrillar) structures (*Fig. 1A*). In contact mode, the cantilever pushes down the membrane and makes the submembrane cytoskeleton visible. It is most clearly observed on the feedback error signal images (*Fig. 1B*), which show the cantilever deflection in each point. The fibrillar structures are indiscernible in semi-contact mode. A similar result was obtained in the studies [8, 25].

The most clearly expressed and rigid intracellular structures are the actin and the microtubule networks [26]. We supposed that the structure of one or both of these networks could be visualized by scanning living astrocytes in contact mode in liquid.

To confirm this assumption, we compared the images obtained by AFM with those obtained by confo-

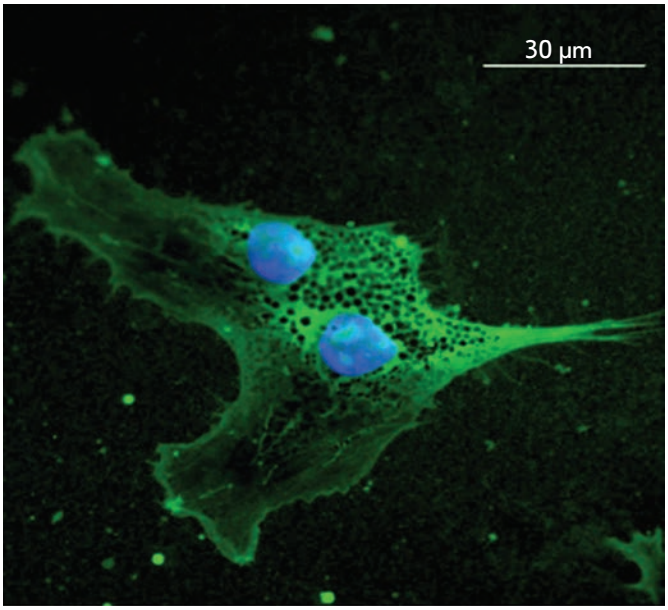

Fig. 2. Immunocytochemical staining of a glial fibrillary acidic protein in the astrocytes of a DRG culture obtained from a chicken embryo. Green colour – Anti-GFAP + Alexa546, dark blue – nuclei stained with DAPI.

cal microscopy upon immunofluorescence staining of astrocytes for α-tubulin and F-actin (*Figs. 1E,F*). The actin cytoskeleton, which is visible upon staining for F-actin, consists of long parallel fibrils (*Fig. 1F*). Staining for α-tubulin (*Fig. 1E*) provides the image showing the arrangement of microtubules in an astrocyte, which form a complex network. A similar network can also be seen on a topography image of a living astrocyte (*Figs. 1A,B*).

Intermediate filaments, which consist of GFAP in astrocytes, either do not form regular fibrillar structures in this culture or are destroyed upon immobilization (*Fig. 2*). Based on the comparison of the obtained images and on the basis of the published data [13, 27], we conclude that, unlike actin and microtubules, intermediate filaments in this case cannot be visualized by AFM.

The fluorescence intensity profiles were measured along the lines selected on the confocal microscopy images (*Fig. 1G,H*). When calculating the profile, the signal is averaged over several lines adjacent to the selected one. Thus, the presence of clearly discernible peaks on the profiles indicates the existence of extensive intracellular fibrils. Since fibrillar structures were detected in all three experiments (*Figs. 1A,E,F*), it cannot be claimed that the filaments observed by AFM in contact mode are necessarily microtubules or actin filaments. It is possible that both systems contribute to the formation of the surface topography (*Fig. 1A*); however, a number of researchers [13, 27] believe that it is actin cytoskeleton that plays the determining role.

It should also be noted that the peak width does not correspond to the diameter of an individual microtubule or actin filament in any of the measured profiles. It is well known [5] that microtubules are extensive α- and β- tubulin copolymers, 10 nm in diameter, whereas the diameter of an actin filament is 7–8 nm. Therefore, the visible structures are bundles of cytoskeleton components. Despite the complexity related to a clear differentiation of various cytoskeleton networks, its visualization by AFM has some advantage over immunocytochemical staining, since the AFM measurements can be performed on living cells in the culture medium.

Thus, the astrocytes of an organotypic culture of dorsal root ganglia obtained from a chicken embryo cultivated on a gelatinous substrate are well adhered, do not shift during scanning, and possess a high level of viability. The gelatinous substrate can efficiently substitute the substrates made of polyornithine/laminine, collagen, etc., which are more expensive and require rather complicated preparations [28].

Force spectroscopy and measurement of the local Young's modulus of living astrocytes

To get more information about the cytoskeleton, we measured the local Young's modulus of the living astrocytes from the force spectroscopy data. The force curves were recorded in the points located along the selected lines (10–20 points per line) or on the grid (from 4 × 4 to 7 × 7 points). Measurements were carried out using two cantilevers (their rigidity values differed by an order of magnitude and were equal to $k_1 = 0.02$ N/m and $k_2 = 0.18$ N/m) in order to demonstrate that the method chosen to calculate the Young's modulus is valid. The values of the Young's modulus of two or three cells were measured using each cantilever. The obtained histograms matched well (*Fig. 3*), and so did the average values of the Young's modulus $E_1 = 2.2 \pm 1.6$ kPa and $E_2 = 2.1 \pm 1.6$ kPa. This proves that the performed measurements are valid. The Young's modulus values determined on living astrocytes fall into a wide range (0.36–9.6 kPa), which is typical of eukaryotic cells. It is known that the Young's modulus values vary from 0.02 to 400 kPa in different eukaryotic cells [14] (the range is from 1 to 40 kPa for astrocytes obtained from rat cerebrum [13]). It is also known that the average Young's modulus of culture-dissociated DRG neurons adhered on polyornithine/laminin [29] is equal to 60 kPa. This fact correlates with the data [11, 30] that the astrocytes are softer than the neurons.

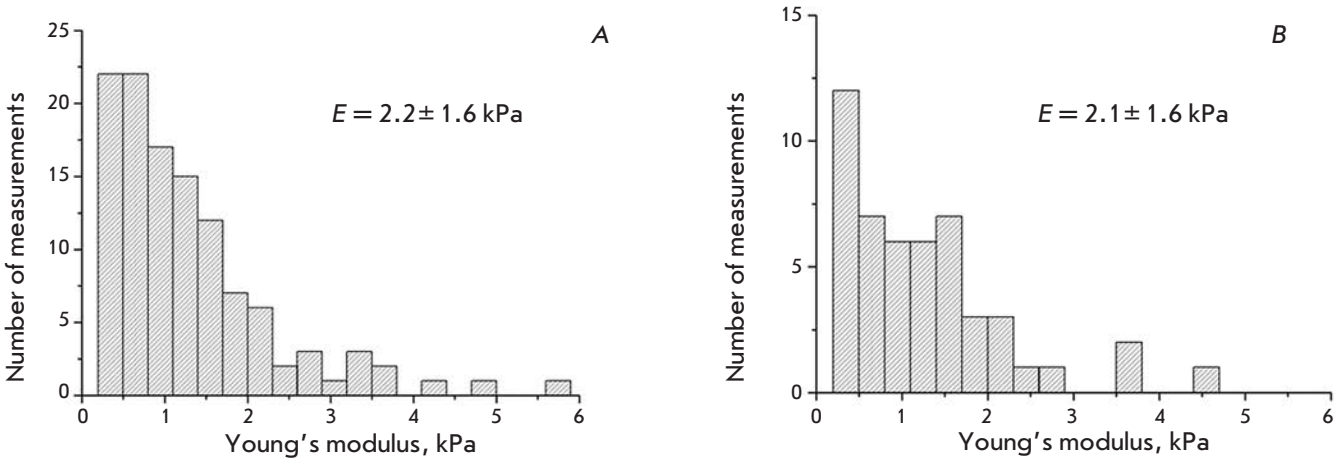

Fig. 3. Histograms of the astrocyte Young's modulus. *A* – obtained with long cantilever PNP-DB, k = 0.02 N/m. *B* – obtained with short cantilever PNP-DB, k = 0.18 N/m.

Mapping of the Young's modulus was also performed; the force curves were recorded in the points located on the grid nodes (*Fig. 4*). On the elasticity map, the lighter squares correspond to the areas with higher rigidity, whereas the darker squares correspond to the areas with lower rigidity (*Fig. 4B*). The force curves are also shown in different points (*Fig. 4C,D,E*). The curve has an abrupt slope above the substrate; above the edge of the cell, the curve is smooth until the cantilever interacts with the substrate. The curves are smooth above the nucleus and more abrupt above the cytoskeleton fibrils. When the force curves along the chosen line were recorded, it was observed that the curve shape and the Young's modulus depended on the presence of the cytoskeleton below the membrane. If there were elements of the cytoskeleton at the reference points (they could be seen on the topographic images), the calculated Young's modulus was higher (*Fig. 5*), which supports the data [13]. It should be mentioned that when a force curve is recorded, the Young's modulus is averaged over the size of the contact area between the cantilever tip and the cell surface. The size of the contact area depends on the probe geometry and indentation depth; in this experiment, it was approximately equal to 700 × 700 nm [31]. This fact can be accounted for by the scattering in the values of the Young's modulus measured above the cytoskeleton elements. Moreover, the fibrils could correspond to the bundles of cytoskeleton filaments of different densities, which impacts the local rigidity. It is obvious from the diagrams of the Young's modulus values (*Fig. 3*) that the majority of points fall into the regions of the cell surface where there are no cytoskeleton elements.

CONCLUSIONS

The obtained data demonstrate that the morphology of astrocytes in an organotypic culture of chicken embryo DRG grown on a gelatinous substrate can be successfully studied by AFM. The cells prepared in this manner are well-adhered, viable, and do not shift substantially during scanning, which makes it possible to use gelatin as an inexpensive and reliable substrate for this culture. The high resolution of the AFM method allows one to observe the cytoskeleton arrangement of a living cell in the culture medium. Unlike confocal microscopy, AFM does not provide information to determine which of the cytoskeleton networks is observed. However, AFM is promising for the study of the cytoskeleton organization in experiments on living cells. Moreover, since the local Young's modulus of a cell is considerably higher at the sites of cytoskeleton fibrils location, force spectroscopy allows one to determine cytoskeleton integrity and rearrangement upon damage. The study of the changes in the cytoskeleton integrity of neuronal cells upon neurodegenerative conditions appears to be a prospective application of AFM. When studying cytoskeleton degradation (one of the key processes in the development of neurodegeneration [32]), force spectroscopy will facilitate a quick, non-invasive and accurate determination of the Young's modulus of living neuronal cells. ●

The present study was supported by the Federal Target-Oriented Program "Scientific and Scientific-Pedagogical Personnel of Innovative Russia for 2009–2013".

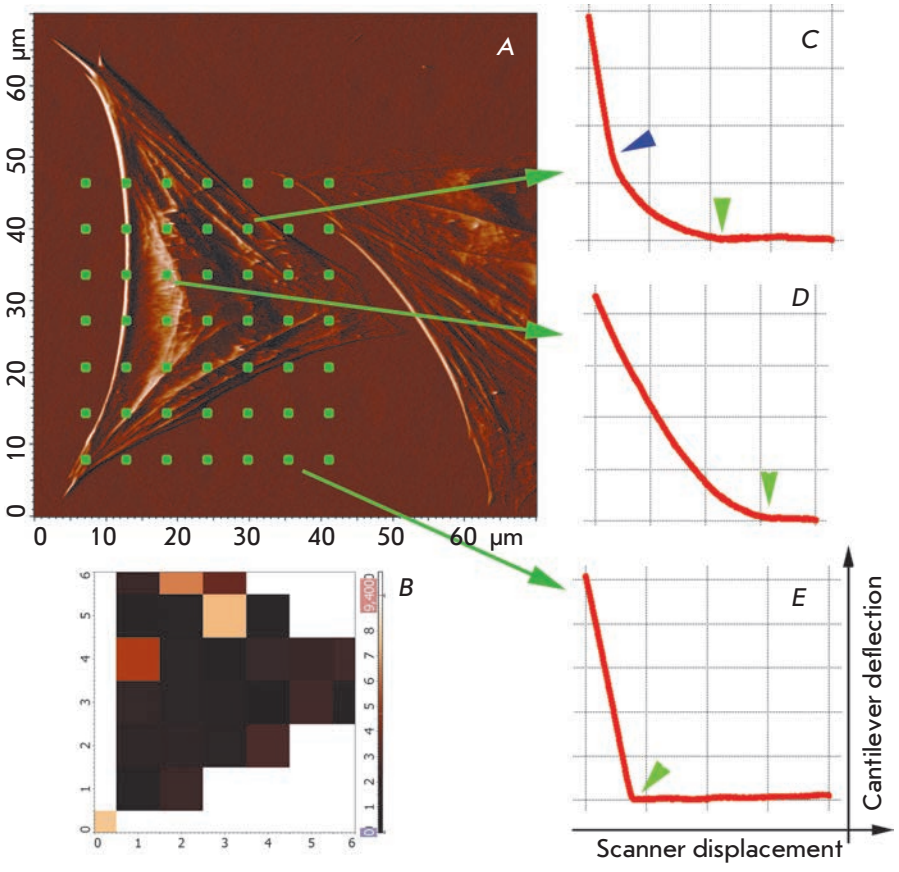

Fig. 4. Mapping the local Young's modulus of the astrocyte. *A* – the deflection image of the living astrocyte and a grid of points where the force curves were obtained. *B* – the map of the local Young's modulus in the grid nodes. The colour scale is in kPa, lighter squares correspond to stiffer areas. *C* – the force curve obtained in a point above the cell edge, the upper part of the curve coincides with the curve obtained on the substrate (E). Green triangular pointers mark the contact point, and blue triangular pointer marks the point where the cantilever touches the substrate. *D* – the force curve obtained in a point above the cell nucleus. The range of the scanner displacement on all curves was 2 μm.

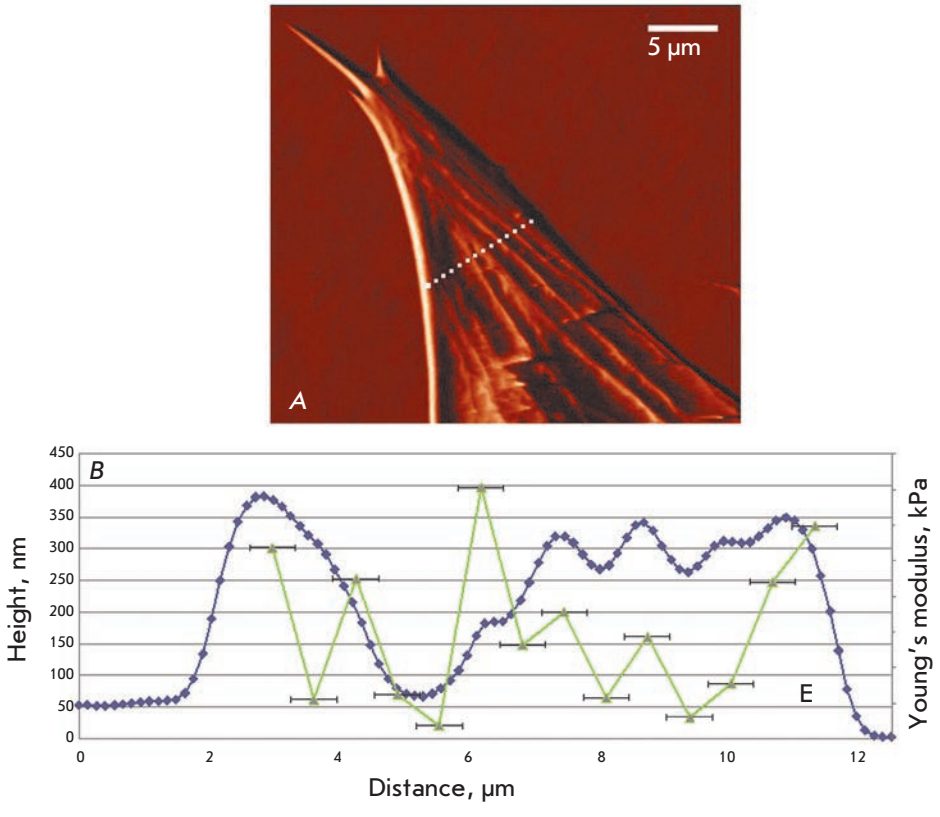

Fig. 5. Mapping the local Young's modulus of the astrocyte. *A* – the image of the astrocyte and the line along which the force curves (14 points) were obtained. *B* – the height profile along the section line (the dark blue curve) and the values of the local Young's modulus (the green points) measured in the corresponding points. Horizontal error bars show the size of the contact area. In the areas where the cytoskeleton fibers are located (local maxima on the dark blue curve), the local Young's modulus increases.

REFERENCES

1. Montgomery D. // Vet. Pathol. Online. 1994. V. 31. P. 145–167.
2. Rodriguez J., Olabarria M., Chvatal A., Verkhratsky A. // Cell Death Differ. 2008. V. 16. P. 378–385.
3. Goczalik I., Ulbricht E., Hollborn M., Raap M., Uhlmann S., Weick M., Pannicke T., Wiedemann P., Bringmann A., Reichenbach A., et al. // Investig. Ophthalmol. Vis. Sci. 2008. V. 49. P. 4578–4589.
4. Maragakis N.J., Rothstein J.D. // Nat. Clin. Pract. Neurol. 2006. V. 2. P. 679–689.
5. Dent E.W., Gertler F.B. // Neuron. 2003. V. 40. P. 209–227.
6. Engel A., Muller D.J. // Nat. Struct. Mol. Biol. 2000. V. 7. P. 715–718.
7. Graham H.K., Hodson N.W., Hoyland J.A., Millward-Sadler S.J., Garrod D., Scothern A., Griffiths C.E.M., Watson R.E.B., Cox T.R., Erler J.T. // Matrix Biol. 2010. V. 29. P. 254–260.
8. Parpura V., Haydon P.G., Henderson E. // J. Cell Sci. 1993. V. 104. P. 427–432.
9. Rotsch C., Radmacher M. // Biophys. J. 2000. V. 78. P. 520–535.
10. Efremov Yu.M., Bagrov D.V., Dubrovinb E.V., Shaitan K.V., Yaminskii I.V. // Biofiz. 2011. V. 56. P. 288-303.
11. Lu Y.B., Franze K., Seifert G., Steinhäuser C., Kirchhoff F., Wolburg H., Guck J., Janmey P., Wei E., Käs J., et al. // Proc. Natl. Acad. Sci. USA. 2006. V. 103. P. 17759–17764.
12. Butt H.J., Cappella B., Kappl M. // Surf. Sci. Rep. 2005. V. 59. P. 1–152.
13. Yamane Y., Shiga H., Haga H., Kawabata K., Abe K., Ito E. // J. Electron Microsc. 2000. V. 49. P. 463–471.
14. Kuznetsova T.G., Starodubtseva M.N., Yegorenkov N.I., Chizhikc S.A., Zhdanov R.I. // Micron. 2007. V. 38. P. 824–833.
15. Kirmizis D., Logothetidis S. // Int. J. Nanomed. 2010. V. 5. P. 137–145.
16. Moore K., Macsween M., Shoichet M. // Tissue Eng. 2006. V. 12. P. 267–278.
17. Cramer L., Desai A. // Fluorescence Procedures for the Actin and Tubulin Cytoskeleton in Fixed Cells. Protocol at http://mitchison.med.harvard.edu/protocols/gen1.html.
18. Braet F., Wisse E. // Meth. Mol. Biol. 2004. V. 242. P. 201–217.
19. Santacroce M., Orsini F., Perego C., Lenardi C., Castagna M., Mari S.A., Sacchi V.F., Poletti G. // J. Microsc. 2006. V. 223. P. 57–65.
20. Costa K.D. // Meth. Mol. Biol. 2006. V. 319. P. 331–361.
21. Lebedev D.V., Chuklanov A.P., Buharev A.A., Drujinina O.S. // Tech. Phys. Let. 2009. V. 35. P. 54–61.
22. Burnham N., Chen X., Hodges C., Matei G.A., Thoreson E.J., Roberts C.J., Davies M.C., Tendler S.J.B. // Nanotechnol. 2003. V. 14. P. 1–6.
23. Sader J.E., Chon J.W.M., Mulvaney P. // Rev. Sci. Instrum. 1999. V. 70. P. 3967–3970.
24. Sneddon I.N. // Int. J. Eng. Sci. 1965. V. 3. P. 47–57.
25. McNally H.A., Borgens R.B. // J. Neurocytol. 2004. V. 33. P. 251–258.
26. Yamada K.M., Spooner B.S., Wessells N.K. // Proc. Natl. Acad. Sci. USA. 1970. V. 66. P. 1206–1212.
27. Yamane Y., Hatakeyama D., Tojima T., Kawabata K., Ushiki T., Ogura S., Abe K., Ito E. // Jpn. J. Appi. Phys. 1998. V. 37. P. 3849–3854.
28. Firouzi M., Sabouni F., Ziaee A.A., Taghikhani M. // Iran. Biomed. J. 2004. V. 8. P. 101–105.
29. Mustata M., Ritchie K., McNally H.A. // J. Neurosci. Meth. 2010. V. 186. P. 35–41.
30. Franze K., Reichenbach A., Kas J. // Mechanosensitivity of the Nervous System/ Ed. Kamkin A., Kiseleva I. Dordrecht: Springer Netherlands; 2009. V. 2. P. 173-213.
31. Braet F., Rotsch C., Wisse E., Radmacher M. // Appl. Phys. A: Materials Sci. & Processing. 1998. V. 66. P. 575–578.
32. George E.B., Glass J.D., Griffin J.W. // J. Neurosci. 1995. V. 15. P. 6445–6452.

An Efficient Method for the Delivery of the Interleukin-2 Gene to Human Hematopoietic Cells using the Fiber-Modified Recombinant Adenovirus

V. N. Rogozhin[1,2]*, D. Yu. Logunov[1], D. V. Shchebliakov[1], M. M. Shmarov[1], E. E. Khodunova[3], I. V. Galtseva[3], R. V. Belousova[2], B. S. Naroditsky[1], A. L. Gintsburg[1]

[1] Gamaleya Research Institute of Epidemiology and Microbiology, Ministry of Health and Social Development of the Russian Federation

[2] Moscow state academy of veterinary medicine and biotechnology named K.I. Skryabin

[3] National Research Center for Hematology, Ministry of Health and Social Development of the Russian Federation

*E-mail: Rogojin_V@mail.ru

Received 01.07.2011

ABSTRACT **Recombinant human adenovirus serotype 5 (Ad5/35F-IL2) with modified fibres containing the C-terminal domain fiber-knob of human adenovirus serotype 35, carrying the gene of recombinant human IL-2, has been designed. As a result of the fiber modification, the adenovirus can efficiently deliver the genetic information to bone marrow leukocytes and the tumor blood cells KG-1A (human myeloblastic leukemia cells) and U937 (human histiocytic lymphoma cells), which are normally resistant to Ad5 infection. The flow cytometry data reveal that the modified Ad5/35F penetrates into a population of monocytes, granulocytes, and blast cells of human bone marrow. The expression of interleukin-2 in CAR-negative bone marrow leukocytes (3682.52 ± 134.21 pg/ml) and the cell lines KG-1A (748.3 ± 32.8 pg/ml) and U937 (421.5 ± 59.4 pg/ml) transduced with adenovirus Ad5/35F-IL2 is demonstrated. The fiber-modified adenovirus can be used as a vector for the efficient gene delivery of interleukin-2 to human normal and tumor hematopoietic cells.**

KEYWORDS **adenovial vector; pseudotyping; interleukin-2; CD46; capsid modification.**

ABBREVIATIONS **Ad – human adenovirus; Ad5 – Ad serotype 5; Ad35 – Ad serotype 35; Ad5/35F – fiber-modified recombinant Ad5; UV – ultraviolet radiation; RBM – red bone marrow; IL2 – human interleukin-2; CAR – coxsackievirus and adenovirus receptor; aa – amino acid residue; pfu – plaque-forming unit.**

INTRODUCTION

Among the vectors most commonly used to deliver genes to human and mammal cells are vectors based on the human adenovirus serotype 5 (Ad5). The advantages of these vectors are numerous; they are capable of transducing both dividing and non-dividing cells [1, 2]; the adenoviral DNA is not incorporated into the host cell genome and retains its extrachromosomal form; adenoviruses can be produced at a titer of over 10^{10} pfu/ml, which enables them to be used as living recombinant vaccines; and they ensure a high expression level of the target gene in a target cell. One of the drawbacks of Ad5-based vectors is their low transducing activity with respect to CAR-deficient and CAR-negative cells. Among those, hematopoeitic cells occupy a significant place. This problem derives from the fact that binding of the adenovirus capsid protein (fiber) and the membrane cell receptor CAR (coxsakievirus-adenovirus receptor) is necessary for the primary interaction between Ad5 and a cell. Therefore, a deficiency or the total absence of these receptors on the cell surface is a factor that limits efficient gene delivery using Ad-5 based adenovectors.

This problem can be overcome via the genetic modification of the adenovirus' fibers. The modification strategy consists in pseudotyping, i.e., the substitution of fibers or their individual domains for the fibers or similar domains of the adenoviruses of other serotypes, which use receptors other than CAR receptors for binding to the cell surface. This approach was first used in 1996 by Gall *et al*; they constructed the Ad5 expressing Ad7 fiber and showed the change in vector tropism [3]. Krasnykh *et al.* [4] and Stevenson *et al.* [5] described the production of chimeric Ad5 vectors containing the N-terminal and central domains of Ad5 fiber and the C-terminal domain of Ad3 fiber.

Substitution of Ad5 fiber for Ad35 fiber (Ad5/35F) was proposed for the efficient transduction of hematopoietic cells [6]. The modification is made possible by the fact that Ad5 and Ad35 use different receptors in order to bind to the cell surface. It is CAR for Ad5 and the CD46 molecule for Ad35 [7]; a high expression level of CD46 was detected on the surface of hematopoietic cells. These chimeric adenoviruses can efficiently transduce human hematopoietic [6] and dendritic cells [8].

The described modification of the Ad5 fiber was used to construct a vector capable of efficiently penetrating CAR-deficient hematopoietic cells, with the purpose of delivering the human interleukin-2 gene. The construction of this vector broadens the potential of using vectors based on human capsid-modified adenoviruses, in particular for genetic therapy in the treatment of leukemia of different etiologies.

EXPERIMENTAL

Plasmid vectors

The pZ35 plasmid containing the Ad5 genome with the Ad35 fiber knob domain and shuttle vector pShuttle-CMV-IL2 containing the human interleukin-2 gene regulated by the human citomegalovirus promoter were previously constructed in the Gamaleya Research Institute of Epidemiology and Microbiology [9]; pShuttle-CMV-EGFP was purchased from Stratagene (United States).

Viruses and bacterial strains

Recombinant Ad5 expressing a green fluorescent protein reporter gene (Ad5-EGFP), recombinant Ad5 expressing the human interleukin-2 gene (Ad5-IL2) obtained earlier in the Gamaleya Research Institute of Epidemiology and Microbiology [9, 10], Eshcerichia coli strains DH5α and BJ5183.

Cell lines

In this study, the following transplantable human cell lines were used: HEK-293 (embryonic kidney cells transformed by the E1 region of the Ad5 genome), KG-1A (myeloid leukemia cells), U937 (monocytic leukemia cells), and the primary leukocyte culture from red bone marrow (RBM) obtained from a healthy volunteer.

Obtainment of recombinant adenoviruses

Plasmid constructions carrying the full size adenovirus genome with the modified fiber (Ad5/35F) and the target gene within the genome were obtained via homologous recombination in *E. coli* BJ5183. To this end, *E. coli* cells were co-transformed with a plasmid pair (pZ35 and pShuttle-CMV-EGFP) in order to obtain the plasmid with a full-size genome Ad5/35F and with green fluorescent protein gene (pAd5/35F-EGFP), and pZ35 and pShuttle-CMV-IL2 to obtain the plasmid with full-size genome of Ad5/35F with the human interleukin-2 gene (pAd5/35F-IL2). Prior to the transformation, pZ35 and shuttle vectors (pShuttle-CMV-EGFP and pShuttle-CMV-IL2) were linearized by PacI and PmeI, respectively. In the shuttle vectors, the target genes (*EGFP* and *IL2*) were regulated by the human cytomegalovirus promoter. Recombinant clones were analyzed using the polymerase chain reaction (PCR) and restriction assay. Recombinant modified vectors Ad5/35F-EGFP and Ad5/35F-IL2 were obtained via the lipofection of plasmid constructions (pAd5/35F-EGFP and pAd5/35F-IL2) into the HEK-293 line cells using Metafectene Pro agent (Biontex, Germany) according to the enclosed protocol. Recombinant adenoviruses were accumulated in HEK-293 cells and detected on the basis of the development of the characteristic cytopathic effect. The presence of the target genes and fiber modification was proven by PCR and restriction assay. Recombinant modified adenoviruses were purified and concentrated by cesium chloride density gradient ultracentrifugation of the lysates of infected cells. The concentration of adenovirus in the purified specimen was determined spectrophotometrically ($\lambda = 260$ nm) using the conversion coefficient 1 OD = 1.12×10^{12} viral particles/ml. The titer of adenoviral specimens was determined by plaque formation assay on HEK-293 cells.

Determination of the physical stability of modified adenoviruses

The physical stability of modified adenoviruses was assessed using the Ad5/35F-EGFP model by determining its thermal stability, according to the procedure described earlier [11].

Transduction of KG-1A and U937 human tumor blood cells with recombinant adenoviruses

KG-1A and U937 cells were seeded into 48-well plates at a concentration of 5×10^4 cells per well. The cells from the leukocytic fraction of human RBM obtained from a healthy donor were extracted by double centrifugation in the density gradient of the Histopaque-1083 commercial preparation (Sigma-Aldrich, Germany) according to the enclosed protocol and seeded into 48-well plates at a concentration of 5×10^4 cells per well. On the following day, the cells were infected with the recombinant modified adenoviruses Ad5/35F-EGFP and Ad5/35F-IL2 and the control adenoviruses with fibers of the wild-type virus and analogous target genes *Ad5-EGFP* and *Ad5-IL2*, at doses of 5×10^3, 10^4, and 5×10^4 viral particles per cell.

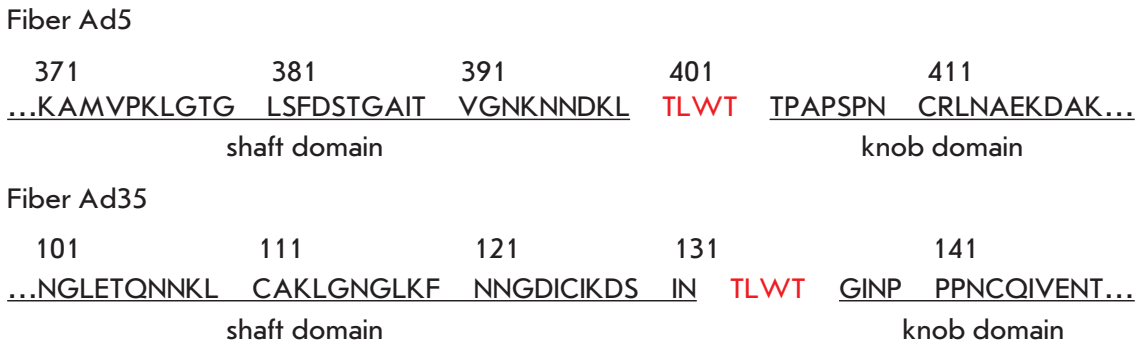

Fig. 1. Amino acid sequences of the C-terminal regions of fibers of human avenoviruses serotypes 5 and 35.

Analysis of the efficiency of penetration of adenoviruses into the cells and the expression level of the target gene

The efficiency of the penetration of the recombinant adenoviruses Ad5-EGFP and Ad/35F-EGFP into cells was assessed 48 h post infection via fluorescent microscopy of the infected cells using the EGFP fluorescence intensity.

The expression level of the human IL2 gene in the cells infected with Ad5-IL2 and Ad5/35F-IL2 was assessed 48 h post infection by determining the IL2 concentration in the culture medium of the infected cells by flow cytofluorimetry using the FlowCytomix Bender Medsystems kit (Austria) according to the enclosed protocol. IL2 concentration in the specimens was calculated using the FlowCytomix Pro 2.2 software.

Determination of leukocyte populations of human RBM which are efficiently transduced by the modified adenovirus

The cells were infected with Ad5/35F-EGFP at a dose of 10^4 viral particles per cell, in order to determine the leukocyte populations of human RBM into which the modified adenovirus is capable of penetrating. Leukocyte populations in RBM, namely monocytes, granulocytes, T- and B-lymphocytes, and blast cells, were determined 24 h post infection via flow cytofluorimetry, using fluorescently labelled antibodies against CD45 (common leukocyte antigen). The virus-infected cells were detected by EGFP fluorescence and correlated with the corresponding leukocyte population.

RESULTS AND DISCUSSION

Obtaining fiber-modified human recombinant adenoviruses serotype 5

The first strategy for obtaining the recombinant adenovirus Ad5/35F described by Shayakhmetov *et al.* [6] consisted in the substitution of the central (shaft) and the C-terminal (knob) Ad5 fiber domains for the analogous domains of the Ad35 fiber. In order to construct the modified virus, we used the new technology based on a single substitution of the C-terminal knob domain of the Ad5 fiber for the knob fibre domain [7]. The C-terminal knob and central shaft domains of the adenovirus fiber are linked by a short amino acid sequence, ensuring the relative mobility of the fiber knob domain. Most human adenoviruses contain a conservative threonine–leucine–tryptophan–threonine (TLWT) sequence in the mobile region between these domains [12]. The N-terminus of the knob domain of the Ad5 and Ad35 fibers also contains this sequence (*Fig. 1*).

Thus, in order to broaden the tropism of the virus relative to CD46-positive cells, and to achieve proper linking of the shaft and knob fibre domains, we substituted the knob domain of the Ad5 fiber (178 aa) for the knob domain of the Ad35 fiber (187 aa) after the TLWT sequence (*Fig. 2*).

Characterization of recombinant modified adenoviruses Ad5/35F

Recombinant modified adenoviruses Ad5/35-EGFP and Ad5/35F-IL2 were characterized according to the

Concentration and titer of recombinant adenoviruses

Virus	Concentration, viral particles/ml	Titer, pfu/ml
Ad5-EGFP	$(4.82 \pm 0.17) \times 10^{12}$	$(3.80 \pm 0.83) \times 10^{10}$
Ad5/35F-EGFP	$(2.54 \pm 0.21) \times 10^{12}$	$(1.22 \pm 0.34) \times 10^{10}$
Ad5-IL2	$(6.97 \pm 0.19) \times 10^{12}$	$(5.85 \pm 0.76) \times 10^{10}$
Ad5/35F-IL2	$(4.23 \pm 0.17) \times 10^{12}$	$(2.12 \pm 0.26) \times 10^{10}$

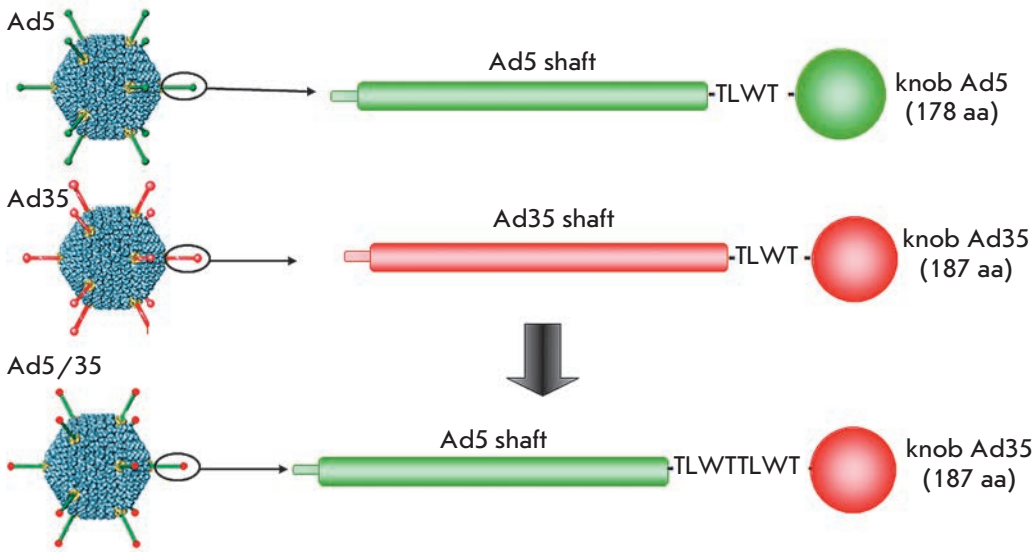

Fig. 2. Scheme for modification of fibers of human adenovirus serotype 5 by substitution of its C-terminal knob domain for the same domain of the fiber of human adenovirus serotype 35.

following parameters: the concentration of viral particles in a sample, titer of the adenoviral sample (*Table*), and the physical stability of adenoviruses upon heating (*Fig. 3*). Unmodified Ad5 samples containing expression cassettes with EGFP (Ad5-EGFP) and human IL2 (Ad5-IL2) genes were used as a control. As can be seen from the *Table*, concentrations and titers of the samples of modified adenoviruses are comparable with the same parameters of the control samples of unmodified adenoviruses. Thus, the modification of the Ad5/35F adenovirus fiber had no considerable effect on its reproduction.

Since the modification of the adenovirus fibers introduced by us could have some impact on the physical stability of adenoviruses, we assessed the stability of Ad5/35F-EGFP upon heating to +37 and +42°C during various time periods as compared with that of unmodified Ad5-EGFP. The thermal stability of Ad5/35F-EGFP virions was shown to be comparable with that of the unmodified Ad5-EGFP adenovirus. Heating the adenovirus samples for 30 min at +37°C did not result in a significant decrease in their infectivity (*Fig. 3A*). The incubation of adenoviruses at +42°C led to the inactivation of adenovirions in both samples: by 11–19% after heating for 15 min and by 23–45% after heating for 30 min (*Fig. 3B*).

The data on the thermal stability of the Ad5/35F-EGFP adenovirus attest to the fact that this modifica-

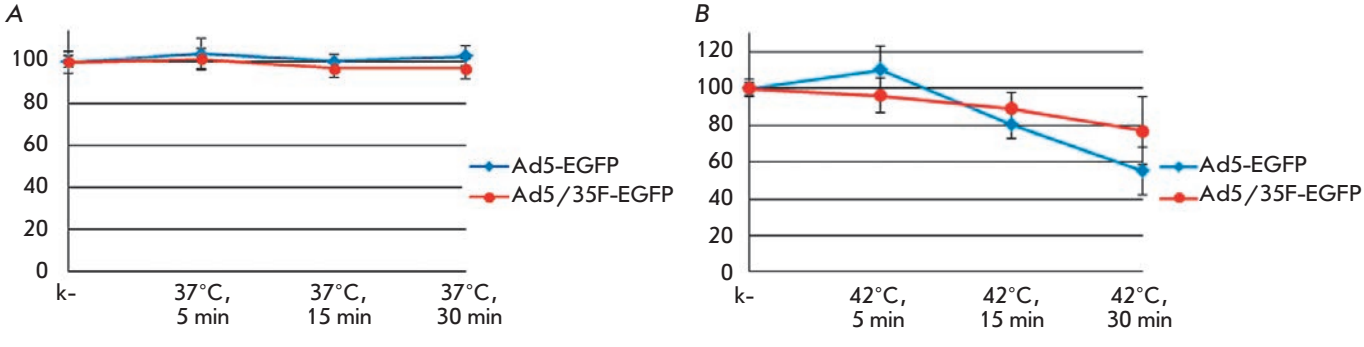

Fig. 3. Thermal stability of fiber-modified adenovirions (Ad5/35F-EGFP) as compared with the unmodified adenovirions (Ad5-EGFP). *A* – Heating of adenovirus samples at +37°C for 5, 15, and 30 min. B – Heating of adenovirus samples at +42°C for 5, 15, and 30 min. Along the X axis, the heating conditions; along the Y axis, the relative efficiency of adenovirus penetration into HEK-293 cells assessed by EGFP fluorescence, %.

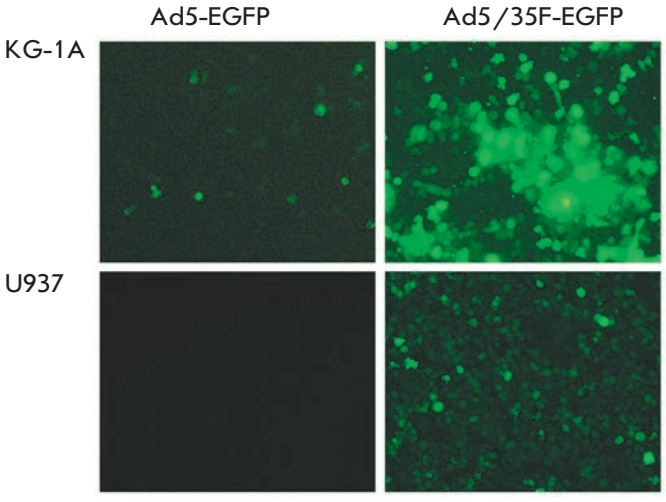

Fig. 4. Penetration efficiency of the modified Ad5/35-EGFP virus into KG-1A and U937 lines of human tumor blood cells 48 h after infection.

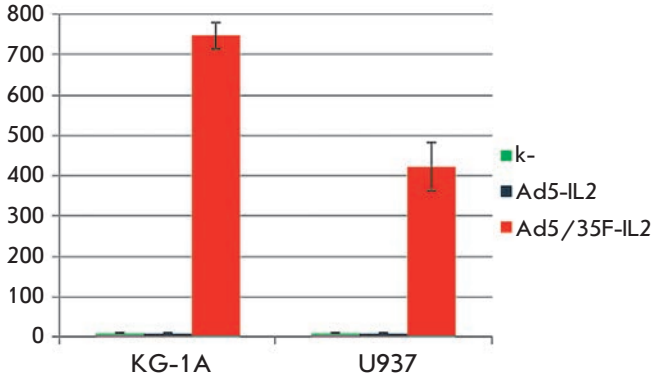

Fig. 5. Expression level of the human interleukin-2 gene in KG-1A and U937 lines of human tumor blood cells transduced with recombinant adenoviruses 48 h after infection. Along the X axis, interleukin-2 concentration in the culture medium of infected cells, pg/ml.

tion of adenovirus fibers has no considerable effect on its physical stability.

Assessment of the efficiency of the delivery of genetic information by Ad5/35F-EGFP and Ad5/35F-IL2 adenoviruses to human hematopoietic tumor cells (KG-1A and U937 cell lines)

We selected KG-1A lines (myeloid leukemia cells) and U937 (monocytic leukemia cells) with a low level of expression of the primary adenoviral receptor CAR [13] and high level of CD46 expression [14], in order to assess the efficiency of *in vitro* penetration of Ad5/35F-EGFP and Ad5/35F-IL2 into human blood tumor cells, and to determine the expression level of the target genes in the virus-transduced cells. The multiplicity of the infection was 5×10^3, 10^4, and 5×10^4 viral particles per cell. The efficiency of the penetration of Ad5/35F-EGFP into the cells was assessed according to the amount of cells expressing the reporter gene *EGFP* and fluorescing under UV irradiation ($\lambda = 395$ nm). It was demonstrated that as a result of fibre modification, the modified Ad5/35F-EGFP penetrated into U937 and KG-1A hematopoietic tumor cells more efficiently in comparison with the unmodified virus (*Fig. 4*). These results are consistent with the data obtained by other researchers who studied the efficiency of penetration of the modified Ad5/35F-EGFP virus into other lines of blood tumor cells [6] and into primary lymphoid and myeloid leukemia cells [15].

The efficiency of expression of the human interleukin-2 gene in the cell lines transduced with the recombinant modified Ad5/35-IL2 adenovirus turned out to be considerably higher than that in the cells transduced with unmodified Ad5-IL2 (*Fig. 5*). The highest concentration of IL2 was noted in the cultural medium of the KG-1A cell line (748.3 ± 32.8 pg/ml) infected with Ad5/35F-IL2. U937 cells transduced with the modified adenovirus expressed the *IL2* gene at a level of 421.5 ± 59.4 pg/ml. In the cells transduced with the unmodified Ad5-IL2 virus, trace amounts of IL2 were expressed.

These results are consistent with the data on the level of CAR and CD46 molecules, the primary receptors for Ad5 and Ad35 adhesion on the surface of the studied cell lines. Hematopoietic cells, including KG-1A and U937 cells, are known to be CAR-negative [13]. Therefore, it is quite understandable that the unmodified Ad5 virtually did not penetrate into these cells; expression of the target genes in them was detected at a trace level. Meanwhile, due to a high level of CD46 expression on the surface of KG-1A and U937 cells [14], the modified Ad5/35F had an enhanced ability to penetrate into these cells, which ensured a high expression level of the target genes in them.

Assessment of the efficiency in delivering the genetic information to normal leukocytes of human red bone marrow (RBM) by recombinant modified adenoviruses

The modified Ad5/35F adenovirus efficiently transduces CAR-negative tumor blood cells and ensures the expression of the target genes introduced into its genome in these cells. It was therefore decided to determine the efficiency in delivering the genetic information via ad-

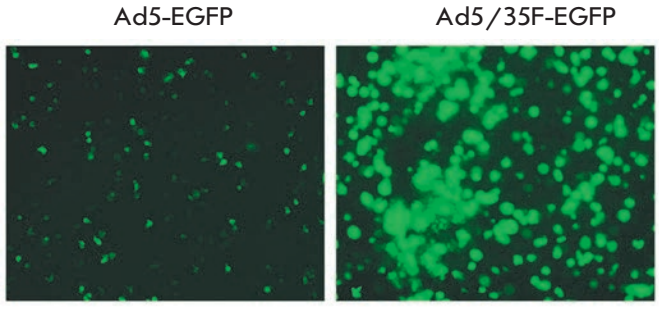

Fig. 6. Penetration efficiency of the modified Ad5/35-EGFP virus into leukocytes of human RBM 48 h after infection.

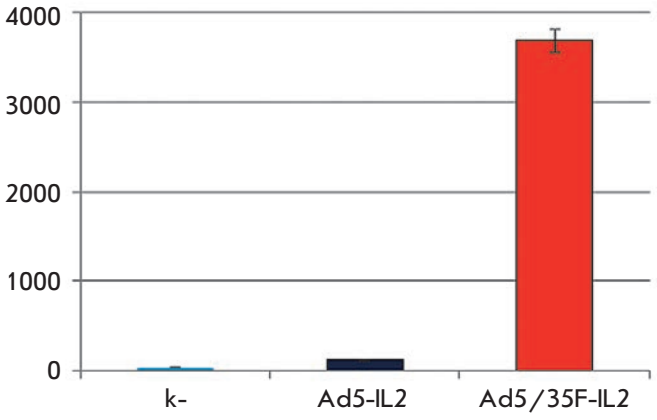

Fig. 7. The level of interleukin-2 expression in leukocytes of human RBM transduced with recombinant adenoviruses, 48 h after infection.

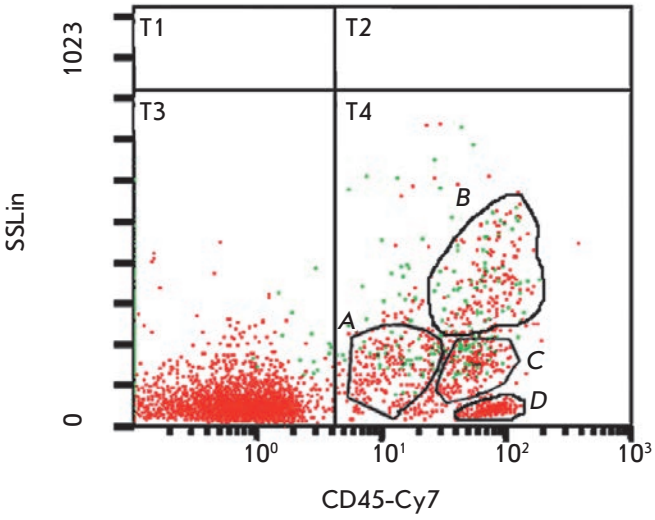

Fig. 8. Determination of leukocyte populations in the human RBM efficiently transduced by recombinant modified adenovirus Ad5/35F-EGFP. Adenovirus-infected cells (fluorescing) are shown in green. *A* – blast cells; *B* – granulocytes; *C* – monocytes; and *D* – lymphocytes.

enovectors (Ad5/35F-EGFP and Ad5/35F-IL2) to the cells of the leukocytic fraction of RBM obtained from a healthy blood donor. The reason for this interest is the potential of using the modified adenovirus as a vector for the efficient selective *ex vivo* delivery of genetic information to hematopoietic and immunocompetent human cells. The leukocytes extracted from a RBM sample taken from a healthy blood donor were transfected with modified (Ad5/35F-EGFP and Ad5/35-IL2) and unmodified (Ad5-EGFP and Ad5-IL2) adenovectors at different doses. As a result, the modified Ad5/35F-EGFP vector was shown to penetrate into RBM leukocytes more efficiently in comparison with Ad5-EGFP, which was indicated by the intense fluorescence of 80% of all cells resulting from the EGFP expression (*Fig. 6*). IL2 concentration upon cell transduction with vectors with the target *IL2* gene in the culture medium of cells infected with the modified Ad5/35-IL2 was equal to 3682.52 ± 134.21 pg/ml; approximately 30-fold higher than the IL2 concentration in the leukocyte culture medium transduced with the unmodified Ad5-IL2 (*Fig. 7*).

Taking into account the fact that the cells of the leukocyte fraction of the RBM contain a number of heterogeneous cell populations, we decided to determine the populations of leukocytes into which the modified adenovirus efficiently penetrates.

RBM leukocytes were infected with the modified Ad5/35F-EGFP at a dose of 5×10^4 viral particles per cell. The populations of cells efficiently transduced by the modified adenovirus were revealed 24 h after infection by flow cytofluorimetry using fluorescently labelled antibodies against the common leukocyte antigen CD45 according to the cell size, the expression level of CD45 antigen, and fluorescence of the infected cells resulting from the expression of the *EGFP* reporter gene (*Fig. 8*). As expected, Ad5/35F-EGFP easily penetrated into RBM monocytes (32.66% of EGFP-positive cells), which confirms the data obtained earlier [16], and transduced granulocytes (42.86% of EGFP-positive cells) and blast cells (27.24% of EGFP-positive cells), which was first demonstrated. Meanwhile, efficiency in penetration of the modified Ad5/35F-EGFP adenovirus in the subpopulation of T- and B-lymphocytes from human RBM was low (0.71% of EGFP-positive cells). The data on the efficient transduction of monocyte, granulocyte, and blast cell populations with the modified Ad5/35F-EGFP adenovirus are consistent with reports of a high level of CD46 expression in pop-

ulations of these cells [17]. However, notwithstanding the data on the level of transcription of the *CD46* gene in T- and B-lymphocytes which is comparable to that in cells of the myeloid differentiation branch [17, 18], the modified adenovirus did not efficiently penetrate into lymphocytes. This could be due to the specific regulation of *CD46* expression at the level of the protein.

CONCLUSIONS

A specific modification consisting in the substitution of the C-terminal knob domain of the Ad5 fiber for the analogous domain of the Ad35 fiber was used to obtain recombinant Ad5 containing the modified fiber and carrying the human *IL2* gene. A manifold increase in efficiency in the penetration of this vector into cells, as compared with the unmodified vector, was demonstrated on KG-1A and U937 line cultures of human tumor blood cells. A 30-fold increase in efficiency in the penetration of the modified vector in comparison with that for the unmodified vector was first demonstrated in experiments on the transduction of the primary leukocyte culture from RBM taken from a healthy donor, which ensures the expression of the human interleukin-2 gene in them. Along with the efficient transduction of RBM monocytes [16], the modified Ad5/35F was first shown to efficiently transduce granulocytes and blast cells of human RBM, while this vector does not penetrate into T- and B-lymphocyte subpopulations.

Based on the results obtained in this study, it can be concluded that the modified Ad5/35F-IL2 adenovirus obtained can be used as a vector for efficient delivery of the human interleukin-2 gene and for its application in the genetic therapy of different types of leukemia, as well as in the design of genetically engineered vaccines capable of efficiently delivering the antigen genes of different pathogens directly to the immunocompetent cells, including dendritic cells, which are professional antigen-presenting cells [19]. ●

This study was supported by the Ministry of Education and Science of the Russian Federation (Government Contract № 02.512.11.2320).

REFERENCES

1. Tang D.C., Jennelle R.S., Shi Z., Garver R.I., Carbone D.P., Loya F., Chang C.H., Curiel D.T. // Hum. Gene Ther. 1997. V. 8. № 17. P. 2117–2124.
2. Tang D.C., Johnston S.A., Carbone D.P. // Cancer Gene Ther. 1994. V. 1. № 1. P. 15–20.
3. Gall J., Kass-Eisler A., Leinwand L., Falck-Pedersen E. // J. Virol. 1996. V. 70. № 4. P. 2116–2123.
4. Krasnykh V.N., Mikheeva G.V., Douglas J.T., Curiel D.T. // J. Virol. 1996. V. 70. P. 6839–6846.
5. Stevenson S.C., Rollence M., Marshall-Neff J., McClelland A. // J. Virol. 1997. V. 71. № 6. P. 4782–4790.
6. Shayakhmetov D.M., Papayannopoulou T., Stamatoyannopoulos G., Lieber A. // J. Virol. 2000. V. 74. P. 2567–2583.
7. Zhang Y., Bergelson J.M. // J. Virol. 2005. V. 79. № 19. P. 12125–12131.
8. Melief C.J., Offringa R. // J. Immunol. 2001. V. 166. P. 5236–5244.
9. Shmarov M.M., Cherenova L.V., Shashkova E.V., Logunov D.Iu., Verkhovskaia L.V., Kapitonov A.V., Neugodova G.L., Doronin K.K., Naroditskiĭ B.S. // Mol. Gen. Mikrobiol. Virusol. 2002. V. 2. P. 30–35.
10. Logunov D.Y., Zubkova O.V., Karyagina-Zhulina A.S., Shuvalova E.A., Karpov A.P., Shmarov M.M., Tutykhina I.L., Alyapkina Y.S., Grezina N.M., Zinovieva N.A., Ernst L.K., Gintsburg A.L., Naroditsky B.S. // J. Virol. 2007. V. 81. № 18. P. 9641–9652.
11. Rogozhin V. N., Belousova R. V., Logunov D.Y., Shmarov M. M., Lunin V.G., Naroditsky B.S. // Vet. Meditsina. 2011. № 2. P. 10-13
12. Guardado-Calvo P., Llamas-Saiz A.L., Fox G.C., Langlois P., van Raaij M.J. // J. Gen. Virol. 2007. № 88. Pt 9. P. 2407–2416.
13. Sakurai F., Mizuguchi H., Yamaguchi T., Hayakawa T. // Mol. Ther. 2003. V. 8. № 5. P. 813–821.
14. Gaggar A., Shayakhmetov D.M., Liszewski M.K., Atkinson J.P., Lieber A. // J. Virol. 2005. V. 79. № 12. P. 7503–7513.
15. Nilsson M., Ljungberg J., Richter J., Kiefer T., Magnusson M., Lieber A., Widegren B., Karlsson S., Fan X. // J. Gene Med. 2004. V. 6. № 6. P. 631–641.
16. Segerman A., Lindman K., Mei Y.F., Allard A., Wadell G. // Virology. 2006. V. 349. № 1. P. 96–111.
17. Christmas S.E., de la Mata Espinosa C.T., Halliday D., Buxton C.A., Cummerson J.A., Johnson P.M. // Immunology. 2006. V. 119. № 4. P. 522–528.
18. Wang G., Liszewski M.K., Chan A.C., Atkinson J.P. // J. Immunol. 2000. V. 164. № 4. P. 1839–1846.
19. Wang H., Liu Y., Li Z., Tuve S., Stone D., Kalyushniy O., Shayakhmetov D., Verlinde C.L., Stehle T., McVey J., et al. // J. Virol. 2008. V. 82. № 21. P. 10567–10579.

GENERAL RULES

Actae Naturae publishes experimental articles and reviews, as well as articles on topical issues, short reviews, and reports on the subjects of basic and applied life sciences and biotechnology.

The journal is published by the Park Media publishing house in both Russian and English.

The journal *Acta Naturae* is on the list of the leading periodicals of the Higher Attestation Commission of the Russian Ministry of Education and Science

The editors of *Actae Naturae* ask of the authors that they follow certain guidelines listed below. Articles which fail to conform to these guidelines will be rejected without review. The editors will not consider articles whose results have already been published or are being considered by other publications.

The maximum length of a review, together with tables and references, cannot exceed 60,000 symbols (approximately 40 pages, A4 format, 1.5 spacing, Times New Roman font, size 12) and cannot contain more than 16 figures.

Experimental articles should not exceed 30,000 symbols (20 pages in A4 format, including tables and references). They should contain no more than ten figures. Lengthier articles can only be accepted with the preliminary consent of the editors.

A short report must include the study's rationale, experimental material, and conclusions. A short report should not exceed 12,000 symbols (8 pages in A4 format including no more than 12 references). It should contain no more than four figures.

The manuscript should be sent to the editors in electronic form: the text should be in Windows Microsoft Word 2003 format, and the figures should be in TIFF format with each image in a separate file. In a separate file there should be a translation in English of: the article's title, the names and initials of the authors, the full name of the scientific organization and its departmental affiliation, the abstract, the references, and figure captions.

MANUSCRIPT FORMATTING

The manuscript should be formatted in the following manner:

- Article title. Bold font. The title should not be too long or too short and must be informative. The title should not exceed 100 characters. It should reflect the major result, the essence, and uniqueness of the work, names and initials of the authors.
- The corresponding author, who will also be working with the proofs, should be marked with a footnote *.
- Full name of the scientific organization and its departmental affiliation. If there are two or more scientific organizations involved, they should be linked by digital superscripts with the authors' names. Abstract. The structure of the abstract should be very clear and must reflect the following: it should introduce the reader to the main issue and describe the experimental approach, the possibility of practical use, and the possibility of further research in the field. The average length of an abstract is 20 lines (1,500 characters).
- Keywords (3 – 6). These should include the field of research, methods, experimental subject, and the specifics of the work. List of abbreviations.
- INTRODUCTION
- EXPERIMENTAL PROCEDURES
- RESULTS AND DISCUSSION
- CONCLUSION

  The organizations that funded the work should be listed at the end of this section with grant numbers in parenthesis.
- REFERENCES

  The in-text references should be in brackets, such as [1].

RECOMMENDATIONS ON THE TYPING AND FORMATTING OF THE TEXT

- We recommend the use of Microsoft Word 2003 for Windows text editing software.
- The Times New Roman font should be used. Standard font size is 12.
- The space between the lines is 1.5.
- Using more than one whole space between words is not recommended.
- We do not accept articles with automatic referencing; automatic word hyphenation; or automatic prohibition of hyphenation, listing, automatic indentation, etc.
- We recommend that tables be created using Word software options (Table → Insert Table) or MS Excel. Tables that were created manually (using lots of spaces without boxes) cannot be accepted.
- Initials and last names should always be separated by a whole space; for example, A. A. Ivanov.
- Throughout the text, all dates should appear in the "day.month.year" format, for example 02.05.1991, 26.12.1874, etc.
- There should be no periods after the title of the article, the authors' names, headings and subheadings, figure captions, units (s – second, g – gram, min – minute, h – hour, d – day, deg – degree).
- Periods should be used after footnotes (including those in tables), table comments, abstracts, and abbreviations (mon. – months, y. – years, m. temp. – melting temperature); however, they should not be used in subscripted indexes (T_m – melting temperature; $T_{p.t}$ – temperature of phase transition). One exception is mln – million, which should be used without a period.
- Decimal numbers should always contain a period and not a comma (0.25 and not 0,25).
- The hyphen ("-") is surrounded by two whole spaces, while the "minus," "interval," or "chemical bond" symbols do not require a space.
- The only symbol used for multiplication is "×"; the "×" symbol can only be used if it has a number to its right. The "·" symbol is used for denoting complex compounds in chemical formulas and also noncovalent complexes (such as DNA·RNA, etc.).
- Formulas must use the letter of the Latin and Greek alphabets.

- Latin genera and species' names should be in italics, while the taxa of higher orders should be in regular font.
- Gene names (except for yeast genes) should be italicized, while names of proteins should be in regular font.
- Names of nucleotides (A, T, G, C, U), amino acids (Arg, Ile, Val, etc.), and phosphonucleotides (ATP, AMP, etc.) should be written with Latin letters in regular font.
- Numeration of bases in nucleic acids and amino acid residues should not be hyphenated (T34, Ala89).
- When choosing units of measurement, SI units are to be used.
- Molecular mass should be in Daltons (Da, KDa, MDa).
- The number of nucleotide pairs should be abbreviated (bp, kbp).
- The number of amino acids should be abbreviated to aa.
- Biochemical terms, such as the names of enzymes, should conform to IUPAC standards.
- The number of term and name abbreviations in the text should be kept to a minimum.
- Repeating the same data in the text, tables, and graphs is not allowed.

GUIDENESS FOR ILLUSTRATIONS

- Figures should be supplied in separate files. Only TIFF is accepted.
- Figures should have a resolution of no less than 300 dpi for color and half-tone images and no less than 500 dpi.
- Files should not have any additional layers.

REVIEW AND PREPARATION OF THE MANUSCRIPT FOR PRINT AND PUBLICATION

Articles are published on a first-come, first-served basis. The publication order is established by the date of acceptance of the article. The members of the editorial board have the right to recommend the expedited publishing of articles which are deemed to be a priority and have received good reviews.

Articles which have been received by the editorial board are assessed by the board members and then sent for external review, if needed. The choice of reviewers is up to the editorial board. The manuscript is sent on to reviewers who are experts in this field of research, and the editorial board makes its decisions based on the reviews of these experts. The article may be accepted as is, sent back for improvements, or rejected.

The editorial board can decide to reject an article if it does not conform to the guidelines set above.

A manuscript which has been sent back to the authors for improvements requested by the editors and/or reviewers is reviewed again, after which the editorial board makes another decision on whether the article can be accepted for publication. The published article has the submission and publication acceptance dates set at the beginning.

The return of an article to the authors for improvement does not mean that the article has been accepted for publication. After the revised text has been received, a decision is made by the editorial board. The author must return the improved text, together with the original text and responses to all comments. The date of acceptance is the day on which the final version of the article was received by the publisher.

A revised manuscript must be sent back to the publisher a week after the authors have received the comments; if not, the article is considered a resubmission.

E-mail is used at all the stages of communication between the author, editors, publishers, and reviewers, so it is of vital importance that the authors monitor the address that they list in the article and inform the publisher of any changes in due time.

After the layout for the relevant issue of the journal is ready, the publisher sends out PDF files to the authors for a final review.

Changes other than simple corrections in the text, figures, or tables are not allowed at the final review stage. If this is necessary, the issue is resolved by the editorial board.

FORMAT OF REFERENCES

The journal uses a numeric reference system, which means that references are denoted as numbers in the text (in brackets) which refer to the number in the reference list.

For books: the last name and initials of the author, full title of the book, location of publisher, publisher, year in which the work was published, and the volume or issue and the number of pages in the book.

For periodicals: the last name and initials of the author, title of the journal, year in which the work was published, volume, issue, first and last page of the article. Must specify the name of the first 10 authors. Ross M.T., Grafham D.V., Coffey A.J., Scherer S., McLay K., Muzny D., Platzer M., Howell G.R., Burrows C., Bird C.P., et al. // Nature. 2005. V. 434. № 7031. P. 325–337.

References to books which have Russian translations should be accompanied with references to the original material listing the required data.

References to doctoral thesis abstracts must include the last name and initials of the author, the title of the thesis, the location in which the work was performed, and the year of completion.

References to patents must include the last names and initials of the authors, the type of the patent document (the author's rights or patent), the patent number, the name of the country that issued the document, the international invention classification index, and the year of patent issue.

The list of references should be on a separate page. The tables should be on a separate page, and figure captions should also be on a separate page.

The following e-mail addresses can be used to contact the editorial staff: vera.knorre@gmail.com, actanaturae@gmail.com, tel.: (495) 727-38-60, (495) 930-80-05